Imperial College London

Identification of chemotherapy resistance drivers in breast cancer cells

A thesis submitted in accordance with the requirements of Imperial College London for the degree of Doctor of Philosophy

By

UTTOM KUMAR

June 2021

Department of Surgery and Cancer
Imperial College London
ICTEM Building
Hammersmith Hospital
Du Cane Road
London
W12 0NN

Statement of Originality

I hereby declare that the contents of this entire thesis include the original data of my own work and that all resources used in the thesis and all the assistants received at the professional and personal levels, for the completion of the study, have been appropriately acknowledged.

Copyright Declaration

The copyright of this thesis rests with the author and is made available under a Creative Commons Attribution Non-Commercial No Derivatives licence. Researchers are free to copy, distribute or transmit the thesis on the condition that they attribute it, that they do not use it for commercial purposes and that they do not alter, transform, or build upon it. For any reuse or redistribution, researchers must make clear to others the licence terms of this work.

Acknowledgement

It is my immense pleasure and proud privilege to express my heartiest regards and deepest sense of gratitude to my respected supervisors, Dr Ernesto Yagüe and Professor R. Charles Coombes, for their constant supervision, total support, and inspiration throughout the period of study. I found myself extremely lucky being a post graduate research student under their supervision. I am thankful to Dr Yagüe for his animating ideas, enthusiastic encouragement, and untiring guidance to carry out this study. I found him as my unforgettable mentor, providing me every support starting from technical issues of experimental design to supervision of everyday laboratory work.

I wish to express my profound reverence and sincere appreciation to Professor Sami Shousha, Centre for Pathology, Department of Medicine, Imperial College Faculty of Medicine, for his generous support in providing the clinical FFPE samples from the Charing Cross tissue bank archives for DNA methylation study and microRNA expression profiling. My special thanks go to Nahal Masrour, Division of Cancer, Imperial College Faculty of Medicine, for helping me with the pyrosequencing work and subsequent data analysis.

I am extremely grateful to Dr Marcos Castellanos-Uribe, Nottingham Arabidopsis Stock Centre (NASC), School of Biosciences, University of Nottingham, for providing me the facility supports for microarray hybridization and processing of whole genome transcriptome analysis, as well as helping me with the array data analysis.

I extend my sincerest thanks to Dr Alison Harrod, Epigenetics and Genome Stability Team, The Institute of Cancer Research, for helping me with the analysis of array data for microRNA expression analysis.

I also thankfully acknowledge Professor Valerie Speirs, Institute of Medical Sciences, School of Medicine Medical Sciences and Nutrition, University of Aberdeen, for making available to us a novel breast cancer cell line isolated from a patient with triple-negative metaplastic breast carcinoma.

My heartiest appreciation to all my fellow lab mates – Zimam Mahmud, Roman Jugov and Anastasia Ardasheva for their help in every possible way they could during my research work. I would like to thank all the supporting staff of the Imperial Centre for Translational and Experimental Medicine (ICTEM) who have helped me to use various equipment and

reagents. I am also thankful to the Commonwealth Scholarship Commission, UK, for funding this study.

Finally, I am indebted to my parents back home for their sacrifice during my stay here in London, and for their inspiration and continuous support.

Abstract

Breast cancer is a heterogenous disease with some subtypes posing a significant treatment challenge due to lack of targeted therapies and chemoresistance, particularly triple-negative metaplastic breast carcinoma (MBC). Here, I report a novel triple-negative MBC derived cell line, BAS, which showed a molecular and phenotypic diversity to the only existing metaplastic HS578T cells. To gain insight behind the chemotherapeutic resistance, I generated doxorubicin (HS-DOX, BAS-DOX) and paclitaxel (HS-TX, BAS-TX) resistant derivatives of both HS578T and BAS cells. Drug sensitivity assays indicated that doxorubicin- and paclitaxel-resistant cells showed a truly multidrug resistant (MDR) phenotype. Both BAS-DOX and BAS-TX showed significant up-regulation of transcription factor FOXC1 and its experimental down-regulation re-sensitized cells to doxorubicin and paclitaxel. Moreover, experimental modulation of FOXC1 expression in MCF-7 and MDA-MB-231 cells corroborated its role in MDR. Genome-wide expression analyses identified up-regulation of *TGFB2* in both BAS-DOX and BAS-TX cells. Pharmacological inhibition of the TGF-β pathway reduced FOXC1 expression and increased drug sensitivity in both BAS-DOX and BAS-TX cells. MicroRNA (miR) expression profiling identified higher endogenous miR-495-3p levels in parental BAS cells that were significantly down-regulated in both BAS MDR cells. Over-expression of miR-495-3p in BAS MDR cells led to re-sensitization to doxorubicin and paclitaxel and down-regulation of *TGFB2* and *FOXC1*, whereas miR-495-3p inhibition in parental BAS cells led to opposite effects. Moreover, miR expression analysis in breast cancer clinical samples identified a miR signature discriminating MBC from invasive ductal carcinoma (IDC).

Additionally, transcription factor FOXA1 also contributes to the MDR in breast cancer cells. Experimental down-regulation of FOXA1 in MCF-7 and T47D cells increased doxorubicin and paclitaxel sensitivity, whereas its over-expression in MDA-MB-231 cells increased resistance to both drugs.

Overall, the present study reveals some novel regulators of chemoresistance in breast cancer cells and thus opens the exploration of new therapeutic strategies.

Table of Contents

Chapter	Title	Page No.
1	**General introduction**	**17-47**
1.1	Breast cancer scenario	17
1.2	Human mammary gland	17
1.3	Molecular subtypes of breast cancer	19
1.4	Breast cancer treatment	20
1.5	Chemotherapy resistance	23
1.6	Cancer metastasis	25
1.7	Epithelial-mesenchymal transition (EMT) of cancer cells	26
1.8	EMT and cancer metastasis	26
1.9	Cancer stem cells (CSCs)	27
1.10	CSC and metastasis	28
1.11	CSC and drug resistance	29
1.12	EMT and CSC	31
1.13	EMT and therapeutic resistance	31
1.14	EMT, CSC and drug resistance	33
1.15	Regulatory network of EMT induction and further development of CSC phenotypes in breast cancer	34
1.16	E-cadherin as a master regulator of EMT, CSC and drug resistance	36
1.17	The forkhead box (FOX) transcription factors family	38
1.18	FOXC1: Structure and function	39
1.19	FOXA1: structure and function	40
1.20	Roles of microRNAs in regulating EMT, CSC and drug resistance	42
1.21	Metaplastic breast carcinoma (MBC)	44
1.22	Aims of the thesis	46
2	**General materials and methods**	**48-63**
2.1	Cell culture and maintenance	48
	2.1.1 Maintenance of cells	48
	2.1.2 Freezing cells for long-term storage	49
	2.1.3 Thawing cells for culture	49
2.2	RNA interference (RNAi) to generate gene down-regulated cell models	50
	2.2.1 Generation stably transfected cells for gene down-regulation	50
	2.2.2 Gene down-regulation by transient transfection of siRNAs	52
2.3	Generation of stably transfected cells for gene over-expression	53
2.4	Clonal isolation	54
2.5	Experimental modulation of miR-495-3p expression	55
2.6	RNA analysis	56
	2.6.1 Isolation of RNA from cells	56
	2.6.2 Synthesis of cDNA	56
	2.6.3 Real-time quantitative PCR (qPCR)	57
2.7	Protein analysis	58
	2.7.1 Protein extraction	58

2.7.2 Estimation of protein concentration 58
2.7.3 SDS-polyacrylamide gel electrophoresis (SDS-PAGE) 59
2.7.4 Electroblotting by wet transfer method 59
2.7.5 Western blotting 59
2.8 Short-term drug sensitivity and long-term drug resistance assays 60
2.8.1 Analysis of short-term drug sensitivity by sulphorhodamine B (SRB) assay 60
2.8.2 Analysis of drug resistance by clonogenic assays 60
2.9 Analysis of population doubling time 61
2.10 Anchorage independent growth assay 61
2.10.1 Soft agar colony formation assay 61
2.10.2 Mammosphere formation assay 62
2.11 Motility assay 62
2.12 Ethical approval 63
3 Characterization of a novel metaplastic breast cancer derived cell line 64-91
3.1 Introduction 64
3.1.1 Histologic characteristics of MBC 64
3.1.2 Clinicopathological features of MBC 64
3.1.3 Prognosis of MBC 65
3.1.4 Chemotherapy resistance in MBC 67
3.1.5 Molecular features of MBC 68
3.2 Aim of the chapter 70
3.3 Materials and methods 71
3.3.1 A novel metaplastic breast cancer derived cell line 71
3.3.2 Short tandem repeat (STR) profiling 71
3.3.3 Analysis of DNA methylation 72
3.4 Results 76
3.4.1 STR profiling of BAS cells identifies a novel breast cancer cell line 76
3.4.2 Phenotypic characterization indicates BAS cells are highly proliferative, motile, and capable to grow in anchorage-independent fashion 78
3.4.3 BAS cell line resembles MBC subclass 1 81
3.4.4 E-cadherin gene promoter methylation status of BAS cells resembles that of MBC patients 87
3.5 Discussion 89
4 FOXC1 is a determinant of MDR phenotype in breast cancer cells 92-127
4.1 Introduction 92
4.1.1 MDR in cancer 92
4.1.2 FOXC1 and cancer prognosis 93
4.2 Aim of the chapter 98
4.3 Materials and methods 99
4.3.1 Generation of drug resistant cell line models 99

4.4 Results 100
4.4.1 Doxorubicin- and paclitaxel-resistant derivatives of metaplastic breast cancer derived cells show a MDR phenotype 100
4.4.2 Upregulation of EMT and CSC markers in metaplastic breast cancer derived MDR cells 105
4.4.3 Assessment of EMT and CSC phenotypes of metaplastic breast cancer derived MDR cells 108
4.4.4 FOXC1 regulates the MDR phenotype in metaplastic derived BAS cells 111
4.4.5 Modulation of FOXC1 expression alters doxorubicin and paclitaxel sensitivity in luminal and basal-like breast cancer cells 113
4.4.6 FOXC1 regulates anchorage independence in breast cancer cells 119
4.5 Discussion 124
5 TGF-β regulates MDR phenotype in metaplastic breast cancer derived cells 128-173
5.1 Introduction 128
5.1.1 Whole transcriptome expression analysis and profiling 128
5.2 Aim of the chapter 130
5.3 Materials and methods 131
5.3.1 Whole transcriptome expression array 131
5.3.2 Preparation of total RNA 133
5.3.3 Preparation of total RNA/ poly-A RNA control mixture 137
5.3.4 Synthesis of first-strand cDNA 137
5.3.5 Synthesis of second-strand cDNA 138
5.3.6 Synthesis of cRNA by *in vitro* transcription 138
5.3.7 Purification and quantitation of cRNA 139
5.3.8 Synthesis of second-cycle single-stranded cDNA 140
5.3.9 Hydrolysis of RNA using RNase H 141
5.3.10 Purification and quantitation of second-cycle single-stranded cDNA 141
5.3.11 Fragmentation and labeling of single-stranded cDNA 142
5.3.12 Cartridge array hybridization 144
5.3.13 Array washing, staining and scanning 146
5.3.14 Analysis of array data 146
5.3.15 Methodological considerations for the generation of gene expression signatures 147
5.4 Results 149
5.4.1 MBC derived cells drug resistance gene expression signatures 149
5.4.2 Metaplastic derived HS578T and BAS cells acquire a MDR phenotype via common cancer hallmarks 160
5.4.3 Inhibition of TGF-β pathway re-sensitizes MDR BAS cells to doxorubicin and paclitaxel 164

5.4.4 Inhibition of TGF-β pathways reduces motility of MDR BAS cells 166
5.5 Discussion 168
5.5.1 MDR phenotype in metaplastic breast cancer derived cells is multi-factorial 168
5.5.2 EMT contributes to the MDR phenotype in metaplastic breast carcinoma 171
5.5.3 Inhibition of TGF-β pathway re-sensitizes MDR BAS cells and decreases their motility 171
6 MiRs regulate chemoresistance in metaplastic breast carcinoma 174-221
6.1 Introduction 174
6.1.1 MiRs in chemotherapy resistance in breast cancer 174
6.2 Aim of the chapter 177
6.3 Materials and methods 178
6.3.1 MicroRNA (miR) expression analysis 178
6.3.2 Total RNA isolation and quantitation 179
6.3.3 FlashTag Biotin HSR RNA labeling 182
6.3.4 Cartridge array hybridization 184
6.3.5 Array washing, staining, and scanning 185
6.3.6 Analysis of array data 186
6.4 Results 187
6.4.1 Metaplastic breast cancer derived cells show distinct miR expression signatures 187
6.4.2 MiR expression profiles of MBC derived cells identify an enrichment of TGF-β signalling pathway 193
6.4.3 MBC derived cells drug resistance miR expression signatures 195
6.4.4 Metaplastic derived HS578T and BAS cells acquire chemotherapeutics resistance via pathways related to aggressive cellular phenotypes 204
6.4.5 MiR-495-3p regulates *FOXC1* and *TGFB2* expression in BAS cells 206
6.4.6 MiR-495-3p regulates MDR phenotype in BAS cells 207
6.4.7 MiR expression analysis of different breast cancer subtypes 209
6.4.8 Discriminatory miR expression signature between MBC and IDC 213
6.4.9 Assessment of resemblance of miRs differentially regulated in breast cancer subtypes to cell lines 216
6.5 Discussion 218
7 FOXA1 regulates chemoresistance in breast cancer cells 222-241
7.1 Introduction 222
7.1.1 Role of FOXA1 in cancer 222
7.2 Aim of the chapter 224

7.3 Results 225
7.3.1 Modulation of FOXA1 expression in breast cancer cellular models 225
7.3.2 Modulation of FOXA1 expression does not alter E-cadherin levels in breast cancer cells 229
7.3.3 FOXA1 regulates the sensitivity of breast cancer cells to doxorubicin and paclitaxel 232
7.3.4 FOXA1 regulates anchorage independence in breast cancer cells 237
7.4 Discussion 239
8 Discussion and future directions 242-248
9 References 249-307
10 Appendices 308-312
Appendix I 308
Appendix II 311
Appendix III 312

List of Tables

Table No.	Title	Page No.
1.1	Drugs used for the treatment of breast cancer	22
2.1	Preparation of transfection complexes of lentivirus constructs	52
2.2	Preparation of transfection complexes of siRNA	53
2.3	Preparation of transfection complexes of miR inhibitor or mimic	55
2.4	Preparation of the 2X reverse transcription (RT) master mix (per 20-µL reaction)	57
2.5	Preparation of the cDNA reverse transcription (RT) reaction	57
2.6	Preparation of PCR reaction mix for one reaction	58
3.1	Description of the cell lines used for DNA methylation analysis	72
3.2	Description of the clinical FFPE samples used for DNA methylation analysis	73
3.3	Thermal cycler program for amplification of the *CDH1* promoter and *LINE1*	75
3.4	Assay design for methylation analysis of *CDH1* promoter and *LINE1*	75
3.5	Primers used for pyrosequencing	75
3.6	Short-tandem repeat (STR) analysis of BAS cells	76
3.7	STR profile comparison of BAS cells with data sets of 2455 cell lines from ATCC, DSMZ, JCRB and RIKEN	77
4.1	Strategy and the concentrations used for generation of drug resistant cell lines	99
4.2	Short-tandem repeat analysis of BAS naïve and drug resistant derivatives	100
4.3	Population doubling times of parental cells and their drug resistant derivatives	102
4.4	Sensitivity of metaplastic breast cancer derived cell lines to different drugs	105
4.5	Sensitivity of cells to doxorubicin and paclitaxel after experimental modulation of FOXC1 levels in metaplastic breast cancer derived MDR cells	111
4.6	Population doubling times of different clones of stably transfected MCF-7 cells over-expressing FOXC1 and their empty vector control clone	116
4.7	Sensitivity of cells to doxorubicin and paclitaxel after experimental modulation of FOXC1 levels in MCF-7 and MDA-MB-231 cells	119
5.1	GeneChip WT PLUS reagent kit contents and storage	132
5.2	Thermal cycler programs for whole transcriptome expression array	133
5.3	Description of the samples used for the whole transcriptome expression analysis	134
5.4	Quality control (QC) parameters of extracted total RNA samples used for the whole transcriptome expression array	135
5.5	Serial dilution of poly-A control stock	137
5.6	Preparation of total RNA/Poly-A RNA control mixture	137
5.7	Preparation of first-strand master mix	138

5.8	Preparation of second-strand master mix	138
5.9	Preparation of IVT master mix	139
5.10	Assessment of cRNA yield	140
5.11	Preparation of cRNA and second-cycle primers mix	141
5.12	Preparation of second-cycle ss-cDNA master mix	141
5.13	Assessment of yield of ss-cDNA	142
5.14	Preparation of fragmentation master mix	143
5.15	Preparation of labeling master mix	143
5.16	Preparation of hybridization master mix for a single reaction	145
5.17	Preparation of hybridization cocktail	146
5.18	Most differentially regulated genes in HS-DOX resistant cells	151
5.19	Most differentially regulated genes in HS-TX resistant cells	152
5.20	Most differentially regulated genes in BAS-DOX resistant cells	153
5.21	Most differentially regulated genes in BAS-TX resistant cells	154
5.22	Differentially regulated genes common between HS-DOX and BAS-DOX resistant cells	155
5.23	Differentially regulated genes common between HS-TX and BAS-TX resistant cells	156
5.24	Differentially regulated genes common between HS-DOX and HS-TX resistant cells	157-158
5.25	Differentially regulated genes common between BAS-DOX and BAS-TX resistant cells	159
5.26	Gene/gene set overlap matrix for HS578T MDR gene expression signature	162
5.27	Gene/gene set overlap matrix for BAS MDR gene expression signature	163
5.28	Gene/gene set overlap matrix for paclitaxel resistance gene expression signature	163
6.1	FlashTag Biotin HSR RNA labeling kit reagents and storage conditions, 10 rxn (P/N 901910)	179
6.2	Description of the cell lines used for miR expression analysis	180
6.3	Description of the clinical samples used for miR expression analysis	182
6.4	RNA input for FlashTag Biotin HSR labeling	183
6.5	Preparation of poly A tailing master mix	183
6.6	Preparation of hybridization master mix for GeneChip miRNA 4.0 array (for a single reaction)	185
6.7	Preparation of hybridization cocktail for GeneChip miRNA 4.0 array	185
6.8	MiRs down-regulated (RMA normalised expression values) in both MBC derived HS578T and BAS cells (Cluster 1)	189
6.9	MiRs up-regulated (RMA normalised expression values) in BAS cells (Cluster 2)	190
6.10	MiRs up-regulated (RMA normalised expression values) in both MBC derived HS578T and BAS cells (Cluster 3)	191
6.11	MiRs up-regulated (RMA normalised expression values) in HS578T cells (Cluster 4)	192-193
6.12	Most differentially regulated miRs in HS-DOX resistant cells	196
6.13	Most differentially regulated miRs in HS-TX resistant cells	197

6.14	Most differentially regulated miRs in BAS-DOX resistant cells	198
6.15	Most differentially regulated miRs in BAS-TX resistant cells	199
6.16	Differentially regulated miRs common between HS-DOX and BAS-DOX resistant cells	200
6.17	Differentially regulated miRs common between HS-TX and BAS-TX resistant cells	201
6.18	Differentially regulated miRs common between HS-DOX and HS-TX resistant cells	201
6.19	Differentially regulated miRs common between BAS-DOX and BAS-TX resistant cells	202-203
6.20	Differentially regulated miRs common to all signatures	203
6.21	Most differentially regulated miRs between metaplastic and IDC	214
7.1	Sensitivity of FOXA1-modulated breast cancer cells to doxorubicin and paclitaxel	234

List of Figures

Figure No.	Caption	Page No.
1.1	Ductal-alveolar unit of human mammary gland with location of the various cell types	19
3.1	Proliferation of HS578T and BAS cells	78
3.2	Motility of BAS, MDA-MB-231 and HS578T breast cancer cells	80
3.3	BAS cells show anchorage-independent growth capacity	81
3.4	BAS cells represent a triple-negative breast cancer molecular subtype	82
3.5	BAS cells express molecular markers of EMT and CSC	84
3.6	Molecular profile of BAS cells resembles MBC subclass 1	85
3.7	Expression profile of metaplastic breast cancer derived BAS cells	86
3.8	Methylation status of E-cadherin gene promoter in MBC patients and a selected panel of breast cancer cell lines	88
4.1	Proliferation of metaplastic breast cancer derived cells and their drug resistant derivatives	101
4.2	Doxorubicin- and paclitaxel-resistant HS578T cells show a MDR phenotype	103
4.3	Doxorubicin- and paclitaxel-resistant BAS cells show a MDR phenotype	104
4.4	Metaplastic breast cancer derived MDR cells show upregulation of different EMT and CSC markers, with significant higher expression of transcription factor FOXC1 in MDR BAS cells	107
4.5	Anchorage independence of metaplastic derived and basal-like MDR breast cancer cells	109
4.6	Motility of metaplastic breast cancer derived MDR cells	110
4.7	Experimental downregulation of FOXC1 leads to re-sensitization of MDR BAS cells to doxorubicin and paclitaxel	112
4.8	Expression of FOXC1 in a selected panel of breast cancer cell lines	113
4.9	Experimental modulation of FOXC1 expression in luminal MCF-7 and basal-like MDA-MB-231 breast cancer cells	115
4.10	Proliferation of stably transfected MCF-7 cells over-expressing FOXC1	116
4.11	Experimental modulation of FOXC1 expression in MCF-7 and MDA-MB-231 cells alters doxorubicin and paclitaxel sensitivity	118
4.12	FOXC1 over-expression in luminal MCF-7 breast cancer cells increases anchorage independence	120
4.13	FOXC1 over-expression in MCF-7 cells does not alter motility	121
4.14	FOXC1 silencing in basal-like MDA-MB-231 cells decrease anchorage independence	123
5.1	Schematic representation of steps involved in the whole transcriptome expression array	131
5.2	Integrity analysis of RNA samples used in the whole transcriptome expression array	136
5.3	Size analysis of fragmented ss-cDNA	144
5.4	Cartridge array	145

5.5	Principal component analysis (PCA)	147
5.6	Number of differentially regulated genes in each MBC derived drug resistant cell and signature	150
5.7	A similar set of hallmarks define the signatures associated with metaplastic breast cancer derived MDR cells	161
5.8	Galunisertib re-sensitizes metaplastic breast cancer derived drug resistant cells to doxorubicin and paclitaxel	165
5.9	Galunisertib inhibits motility of metaplastic breast cancer derived MDR cells	167
6.1	Schematic representation of FlashTag Biotin HSR RNA labeling for analysis by GeneChip miRNA arrays	178
6.2	GeneChip cartridge array for miR	184
6.3	Identification of the MBC derived cells miR expression signatures	188
6.4	MiR expression profile analysis highlights TGF-β signalling pathway in MBC derived cells	194
6.5	Pathways associated with chemotherapeutics resistance in MBC derived cells	205
6.6	Experimental modulation of miR-495-3p alters *FOXC1* and *TGFB2* expression in BAS cells	207
6.7	Experimental modulation of miR-495-3p expression in BAS cells and their drug resistant derivatives (BAS-DOX and BAS-TX MDR cells) alters doxorubicin and paclitaxel sensitivity	208
6.8	MiR expression profiling of different subtypes of breast cancer	211
6.9	MiR expression profile analysis highlights pathways associated with breast cancer	212
6.10	Pathways associated with discriminating miR expression signature between MBC and IDC	215
6.11	Analysis of miR expression resemblance between breast cancer clinical samples and cell lines	217
7.1	Expression of FOXA1 and E-cadherin in a selected panel of breast cancer cell lines	226
7.2	Experimental modulation of FOXA1 expression in breast cancer cells	228
7.3	E-cadherin expression remains unaffected upon FOXA1 knock-down in MCF-7 and T47D cells	229
7.4	Transcriptional regulation analysis of E-cadherin gene in FOXA1-modulated breast cancer cells	231
7.5	Experimental modulation of FOXA1 expression in breast cancer cells alters doxorubicin and paclitaxel sensitivity	234
7.6	FOXA1 knock-down in breast cancer cells decreases long-term resistance to doxorubicin and paclitaxel	235
7.7	Analysis of hormone receptors and key drug resistance markers expression upon FOXA1 modulation	236
7.8	Experimental modulation of FOXA1 expression alters anchorage independence in breast cancer cells	238
8.1	Regulators of multidrug resistance in breast cancer cells	243

Chapter 1: General introduction

1.1 Breast cancer scenario

Cancer is the second leading cause of death worldwide. In 2018 alone, it caused an estimated deaths of 9.6 million globally, which means one in six deaths is from cancer (World Health Organization, n.d.; Bray *et al.*, 2018). Among many different types of cancer, breast cancer is the most common type of cancer both in the developed and developing countries, affecting more than 2 million women globally each year (World Health Organization, n.d.; Harbeck *et al.*, 2019). It was the most prevalent form of cancer globally across all the income levels with the only exception of upper middle-income countries where ranked as two after the lung cancer in 2018 (WHO, n.d.). Overall, breast cancer ranked as the fifth cause of cancer associated death, which accounted for 685,000 deaths in 2020 (World Health Organization, n.d.). Breast cancer is the most common cancer type in US women after skin cancer and is the second leading cause of cancer death among women (American Cancer Society, 2017). Over a most recent period of 5-year (2012-2016), there was a slight increase in the breast cancer incidence rate by 0.3% per year in the United States (American Cancer Society, 2017; DeSantis *et al.*, 2019). Currently, an average risk of developing breast cancer in American women at some point in their lifetime is about 13%, which means there is a 1 in 8 chance that she may have developed breast cancer (American Cancer Society, 2017).

1.2 Human mammary gland

The mammary gland is an exocrine gland located in human breast and is responsible for production and delivery of milk. Normal mammary glands are branching epithelial structures composed of excretory ducts and secretory alveoli organized in lobules (**Figure 1.1**) (Sopel, 2010; Cristea & Polyak, 2018). The intralobular ducts together with clusters of alveoli form the lobules or terminal ductal-lobular units (TDLUs), which are known as the functional units of the breast (Stingl *et al.*, 2005). Milk is carried proximally via a series of branching ducts to the nipple upon synthesis within the differentiated acini of the gland. The epithelium of duct and alveoli consists of two differentiated cell types arranged into two layers, an inner layer of luminal epithelial cells and an outer layer of myoepithelial cells bordering basal lamina (**Figure 1.1**) (Sopel, 2010; Cristea & Polyak, 2018).

Luminal epithelial cells are cuboidal to columnar in shape. During lactation, luminal cells within the distal ducts and alveoli synthesize and secrete milk components. Markers expressed by luminal epithelial cells include keratin 18 (CK18), keratin 19 (CK19), CD24, CD133 and MUC1 (luminal cells-specific glycoprotein). However, some luminal epithelial cells especially located in large duct do not express keratin 18 (Stingl *et al.*, 2005). Epithelial cell adhesion molecule (EpCAM; also known as epithelial specific antigen or ESA) displays strong expression in luminal cells and is localized primarily to their basal and lateral membranes. Importantly, luminal cells exclusively express E-cadherin (Sopel, 2010).

Myoepithelial cells are specialized contractile epithelial cells located between the basement membrane and the luminal cells (Stingl *et al.*, 2005). They are attached to the luminal cells by desmosomes, and to the basement lamina by hemidesmosomes. In excretory ducts, myoepithelial cells form an almost continuous layer or sheath. However, in the secretory unit or alveoli, they tend to acquire basket-like shape, with sparser distribution that allows some luminal cells to be in contact with the basement membrane (Stingl *et al.*, 2005; Sopel, 2010). Mature myoepithelial cells are morphologically similar to smooth muscle cells, although they demonstrate features characteristics of epithelial cells, such as the expression of specific cytokeratin filaments. The intermediate filaments of myoepithelial cells are comprised mostly of cytokeratins, particularly CK5, CK14, and CK17. Interestingly, myoepithelial cells express proteins typically found in the contractile apparatus of smooth muscle cells, such as α-actin of smooth muscles (SMA), α-actinin, myosin heavy chains, vinculin, and calponin. The cellular contraction of myoepithelial cells is mediated by the cytoplasmic bundles of actin microfilaments and myosin filaments (Sopel, 2010).

Myoepithelial cells are primarily responsible for milk ejection in response to oxytocin action. They also participate in mammary gland morphogenesis during development, and play a role modulating the proliferation and differentiation of luminal cells, as well as in the formation of extracellular matrix (ECM), and thus contributing to the synthesis of ECM components (Sopel, 2010).

Although differentiated luminal and myoepithelial cells constitute more than 90% of the epithelial cells present in the mammary gland, there are some cells with an undifferentiated morphology. An example of these cells is the cap cells that line the terminal end buds (TEBs) of elongating ducts (Stingl *et al.*, 2005). The cap cells are considered as multipotent stem cells, as they can take on either a luminal or myoepithelial lineage (Sopel, 2010).

Interestingly, these cells exhibit phenotype intermediate between luminal and myoepithelial cells. For example, they share the expression of markers related to both lineages, such as vimentin, α-actin of smooth muscles (SMA), and MUC1 (Stingl *et al.*, 2005).

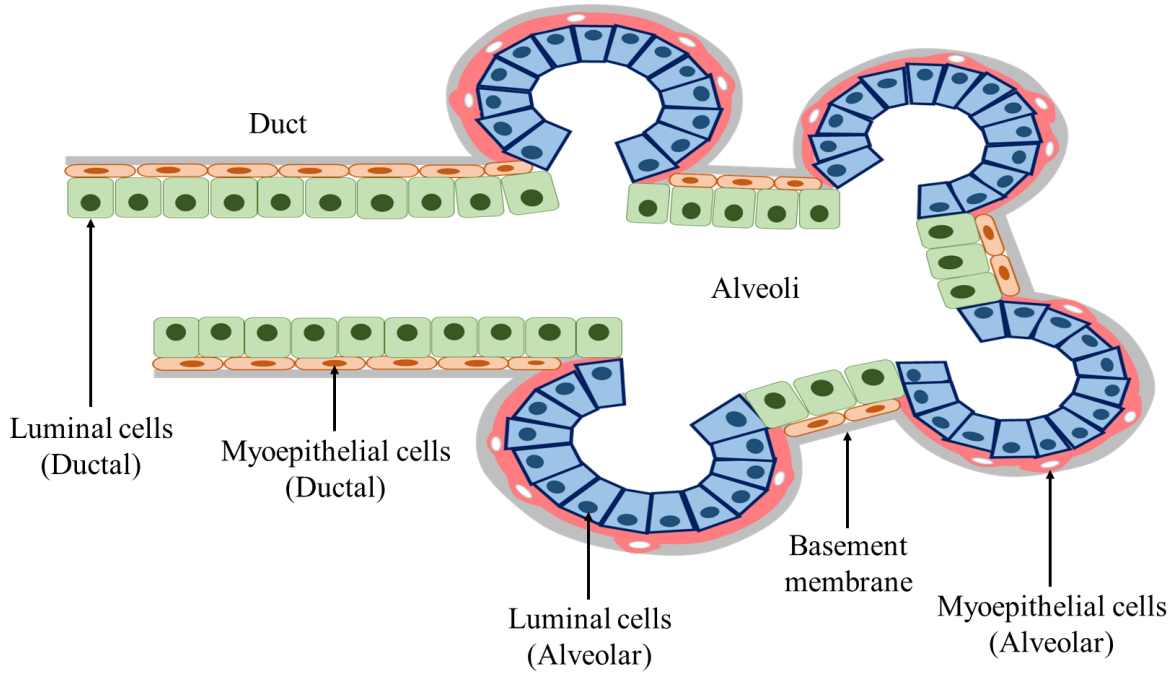


Figure 1.1: Ductal-alveolar unit of human mammary gland with location of the various cell types. Luminal epithelial cells of the duct and alveoli form the inner layer. Myoepithelial cells surround the luminal epithelial layer and are in direct contact with the basement membrane. The figure was prepared in Microsoft PowerPoint and is based on published information (Sopel, 2010; Tordonato, Di Fiore & Nicassio, 2015; Cristea & Polyak, 2018).

1.3 Molecular subtypes of breast cancer

Breast cancer is recognized to be a complex and molecularly heterogenous disease (Charafe-Jauffret *et al.*, 2006; Kao *et al.*, 2009). Prognostication and patient's stratification for appropriately targeted drug therapy are depended largely on the expression of mainly three markers, estrogen receptor (ER), progesterone receptor (PR) and ERBB2/HER2 (Subramaniam & Isaacs, 2005).

More recently, a molecular taxonomy of breast cancer has been introduced using DNA microarray studies. This distinguishes five major subtypes of breast cancer (luminal A, luminal B, basal, ERBB2-overexpressing and normal-like) taking account of their differential

gene expression profiles, underlying DNA copy number alterations (CNAs), and associated clinical outcomes (Perou *et al.*, 2000; Sørlie *et al.*, 2001; Chin *et al.*, 2006; Bergamaschi *et al.*, 2006). Both luminal A and luminal B tumour subtypes are ER positive and the markers they express share with the cells of luminal epithelial layer of normal breast duct lining. Contrasts between these two subtypes are that luminal A tumour is genetically simple, whereas high proliferation rates and frequent DNA amplification are observed with luminal B tumour. They also differ in prognosis where luminal A is associated with favourable outcome, but the luminal B exhibits less favourable. The expression markers of basal-like tumours share with the basal or myoepithelial cells of normal breast ducts. These tumours are ER negative and mostly associated with poor prognosis. The ERBB2-overexpressing subtype shares expression of genes that are co-amplified with ERBB2, and the normal-like is associated with expression patterns of normal breast tissue (Kao *et al.*, 2009).

1.4 Breast cancer treatment

The treatments for breast cancer are continuously evolving and multiple treatment options have been in use today for the management of breast cancer patients, such as surgery, radiotherapy, systemic adjuvant therapy, etc. The selection of appropriate treatment options for better patient outcome mainly depends on tumour histologic grade, lymph node involvement, hormone receptors status (oestrogen and progesterone receptors), ERBB2 overexpression, menopausal status, comorbidities, and patient age (Maughan, Lutterbie & Ham, 2010). Lobular carcinoma *in situ* does not warrant any treatment, as it usually does not turn into invasive breast cancer, but the affected women should be under continuous monitoring to assess such risk (American Cancer Society, 2019b). In contrast, ductal carcinoma in situ (DCIC), which has high tendency to progress into invasive breast cancer, is treated with breast-conserving surgery followed by radiotherapy (Solin *et al.*, 1991, 1996). Early-stage invasive breast cancers (stages I and II) are primarily treated with local and regional treatment, such as breast-conserving surgery and radiotherapy (JAMA, 1991; Litière *et al.*, 2012). The evaluation of regional lymph node involvement is an integral part during surgery, as it determines the need for subsequent radiotherapy and systemic adjuvant therapy (Maughan, Lutterbie & Ham, 2010). Typically, radiotherapy to whole-breast following breast-conserving surgery is recommended to treat subclinical disease, that might otherwise cause local recurrence (Abe *et al.*, 2005). Patients with node-positive disease are those to

benefit most from systemic adjuvant therapy. Practically, women with early-stage breast cancer almost invariably receive systemic therapies, including chemotherapy, endocrine therapy, and tissue targeted therapy, following local therapy (surgery, radiotherapy, or both) (Maughan, Lutterbie & Ham, 2010). **Table 1.1** summarizes medications used as systemic therapy to treat breast cancers. Chemotherapies are commonly used as a standard care to treat node-positive disease or a tumour larger than 1 cm in size (Maughan, Lutterbie & Ham, 2010). Hormone receptors-negative patients benefit more from chemotherapy and the selection of appropriate patients for chemotherapeutics treatment is also influenced by patient age and comorbidities (Partridge, Burstein & Winer, 2001; Goldhirsch *et al.*, 2007). The hormone receptors-positive disease is treated with hormone or endocrine therapies, including selective oestrogen receptor modulators (SERMs), selective oestrogen receptor degrader (SERD), aromatase inhibitors, luteinizing hormone-releasing hormone agonists, and progestins (Reinbolt *et al.*, 2015; American Cancer Society, 2019a). The tumours expressing specific biomarkers can also be treated with systemic targeted therapies. For example, a monoclonal antibody, trastuzumab is indicated for the treatment of tumours overexpressing ERBB2 (Ju, Zhu & Yuan, 2018). The standard treatment for locally advanced breast cancer (Stage III) is induction, also called neoadjuvant, chemotherapy or endocrine therapy to reduce the tumour burden, followed by local therapy, such as surgery (breast-conserving surgery or mastectomy), radiotherapy, or both (Hortobagyi, 1994; Giordano, 2003). However, for stage III inflammatory breast cancer, mastectomy followed by chest wall radiation is recommended after neoadjuvant chemotherapy due to the aggressive behaviour of this cancer type (Maughan, Lutterbie & Ham, 2010). The metastatic breast cancer (stage IV) is associated with poor prognosis with a five-year survival of only about 27 percent patients. The main objectives in the treatment of patients with metastatic breast cancer are palliative care and prolongation of life (Liu *et al.*, 2020). All possible treatment options, such as chemotherapy, endocrine therapy, radiotherapy, and limited surgery, are used to achieve these main goals with metastatic breast cancer patients (American Cancer Society, 2019a).

Table 1.1: Drugs used for the treatment of breast cancer

Therapy Type	Drug		
Chemotherapy	**Anthracyclines** • Doxorubicin • Epirubicin	**Taxanes** • Paclitaxel • Docetaxel	**Others** • 5-Fluorouracil or Capecitabine • Cyclophosphamide • Carboplatin
Endocrine Therapy	***Oestrogen receptors blockers***		
	Selective oestrogen receptor modulators (SERMs) • Tamoxifen • Toremifene		
	Selective oestrogen receptor degrader (SERD) • Fulvestrant		
	Drugs that lower oestrogen levels		
	Aromatase inhibitors (AIs) • Letrozole • Anastrozole • Exemestane	**Luteinizing hormone-releasing hormone (LHRH) analogues** • Goserelin • Leuprolide	
	Progestins		
	• Megestrol acetate • Medroxyprogesterone acetate		
Targeted therapy	***For HER2-positive breast cancer***		
	Monoclonal antibodies • Trastuzumab • Pertuzumab • Margetuximab	**Antibody-drug conjugates (ADCs)** • Ado-trastuzumab emtansine • Fam-trastuzumab deruxtecan	
	Kinase inhibitors • Lapatinib • Neratinib • Tucatinib		
	For hormone receptor-positive breast cancer		
	Cyclin-dependent kinase 4/6 (CDK4/6) inhibitors • Palbociclib • Ribociclib • Amebaciclib		**mTOR inhibitor** • Everolimus
	PI3K inhibitor • Alpelisib		
	For women with BRCA gene mutation		
	PARP inhibitors • Olaparib • Talazoparib		
	For triple-negative breast cancer		
	Antibody-drug conjugate (ADC) • Sacituzumab govitecan		

Source: American Cancer Society (American Cancer Society, 2019a)

1.5 Chemotherapy resistance

Breast cancer is a heterogenous disease exhibiting at least five major molecular subtypes, including luminal A, luminal B, HER2 enriched, basal-like and normal-like (Bernardo *et al.*, 2013). While luminal A tumours, which express estrogen receptor (ER)-α, appear to show a more favourable prognosis partly because of initial good response to anti-hormone therapies, a third of women with early stage breast cancer tend to develop resistance and relapse, following long term treatment (EBCTCG, 2005; Fan, Chang & Fu, 2015). Patients with basal tumours have a poorer prognosis due to intrinsic chemotherapy resistant properties of these tumours and lack of targeted therapies (Rakha, Reis-Filho & Ellis, 2008).

Though a noteworthy progress has been made in understanding the underlying molecular mechanisms of chemotherapy resistance and many new targeted therapies came into clinical practice, drug resistance still remains an unsolved clinical problem (Lage, 2008). A strategy to employ multiple drugs with different chemical structures that act via completely different mechanisms of action is not the way to avoid this problem, because cancer cells are capable to develop resistance simultaneously to many different chemotherapeutics, a multidrug resistance (MDR) phenomenon (Lage, 2008). The therapy failure due to drug resistance can be attained broadly by two main ways: pharmacological and cellular mechanisms. An acquisition of drug resistance phenotype by cancer cells involves a complex network of cellular pathways and multiple molecular mechanisms that can be switched on and off simultaneously and/or sequentially (Lage, 2008). Cellular mechanisms by which cancer cells attain MDR phenotype includes alteration of cell cycle checkpoints, drug targets modification, reduced cellular drug uptake and increased membrane-embedded transporters mediated drug efflux (Gottesman & Pastan, 1993; Raz *et al.*, 2014; Zhou *et al.*, 2015). One of the predominant mechanisms of resistance to conventional chemotherapeutics is increased drug efflux by membrane-bound drug extrusion pump called ABC-transporters such as ABCB1 (MDR1/P-glycoprotein), ABCC1 (multidrug resistance-associated protein 1, MRP1) and ABCG2 (breast cancer resistance protein, BCRP) (Lage & Dietel, 2000; Schinkel & Jonker, 2003). ABC-transporters catalyse ATP-dependent extracellular transport of structurally diverse compounds through cellular membrane leading to decreased intracellular drug concentration, and thereby the extruded drug cannot interact with their target molecules (Borst & Oude Elferink, 2002; Lage, 2008). Beside the cytoplasmic membrane localization, ABC-transporters are also found to be expressed in the intracellular membranes, like nuclear membrane or vesicular membranes (Dietel *et al.*, 1990; Surowiak *et al.*, 2006). This prevents

the accumulation of drugs in the nucleus to interact with their target molecules, or causes the drug entrapped in membrane-surrounded compartment, respectively. An overexpression of ABC-transporters due to gene amplifications or transcriptional and epigenetic changes to their expression is often associated with MDR phenomenon as it causes increased efflux of antineoplastic agents out of the cells so that tumour cells are no longer exposed to drugs long enough to produce cytotoxic effects (Meng *et al.*, 2006; Dallas *et al.*, 2009).

Modulation of cell cycle arrest or cell death pathways induced by the chemotherapeutic agents is another established mechanism in the development of drug resistance (Lage, 2008). Alteration of both apoptotic and anti-apoptotic mechanisms may contribute to the acquisition of drug resistant phenotypes of carcinoma cells (Okada & Mak, 2004; Brown & Attardi, 2005). Consequently, changes in the expression of cellular proteins responsible for maintaining homeostasis between these pro-apoptotic and anti-apoptotic mechanisms, such as B-cell lymphoma-2 (BCL-2) proteins family, may be important factors leading to the development of drug resistant phenotype (Johnstone, Ruefli & Lowe, 2002; Mashima & Tsuruo, 2005).

Activation of the DNA repair pathways is another mechanism causing drug resistance since many classical cytotoxic drugs directly target DNA molecule (Lage & Dietel, 1999; Ferreira, Tolis & Giaccone, 1999; Gerson, 2004; Bradbury & Middleton, 2004). Proteins involved as regulators of DNA repair pathways like PARP, p53 or BRCA1 may contribute to chemotherapy resistance (Lage, 2008). For example, MGMT (O^6-methylguanine-DNA-methyltransferase), an important DNA repair protein responsible for maintaining the integrity of cellular DNA, is involved in the resistance of cancer cells to methylating agents. This is because damage caused by these drugs provides a perfect substrate for MGMT (Gerson, 2004).

A hypothesis that draws a particular attention in recent years is the cancer stem cell (CSC) concept of MDR. According to the CSC model of MDR, the small subpopulation of this CSCs in the malignancy are intrinsically chemotherapeutic resistant because of their high levels of MDR-associated ABC-transporters content such as ABCB1 and ABCG2 as well as their capacity to repair DNA (Dean, Fojo & Bates, 2005; Lou & Dean, 2007). For this reason, drug treatment becomes ineffective and condition relapses after certain time because CSCs support the regeneration of tumour mass.

Therefore, a key to developing new cancer treatments as well as improving patient outcomes and increasing survival is solely dependent on the understanding and overcoming resistance to current therapies.

1.6 Cancer metastasis

Metastasis is the development of secondary tumours at distant anatomic sites from a primary tumour (Geiger & Peeper, 2009). This is considered as the major cause of most cancer related deaths (Fidler, 2003). The pathogenesis of a cancer metastasis involves a long series of sequential and interrelated steps including cellular transformation, local invasion, intravasation, survival in the circulation, migration to distant anatomic sites, extravasation, and finally colonization and metastasis in some of those sites (Gupta & Massagué, 2006). Each step in the entire process can be rate limiting, which means faulty at any of the steps can cause cessation of metastasis (Poste & Fidler, 1980; Fidler, 2002). The intrinsic properties of the cancer cells and host responses mutually determine the outcome of the process (Fidler, 2003). The metastatic potential of malignant cells is regulated by various genetic events such as mutation that cause transient or permanent changes in DNA, RNA, or proteins (Fidler, 2003; Hanahan & Weinberg, 2011). Most of the cancer types share similar steps to be metastasized, albeit the genetic variability in tumorigenesis of different cancers. Extensive vascularization or angiogenesis is both important for the initial tumour cells proliferation and the formation of secondary tumours as it supplies the nutrients for the expanding tumour mass. Loosing cellular attachment initially to be able to detach the cells from their original tumour site and then regaining this property so that they can adhere to the capillary beds of distant organs is an important attribute gained by the metastatic cancer cells. Several adhesion molecules play a significant role in the loss or gain of this property. Resistance to anoikis, a form of apoptosis induced by loss of cell adhesion, is another important property conferring the ability of the cancer cells to survive in the circulation during the metastatic cascade since most of the circulating tumour cells are rapidly destroyed due to induction of apoptosis when they loss their attachment to the extracellular matrix (ECM). Finally, proliferative capacity of the tumour cells within the organ parenchyma at secondary sites completes the metastatic process (Woodhouse, Chuaqui & Liotta, 1997; Fidler, 2003; Onder *et al.*, 2008).

The organ specific development of metastases is explained by the well-known Paget's seed and soil hypothesis. According to this hypothesis, metastasis develops only when a

subpopulation of tumor cells with metastatic potential (the 'seeds') finds compatible organ microenvironments (the 'soil'). The "seed and soil" hypothesis involves three principles. First, neoplasms contain heterogenous subpopulations of cells, each of which have different proliferative, angiogenic, cohesive, motility, and invasive properties. Second, the metastatic process is selective for cells that can successfully complete all the steps of metastasis, starting from local invasion to finally extravasation into, and multiplication within, secondary organ parenchyma. This assumes that metastasis supports survival and growth of a few subpopulations of cells pre-existing within the primary tumor and thus, different metastases can arise from proliferation of different single cells. Third, crosstalk between metastatic cells and homeostatic mechanisms determines the outcome of metastasis (Fidler, 2002, 2003).

1.7 Epithelial-mesenchymal transition (EMT) of cancer cells

The cellular process involving conversion of polarized, adherent epithelial cells into highly motile individual fibroblastoid or mesenchymal cell is known as epithelial to mesenchymal transition (EMT) (Huber, Kraut & Beug, 2005; Luo, Brooks & Wicha, 2015). EMT is a vital process during embryogenesis and chronic inflammation and fibrosis, as well as has been implicated in the cancer progression (Huber, Kraut & Beug, 2005; Liu *et al.*, 2005; Potenta, Zeisberg & Kalluri, 2008; Zeisberg *et al.*, 2007; Thiery, 2002; Nieto, 2013). In epithelial cells, several junctional structures, like tight junctions and adherent-type junctions, attach to the actin and intermediate cytoskeleton to form a tightly interconnected network (Liu *et al.*, 2005). During EMT, epithelial cells lose their cell-cell contacts and remodel the cytoskeleton network, with the ultimate consequences of loss of epithelial cell polarity and gain of a mesenchymal-like phenotype (Liu *et al.*, 2005; Nieto, 2013).

1.8 EMT and cancer metastasis

From a mechanistic viewpoint, at least four interrelated processes are needed for cancer cells to transform into metastatic cancer cells: EMT, remodelling of the ECM, migration to specific distant anatomic sites, and neoangiogenesis. Cancer progression is thought to be initiated by EMT where the ultimate migratory cells invade adjacent tissues and enter into the circulation (Thiery, 2003; Luo, Brooks & Wicha, 2015). The disruption of cell-cell adhesion and cell polarity of epithelial cells in primary tumour during EMT induction allows the EMT

cancer state to induce hypoxia, hyperactivation of various growth factors production by the tumour microenvironment and undergo metabolic changes (Craene & Berx, 2013). This causes biochemical changes in the polarized epithelial cell enabling its acquisition of mesenchymal-like phenotype, where the cells acquire migratory ability and resistance to apoptotic death in the circulation. As a result, these cells can migrate to distant anatomical sites (Kalluri & Neilson, 2003). Once the circulating tumour cells arrive at the site of metastasis, a reciprocal program, called mesenchymal to epithelial transition (MET), is induced to help disseminated tumour cells to adhere at its new site and form metastatic colonies at distal organs (Kalluri & Weinberg, 2009; Luo, Brooks & Wicha, 2015).

Thus, treatment strategy targeting EMT alone at late stage of cancer when the tumour cells have already disseminated from their primary site may be counterproductive, as the inhibition of EMT at this stage may cause stimulation of metastasis by promoting MET. Therefore, inhibition of both EMT and MET could be a promising strategy to develop new therapeutics in future (Luo, Brooks & Wicha, 2015; Liu *et al.*, 2017).

1.9 Cancer stem cells (CSCs)

CSCs are described as a subpopulation of cancer cells within a tumour with the potential to self-renew and to generate heterogeneous lineages of cancer cells that constitute a tumour (Hemmati *et al.*, 2003). These cells are also called "tumorigenic cells", or "tumour initiating cells". Typically, they comprise approximately 1% of the whole tumour cells mass (Hirschmann-Jax *et al.*, 2004). Cancer stem cell (CSC) theory assumes that most solid tumours exhibit a hierarchical organization and sustain a distinct subpopulation of CSCs (Visvader & Lindeman, 2008). According to this theory cancer arises from stem-like cells with the tumorigenic mutations and sometimes that have undergone epigenetic modifications too, resulting in the acquisition of dysregulated self-renewal capability. Accumulation of further tumorigenic mutations in these stem-like cells, owing to their increased lifespan, leads to the generation of cancer stem cells (CSCs) (Luo *et al.*, 2015).

Cancer stem cells were first detected in acute myeloid leukaemia in 1997 (Bonnet & Dick, 1997). These cells share the similar properties of normal stem cells, like capacity to self-renew and differentiation into many different cell types, and express unique signatures of stem cell such as $CD34^+$, $CD38^-$ phenotype (Bonnet & Dick, 1997). Breast cancer stem cells (BCSC) were first identified in 2003 in any solid tumour and are characterized by the

expression of cell surface antigens including $CD24^-$ and $CD44^+$, markers responsible for stemness and capacity to migrate, invade and proliferate (Luo, Brooks & Wicha, 2015; Koury, Zhong & Hao, 2017). The presence of CSCs has also been found in variety other carcinomas, beyond the initial identification in acute myeloid leukaemia and breast cancer, with the expression of some new markers like $CD133^+$ cells in brain tumour, colorectal carcinoma (CRC) and pancreatic cancer (O'Brien *et al.*, 2007; Hermann *et al.*, 2007; Reik, 2007).

Signalling pathways that play an important role in developmental process such as embryogenesis are reactivated during cancer progression initiated by the CSCs, like WNT-, Hedgehog- and Notch-dependent pathways (Singh *et al.*, 2004). There have been various epigenetic processes, like DNA methylation, histone modification and chromatin remodelling, which cause regulation of gene expression and cell fate determination without any changes to the DNA sequences. These epigenetic events may allow for CSC differentiation (Esteller, 2007). An epigenetic mechanism that has the vital role in cancer stem cells is DNA methylation. For example, DNA hypermethylation at CpG islands can cause silencing of genes that function tumour suppressors, contributing the formation of cancer stem cells (Ohm *et al.*, 2007; Jones & Baylin, 2007; Klarmann, Decker & Farrar, 2008). Another example where epigenetic DNA methylation plays an important role on regulating pathways related to cancer stem cells is the WNT/β-catenin signalling pathway, in which DNA methylation causes silencing of several WNT inhibitors including WIF-1 and AXIN2, resulting in aberrant activation of this pathways in breast and bladder cancers (Klarmann, Decker & Farrar, 2008; Koinuma *et al.*, 2006).

1.10 CSC and metastasis

Cancer metastasis is a very complex process where the disseminated tumour cells must pass through many steps of metastatic cascade to form secondary tumour at distal organs. Though a large number of cancer cells is released into the circulation from the primary tumour, micro-metastatic growth is initiated by only a small fraction of these cells (~2%) and the fraction of circulating tumour cells that can form sizeable macro-metastases at distal organs is estimated to be around ~0.02% (Cameron *et al.*, 2000; Chambers, Groom & MacDonald, 2002; Fidler, 2003; Gupta & Massagué, 2006). Therefore, metastatic colonization, the last step of metastasis, is a highly inefficiency process and only a small subpopulation of

disseminated cancer cells can accomplish (Malanchi *et al.*, 2012). The gene expression profile of breast cancer stem cells indicated invasive gene signature correlation with increased metastasis and poor overall survival (Liu *et al.*, 2007). This is further supported by the observation that metastatic bone marrow cancer cells of breast cancer patents exhibit CSC phenotype (Balic *et al.*, 2006). In a study using a mouse xenograft model, the metastatic cancer cells of human triple-negative breast cancer were found to be CD44+ and able to form tumours following transplantation in immunocompromised mice (Liu *et al.*, 2010). Moreover, the $CD44^{+}/CD24^{-}$ breast cancer stem cell lines can form mammospheres in non-adherent serum free medium, an *in vitro* surrogate of assessing tumour-initiating ability (Borgna *et al.*, 2012). Accumulated evidence suggests that cancer stem cells mediate metastasis and contribute to treatment resistance and disease relapse (Luo, Brooks & Wicha, 2015).

A concept called "migrating stem cell" was first established in 2005. This theory supports the existence of mobile cancer stem cell (Brabletz *et al.*, 2005). A strong support of this CSC theory was evident by the *in vitro* identification of a subset of cells with stem cell properties, from human brain tumours (Liu *et al.*, 2017). The property of cancer stem cells maintaining tumour microenvironment regulated plasticity to transition between mesenchymal-like (EMT) and epithelial-like (MET) states enables them to metastasize, where EMT-CSCs allow tumour cells dissemination, and the MET-CSCs are responsible for metastatic colonization. The mesenchymal phenotype of EMT-CSCs allows them to invade the surrounding tissue and enter the circulation, where they survive owing to their intrinsic quiescence and anoikis resistance. Once the EMT-CSCs form micro-metastases in distal organs after extravasation of the circulation, the reciprocal program MET is initiated by the tumour microenvironment due to extreme plasticity of CSCs. These MET-CSCs allow them to form macro-metastases (Luo, Brooks & Wicha, 2015). Therefore, the cancer stem cells are considered as most tenacious "seed" capable to colonize successfully in a foreign "soil" (Liu *et al.*, 2017).

1.11 CSC and drug resistance

The CSC concept explains that the limited efficacy of conventional chemotherapy due to its inability to eradicate the rare subpopulation of CSC, thereby causing disease relapse. An increasing body of evidence supports that the CSCs are naturally resistant to chemo- and radiotherapy (Shibue & Weinberg, 2017; Phi *et al.*, 2018; Steinbichler *et al.*, 2018). A high percentage of CSC at baseline in acute myeloid leukaemia (ALM) patients correlated with a

poor prognosis (van Rhenen *et al.*, 2005). Another study demonstrated that the cellular origin of relapse in some patients with AML is due to the presence of rare subpopulation of cells with a CSC phenotype before initiation of therapy (Shlush *et al.*, 2017). In breast cancer, several clinical studies shown the intrinsic resistance of breast cancer stem cell to neoadjuvant chemotherapy (Luo, Brooks & Wicha, 2015). For example, the residual tumour tissues after twelve weeks of chemotherapy contained a significantly increased percentage of $CD24^{-}/CD44^{+}$ breast cancer stem cells and exhibited more tumoursphere forming activity (Li *et al.*, 2008). Additionally, a high recurrence following new adjuvant chemotherapy was found to be associated with the presence of residual $ALDH^{+}$ cells, a marker for MET-like breast cancer stem cells (Alamgeer *et al.*, 2014).

The therapy resistant properties of CSCs are mediated by several different mechanisms, including dormancy of CSC, increased capacity to DNA damage repair and drug efflux, decrease apoptosis and interaction of CSCs with their supporting microenvironment (Steinbichler *et al.*, 2018). Chemoradiotherapy mainly targets the proliferating cells. CSCs are capable to induce cell cycle arrest, thereby enter into a dormant state and evade the antineoplastic agents (Phi *et al.*, 2018). Chemotherapy resistance due to increased drug efflux is caused by the expression of high levels of multidrug resistance (MDR) transporters, such as ABCB1 and ABCG2 (Steinbichler *et al.*, 2018). The properties of the CSCs to actively repair DNA damage is attributed to their radioresistance. For example, CD133+ glioblastoma cells were found to repair DNA damage more efficiently than corresponding CD133- cells (Steinbichler *et al.*, 2018). One study explained the increased radioresistance of mesenchymal CSCs is due to overexpression of N-methyltransferase, which causes depletion of the accessible amounts of nicotinamide, an inhibitor of cellular DNA repair mechanisms (D'Andrea *et al.*, 2011). Moreover, CSCs cause upregulation of reactive oxygen species (ROS) scavengers when irradiated, thereby lowering the levels of ROS, which are responsible for radiation induced DNA damage (Skvortsova *et al.*, 2015). The antiapoptotic phenotype of CSCs is mainly due to higher expression of B-cell lymphoma-2 (BCL-2) family of proteins (Steinbichler *et al.*, 2018). In breast and prostate cancers, CSCs were found to overexpress BCL-2 (Lang *et al.*, 2011; Domingo-Domenech *et al.*, 2012). This overexpression of BCL-2 in prostate CSCs is due to upregulation of developmental pathways, such as Notch and Hedgehog signalling pathways (Domingo-Domenech *et al.*, 2012; Merchant & Matsui, 2010). Moreover, WNT/β-catenin signalling pathways plays an important role in the acquisition of antiapoptotic phenotype (Heidel *et al.*, 2012).

1.12 EMT and CSC

The EMT program plays a vital role in transforming non-stem cancer cells into stem cell states (Liu *et al.*, 2017). For example, EMT induction stimulates the acquisition of stem and tumorigenic properties in mammary tumour progression model (Morel *et al.*, 2008). Generally, the gene signatures related to stemness and CSC numbers tend to be upregulated by induction of EMT (Luo, Brooks & Wicha, 2015). A study showed that induction of EMT in immortalized human mammary epithelial cells involved the expression of stem cell markers, and these cells exhibited CSC phenotypes, such as an increased ability to form mammosphere in suspension culture and colonies in soft agar as well as enhanced tumorigenicity in nude mice (Mani *et al.*, 2008). A similar molecular and phenotypic alteration conferring CSC attributes in epithelial carcinoma cells was observed with experimental activation of EMT, via either overexpression of EMT-associated transcription factors, such as Twist1 or Snail1, or treatment with transforming growth factor β (TGF-β) (Mani *et al.*, 2008; Morel *et al.*, 2008). Furthermore, luminal lineage cells in normal breast tissue were found to acquire a stem-like state by the overexpression of EMT related transcription factors Slug and Sox9 (Guo *et al.*, 2012). The association between EMT and CSC suggests that induction of EMT program is an important mediator in transitioning the luminal type of cell to a more mesenchymal stem-like CSC (Luo, Brooks & Wicha, 2015). Thus, the EMT program is responsible for non-stem to stem-like dedifferentiation. Additionally, CSCs are, by definition, capable to differentiate into non-CSCs, which form the bulk of the tumour mass. This stem-like to non-stem differentiation is triggered by the MET program. Therefore, the phenotypic plasticity of carcinoma cells, demonstrating their ability to transition back-and-forth between CSCs and non-CSCs, is caused by the reversibility of both the EMT and MET programmes (Shibue & Weinberg, 2017).

1.13 EMT and therapeutic resistance

Various clinical studies indicate that expression of EMT associated gene signatures in tumour samples result in therapeutic resistance, thereby poor clinical outcome (Shibue & Weinberg, 2017). For example, gene expression analyses in patients with non-small cell lung carcinoma have identified a 76-gene EMT signature as a potential tool to predict clinical resistance to EGFR or PI3K inhibitors (Byers *et al.*, 2013). In human pancreatic cancer, experimental evidence revealed that the transcription factor Zeb1 and other regulators of EMT help

maintain the drug resistance phenotype in cancer cells, suggesting the contribution of EMT in drug resistance (Arumugam *et al.*, 2009). It is increasingly recognized that EMT is associated with treatment resistance in breast cancer (Huang, Li & Ren, 2015).

Factors that contribute to the induction of EMT, including transcription factors, cytokines, and signalling pathways, also play an important role in the drug resistant in various types of carcinoma (Huang, Li & Ren, 2015; Du & Shim, 2016). EMT-related transcription factors, such as Snail, Slug, Twist, Zeb, contribute to the acquisition of drug resistance in various types of cancer (Du & Shim, 2016). For instance, aberrant expression of transcription factor Snail or Slug is involved in the protection against genotoxic stress induced apoptosis in breast adenocarcinoma cells (Kajita, McClinic & Wade, 2004), and upregulation of Akt2, caused by the elevated expression of transcription factor Twist, in highly invasive breast cancer cell lines promotes resistance to paclitaxel (Cheng *et al.*, 2007). Moreover, Twist plays also an important role in the resistance to oxaliplatin in colorectal carcinoma (Deng *et al.*, 2016).

Several EMT-related cytokines, such as TGF-β, tumour necrosis factor α (TNF-α), fibroblast growth factor (FGF), are associated with drug resistance. A recent study has demonstrated that chemotherapeutics induce activation of TGF-β pathway in breast cancer cells or higher levels of secreted active TGF-β in the tumour microenvironment caused EMT, leading to the resistance to chemotherapy (Bandyopadhyay *et al.*, 2010). In a colon carcinoma cell line, doxorubicin treatment induces EMT, via upregulation of TGF-β signalling pathways, and confers chemotherapy resistance (Li *et al.*, 2015). Another important inflammatory cytokine, TNF-α, also contributes to both EMT and drug resistance. Breast cancer cells exposed to TNF-α undergo EMT changes and exhibit multidrug resistant phenotype (Huang, Li & Ren, 2015). Furthermore, FGF expression is better correlated with paclitaxel resistance in patients with breast cancer, than P-glycoprotein (P-gp), p53, or BCL-2 expression (Gan, Wientjes & Au, 2006). Since FGF is linked to EMT induction, FGF-mediated chemotherapy resistance may be due to EMT (Huang, Li & Ren, 2015).

Many signalling pathways that are related to the EMT, such as Notch, Hedgehog, WNT, and NF-κB also contribute to drug resistance. A study revealed that a combination of a Notch inhibitor and transtuzumab treatment partially reverses transtuzumab-resistance in HER-2+ breast cancer. Thus, inhibition of Notch signalling may be an important target in the treatment of this type of recurrent breast cancer (Pandya *et al.*, 2011). Activation of the Hedgehog signalling pathway involved in the resistance to anti-epidermal growth factor

receptor (EGFR) targeted drugs, tyrosine kinase inhibitors (TKIs) through induction of EMT in non-small cell lung cancer (NSCLC) cells (Della Corte *et al.*, 2015). Overexpression of Wnt3 is a key mediator in the activation of WNT/β-catenin signalling pathway, which causes EMT induction and hence, rendering HER-2 overexpressing breast cancer cells resistant to transtuzumab (Wu *et al.*, 2012). The NF-κB pathway is a regulator of EMT and plays a key role in the resistance to chemotherapeutic agents (Orlowski & Baldwin, 2002). Inhibition of this pathway was found to cause sensitization of breast cancer cells to doxorubicin (Tapia *et al.*, 2007).

Collectively, these observations clearly demonstrate that EMT program plays a significant contribution in the development of chemotherapeutic resistance in many different types of carcinomas.

1.14 EMT, CSC and drug resistance

The functional link between EMT program and the CSC phenotype has provided us an opportunity to understand the phenomenon of chemotherapeutic resistance at molecular level in multiple cancer types. CSCs are more refractory to conventional chemotherapy and radiotherapy, compared to the non-CSCs population within the same tumour (Lage, 2008; Shibue & Weinberg, 2017; Phi *et al.*, 2018; Steinbichler *et al.*, 2018). This drug resistance phenotype of CSCs is may be due their high ABC-transporter expression, capacity to DNA repair, increased expression of antiapoptotic proteins and dormancy (Lage, 2008; Shibue & Weinberg, 2017; Steinbichler *et al.*, 2018). Interestingly, accumulating evidence suggests that the signalling pathways activated during EMT induction are similar to those driving CSCs, such as WNT, Notch and Hedgehog signalling pathways (Du & Shim, 2016). Importantly, cancer cells attain stem cell-like characteristics because of EMT programming. Thus, EMT and CSC are tightly interlinked, and are often associated with the acquisition of drug resistance (Lage, 2008; Singh & Settleman, 2010; Zhou *et al.*, 2014; Luo, Brooks & Wicha, 2015; Huang, Li & Ren, 2015; Liu *et al.*, 2017; Shibue & Weinberg, 2017; Asaduzzaman *et al.*, 2017). Interestingly, clinical evidence points toward the association of drug resistance with the EMT and CSCs. For instance, the residual tumors after chemotherapy show an enrichment of the CSCs and have all the hallmarks related to EMT (Dave *et al.*, 2012). A further illustration of the interplay between EMT, CSC and drug resistance comes from the characterization of the metaplastic breast cancers. This category of breast cancers is highly

aggressive and intrinsically resistant to chemotherapy. A study shows that MBCs are enriched in EMT and stem-like characteristics, attributing an association of chemoresistance with these two phenotypes (Hennessy *et al.*, 2009). The association between these three phenotypes is recognized as an 'axis of evil' in the war on cancer (Singh & Settleman, 2010). Therefore, further studies of the nexus between EMT programming, the CSC phenotype and drug resistance will be of great interest to develop new treatment modalities to eradicate CSCs and overcome drug resistance.

1.15 Regulatory network of EMT induction and further development of CSC phenotypes in breast cancer

Developing new therapies to target breast cancer stem cells depends mostly on the understanding pathways related to EMT induction and hence, development of CSC phenotypes. There are multiple signalling pathways involved in the EMT induction, including WNT, TGF-β, TNF-α/NF-κB, receptor tyrosine kinase (RTK), Notch and Hedgehog signalling pathways (Huber, Kraut & Beug, 2005; Kotiyal & Bhattacharya, 2014; Han *et al.*, 2015).

WNT signalling pathways causes activation and stabilization of β-catenin leading to its accumulation in the cytoplasm and further translocation into the nucleus, where it regulates transcription of many target genes. This ultimately leads to accumulation of Snail1, which is a transcriptional repressor of E-cadherin and, thus, downregulating E-cadherin resulting in EMT induction (Wang & Zhou, 2011).

The TGF-β signalling pathway, a potent EMT inducer, appears to play a dual role in carcinogenesis. TGF-β acts as a tumour suppressor during the early stages of tumour growth while with continuous disease progression, the growth inhibitory response to TGF-β is decreased and it plays an important role in tumorigenesis and metastasis via EMT induction (Massagué, 2008; Heldin, Landström & Moustakas, 2009). TGF-β pathway induces expression of many transcription factors that initiate EMT, including Snail, Slug, Twist and ZEB1/2 (Miettinen *et al.*, 1994; Wang & Zhou, 2011; Lamouille, Xu & Derynck, 2014). Moreover, TGF-β signalling cooperates with other signalling pathways, including Notch, WNT/β-catenin, NF-κB and RTK, to induce EMT and help maintain the mesenchymal phenotype of metastatic breast cancer cells (Wang & Zhou, 2011).

The developmental signalling pathway Notch plays a significant role in cell fate determination and maintenance of progenitor cell population. Notch signalling requires cooperation with other signalling pathways to promote EMT. For example, cross-talk between TGF-β and Notch signalling through Smad3 promotes Slug expression, which causes down-regulation of E-cadherin expression, leading to induction of EMT (Leong *et al.*, 2007). Another developmental signalling pathway, Hedgehog, has been reported to be involved in the maintenance of cancer stem cell (CSC) phenotypes in the basal-like breast cancer cells (Han *et al.*, 2015; Bhateja *et al.*, 2019). Activation of Hedgehog signalling pathway leads to expression of Snail family member transcription factors via GLI-dependent transcriptional activation and, hence, contributes to EMT (Huber, Kraut & Beug, 2005; Du & Shim, 2016).

The pro-inflammatory cytokine TNF-α is involved in the many steps of tumorigenesis, including proliferation, invasion, angiogenesis, and metastasis (Wu & Zhou, 2010). The signalling cascade initiated by TNF-α allows the translocation of free NF-κB into the nucleus, thereby inducing expression of many EMT-related transcription factors, such Snail, Slug, Twist, Zeb1 and Zeb2 (Min *et al.*, 2008).

Additionally, RTK signalling pathways also contribute to the EMT program and cancer cell invasion (Yang & Weinberg, 2008). Growth factors, like epidermal growth factor (EGF), fibroblast growth factor (FGF), or hepatocyte growth factor (HGF), function through activation of RTKs (Wang & Zhou, 2011). Signalling via either downstream effectors such as MAPK or PI3K is also necessary to regulate EMT along with TGF-β (Gotzmann *et al.*, 2004).

Interestingly, activation of these signalling pathways ultimately leads to an expression of several EMT-related transcription factors (EMT-TFs), including SNAIL factors (Snail and Slug), bHLH factors (E12 and E47, Twist1 and Twist2) and ZEB factors (Zeb1 and Zeb2). Binding of these EMT-TFs to specific DNA sequences has been shown to regulate EMT-target genes (Lamouille, Xu & Derynck, 2014).

Recently, forkhead box (FOX) transcription factors have been identified as important EMT-TFs (Du & Shim, 2016). A study revealed that FOXC1, a member of the FOX transcription factor family, is a potent EMT-inducer in breast cancer (Taube *et al.*, 2010). Moreover, breast cancer circulating tumour cells, which are associated with distant metastasis following EMT, express high levels of FOXC1 (Powell *et al.*, 2012; Yu *et al.*, 2013). FOXC2, another

member of FOX protein family, also contributes to the EMT and stem-like phenotypes in breast cancer. Down-regulation of FOXC2 expression in EMT-induced human mammary epithelial cells reverses the mesenchymal and stem-like phenotypes, whereas its overexpression in transformed mammary epithelial cells leads to the opposite effects (Hollier *et al.*, 2013).

Furthermore, current findings demonstrate that microRNAs (miRs) are also involved in EMT related diverse signalling pathways by regulating expression of several EMT-TFs as well as targeting genes involved in the maintenance of epithelial or mesenchymal phenotypes, thereby function as master regulators of EMT (Wang & Zhou, 2011; Kotiyal & Bhattacharya, 2014; Lamouille, Xu & Derynck, 2014; Du & Shim, 2016). For example, miR-200 family of microRNAs regulate EMT in breast cancer by directly targeting EMT-TFs, Zeb1 and Zeb2 (Gregory *et al.*, 2008; Bai *et al.*, 2014). Down-regulation of miR-125b was found to be associated with EMT phenotype in paclitaxel-resistant breast carcinoma cells (Yang *et al.*, 2015). MiR-34c down-regulation promotes EMT and self-renewal in breast tumour initiating cells (Yu *et al.*, 2012) and overexpression of miR-671-5p reverses EMT phenotype in breast cancer cells by downregulating FOXM1 expression (Tan *et al.*, 2016b).

1.16 E-cadherin as a master regulator of EMT, CSC and drug resistance

Epithelial cells undergoing EMT show a characteristic decrease in E-cadherin levels resulting in the loss of their morphology, increased motility and gain the ability to degrade the extracellular matrix and invade other tissues (Onder *et al.*, 2008). In addition to E-cadherin loss, cells acquiring mesenchymal phenotypes during the progression of EMT are also found to cause an upregulation of N-cadherin, and the phenomenon is termed as “cadherin switch” (Hopkins, Coatham & Berry, 2017). Loss of E-cadherin is a hallmark of EMT program (Liu *et al.*, 2005; Asaduzzaman *et al.*, 2017).

E-cadherin is a single-span transmembrane glycoprotein which extracellular domain establishes homophilic contacts with the neighbouring cells forming adherens junctions and intracellular or cytoplasmic domain binds with three catenin proteins (α, β and p120), leading to link with actin cytoskeleton (Onder *et al.*, 2008). Loss of E-cadherin causes accumulation free β-catenin in the cytoplasm which otherwise bound to C-terminus of E-cadherin and eventual translocation into the nucleus and induces the expression of a number of genes involved in EMT (Onder *et al.*, 2008; Asaduzzaman *et al.*, 2017).

In human tumours, there are several mechanisms causing loss or reduction of E-cadherin expression, including chromosomal deletions, somatic mutations, proteolytic cleavage, and promoter silencing of the *CDH1* gene (Hirohashi, 1998; Berx *et al.*, 1998; Strathdee, 2002; Maretzky *et al.*, 2005). The silencing of the E-cadherin gene occurs mainly by epigenetic processes, such as DNA hypermethylation, chromatin remodelling, and transcriptional repression in most carcinomas (Liu *et al.*, 2005).

Hypermethylation of *CDH1* promoter resulting in transcriptional down-regulation of E-cadherin gene has been found in many tumours, including breast carcinoma, oesophageal carcinoma, gastric carcinoma, and oral carcinoma (Liu *et al.*, 2005). Chromatin remodelling via histone acetylation or deacetylation is also play a significant contribution on the transcriptional regulation of gene expression. The status of histone acetylation or deacetylation depends on the recruitment of enzymes called histone acetyltransferase (HAT) or histone deacetylase (HDAC) (Strahl & Allis, 2000). A study reported that constraints imposed by the HDAC on the structure of chromatin was suggested to cause down-regulation of E-cadherin in metastatic breast cancer cells (Liu *et al.*, 2005).

Down-regulation of E-cadherin by transcriptional repressors is well-established. Several EMT-related transcription factors, including Snail family factors (Snail and Slug), bHLP family factors (E12/E47 and Twist1/2), and two-handed zinc factors family (Zeb1/2), have been reported to show major contribution in E-cadherin repression (Liu *et al.*, 2005; Yook *et al.*, 2006; Vincent *et al.*, 2009). The human *CDH1* gene promoter also has binding sites for upregulating transcription factors, including EP300, RUNX1 and FOXA1 (Liu *et al.*, 2005; Asaduzzaman *et al.*, 2017). The roles of these transcriptional activators regulating E-cadherin expression, thereby controlling EMT induction and associated CSC and drug resistant phenotypes in different carcinomas, particularly breast cancers, have not yet been fully characterized.

EP300 functions as a histone acetyltransferase (HAT) and thus remodels chromatin structure to epigenetically regulate transcription of E-cadherin gene (Ogryzko *et al.*, 1996). Moreover, it is also involved in cell proliferation and differentiation (Goodman & Smolik, 2000). Loss of heterozygosity and truncating mutations of EP300 have been reported to be associated with several malignancies, such as human colon, breast, and ovarian carcinoma (Gayther *et al.*, 2000; Bryan *et al.*, 2002). A study showed that EP300 deficiency in colon carcinoma cells induces changes in phenotypes characteristic of EMT (Krubasik *et al.*, 2006). Recently, using

breast cancer cellular models our lab has found that EP300 silencing in luminal cells confers drug resistance, together with increased *in vitro* tumorigenicity and CSC populations, while its ectopic expression in basal-like cells causes epithelial, differentiated and drug sensitive phenotype. Gene expression analysis revealed down-stream EP300 targets associated with EMT, CSC and drug resistance, including *ABCG2* (stemness), *BCL2* and *TNFRSF11B* (apoptosis), *ITGA2/3* (migration) and *TGFB2* (metastasis). Moreover, a strong down-regulation of EP300, and the corresponding either absent or low levels of E-cadherin expression, were also observed in metaplastic breast carcinoma, a rare, but aggressive form of invasive breast cancer with morphological features of EMT (Asaduzzaman *et al.*, 2017). All these observations depict the role of EP300 regulating E-cadherin expression and further development of EMT, CSC and drug resistant phenotypes in breast carcinomas. However, two other transcription activators of E-cadherin, such as forkhead box transcription factor FOXA1 and RUNX1, are less well characterized in relation to these perspectives.

1.17 The forkhead box (FOX) transcription factors family

The FOX family members are a group of highly evolutionary conserved transcription factors with a common DNA-binding domain of 110 amino acids known as winged-helix or forkhead box domain (FHD) (Myatt & Lam, 2007; Zhu, 2016). The FHD structure consists of three α-helices, three β-sheets and two wing regions located on either side of the third β-sheet- this assembly creates a butterfly-like characteristic and hence, the domain is named as such (Hannenhalli & Kaestner, 2009). To date, more than fifty different FOX transcription factors have been identified in human which belong to subclasses ranging from FOXA to FOXS (Hannenhalli & Kaestner, 2009; Lam *et al.*, 2013; Zhu, 2016). The FOX family proteins play pivotal roles in many biological processes, including cell proliferation, differentiation, survival, and death (Lehmann *et al.*, 2003; Lam *et al.*, 2013). Thus, deregulation of these proteins is involved with many pathological conditions, including development and progression of cancers (Myatt & Lam, 2007; Lam *et al.*, 2013). Current findings show that members of different subclasses of FOX proteins, including FOXA, FOXC, FOXM, FOXO and FOXP, contribute to initiation and progression of many different cancers, and are related with clinical outcomes (Lam *et al.*, 2013; Han *et al.*, 2017).

1.18 FOXC1: Structure and function

The human *FOXC1* gene is located at chromosome 6p25 encoding a 533 amino acids protein (Nishimura *et al.*, 1998). Structurally, FOXC1 phosphoprotein consists of a forkhead DNA-binding domain (FHD), followed by a transcription-inhibitory domain located between N- and C-terminal transactivation domains (Berry, Saleem & Walter, 2002; Berry, Mirzayans & Walter, 2006). The transcriptional activity of FOXC1 is regulated via its transactivation domains as well as phosphorylated inhibitory domain, where both N-and C-terminal activation domains are required for the maximal transactivation of FOXC1, whereas the phosphorylated inhibitory domain mitigates the activity of these domains (Berry, Saleem & Walter, 2002). FOXC1 protein has two nuclear localization sequences (NLS), which help translocate to the nucleus (Han *et al.*, 2017; Elian, Yan & Walter, 2018). Once in the nucleus, forkhead box domain (FHD) of FOXC1 binds to the DNA and regulates expression of many genes (Elian, Yan & Walter, 2018). A large body of evidence indicates that FOXC1 plays vital roles in many physiological and pathological processes (Han *et al.*, 2017; Elian, Yan & Walter, 2018; Wang *et al.*, 2018b).

FOXC1 is involved in many stages during embryonic development, like neural crest, mesodermal and ocular development (Han *et al.*, 2017; Elian, Yan & Walter, 2018). FOXC1-kockout mice die at birth due to multiple complications, including eye defects, hydrocephalus and skeletal abnormalities (Kume *et al.*, 1998). FOXC1 interacts with Hedgehog signalling pathway via binding directly with its transcription factor Glioma-associated oncogene family zinc finger 2 (GLI2) to regulate endochondral ossification (Yoshida *et al.*, 2015). Moreover, FOXC1 also plays an important role in the kidney, urinary tract, and reproductive development (Kume, Deng & Hogan, 2000; Wilm *et al.*, 2004).

Interestingly, both increased and decreased FOXC1 function are linked to pathological conditions (Elian, Yan & Walter, 2018). For example, a reduced FOXC1 function due to mutations is associated with Axenfeld-Rieger Syndrome (ARS), an autosomal dominant disease that mainly affects the development of the anterior segment of the eye, whereas increased levels of FOXC1 have been linked to many aspects of cancer progression, including cancer cell proliferation, differentiation, survival and metastasis (Nishimura *et al.*, 1998; Mears *et al.*, 1998; Tümer & Bach-Holm, 2009; Han *et al.*, 2017; Elian, Yan & Walter, 2018). FOXC1 has been reported to be involved in several different cancer types, such as breast cancer, hepatocellular carcinoma, endometrial cancer, lymphoma, pancreatic cancer, and non-small cell lung cancer (Sizemore & Keri, 2012; Xia *et al.*, 2013; Xu *et al.*, 2012; Wei

et al., 2013; Jin *et al.*, 2014; Elian, Yan & Walter, 2018). FOXC1 is a biomarker as well as a key prognostic indicator for basal-like breast cancer (BLBC) (Han *et al.*, 2017; Elian, Yan & Walter, 2018). In fact, poor prognosis in BLBC because of the acquisition of aggressive cellular phenotypes, such as increased cell proliferation, migration, and invasion, is due to elevated expression of FOXC1 (Ray *et al.*, 2010, 2011). Over-expression of FOXC1 in breast cancer cells, which harbour moderate endogenous FOXC1 levels, is found to increase cell proliferation, migration, and invasion. In contrast, down-regulation of FOXC1 in breast cancer cells with high endogenous FOXC1 levels decreases cell proliferation, migration, and invasion. Interestingly, ectopic expression of FOXC1 in mammary epithelial cells induces EMT as evident by the gain of mesenchymal phenotypes, with an up-regulation of basal marker P-cadherin and a down-regulation of epithelial marker E-cadherin (Ray *et al.*, 2010). Therefore, modulation of FOXC1 functions may unveil new treatment modalities for patients with breast cancer.

1.19 FOXA1: structure and function

Forkhead box transcription factor FOXA1, also known as Hepatocyte nuclear factor 3α (HNF-3α), contains a winged helix DNA-binding domain located between N-and C-terminal transactivation domains (Nakshatri & Badve, 2009). The DNA-binding domain binds directly with major groove of DNA consensus sequence in a base specific manner and is important for target site recognition (Clark *et al.*, 1993; Cirillo & Zaret, 2007; Nakshatri & Badve, 2009). FOXA family transcription factors are considered as pioneer factors because of their unique ability to initiate transcriptional regulatory programs by binding to target DNA sequence in the silent chromatin as an early event in a dominant manner (Nakshatri & Badve, 2009; Augello, Hickey & Knudsen, 2011). For example, binding of FOXA1 to the chromatin as a pioneer factor allows to open the chromatin structure and thereby, facilitates the hormone receptors (ERα and AR)/chromatin interactions at regulatory *loci* near hormone responsive genes (Carroll *et al.*, 2005; Laganière, Deblois & Giguère, 2005; Eeckhoute *et al.*, 2006; Lupien & Brown, 2009; Wang *et al.*, 2009). Current findings suggest that the ability of FOXA1 to open silent chromatin as a pioneer factor depends on the co-recruitment of positive and negative coregulatory proteins (Nakshatri & Badve, 2009). For example, recruitment of Transducin-like enhancer of split3 (TLE3) by FOXA1 to chromatin represses FOXA1 target genes due to formation of locally closed chromatin (Sekiya & Zaret, 2007). Thus, these coregulatory proteins may determine the cell-type specific function of FOXA1.

FOXA1 plays important roles in the regulation of development of endodermal layer and organogenesis during mammalian embryonic development as well as in metabolism and homeostasis in the adult (Wang *et al.*, 2018a). The role of FOXA1 in human carcinogenesis has not yet been fully defined, as both pro- and anti-tumorigenic functions have been reported (Augello, Hickey & Knudsen, 2011). For example, clinical analyses in patients with pancreatic carcinoma suggests that FOXA1 expression is inversely correlated with disease progression and aggressiveness, where loss of FOXA1 expression is observed in poorly differentiated disease (Song, Washington & Crawford, 2010). On the other hand, FOXA1 was identified as a potential oncogene, overexpressing in almost 70% thyroid cancer cases, and its expression was associated with highly proliferative, but poorly differentiated tumour phenotypes (Nucera *et al.*, 2009). Moreover, amplification or overexpression of FOXA1 have also been reported in both oesophageal and lung cancers, respectively (Lin *et al.*, 2002).

FOXA1 is identified as a master regulator of development of tissues mainly dependent on sex hormone signalling, like the breast and prostate glands (Augello, Hickey & Knudsen, 2011). This also implies that FOXA1 may play potential roles in hormone-dependent cancers, including prostate and breast cancers. Several studies reported that metastatic tissues from patients with prostate carcinoma were found to have high FOXA1 levels and thus, FOXA1 expression is strongly associated with the development of metastatic disease in prostate adenocarcinoma (Augello, Hickey & Knudsen, 2011; Robbins *et al.*, 2011; Jain *et al.*, 2011). Moreover, high FOXA1 expression is associated with poor prognosis in the majority of prostate cancers (Augello, Hickey & Knudsen, 2011). In breast cancers, FOXA1 expression is associated with luminal subtype tumours, and helps maintain the breast cancer luminal phenotype both ER-dependent and ER-independent mechanisms (Bernardo *et al.*, 2013). Importantly, high FOXA1 expression is associated with favourable prognosis in ERα-positive luminal breast cancer (Thorat *et al.*, 2008). Interestingly, recent studies suggest a quite unexpected role of FOXA1 in a subtype of ERα-negative breast tumour, which is also known as molecular apocrine breast cancer, due to the presence of apocrine-like histological features, with a gene signature related to oestrogen signalling (Augello, Hickey & Knudsen, 2011). In this type of breast cancer, FOXA1 was found to cause AR to bind to the sites normally occupied by ERα in luminal breast cancer, inducing ERα-like gene expression. Thus, it is suggested that FOXA1 can reprogram AR to function as surrogate for ERα (Robinson *et al.*, 2011).

1.20 Roles of microRNAs in regulating EMT, CSC and drug resistance

MicroRNAs (miRs) are a type of single-stranded non-coding RNAs (18- to 24-nucleotide) that negatively regulate gene expression by translational repression via partial complementation to 3'-untranslated region (3'-UTR) of target mRNAs (Reinhart *et al.*, 2000). MiRs play vital roles in many different biological processes and hence dysregulation of their expression leads to pathological conditions, including cancers (Calin *et al.*, 2002; Jang *et al.*, 2012). MiR genes are frequently located at genomic regions involved in cancers and have been reported to function as both oncogenes and tumour suppressors (Calin *et al.*, 2004; He *et al.*, 2005; Bonci *et al.*, 2008). For example, miR-122 was found to be down-regulated in breast cancer and its overexpression caused inhibition of cell proliferation and tumorigenesis, suggesting the role of miR-122 as a tumour suppressor (Wang, Wang & Yang, 2012; Ouyang *et al.*, 2014). In contrast, miR-221 was significantly up-regulated in breast cancer cells and its upregulation promoted breast cancer cells proliferation and invasion. Thus, miR-221 appears to function as an oncomiR (Falkenberg *et al.*, 2013; Ouyang *et al.*, 2014).

Several studies have associated miRs with chemotherapy resistance (Yang *et al.*, 2008; Zhou *et al.*, 2010; Hu *et al.*, 2016a; Zhou *et al.*, 2014). A study showed that miR-140 determines the chemotherapeutic sensitivity to 5-fluorouracil (5-FU) in osteosarcoma, where inhibition of endogenous miR-140 was shown to sensitize the resistant cancer cells to 5-FU, whereas overexpressed tumour cells were more resistant to the same drug (Song *et al.*, 2009). Another study reported miR-214 causes cell survival and induces cisplatin resistance in human ovarian cancer cells (Yang *et al.*, 2008). In breast cancer, miR-221/222 confers resistance to tamoxifen (Miller *et al.*, 2008). A significant down-regulation of miR-200b was noted in docetaxel-resistant non-small cell lung cancer (NSCLC) (Rui *et al.*, 2010). Down-regulation of miR-34a was associated with gain of chemotherapeutic resistant phenotype in both prostate and breast cancer cells (Fujita *et al.*, 2008; Chen *et al.*, 2010). Moreover, an interesting phenomenon was observed with pancreatic carcinoma, in which cancer stem cells (CSCs) showed loss of miR-34, suggesting that miR-34 might be involved in pancreatic CSC phenotype and subsequently drug resistance (Ji *et al.*, 2009b).

A large body of literature indicates that aberrant miRs expression is correlated with EMT and development of CSC phenotype, two key phenomena associated with the development of drug resistance in cancers (Wang *et al.*, 2010; Zhou *et al.*, 2014; Dong *et al.*, 2021). MiRs can regulate EMT by regulating the expression EMT-related transcription factors (EMT-TFs)

(Wang *et al.*, 2010; Du & Shim, 2016). For example, the miR-200 family, which comprises miR-200a, miR-200b, miR-200c, miR-141 and miR-429, negatively regulate EMT by directly targeting EMT-TFs, ZEB1 and ZEB2 (Park *et al.*, 2008; Gregory *et al.*, 2008), two repressors of E-cadherin, a hallmark of EMT. An ectopic expression of miR-200 in cancer cell lines caused up-regulation of E-cadherin and reduced their motility, whereas inhibition of miR-200 resulted in down-regulation of E-cadherin, increased vimentin expression, and EMT induction (Park *et al.*, 2008). Moreover, miR-200 family members, miR-200b and miR-200c, were also significantly down-regulated in gemcitabine-resistant pancreatic carcinoma cells, which show the characteristics feature of EMT. Interestingly, re-expression of the miR-200 family caused reversal of EMT phenotype, with the down-regulation of mesenchymal markers, such as ZEB1, Slug and vimentin (Li *et al.*, 2009). Another study reported miR-200 family members (miR-200a, miR-200b and miR-141) were down-regulated in nintedanib-resistant non-small cell lung cancer (NSCLC), which shows characteristics expression of EMT markers, such as decrease in E-cadherin levels and up-regulation of ZEB1 and vimentin (Nishijima *et al.*, 2016). In epithelial ovarian carcinoma, miR-186 was down-regulated in cisplatin resistant cancer cells showing EMT phenotype with increased Twist1 expression. Re-expression of miR-186 in these cells led to reversal of EMT phenotype, reduced Twist1 expression and transformed them more sensitive to cisplatin, as miR-186 directly targets Twist1 and negatively regulates its expression (Zhu *et al.*, 2016). MiR-29b was significantly down-regulated in metastatic prostate cancer cells and its ectopic expression can reverse EMT in prostate cancer cell by repressing Snail expression (Ru *et al.*, 2012). Tamoxifen-resistant breast cancer cells displaying mesenchymal features and increased invasiveness showed substantial down-regulation of miR-375 and its re-expression partly reversed EMT and sensitized resistant cells to tamoxifen (Ward *et al.*, 2013).

In addition to regulating the expression of EMT-TFs, miRs can also regulate the expression of many genes directly involved in the maintenance of epithelial or mesenchymal phenotype, such as these encoding adhesion molecules and signalling mediators, and thereby regulate EMT (Lamouille, Xu & Derynck, 2014). For example, up-regulation of miR-9 in breast cancer cells represses E-cadherin expression, resulting in increased cell motility and invasiveness, the typical mesenchymal characteristics (Ma *et al.*, 2010). Another study reported that over-expression of miR-194 in hepatic mesenchymal cells caused down-regulation of N-cadherin and suppression of their migration and invasion properties (Meng *et al.*, 2010). MiR-489 regulates EMT and chemo-resistant in breast cancer cells via negatively

regulating Smad3 expression. The drug resistant cells showed EMT phenotype with decreased expression of miR-489 and increased Smad3 expression, compared to corresponding parental cells, and forced expression of miR-489 reduced Smad3 levels and reversed EMT properties as well as chemoresistance (Jiang *et al.*, 2014).

Accumulated evidence indicated that miRs also regulate cancer stem cell (CSC), a key to develop chemotherapy resistance (Wang *et al.*, 2010). For example, miR-200c was down-regulated in human breast cancer stem cells (BCSCs). Importantly, expression of miR-200c in BCSCs inhibited their tumorigenicity *in vivo*, reflecting its role in regulating CSC phenotype (Shimono *et al.*, 2009). Moreover, miR-200 family miRs were reported to be strongly down-regulated in $CD44^{+}/CD24^{-}$ population of human breast cancer cells (Wang *et al.*, 2010). Another miR which plays vital role in regulating stem-like phenotypes of tumour-initiating cell (T-ICs) in breast cancer is miR-30. A study showed that miR-30 was down-regulated in breast T-ICs and its forced expression in breast T-ICs reduced tumorigenicity *in vivo*, whereas blocking miR-30 expression in differentiated breast cancer cells resulted in enhanced tumorigenicity *in vivo* (Yu *et al.*, 2010). In pancreatic cancer, miR-34 is involved in the survival and maintenance of cancer stem cell (CSC). The human pancreatic cancer stem cells show loss of miR-34 and elevated levels of Notch/BCL2, and restoration of miR-34 expression in the pancreatic cancer cells causes down-regulation of anti-apoptotic protein BCL2 and developmental pathway protein Notch, as well as a decrease in the tumour initiating cell population and tumorigenicity (Ji *et al.*, 2009b). In hepatocellular carcinoma, expression of miR-181 is associated with an enrichment of cancer stem cell (CSC) population and the progenitor cells isolated from tumour show up-regulation of miR-181 family members expression (Ji *et al.*, 2009a).

Thus, miRs could represent a potential therapeutic avenue in the treatment of breast cancer. Therefore, a continuous effort is made here to identify new miR candidates responsible for chemotherapeutic resistance in breast cancer, particularly triple-negative metaplastic breast carcinoma.

1.21 Metaplastic breast carcinoma (MBC)

Metaplastic breast carcinoma (MBC) is a morphological subtype of breast cancer accounting for only 0.2-5% of all invasive breast cancers (Lien *et al.*, 2007; Weigelt *et al.*, 2014). MBC is an umbrella term for a histologically diverse and unique collection of tumours

characterized by the coexistence of glandular and non-glandular component (Zhang, Toy & Kleer, 2012). The non-glandular component includes cells arising from metaplastic differentiation (Brenner *et al.*, 1998). Classically, these metaplastic changes lead to development of carcinomatous (squamous) and sarcomatous components, including spindle, osseous, and chondroid morphology (Reddy *et al.*, 2020). MBCs almost invariably (>90%) exhibit a triple negative breast cancer (TNBC) phenotype (Hennessy *et al.*, 2009; Weigelt, Kreike & Reis-Filho, 2009). However, MBCs differ from conventional TNBC in gene expression profiles. Compared to TNBC gene expression profile, MBC tumours show more up-regulation of EMT-related genes (McQuerry *et al.*, 2019). Moreover, proteomic analyses also identified EMT as the top upregulated pathway in the MBC proteome compared to conventional TNBC (Reddy *et al.*, 2020; Djomehri *et al.*, 2020). In comparison with non-metaplastic TNBC, MBCs are associated with a worse prognosis with twice the risk of recurrence and a shorter disease-free and overall survival (Nelson *et al.*, 2015). This is attributed to their very aggressive nature, inherent chemotherapeutic resistance and high tendency to metastasize, with the exception of low-grade adenosquamous carcinoma and fibromatosis-like carcinoma variants (McMullen, Zoumberos & Kleer, 2019). Thus, EMT might contribute to the aggressiveness and lethality of MBC.

Three hypotheses have been postulated to explain the biphasic phenotype (that is, coexistence of carcinomatous and sarcomatous components within the same tumour) of MBC. The collision theory suggests these components arise from separate progenitor cells. In contrast, the combination theory describes that both carcinomatous and sarcomatous components are derived from a common multipotent progenitor cell. Another theory called conversion/metaplastic theory hypothesizes that the sarcomatous components results from conversion or metaplasia of carcinomatous components (Schwartz *et al.*, 2013). Furthermore, the frequent expression of myoepithelial markers, such as p63, CD10 and smooth muscle actin, in tumours also suggest that MBC may originate from myoepithelial cells (Leibl *et al.*, 2005).

Several studies indicate that MBCs display multiple molecular alterations, such as similarity in EMT signatures, EGFR overexpression, mutations in the *PIK3CA* gene and loss of *PTEN*, enhanced nitric oxide (NO) activity, aberrant β-catenin expression, enhanced expression of PD-L1, and high frequency of p53 and *TERT* promoter mutations (Reddy *et al.*, 2020). Thus, targeting these molecular alterations may provide new therapeutic options for MBCs. Currently, the standard treatment guidelines with systemic chemotherapy used for MBCs are

the same that followed for conventional TNBC, despite the poorer clinical outcomes (Jung *et al.*, 2010; Chen *et al.*, 2011). Therefore, more research is necessary to understand the pathobiology of this aggressive breast cancer subtype leading to development of new and effective treatments.

1.22 Aims of the thesis

The general aim of the present study was to identify the potential regulators of chemotherapy resistance in breast cancer cells, with a particular focus on metaplastic breast carcinoma (MBC) derived cells. MBC is an aggressive malignancy with very poor prognosis, which is mainly due to their inherent or acquired chemotherapy-refractory properties. Moreover, the genetic and phenotypic variation within the different subclasses of MBC poses additional treatment challenges. This requires firstly a spectra of cell line models that could be workhorses to study more comprehensively *in vitro* the pathobiology of MBC, and secondly identification of chemotherapy resistance drivers, especially related to multidrug resistance (MDR) phenotype, that could provide novel therapeutic strategies for this notorious category of breast cancer. Additionally, regulation of MDR beyond the MBC subtype was also within the scope of the study. Specifically, FOXC1 and FOXA1 were selected to identify their role, if any, in regulating MDR and its associated EMT and CSC phenotypes.

The specific aims of the project were-

1. to characterize a novel MBC derived cell line molecularly and phenotypically, with a particular interest on EMT and CSC properties.
2. to generate and characterize, with respect to EMT and CSC attributes, chemotherapy resistant derivatives of MBC derived cell lines.
3. to investigate the effect of experimental modulation of FOXC1 expression on sensitivity/resistance towards conventional chemotherapeutics, such as doxorubicin and paclitaxel, as well as on EMT and CSC characteristics.
4. to identify drug resistance gene expression signatures for MBC derived cells by genome-wide expression profiling of their chemotherapy resistant derivatives.
5. to establish miR expression signatures for MBC derived cell lines, as well as to identify their drug resistance miR expression signatures, by miR expression analyses using a small panel of breast cancer cell lines, including MBC derived cells and their chemotherapy resistant derivatives.

6. to examine if any discriminatory miR expression signature for MBC, particularly related to EMT, CSC and drug resistance, can be obtained by miR expression profiling in a small panel of breast cancer clinical samples, including MBC.
7. to identify if experimental modulation of FOXA1 expression affects chemotherapy sensitivity/resistance, as well as EMT and CSC properties.

Chapter 2: General materials and methods

2.1 Cell culture and maintenance

All the cell culture work was performed in a class II laminal flow hood (BioMAT 2, MAT, Derby, UK) using disposable sterile plastic-wares. Cells were grown in a humidified Galaxy 170R incubator maintained at 37^0C and 5% CO_2 (RS Biotech, Ayrshire, UK).

2.1.1 Maintenance of cells

European Cell Culture Collection cell lines MCF-7, T47D, MDA-MB-231 and HS578T were acquired from Sigma-Aldrich (St. Louis, MO, USA). CAL51 cells were acquired from the German Resource Centre for Biological Material (DSMZ, Braunschweig, Germany). SK-BR-3 cells were a gift from L. Buluwela (Imperial College London). These cells were cultured in low glucose (1 g/L) Dulbecco's Modified Eagle's Medium (DMEM) (Lonza, Walkersville, MD, USA) supplemented with 10% of foetal calf serum (FCS), and 100 U/mL of penicillin, 0.1 mg/mL of streptomycin and 4 mM of L-glutamine (Sigma-Aldrich, St Louis, MO, USA). The medium for HS578T cells contained, in addition, 10 µg/mL of recombinant human insulin (Sigma-Aldrich, St Louis, MO, USA). The non-tumorigenic breast cell line, MCF-10A was a gift from L. Buluwela (Imperial College London), and was routinely cultivated in HuMEC Ready Medium consisting of HuMEC Basal Serum-Free Medium supplemented with HuMEC Supplement Kit, which includes 5 mL of a supplement mix containing epidermal growth factor, hydrocortisone, isoproterenol, transferrin, and insulin, and 25 mg of bovine pituitary extract (Gibco, Thermo Fisher Scientific, Waltham, MA, USA). Cells were maintained at 37^0C in a humidified incubator with an atmosphere of 5% CO_2. All cells were sub-cultured and maintained by serial passaging as suggested by the American Type Culture Collection (ATCC) using 25 g/L trypsin solution (Sigma-Aldrich) in 0.02% ethylenediaminetetraacetic acid (EDTA) (Sigma-Aldrich). All cells were routinely tested for mycoplasma contamination using a MycoAlert Mycoplasma Detection Kit (Lonza, Rockland, ME, USA). Normal human mammary epithelial cells (HMECs) were obtained from the Breast Cancer Now Tissue Bank, UK, and expanded in HuMEC Ready Medium (Gibco, Thermo Fisher Scientific). Doxorubicin-resistant CAL51 cells (CALDOX) were generated previously in the laboratory and routinely grown in the presence of 0.4 µM doxorubicin (Raguz *et al.*, 2013).

2.1.2 Freezing cells for long-term storage

Cells grown in 75 cm^2 culture flasks at a confluency of ~75% were frozen in 3 vials with ~1 mL cryomedium each. Cryomedium was made of 10% of tissue culture grade DMSO in foetal calf serum (FCS) except for BAS cells which was composed of 10% tissue culture grade DMSO, 10% FCS in complete Keratinocyte serum-free medium (KSFM). Briefly, cells were trypsinized after washing with sterile phosphate buffered saline (PBS), quenched with medium containing 10% FCS, and spun at 100 x *g* for 3 minutes. After aspiration of the supernatant, cryomedium (normally between 0.5-1.0 mL per cryovial) was added in a stepwise fashion resuspending the cells to avoid any clumps, transferred into cryovials, and immediately put in a Mr Frostie and kept at -80^0C overnight. Finally, cryovials were transferred to a liquid nitrogen (LN) vessel avoiding a sudden increase in temperature (i.e., keeping the vial in dry ice during transit).

2.1.3 Thawing cells for culture

Vials from liquid nitrogen storage were put immediately (or after short transit from the LN storage facility in dry ice) in a 37^0C water bath. Once thawed, the vial was taken immediately to tissue culture (T/C) hood, and cells' suspension in cryomedium was transferred to a 15 mL Falcon tube and ~10 mL of culture medium at 37^0C was added slowly and gently moving the tube so that DMSO diffuses out of the cells. Cells were treated gently avoiding vigorous pipetting and spun at 100 x *g* for 3 minutes in a standard T/C centrifuge. After aspiration of the supernatant, 1 mL of the culture medium at 37^0C was added with a Gilson and resuspended well to avoid any clumps and transferred to an appropriate T/C flask already with the required volume of culture medium at 37^0C. The flask was then incubated in a humidified incubator set to 37^0C temperature and 5% CO_2 level.

In case of very sensitive cells such as human mammary epithelial primary cells, once thawed the vial was immediately taken to the T/C hood and cells' suspension in cryomedium was directly added to the appropriate T/C flask already with the required volume of culture medium at 37^0C. After incubation overnight, medium was replaced with the fresh culture medium at 37^0C on next day.

2.2 RNA interference (RNAi) to generate gene down-regulated cell models

Both stable and transient transfection methods were used. Cell lines down-regulating *FOXA1* were generated by stable transfection, whereas down-regulation of *FOXC1* expression was performed transiently, after initial attempts to obtain stably transfected cells with robust and maintained *FOXC1* down-regulating were unsuccessful.

2.2.1 Generation stably transfected cells for gene down-regulation

Down-regulation of *FOXA1* in MCF-7 and T47D was obtained by stable expression of hairpins in the lentiviral vector pGIPZ (Horizon Discovery, Waterbeach, UK). After an initial trial of 6 different hairpins from the RNAi Consortium (Broad Institute, Cambridge, MA, USA), two different hairpins giving the best down-regulation in each cell line were selected (V3LHS_399489-mature antisense 5'-TCTCGAACATGTTGCCGGA-3' and V2LHS_16780-mature antisense 5'-GTTATGTAAATATACGGAG-3' for MCF-7 cells and V3LHS_414344-mature antisense 5'-GTCTTGCTATATAACAGCA-3' and V2LHS_16780 for T47D cells).

Isolation of plasmid DNA

Plasmid DNA cloned into *E. coli* DH5α was isolated using the QIAGEN Plasmid Maxiprep Kits (Qiagen, Hilden, Germany), following the manufacturer's instructions. A single colony from a freshly streaked ampicillin (100 µg/mL) selective LB-agar plate was picked and inoculated a starter culture of 5 mL LB-broth medium containing the same selection antibiotic, ampicillin (100 µg/mL), and incubated at 37^0C with vigorous shaking (300 rpm) until growth observed. The starter culture was mixed to 500 mL of ampicillin (100 µg/mL) selective LB-broth medium and incubated overnight at 37^0C with vigorous shaking (300 rpm). The bacterial cells grown were harvested by centrifugation at 6000 x *g* for 15 minutes at 4^0C. The cells' pellet thus obtained was resuspended with 10 mL of Buffer P1 (with which RNase A was already added at a concentration of 100 µg/mL). Next, 10 mL of Buffer P2 was added to the cells' suspension, mixed thoroughly, and incubated at room temperature for 5 minutes. After lysis, 10 mL of chilled Buffer P3 was added to the lysate, mixed thoroughly, incubated on ice for 20 minutes, and centrifuged (20,000 x *g*) for 30 minutes at 4^0C. The supernatant containing plasmid DNA was promptly transferred into 50 mL Falcon tube by sterile cotton gauze filtration to eliminate any suspended or particulate materials left after

centrifugation. The supernatant was then applied to a QIAGEN-tip 500 (already equilibrated with 10 mL of Buffer QBT) and allowed to enter the resin. QIAGEN-tip was washed with 2 x 30 mL Buffer QC. DNA was eluted with 15 mL Buffer QF into 50 mL Falcon tube. Afterward, the eluted plasmid DNA was precipitated by adding 10.5 mL (0.7 volumes) isopropanol to the eluted DNA, mixed well, and kept standing overnight at room temperature. Next day, the mixture containing the precipitated DNA was centrifuged at 200 x *g* for 30 minutes at 4^0C and the supernatant was carefully decanted. The DNA pellet thus obtained was resuspended with 1.5 mL of 70% ethanol and transferred to an Eppendorf tube and spun at 15000 x *g* for 5 minutes. The supernatant was aspirated carefully with micropipette without disturbing the pellet. After air-drying for 10 minutes, the DNA was dissolved in a suitable volume of TE buffer (pH 8.0), and the concentration determined using a NanoDrop ND1000 spectrophotometer (Thermo Fisher Scientific).

Lentiviral transfection

Lentiviruses were produced in HEK293T cells. The producer cells were seeded in a 10 cm dish at a confluence of 20-30%. On the next day morning, the culture medium of HEK293T (high glucose DMEM with 10% FCS) was replaced with fresh medium and in the late afternoon, transfection complexes of second-generation lentiviral constructs (a lentiviral expression plasmid, a packaging plasmid and a pseudotyping plasmid) and a transfection reagent, polyethyleneimine (PEI) (Polysciences), were prepared with Opti-MEM (Gibco, Life Technologies, UK) as described in **Table 2.1**. After incubation for 30 minutes at room temperature, the transfection complexes were added to the HEK293T culture dish dropwise, distributed gently and left overnight in the incubator. Next day, the recipient cells were seeded in a 75 cm^2 flask to have 1-2 million cells. In the morning, the HEK293T culture medium was replaced with fresh medium, which was again changed with 6-8 mL of recipient cells' medium in the night. On the following day, the virus containing recipient cells' medium was collected with substitution of fresh medium, filtered and polybrene (Sigma-Aldrich, Poole, UK) was added at a concentration of 1 μL per mL of medium. The recipient cells' medium was then replaced with this virus containing medium. This process of infection was carried out thrice at an interval of three hours. Next day, the recipient cells' medium was changed with virus-free fresh medium. After 2-3 days, the efficiency of transfection was assessed by visualising fluorescent glow, as pGIPZ carries EGFP reporter, using an EVOS

FL Cell Imaging System (Thermo Fisher Scientific, Waltham, MA, USA), and puromycin was added (1 µg/mL). After approximately 15 days clones were visible (>100 clones per flask) and were pooled by trypsinization and expanded.

Table 2.1: Preparation of transfection complexes of lentivirus constructs

Component	Volume/10 cm culture dish (µL)
Lentiviral Expression Plasmid (pGIPZ or pGIPZ sh constructs for FOXA1)	Volume equivalent to 20 µg
Pseudotyping Plasmid (pVSV-G)	Volume equivalent to 2 µg
Packaging Plasmid (pPAX2)	Volume equivalent to 8 µg
Polyethyleneimine (1 mg/mL, sterile and adjusted to pH 7.0)	75
Opti-MEM	Variable
Total Volume	**500**

2.2.2 Gene down-regulation by transient transfection of siRNAs

Down-regulation of *FOXC1* in MDA-MB-231 and doxorubicin- and paclitaxel-resistant derivatives of novel metaplastic breast cancer derived BAS (BAS-DOX and BAS-TX, respectively) cells was performed as described (Adams *et al.*, 2015). Cells were transfected with ON-TARGET plus SMART pool *FOXC1* siRNA oligonucleotides (Horizon Discovery, Waterbeach, UK) using HiPerFect transfection reagent (Qiagen, Hilden, Germany) following manufacturer's instructions. GFP siRNA (Ambion, Thermo Fisher Scientific, Waltham, MA, USA) was used as a negative control. Briefly, the day before transfection, cells (1 x 10^5 / well) were seeded in 6-well plate with an appropriate culture medium and incubated under normal culture conditions (typically 37^0C and 5% CO_2). On the day of transfection, the transfection complexes were prepared by mixing the components described in **Table 2.2** and incubating at room temperature for 10 minutes. The culture medium was replaced with 2.3 mL of fresh medium per well (without antibiotics). The transfection complexes (100 µL per well) were added dropwise onto the cells and the culture plate was gently swirled to ensure uniform distribution of the transfection complexes. Cells with the transfection complexes were incubated as usual and the gene silencing was monitored after an appropriate time. The culture medium was changed as required.

Table 2.2: Preparation of transfection complexes of siRNA

Component	Volume/well of 6-well plate (µL)	Final Concentration
siRNA (siFOXC1 at 20 µM stock and siGFP at 50 µM stock)	Variable (to get the final siRNA concentration after adding the complexes to cells)	40 nM
HiPerFect Reagent	12	
Culture Medium (without serum and antibiotics)	Variable	
Total Volume	**100**	

2.3 Generation of stably transfected cells for gene over-expression

MDA-MB-231 over-expressing *FOXA1* and MCF-7 over-expressing *FOXC1* were generated by stable transfection using FuGENE 6 transfection reagent (Promega, Madison, WI, USA) following the manufacturer's instructions.

Cloning vectors used and their constructs

Over-expression of *FOXA1* and *FOXC1* was obtained by stable expression of pcDNA3.1(-)-derived constructs carrying the full-length cDNA. *FOXA1* and *FOXC1* cDNAs were synthesized by GenScript Biotech (Leiden, The Netherlands) and cloned into the *Xho*I and *Eco*RI sites of pcDNA3.1(-) (Thermo Fisher Scientific, Waltham, MA, USA) incorporating a GCCACC Kozak sequence immediately before the ATG initiation codon.

Plasmid DNA isolation, linearization, and purification

All the plasmids cloned into *E. coli* DH5α were isolated using QIAGEN Plasmid Maxi Kits (Qiagen, Hilden, Germany), following the manufacturer's instructions. Plasmid DNA was linearized with *Pvu*I (pcDNA3.1 empty vector and *FOXA1* construct) or *Sca*I (*FOXC1* construct) following standard molecular biology techniques using 40 µg plasmid and 160 U (*Pvu*I) or 400 U (*Sca*I) of enzyme. The linearized plasmids were then purified by phenol-chloroform extraction and ethanol precipitation. DNA pellets were resuspended in TE buffer (10 mM Tris, 1 mM EDTA, pH 8.0) and the concentration determined using a NanoDrop ND1000 spectrophotometer (Thermo Fisher Scientific).

Cell transfection

Cells were seeded in 25 cm^2 culture flasks to reach 50-60% confluence while transfecting. On the day of transfection, 24 µL of FuGENE 6 Transfection Reagent (Promega, Madison, WI, USA) were added to Opti-MEM (Gibco, Thermo Fisher Scientific, Waltham, MA, USA) for a final volume of 325 µL (after addition of DNA in next step), mixed well and incubated at room temperature for 5 minutes. Next, the volume equivalent to 16 µg of linearized plasmid DNA (at a ratio of DNA to FuGENE 6 of 1:1.5) was added to the Opti-MEM/FuGENE 6 Transfection Reagent mix, following the manufacturer's instructions and incubated at room temperature for 15 minutes. Finally, the culture medium was replaced with 6.5 mL of antibiotic-free medium, and the transfection reagent/DNA complexes were added dropwise to the cells and mixed gently. Two days post-transfection, antibiotic selection was added and maintained with 1 mg/mL of G418 (Sigma-Aldrich, St. Louis, MO, USA).

2.4 Clonal isolation

Isolation of individual clones from a pooled population (MCF-7 cells down-regulating FOXA1 and MCF-7 cells transfected with pcDNA3.1 empty vector as well as overexpressing FOXC1) was performed using stainless steel cloning cylinders. Briefly, the cells were seeded at variable low densities in 20-cm culture dishes to ensure the likelihood of getting single-cell derived clones. The culture dishes containing the well-isolated clones were examined with an inverted microscope and satisfactory colonies located and marked with a circle around them on the bottom of the dish with a marking pen. After aspiration of the culture medium, the plate was rinsed twice with PBS to remove any floating cells. Using sterile medium forceps, a cloning cylinder was picked up and the flat bottom of the cylinder was gently pressed into smooth silicone grease and removed with a sudden vertical motion. The cylinder was set over a colony following the marking and gently pressed the cylinder down evenly with forceps. The position of the cylinder over the colony was verified with the microscope to ensure it encircled a single colony. The colony within the cloning cylinder was then trypsinized, quenched with a medium containing 10% FCS, and the cells gently aspirated with a micropipette and transferred to a suitable culture vessel containing the appropriate volume of culture medium at 37^0C. Finally, cells were incubated as usual and expanded.

2.5 Experimental modulation of miR-495-3p expression

Inhibition of miR-495-3p expression in BAS cells and its over-expression in doxorubicin- and paclitaxel-resistant derivatives of BAS cells (BAS-DOX and BAS-TX, respectively) was performed with hsa-miR-495-3p miRCURY LNA miRNA Inhibitor (Qiagen) and MISSION microRNA mimic hsa-miR-495 (Sigma-Aldrich), respectively. Negative control A miRCURY LNA Inhibitor Control (Qiagen) and MISSION miRNA, Negative Control 1 (Sigma-Aldrich) were used as their corresponding negative controls. The sequences for miR-495-3p inhibitor and its negative control were 5'-AGAAGTGCACCATGTTTGTT-3' and 5'-TAACACGTCTATACGCCCA-3', respectively. The miR-495 mimic mature sequence was 5'-AAACAAACAUGGUGCACUUCUU-3' and mimic negative control sequence was 5'-GGUUCGUACGUACACUGUUCA-3'. Cells were transfected with miR-495-3p inhibitor or mimic and the respective negative control using HiPerFect transfection reagent (Qiagen, Hilden, Germany) following the manufacturer's instructions. Briefly, cells (2 x 10^5 / well) were seeded in 6-well plate with appropriate culture medium and incubated under normal culture conditions (typically 37^0C temperature and 5% CO_2). Next day, transfection complexes were prepared with the components described in **Table 2.3**, gently mixed and incubated at room temperature for 10 minutes. The culture medium was replaced with 2.3 mL of antibiotic free fresh medium per well. The transfection complexes (100 µL per well) were then added dropwise onto the cells and the culture plate was gently swirled to allow homogeneous distribution of the transfection complexes. Cells with transfection complexes were incubated as usual and target genes expression were monitored after an appropriate time. The culture medium was replaced as required.

Table 2.3: Preparation of transfection complexes of miR inhibitor or mimic

Component	Volume/well of 6-well plate (µL)	Final Concentration
MiR-495-3p inhibitor and negative control or miR-495 mimic and negative control (20 µM stock)	4.8	40 nM
HiPerFect Reagent	15	
Culture Medium (KSFM without supplements and antibiotics)	80.2	
Total Volume	**100**	

2.6 RNA analysis

2.6.1 Isolation of RNA from cells

Total RNA was isolated using RNeasy Mini Kit (QIAGEN) following the manufacturer's instruction. Cells grown at a confluence of 80-90% were trypsinized following the standard procedure, washed twice with cold PBS, and the cells' pellet obtained was loosen thoroughly by flicking the tube and lysed with 600 µL Buffer RLT by pipetting up and down. The lysate was then homogenized by passing through a blunt 20-gauge needle fitted to an RNase-free syringe at least five times. Next, one volume of 70% ethanol (600 µL) was added to the homogenized lysate and mixed well by pipetting. Afterward, 700 µL of the sample (including precipitates that formed) was loaded onto an RNeasy spin column assembled with a 2 mL collection tube and spun at ≥8000 x *g* for 15 seconds. The flow-through was discarded, and the spin column was reassembled with its collection tube. This process was repeated with the remaining sample volume (exceeding 700 µL) using the same RNeasy spin column. The column was washed once with 700 µL Buffer RW1 by centrifugation at ≥8000 x *g* for 15 seconds followed by twice with 500 µL Buffer RPE by centrifugation at ≥8000 x *g* for 15 seconds (first time) and for 2 minutes (second time), according to the manufacturer's instructions. The flow-through was discarded after each centrifugation. The column was spun at full speed for 1 minute with a new 2 ml collection tube to remove any residual wash buffer. The column was then assembled with a new 1.5 mL collection tube and 50 µL of RNase-free water was added directly to the spin column membrane. The elution of RNA was done by spinning the column at ≥8000 x *g* for 1 minute. The concentration of the isolated RNA was determined using a NanoDrop ND1000 spectrophotometer (Thermo Fisher Scientific) and stored at -80^{0}C until further manipulation.

2.6.2 Synthesis of cDNA

Single-stranded complementary DNA (cDNA) was synthesized from total RNA using a High Capacity cDNA Reverse Transcription Kits (Applied Biosystems, USA) with random primers in a thermal cycler according to the manufacturer's instruction. The input amount of total RNA used was 2 µg per 20-µL reaction. On ice, the 2X reverse transcription (RT) master mix was prepared using the kit components as described in **Table 2.4**. The cDNA reverse transcription reaction was prepared with 2X RT master mix and RNA sample and adjusted to a final volume of 20 µL with nuclease-free water (**Table 2.5**). Finally, reverse transcription

was performed in a thermal cycler (G-storm) following the thermal cycler program described in the protocol (Step 1: 25^0C for 10 minutes, Step 2: 37^0C for 120 minutes, Step 3: 85^0C for 5 minutes, and Step 4: 4^0C until sample was recovered for storage). The cDNA thus obtained was stored at -20^0C until further use.

Table 2.4: Preparation of the 2X reverse transcription (RT) master mix (per 20-µL reaction)

Component	Volume/Reaction (µL)
10X RT Buffer	2.0
25X dNTP Mix (100 mM)	0.8
10X RT Random Primers	2.0
Multiscribe Reverse Transcriptase	1.0
Nuclease-free Water	4.2
Total per Reaction	**10.0**

Table 2.5: Preparation of the cDNA reverse transcription (RT) reaction

Component	Volume/Reaction (µL)
2X RT Master Mix	10.0
Total RNA Sample	Volume equivalent to 2 µg
Nuclease-free Water	Variable
Total Volume	**20.0**

2.6.3 Real-time quantitative PCR (qPCR)

qPCR was performed with a StepOnePlus Real-Time PCR system (Applied Biosystems) using cDNA as a template. First, a cDNA standard was prepared by pooling equal amounts of all diluted cDNA samples. Following a serial dilution technique, four dilutions of the standard in nuclease-free water (1/4, 1/16, 1/64 and 1/256) were prepared for the generation of a standard curve points, including a negative control (Nuclease-free water). Next, the PCR reaction was prepared in 96-well reaction plate (Applied Biosystems) with 2 µL of diluted cDNA sample (or standards, or nuclease-free water; depending on the plate layout) and 18 µL of reaction mix prepared with the components described in **Table 2.6**, for a final reaction volume of 20 µL. The amplification conditions were as follows: 10 minutes at 95^0C, followed by 40 cycles of 3 seconds at 95^0C and 30 seconds at 60^0C. Expression of *RPS14* and *RPLP0*

mRNAs was used to normalize the RNA input. All measurements were performed in triplicate. Analysis of gene expression was performed with the relative standard curve method. The statistically significant difference between the experimental groups was estimated using a Student *t*-test at a confidence interval of >95% ($p<0.05$). Primers used for the qPCR are listed in **Appendix I**.

Table 2.6: Preparation of PCR reaction mix for one reaction

Component	Volume/Reaction (µL)
Forward Primer for Target Gene (20 µM)	0.5
Reverse Primer for Target Gene (20 µM)	0.5
Nuclease-free Water	7.0
PowerUp SYBR Green Master Mix [2X] (Applied Biosystems)	10.0
Total Volume	**18.0**

2.7 Protein analysis

2.7.1 Protein extraction

Cells were trypsinized following the standard procedure, washed twice with cold PBS, and the cell pellet obtained was flash frozen in dry ice and kept at -80^{0}C until needed. On ice, the frozen cell pellet was lysed in 2 volumes of NP-40 lysis buffer [1% (v/v) Nonidet P-40, 150 mM sodium chloride, 50 mM Tris-HCl (pH 7.6), 5 mM EDTA, 1 mM sodium fluoride, 1 mM phenylmethylsulfonyl fluoride (PMSF), 1 mM sodium orthovanadate and one cOmplete protease inhibitor cocktail tablet (Roche Diagnostics, UK) per 10 mL of solution, according to manufacturer's instruction] for 10 minutes with meanwhile vortexing. The lysate was centrifuged at 15000 x *g* for 10 minutes at 4^{0}C, and the supernatant was carefully transferred to a clean Eppendorf tube and kept at -80^{0}C until further manipulation.

2.7.2 Estimation of protein concentration

The protein concentration was determined by bicinchoninic acid (BCA) assay using Pierce BCA protein assay kit (Thermo Fisher Scientific) following the manufacturer's instructions. Optical density (OD) was quantified at 562 nm using a Sunrise microplate reader (Tecan, Männedorf, Switzerland) and protein concentration was calculated against a standard curve.

The protein lysate was first diluted with distilled water at a ratio of 1:5, and this diluted sample was used for the estimation.

2.7.3 SDS-polyacrylamide gel electrophoresis (SDS-PAGE)

SDS-PAGE gels (5 to 10%) were prepared with varying amounts of bis-acrylamide solution depending on the molecular weight of target protein. The protein sample (10-20 µg) was first denatured by heating at 100^0C for 5 minutes with 6X SDS Laemmli buffer [6% SDS, 1.05 M DTT, 187.5 mM Tris-HCl (pH 6.8), 75% glycerol, 0.3% Bromophenol blue]. The denatured protein sample was loaded onto the stacking well of SDS-PAGE gel and run in a running buffer (25 mM Tris, 190 mM glycine and 0.1% w/v SDS) at 60V to pass through the stacking part of the gel, and afterward at 90V through the resolving gel, using Mini-Protean III apparatus (Bio-Rad Laboratories, Hemel Hempstead, UK).

2.7.4 Electroblotting by wet transfer method

The proteins in the sample thus resolved were transferred to the nitrocellulose membrane (BioTrace NT) in transfer buffer [25 mM Tris, 190 mM glycine and 20% (v/v) ethanol] at 90V for 90 minutes on ice using Trans-Blot Cell (Bio-Rad) wet transfer system.

2.7.5 Western blotting

The membrane was then blocked with 5% (w/v) bovine serum albumin (BSA) in 1xTBS-0.05% Tween-20 (TBST, pH 7.5) for 1 hour at room temperature and then incubated with primary antibody against protein of interest at 4^0C overnight. Next day, the membrane was washed with TBST thrice for 5 minutes each at room temperature, followed by incubation with horseradish peroxidase (HRP) linked anti-rabbit or anti-mouse secondary antibody (Dako, Agilent, Santa Clara, CA, USA), depending on the species of primary antibody, at 1:2000 dilution in TBST for 1 hour at room temperature. Finally, the membrane was washed again 5 times for 5 minutes each to remove the unbound secondary antibody and the bands were visualised using enhanced chemiluminescence (ECL) detection system (PerkinElmer, Inc., Massachusetts, USA). β-actin was used as a loading control. The details of primary antibodies used are described in **Appendix II**.

2.8 Short-term drug sensitivity and long-term drug resistance assays

2.8.1 Analysis of short-term drug sensitivity by sulphorhodamine B (SRB) assay

The sensitivity of the cancer cells toward a chemotherapeutic agent was assessed *in vitro* by SRB colorimetric assay (Vichai & Kirtikara, 2006). Briefly, cells were trypsinized, counted, seeded at a density of 2 x 10^3 cells per well of 96-well corning cell culture plate in six replicates for each drug concentration, and incubated overnight so that the cells adhere to the plate. Next day, cells were treated with a range of drug concentration determined by initial exploratory experiments, including a drug control group where no drug was added. The duration of drug treatment is relative to the proliferation rate of the cell lines, and cells were exposed to the drug for a period of their respective appropriate doubling time. After the drug treatment period, cells were fixed with 100 µL of cold 40% (w/v) trichloroacetic acid (TCA) (Sigma-Aldrich) per well for an hour at 4^0C, washed the plate four times with water, and stained with 100 µL per well of 0.4% (w/v) SRB (Sigma-Aldrich) in 1% (v/v) acetic acid by slow shaking for an hour at room temperature. The plate was washed repeatedly (usually four times) with 1% (v/v) acetic acid to remove excess dye and left to air-dry overnight. Finally, the protein-bound SRB dye was dissolved in 200 µL per well of 10 mM Tris base solution by shaking for an hour at room temperature, and the optical density (OD) was quantified at 490 nm using a Sunrise microplate reader (Tecan, Männedorf, Switzerland).

2.8.2 Analysis of drug resistance by clonogenic assays

A clonogenic assay was employed to evaluate the long-term resistance of the cells against the chemotherapeutic agents and assess the ability of cells to proliferate after exposure to toxic drug concentration thus forming colonies. Cells ($5x10^3$) were seeded into 6-well corning cell culture plate, at least in duplicate for each drug concentration. Next day, cells were treated with a single pulse of doxorubicin (Tocris Bioscience, Bristol, UK) or paclitaxel (Tocris Bioscience, Bristol, UK) at various drug concentration for 3 days. Cells were maintained for 14 days in culture with drug-free medium changing every three days. At the end of this period, the culture medium was aspirated, washed gently twice with 1X-PBS, and the drug resistant clones were fixed with 100% methanol for 10 minutes at room temperature. After aspiration of the methanol, clones thus fixed were stained with 0.5% (w/v) crystal violet (Sigma-Aldrich) in 25% (v/v) methanol by slow shaking for an hour at room temperature. The excess dye was washed off with tap water and plate was left to dry overnight. Digital

images of the colonies were taken using a camera and the stain was solubilized with 33% (v/v) acetic acid, and the optical density (OD) was measured 490 nm using a Sunrise microplate reader (Tacan, Männedorf, Switzerland).

2.9 Analysis of population doubling time

The SRB assay is used for the determination of cell density (Vichai & Kirtikara, 2006) and thus can be a surrogate for the estimation of population doubling time. This method measures cellular protein content owing to the ability of SRB dye to bind, under mild acidic conditions, to protein components of cells fixed to the culture plate. The amount of dye extracted from stained cells, under basic conditions with a suitable SRB solubilization buffer, is directly proportional to the cell mass due to stoichiometric binding of SRB to cellular protein. As described in the **section 2.8.1**, cells were seeded at a density of 2 x 10^3 cells per well in six replicates into 5 different 96-well coring cell culture plates. Next day (considered as 0 hour), cells in one plate were fixed with cold 40% (w/v) trichloroacetic acid (TCA), washed four times with tap water, and air-dried the plate overnight. This process of cells fixation was repeated every 24 hours with one plate for a period of 96 hours. The plates were stained with 0.4% (w/v) SRB (Sigma-Aldrich) in 1% (v/v) acetic acid, washed off excess dye with 1% (v/v) acetic acid, and left to air-dry overnight. Finally, the protein-bound SRB dye was dissolved in 200 µL per well of 10 mM Tris base solution by shaking for an hour at room temperature, and the optical density (OD) was quantified at 490 nm using a Sunrise microplate reader (Tecan, Männedorf, Switzerland). Doubling time was obtained from the best-fit curve generated by plotting OD vs time (hour) in Excel (Microsoft Corporation).

2.10 Anchorage independent growth assay

2.10.1 Soft agar colony formation assay

Soft agar colony formation assay was used to assess the anchorage-independent growth capability of cancer cells *in vitro* (Borowicz *et al.*, 2014). Cells (2 x 10^4) were seeded in complete DMEM (except for BAS cells and its drug resistant derivatives, which used complete KSFM) containing 0.3% soft agar noble (Difco Laboratories, Detroit, MI, USA) into 6-well corning cell culture plate with a bottom layer of solidified 0.6% agar noble in the same medium. Six replicate cultures for each cell type were maintained for 4 weeks in a

humidified incubator at 37^0C and 5% CO_2 level, with 300 µL fresh culture medium added twice a week. After 4 weeks, colonies larger than a predetermined reasonable size cut-off of 100 µm in diameter were counted and imaged using an EVOS FL Cell Imaging System (Thermo Fisher Scientific, Waltham, MA, USA). Clone forming efficiency was calculated relative to the total number of plated cells x100.

2.10.2 Mammosphere formation assay

The capacity of breast cancer stem cells (BCSCs) to propagate in anchorage-independent growth conditions was assessed by the mammosphere formation assay (Lombardo *et al.*, 2012). Cells (4 x 10^3) were seeded, at least in duplicate, in ultra-low attachment 6-well cell culture plates (Corning, NY, USA) with DMEM/F12 (except for BAS cells and its drug resistant derivatives, which used complete KSFM) supplemented with 20 ng/mL epidermal growth factor (EGF, Sino Biologics, Wayne, PA, USA), 20 ng/mL basic fibroblast growth factor (bFGF, Thermo Fisher Scientific, Whaltham, MA, USA) and 1X B27 (Thermo Fisher Scientific, Whaltham, MA, USA). Fresh medium (500 µL) was added every 3-5 days. After two weeks, spherical clusters of cells larger than a predetermined reasonable size cut-off of 100 µm in diameter were counted and imaged using an EVOS FL Cell Imaging System (Thermo Fisher Scientific, Waltham, MA, USA). Sphere forming efficiency was calculated relative to the total number of plated cells x100.

2.11 Motility assay

Scratch assay is used to assess the cell migration *in vitro*. This method involves creating a scratch in a cell monolayer and measuring the closure of the scratch over a period. The protocol was adapted from Liang *et al.* (Liang, Park & Guan, 2007). Cells were plated in 6-well plate in triplicate and grown until reached at 80% confluency. The plate was washed with PBS and a straight-line scratch was created by scarping the cell monolayer with a p200 pipette tip. The plate was washed again with PBS to remove the debris and then replaced with 2 mL of DMEM supplemented with 0.5% (v/v) FCS and 100 U/mL penicillin, 0.1 mg/mL streptomycin and 4 mM L-glutamine, except for BAS cells and its drug resistant derivatives which was KSFM supplemented with antibiotic-antimycotic. To ensure that the same field of each scratch is imaged over time, marks that served as reference points were made for two

sites of each scratch on the outer bottom of the plate with a maker pen. The plate was then incubated in a tissue culture incubator at 37^0C. Six visual fields were acquired at each time point with EVOS FL Cell Imaging System (Thermo Fisher Scientific, Waltham, MA, USA). The percent scratch closure was calculated by dividing the size of the gap in micrometers measured at time over that of at zero hour.

2.12 Ethical approval

All procedures performed in this study involving human clinical samples in accordance with the ethical standards of the Imperial College Healthcare Tissue Bank (R14086 and R17041) and Breast Cancer Now Tissue Bank (BCNTB-TR000054).

Chapter 3: Characterization of a novel metaplastic breast cancer derived cell line

3.1 Introduction

3.1.1 Histologic characteristics of MBC

Breast cancer is a heterogenous disease and its classification based on morphological and phenotype characteristics is routinely used in the clinic. Metaplastic breast carcinoma (MBC) is a rare poorly differentiated form of breast cancer (Beatty *et al.*, 2006), typically characterized by the coexistence of various combinations of adenocarcinoma with epithelial and mesenchymal components, resulting in various histopathological patterns (Song *et al.*, 2013). In fact, the tumours of this subtype of breast malignancies are composed of adenocarcinoma admixed with heterogenous histological elements, including spindle, squamous, and chondroid neoplastic cells (Rayson *et al.*, 1999). However, MBCs differ from typical adenocarcinoma in terms of clinicopathological features (Park *et al.*, 2010).

Classically, MBC is characterized by the histological evidence of both carcinomatous and sarcomatous components within the same tumour. Based on the relative abundance of these components in a tumour, MBCs have been classified in two subclasses. MBC subclass 1 has a predominant histological presence of carcinomatous components with only focal sarcomatous components, which is less than 10% of whole-tumour components. In contrast, MBC subclass 2 is composed predominantly of sarcomatous components and focally of carcinomatous components (< 10% of whole-tumour components) (Lien *et al.*, 2007).

3.1.2 Clinicopathological features of MBC

MBCs differ from typical invasive ductal carcinomas (IDCs) in terms of several clinical and pathological aspects, including age at time of presentation, tumour size and lymph node involvement (Park *et al.*, 2010; Song *et al.*, 2013; Schwartz *et al.*, 2013; Tray, Taff & Adams, 2019). MBCs occur more frequently in women older than 50 years, with a median age at the time of presentation found to be in the literature around 59 years (González-Martínez *et al.*, 2020). Interestingly, different histological subtypes of MBC also vary considerably at the age of patients during the time of presentation, with mean age of occurrence for MBC with chondroid differentiation was 71 years and that of for the squamous and spindle cell carcinoma were 48 and 56 years, respectively (Piscuoglio *et al.*, 2017). This category of

breast cancers is most often diagnosed as a rapidly growing mass, with sizes at presentation larger than the invasive ductal carcinoma (Bian *et al.*, 2016). The size of tumour in patients diagnosed with MBC is in general greater than 2 cm (Schwartz *et al.*, 2013; González-Martínez *et al.*, 2020). MBCs are usually diagnosed as a localized disease (nearly 90% of MBCs), but about half of the patients who are initially diagnosed as a local disease tend to develop distal metastasis, almost twice the observed in conventional TNBC (Abouharb & Moulder, 2015; El Zein *et al.*, 2017). Interestingly, the incidence of *de novo* stage IV disease (metastatic condition) is significantly higher with MBC than that found with conventional IDC. A study showed that 10.3% of patients with MBC present with *de novo* metastatic condition, compared to only 0.9% of incidence in patients with IDC (Park *et al.*, 2010). Involvement of axillary lymph nodes is less frequent with MBC despite the larger size of tumour, compared to the other types of breast cancers of same tumour sizes (Park *et al.*, 2010; Schwartz *et al.*, 2013; Tray, Taff & Adams, 2019). The incidence of metastases to axillary lymph nodes was found to be about 15-20% of all surgical cases (Pezzi *et al.*, 2006; Langlands *et al.*, 2016). Metastases only to lung occur more frequently with MBC compared to TNBC. In one study involving 22,433 patients (1112 MBC and 21,321 TNBC) reported that the incidence of lung-only metastases was 41.7% of metastatic cases, whereas that of for TNBC was 18.5% of metastatic cases (He *et al.*, 2019). MBC also tends to pose higher risk of local recurrence than the typical breast cancer (Park *et al.*, 2010; Schwartz *et al.*, 2013; Song *et al.*, 2013). A study showed that 53% patients with node-negative primary MBC recurred locally within two years which is significantly higher than that observed with typical adenocarcinoma of the breast, where local recurrence rate was found to be 17-20% patients with node-negative disease at five years (Carter, Allen & Henson, 1989; Rayson *et al.*, 1999). Molecularly, several studies reported around 80-84% of MBCs are triple-negative breast cancer subtype, which is significantly higher than the incidence rates found in IDC (around 16.7-20%) (Park *et al.*, 2010; Jung *et al.*, 2010). Interestingly, over-expression of Ki67 is more common in patients with MBC (87%), compared to IDC patients (63%) (Song *et al.*, 2013).

3.1.3 Prognosis of MBC

Accumulated evidence indicated MBCs are associated with poor prognosis. Song *et al.* demonstrated that the 5-year overall survival (OS) rate among a group of patients with MBC was lower than that of a group of patients with IDC (54.5% versus 85.1%) (Song *et al.*,

2013). The similar phenomenon was also observed for the 5-year disease-free survival (DFS) rate, with 45.5% in MBC versus 71.2% in IDC. Moreover, both the 5-year OS and 5-year DFS were reported to be significantly related to the tumour size (>5 cm), involvement of lymph nodes and over-expression of Ki67. These factors were considered as indicators of poor prognosis in patients with MBC (Song *et al.*, 2013). Another study conducted by Jung *et al.* noted that the 5-year overall survival (OS) rate was 62.8% in group of MBC patients and 92% in IDC patients' group. Similarly, the 5-year disease-free survival (DFS) rate for MBC group was 41.8% and that of for IDC group was 87.3% (Jung *et al.*, 2010). With regards both the DFS and OS, MBC showed poorer prognosis than the any subtype of IDC (5-year DFS rate: 41.8% for MBC versus 88.5% for Luminal A, 78.7% for Luminal B, 81.8% for triple-negative IDC and 75.4% for HER2-positive subtype; 5-year OS rate: 62.8% for MBC versus 93.3% for Luminal A, 91.7% for Luminal B, 87.0% for triple-negative IDC and 83.6% for HER2-positive subtype) (Jung *et al.*, 2010).

Interestingly, MBC subtypes also vary in prognosis. Song *et al.* reported that spindle cell carcinoma was the worst and carcinosarcoma was the best, considering the 5-year overall survival (OS). The 5-year OS rate for spindle cell carcinoma was 40% versus 50% in squamous cell carcinoma, 56.3% in adenosquamous carcinoma and 75% in carcinosarcoma (Song *et al.*, 2013). Rakha *et al.* also observed a significant association between MBC subtypes and disease prognosis in a large international multicentre series of MBC (n=405). Although a significant difference in outcome was observed between matrix producing and squamous carcinomas, both were associated with a better prognosis while spindle and mixed spindle and squamous carcinomas were involved with the worst outcome (Rakha *et al.*, 2015). Another study reported spindle cell carcinoma is associated with more aggressive biological characteristics compared to squamous cell carcinoma as well as MBC with heterologous mesenchymal differentiation (McCart Reed *et al.*, 2019; González-Martínez *et al.*, 2020).

On the other hand, variation in MBC prognosis based on receptors status is somewhat conflicting. Mills *et al.* demonstrated no significant difference in prognosis between triple-negative MBC and non-triple-negative MBC (Mills *et al.*, 2018). In contrast, Ong *et al.* noted that triple-negative MBC was associated with a worse prognosis compared to oestrogen receptor-positive MBC, except HER2-postive MBC, which was comparable to triple-negative MBC (Ong *et al.*, 2018).

3.1.4 Chemotherapy resistance in MBC

The poor prognosis in MBCs might be attributed to their intrinsic chemo-refractory nature. Patients with MBC usually do not respond well to systemic chemotherapy (Al Sayed *et al.*, 2006; Weigelt *et al.*, 2014). Moreover, MBCs have been reported to be relatively resistant to DNA-damaging chemotherapeutics compared to conventional TNBCs (Weigelt *et al.*, 2014). Poor response of MBC to systemic therapy has been observed in both neoadjuvant and adjuvant chemotherapy settings. Several studies demonstrated that effectiveness of neoadjuvant chemotherapy was very minimal to reduce the tumour burden as well as preventing disease progression. In a single institutional study by Al-Hilli *et al.* analysing the response of MBC to neoadjuvant chemotherapy (NAC) employing 18 MBC patients, the pathological complete response (pCR) was observed in two patients (11%) and another two patients were found to develop metastatic condition during NAC, suggesting that MBCs are poor responsive to NAC (Al-Hilli *et al.*, 2019). From a retrospective study of MBC patients who received NAC at the M.D. Anderson Cancer Centre between 1985 and 2001, Hennessy *et al.* reported only 10% pathological complete response (pCR) rate was observed to NAC (Hennessy *et al.*, 2006). Furthermore, Chen *et al.* reported 83% of disease progression rate during NAC in their single-institute retrospective study. Notably, no responses were observed in patients who received anthracycline-, vinorelbine-, or cyclophosphamide-based chemotherapy and the partial response rate was 17.6% among patients who received taxane-based chemotherapy (Chen *et al.*, 2011).

Limited efficacy of systemic chemotherapy in metastatic MBC patients has also been reported. A retrospective study noted that the response rate to systemic chemotherapy in a group of metastatic MBC patients was only 16.7%, whereas that found in metastatic IDC patients was between 21 and 75% (Cardoso *et al.*, 2009; Chen *et al.*, 2011). Rayson *et al.* analysed the outcomes of palliative chemotherapy in 7 metastatic MBC patients who received a variety of chemotherapy regimens. Only one patient treated with doxorubicin showed partial response for a period of four months (Rayson *et al.*, 1999). In another study involving 23 metastatic MBC patients treated with a variety of palliative chemotherapy regimens, only 5 patients (21.7%) were reported to show a partial response to therapy (Song *et al.*, 2013). Recently, Takala *et al.* noted only 2 patients showed a partial response to palliative chemotherapy in a cohort of 14 metastatic MBC patients (Takala *et al.*, 2019).

3.1.5 Molecular features of MBC

The inherent chemotherapy-refractory behaviour of MBC could consequently be suggestive of being caused by EMT and CSC. Multiple studies revealed that MBCs are enriched in markers of EMT as well as inducers of CSC characteristics (Lien *et al.*, 2007; Hennessy *et al.*, 2009; Creighton, Chang & Rosen, 2010; Taube *et al.*, 2010). Zhang *et al.* reported that MBC exhibits frequent loss of E-cadherin and an up-regulation of EMT inducer Zeb1. Importantly, all the mesenchymal metaplastic components in the cohort of 27 metaplastic carcinomas showed aberrant (reduced or absent) E-cadherin expression. As expected, the over-expression of ZEB1, a transcriptional repressor of E-cadherin and thus an EMT inducer, was detected in the non-glandular, metaplastic components. This group also demonstrated that MBCs express CSC markers, where they found ALDH-1^+ cells in 17 out of 27 (63%) metaplastic carcinoma cases and $CD44^+/CD24^-$ cells in 12 out of 27 (44%) metaplastic cases (Zhang, Toy & Kleer, 2012). A comparative transcriptional profiling of 28 MBCs with common breast cancers by Hennessey *et al.* reported that MBC showed a characteristic low expression of GATA3-regulated genes and of genes involved in cell-cell adhesion, with enrichment for markers linked to EMT and CSC. Indeed, MBC exhibited a marked elevation of CD44/CD24 and CD29/CD24 ratios; an up-regulation of EMT-related transcription factors, Twist1 and Snail homologue 2 (SNAI2/Slug), as well as frequent genomic aberrations activating the phosphatidylinositol-3 kinase (PI3K)/AKT pathway. These factors could consequently lead to the poor prognosis of MBC and suggest mechanisms for its chemoresistance properties (Hennessy *et al.*, 2009). Another study by Taube *et al.* demonstrated that the gene expression signature of metaplastic breast cancers correlates with the EMT core signature, which consists of common differentially expressed genes (159 down-regulated and 87 up-regulated) induced by different EMT-inducing signals, including up-regulation of Goosecoid, Twist1, Snail, and TGFβ1, and down-regulation of E-cadherin. Moreover, this group also studied gene expression pattern of EMT related transcription factors in breast cancer subtypes, particularly in basal-like, HER2-positive, luminal, claudin-low, and metaplastic, and revealed that Snail, Slug, Zeb1, Twist1, and FOXC1 transcription factors are up-regulated in MBC tumours. Notably, down-regulation of *CDH1* gene, which encodes E-cadherin, is also found in MBC tumour subtype. Interestingly, expression level of FOXC1 demonstrated to be a powerful prognostic indicator. Tumours with high levels of *FOXC1* gene expression were associated with poorer survival outcome (Taube *et al.*, 2010). Hayes *et al.* found aberrant (nuclear or cytoplasmic or both) localization of β-catenin in 33

out of 36 (91.7%) primary MBCs. This provides an evidence of Wnt signalling pathway activation and hence, induction of EMT in this category of breast cancer (Hayes *et al.*, 2008).

In one study by Lien *et al.* including 44 breast tissue samples (4 metaplastic breast carcinoma, 34 ductal carcinomas of breast and 6 normal breast samples), transcriptional profiling using oligonucleotide microarrays identified gene signature discriminating MBCs from ductal carcinomas of breast (DCBs). Notably, many genes related to maintenance of epithelial phenotype, for example *CDH1*, were down-regulated in MBC, whereas several genes involved in synthesis, remodelling and adhesion of extracellular matrix, were up-regulated in MBCs. In addition, *ESR1* and *ERBB2* were also found to be down-regulated in MBCs. Importantly, this group demonstrated that the genetic difference between MBC subclasses accounts for their differences in morphological features and identified 35 discriminator genes between MBC subclasses. All these genes were up-regulated in MBC subclass 2, which shows prominent sarcomatous growth. Functionally, many of these discriminator genes are involved in different biological processes, including cell-cell matrix adhesion (*COL18A1*, *MCAM*, *COL16A1*, *AGC1*, *THBS2*, *EDIL3*, *POSTN*, *THBS1* and *PKD2*), development (*EDIL3*, *POSTN*, *MSX1*, *SFRP4*, *SFRP2*, *THBS1*, *PRRX1*, *TBX2* and *HOXA7*), signal transduction (*TIMP3*, *SPARC* and *PDGFRA*), metabolism (*AADMTS5* and *HTRA3*), ion transport (*KCNE4* and *PKD2*) and transcription (*MSX1*, *PRRX1*, *TBX2* and *HOXA7*). In addition to MBC subclasses differentiation, these 35 discriminator genes set was also capable of successfully separating MBC from DCB (Lien *et al.*, 2007).

3.2 Aim of the chapter

Given the distinct genetic and morphological features observed in MBCs, a better understanding the characteristics of MBCs, particularly their inherent chemoresistance phenotype, is germane to identify novel therapeutic strategies for this rare category of breast cancer. To explore their pathobiology more fully it is important to acquire a spectrum of cell lines that adequately reflect the genetic and morphological heterogeneities of different subclasses of MBC. Although several cell lines are available which broadly reflect the molecular subgroups of breast cancer, cell lines from some of the rarer subtypes have yet to be documented (Neve *et al.*, 2006; Holliday & Speirs, 2011). As MBCs are almost invariably triple-negative, the only cell line for MBC to date has been reported to be HS578T (Hackett *et al.*, 1977). Thus, it is of upmost necessity to have additional cell lines to cover the molecular and phenotypic diversity of this rare but aggressive type of breast cancer. Here, I aimed to molecular and phenotypic profiling of a new breast cancer cell line derived from metaplastic breast cancer.

3.3 Materials and methods

3.3.1 A novel metaplastic breast cancer derived cell line

A novel breast cancer cell line was obtained as a generous gift from Prof. Valerie Speirs, Institute of Medical Sciences, School of Medicine Medical Sciences and Nutrition, University of Aberdeen, United Kingdom, who had derived this breast cancer cell line from primary cultures of mammary epithelial cells established from an elderly patient with grade II, triple-negative, lymph node negative metaplastic breast carcinoma with foci of squamous cell differentiation. After an initial period of senescence, some cells underwent spontaneous immortalization and adopted cobblestone morphology reminiscent of epithelial cells forming vaguely cohesive groups. A subpopulation was isolated with β4-integrin positive selection using immunomagnetic beads (Dynabeads sheep anti-Rat IgG, Invitrogen, Thermo Fisher Scientific, Waltham, MA, USA) bound to a β4-integrin antibody (ab110167, Abcam, Cambridge, UK) following established procedures and those recommended by the manufacturer (Gomm *et al.*, 1997; Holliday *et al.*, 2009). The separated cells expressed high levels of β4-integrin and basal cytokeratin 17 and was negative for the luminal epithelial marker, epithelial membrane antigen (EMA). Cells, hereby termed BAS, were routinely grown in Keratinocyte serum-free medium (KSFM) (Gibco, Thermo Fisher Scientific, Waltham, MA, USA) supplemented with bovine pituitary extract, recombinant epidermal growth factor, 10 µg/L of cholera toxin (Sigma-Aldrich, St. Louis, MO, USA), and antibiotic-antimycotic (Sigma-Aldrich, Poole, UK). Cells were maintained in a humidified incubator with 37^0C temperature and 5% CO_2 level and routinely tested negative for mycoplasma contamination using a MycoAlert Mycoplasma Detection Kit (Lonza, Rockland, ME, USA).

3.3.2 Short tandem repeat (STR) profiling

The identity of BAS cells was verified using STR profiling by the NorthGene Limited, Newcastle, United Kingdom. Briefly, genomic DNA from BAS cells were extracted using Zygem PremGem DNA extraction kit and amplified using PowerPlex Fusion STR chemistry kit (Promega Corporation, United Kingdom) with a 25-cycle PCR, following the manufacturer's instructions.

3.3.3 Analysis of DNA methylation

Isolation of genomic DNA from cell lines

A GenElute Mammalian Genomic DNA Miniprep Kit (Sigma-Aldrich) was used for the isolation of genomic DNA. Cells in 25 cm^2 culture flasks were grown to a confluency of 80-90%, trypisinized, washed twice with phosphate buffered saline (PBS), centrifuged, and the pellet resuspended thoroughly in 200 µL of Resuspension Solution. After incubation with 20 µL of RNase A solution for 2 minutes at room temperature, cells were lysed by adding 20 µL of the Proteinase K solution (20 mg/mL), followed by 200 µL of Lysis Solution C, mixing homogeneously by pipetting gently up and down, and incubating at 70^0C for 10 minutes. DNA binding to columns and elution of genomic DNA followed exact protocols recommended by the manufacturer. Isolated DNA concentration was determined using a NanoDrop ND1000 spectrophotometer (Thermo Fisher Scientific). A260/A280 ratio was used as a quality control (QC) parameter to determine the purity of isolated DNA. All the samples were stored at 2-8^0C until further manipulation. The description of the cell lines used are described in **Table 3.1**.

Table 3.1: Description of the cell lines used for DNA methylation analysis

Sample ID	Sample Name	Conc. (ng/µL)	A260/A280
1	MCF-7	230.5	1.88
2	T47D	360.8	1.88
3	CAL51	191.1	1.84
4	MDA-MB-231	117.9	2.00
5	HS578T	151.1	1.84
6	BAS	86.8	1.90

Isolation of genomic DNA from clinical FFPE samples

Genomic DNA from clinical FFPE samples was isolated using a QIAamp DNA FFPE Tissue Kit (Qiagen). Clinical samples (n = 14) from a previous study (Asaduzzaman *et al.*, 2017) were used, comprising cosmetic reduction mammoplasties (CRM) and metaplastic breast cancer. Four 10-µm thick sections were used per sample in a single 1.5 mL microcentrifuge tube. Briefly, 1 mL of xylene was mixed with each sample by vigorous vortexing for 10 seconds. After centrifugation (~14,000 x g) for 2 minutes at room temperature, the supernatant was removed carefully by pipetting without disturbing the pellet. Next, 1 mL of

100% ethanol was added to the pellet, vortexed, and centrifuged at full speed for 2 minutes at room temperature. The supernatant was removed carefully, keeping the pellet undisturbed, and the pellet was incubated at room temperature for 10 minutes with the tube open to evaporate the residual ethanol. The pellet was resuspended in 180 µL Buffer ATL, and 20 µL proteinase K was added and mixed by vortexing. The sample was incubated at 56^0C for 1 hour. Tissue dissociation was monitored visually, and samples were further incubated with additional proteinase K and longer incubation times when necessary. All samples were then incubated at 90^0C for 1 hour. After briefly centrifugation of the tube, 200 µL Buffer AL was added to the sample, and mixed thoroughly by vortexing. Then 200 µL of 100% ethanol was added, mixed again thoroughly by vortexing to yield a homogeneous solution, and centrifuged the tube briefly. The entire lysate was carefully transferred to the QIAamp MinElute column. All subsequent procedures followed exactly those recommended by the manufacturer. The concentration of the isolated DNA was determined using a NanoDrop ND1000 spectrophotometer (Thermo Fisher Scientific). A260/A280 ratio was used as a quality control (QC) parameter to determine the purity of isolated DNA. All the samples were stored at 2-8^0C until further manipulation. The description of the clinical FFPE samples used is further described in **Table 3.2**.

Table 3.2: Description of the clinical FFPE samples used for DNA methylation analysis

Sample ID	Sample Name	Conc. (ng/µL)	A260/A280	Sample type
1	CRM 1	223.9	2.03	Normal (n=3)
2	CRM 2	165.2	1.97	
3	CRM 3	48.5	2.00	
4	Metaplastic 1	171.0	1.95	Metaplastic (n=11)
5	Metaplastic 2	133.0	1.99	
6	Metaplastic 3	118.4	1.95	
7	Metaplastic 4	184.1	1.98	
8	Metaplastic 5	9.3	1.76	
9	Metaplastic 6	110.8	1.98	
10	Metaplastic 7	183.0	2.05	
11	Metaplastic 8	142.8	1.80	
12	Metaplastic 9	134.0	1.97	
13	Metaplastic 10	99.5	1.88	
14	Metaplastic 11	433.8	1.84	

Pyrosequencing

The methylation status of well-characterized 21 CpG sites in the *CDH1* gene promoter (Reinhold *et al.*, 2007) from metaplastic breast cancer biopsies and cell lines was determined by pyrosequencing following bisulphite modification of DNA essentially described (Mahmud *et al.*, 2019). Briefly, the isolated genomic DNA from FFPE tissue samples and cell lines was bisulphite treated using EZ DNA Methylation Kit (Zymo Research, Irvine, CA, USA). PCR amplification of the *CDH1* promoter and *LINE1* was performed with FastStart Taq DNA polymerase (Roche, Basel, Switzerland) using the thermal cycler program described in **Table 3.3**. The *CDH1* primers were designed using PyroMark Assay Design 2.0 software (Qiagen) to amplify 4 regions in the proximal *CDH1* promoter, and the *LINE1* primers used as described (Raguz *et al.*, 2013) (**Table 3.4 and 3.5**). After PCR and verification of amplification by agarose gel electrophoresis, the biotinylated PCR products were purified with streptavidin-coated Sepharose beads (GE Healthcare, Chalfont St Giles, UK) and Vacuum Prep Tool (Qiagen, Crawley, UK) as recommended by the manufacturer. The sequencing primer was annealed to the purified single-stranded PCR product, and the pyrosequencing was performed using PyroGold Reagent Kit (Qiagen, Crawley, UK) with Pyromark Q96 MD instrument following the manufacturer's protocol. The percentage methylation at individual CG sites was analysed using Pyro Q-CpG software (Qiagen, Crawley, UK). All runs contained a set of controls constructed by serial dilutions of a hypermethylated DNA (CpGenome Universal Methylated DNA, Millipore, Whatford, UK) in the whole genome amplified normal female genomic DNA (GE Healthcare Life Sciences, Little chalfornt, UK), which was used as an unmethylated standard. Untreated normal female genomic DNA (Promega, Madison, WI, USA) was also used as a control. The global DNA methylation levels of the sample were assessed by its surrogate *LINE1* methylation analysis (Ohka *et al.*, 2011).

This part of pyrosequencing was performed in collaboration with Nahal Masrour, Division of Cancer, Imperial College Faculty of Medicine, Hammersmith Hospital Campus, Du Cane Road, London W12 0NN, United Kingdom.

Table 3.3: Thermal cycler program for amplification of the *CDH1* promoter and *LINE1*

Step	Name	Temperature	Time	Number of cycles
1	Initial Denaturation	95^0C	6 min	1 cycle
2	Denaturation	95^0C	30 sec	45 cycles
	Annealing	53^0C (*LINE1*) or 58^0C (*CDH1*)	30 sec	
	Extension	72^0C	30 sec	
3	Final Extension	72^0C	5 min	1 cycle
4	Hold	4^0C		

Table 3.4: Assay design for methylation analysis of *CDH1* promoter and *LINE1*

Gene	Region	Amplicon size (bp)	CpG analysed	Sequence analysed
CDH1	1	114	3-7	AAACRAAACTAACRACCCRCCCACCCRACCTCRC ATAAACRCRATAACCCTCTAACCTAAAATTACTA
	2	138	11-15	TTAGYGGTAYGGGGGGYGGTGTTTTYGGGGTTT ATTTGGTTGTAGTTAYGTATTTTTTTT TAGTGG
	3	140	19-25	AGTTYGTTTTAGTTYGGTTYGATTYGATYGTATT YGGYGTTTGTTTTYGTT
	4	125	22-29	RAAAACRCCRAACRAAAACAAACRCCRAATACR ATCRAATC
LINE1		146	1-3	TTCGTGGTGCGTCGTTTTTTAAGTCGGTTT

Table 3.5: Primers used for pyrosequencing

Gene	Region	Primer	Sequence
CDH1	1	Forward	5'-Biotin-TTTAGTAATTTTAGGTTAGAGGGTTA-3'
		Reverse	5′-TCACCTACCCACCACAACCAATCAACAA-3'
		Sequencing	5′-CAACAACCCCAACCCCTCCCCA-3'
	2	Forward	5′-ATTGGTTGTGGTAGGTAGGTGAATT-3'
		Reverse	5′-Biotin-AACTTCCCCAAACTCACAAATACTTTAC-3'
		Sequencing	5′-GTAGGTGAATTT TTAGTTAA-3'
	3	Forward	5′-GGAATTGTAAAGTATTTGTGAGTTTG-3'
		Reverse	5′-Biotin-AAAAACTACCACTCCAAAAACCCATA-3'
		Sequencing	5′-GTTTGAGGAAGTTAGTTTAGATTTT-3'
	4	Forward	5′-Biotin-TGTGAGTTTGAGGAAGTTAGTTTAGAT-3'
		Reverse	5′-AAAAACTACCACTCCAAAAACCCATAAC-3'
		Sequencing	5′-CAAAAACCCATAACTAACC-3'
LINE1		Forward	5'-GGATTTTTTGAGTTAGGTGTGGG-3'
		Reverse	5'-Biotin-CAAAAATCAAAAAATTCCCTTTCC-3'
		Sequencing	5'-AGGTGTGGGATATAGT-3'

3.4 Results

3.4.1 STR profiling of BAS cells identifies a novel breast cancer cell line

As the BAS cell line was derived from primary culture of mammary epithelial cells established from a patient with MBC, I aimed to do STR profiling (typing) of this newly isolated cell line, as an identity control for a human cell line (Masters *et al.*, 2001). For this, I outsourced STR analysis and identified the STR microsatellite loci profile of BAS cells (**Table 3.6**). Next, the uniqueness of BAS cell line was ensured by comparing the STR profile with a large interactive database of STR profiles of human cell lines distributed by ATCC, DSMZ, JCRB and RIKEN, with an arbitrarily set match criteria of 95% (Dirks *et al.*, 2010). In comparison with reference STR profiles of 2455 human cell lines currently available in these databases, the STR profile of isolated metaplastic breast cancer derived BAS cells was shown to be entirely different, confirming the unique identity of our new cell line (**Table 3.7**).

Table 3.6: Short-tandem repeat (STR) analysis of BAS cells

Locus	BAS
AMEL	X, X
D13S317	8, 13
D16S539	12, 12
CSF1PO	10, 11
TH01	9.3, 9.3
vWA	14, 17
D7S820	8, 12
D5S818	11, 11
TPOX	8, 11

Table 3.7: STR profile comparison of BAS cells with data sets of 2455 cell lines from ATCC, DSMZ, JCRB and RIKEN

EV[a]	Cell No	Cell name	Locus names							
			D5S818	D13S317	D7S820	D16S539	VWA	TH01	AM	TPOX	CSF1PO
	Query (BAS)		*11,11*	*8,13*	*8,12*	*12,12*	*14,17*	*9.3,9.3*	*x,x*	*8,11*	*10,11*
0.72(26/36)	CRL-7888	Hs 801.Pl	9,12	**8**,12	**8**,**12**	9,**12**	**17**,18	**9.3**,**9.3**	**X**,**X**	**8**,**11**	**10**,**11**
0.72(26/36)	HTB-14	U-87MG	**11**,12	**8**,11	**8**,9	**12**,**12**	15,**17**	**9.3**,**9.3**	**X**,**X**	**8**,8	**10**,**11**
0.72(26/36)	JCRB0240	MCAS	**11**,13	**8**,12	**8**,11	**12**,**12**	**14**,**17**	6,8	**X**,**X**	**8**,**11**	**10**,**11**
0.67(24/36)	203	SK-N-MC	**11**,**11**	11,11	**8**,8	**12**,**12**	**17**,18	**9.3**,**9.3**	**X**,**X**	9,**11**	**10**,10
0.67(24/36)	731	CAKI-1	**11**,12	11,11	**8**,**12**	**12**,**12**	15,**17**	6,8	**X**,**X**	**8**,**11**	**10**,**11**
0.67(24/36)	749	U-CH2	10,**11**	11,11	**8**,**12**	**12**,**12**	**17**,17	**9.3**,**9.3**	**X**,**X**	**8**,8	**11**,12
0.67(24/36)	ACS-1011	ATCC-DYR0100 hiPSC	**11**,**11**	11,**13**	9,10	**12**,**12**	**14**,19	**9.3**,**9.3**	**X**,Y	**8**,**11**	7,**11**
0.67(24/36)	ACS-1019	ATCC-DYS0100 hiPSC	**11**,**11**	11,**13**	9,10	**12**,**12**	**14**,19	**9.3**,**9.3**	**X**,Y	**8**,**11**	7,**11**
0.67(24/36)	CRL-1486	HEPM	**11**,13	**8**,12	**8**,10	11,**12**	**17**,18	6,**9.3**	**X**,**X**	**8**,**11**	**10**,**11**
0.67(24/36)	CRL-1692	HISM	**11**,**11**	**8**,11	11,**12**	**12**,13	16,**17**	9,**9.3**	**X**,**X**	**8**,**11**	**11**,12
0.67(24/36)	CRL-2270	MC-IXC	**11**,**11**	11,11	**8**,8	**12**,**12**	**17**,18	**9.3**,**9.3**	**X**,**X**	9,**11**	**10**,10
0.67(24/36)	CRL-5846	NCI-H847	**11**,12	**13**,13	**8**,**12**	**12**,**12**	**17**,18	6,6	**X**,**X**	**8**,8	**10**,**11**
0.67(24/36)	CRL-7090	Hs 142.Sp	9,**11**	12,**13**	**8**,9	9,**12**	**14**,18	7,**9.3**	**X**,**X**	**8**,**11**	**10**,**11**
0.67(24/36)	CRL-7091	Hs 142.Th	9,**11**	12,**13**	**8**,9	9,**12**	**14**,18	7,**9.3**	**X**,**X**	**8**,**11**	**10**,**11**
0.67(24/36)	CRL-7171	Hs 209.Sp	**11**,**11**	12,**13**	**8**,9	8,**12**	**14**,**17**	6,8	**X**,**X**	**8**,**11**	8,**10**
0.67(24/36)	CRL-7935	R1192	**11**,12	11,12	**8**,**12**	**12**,**12**	15,**17**	6,8	**X**,**X**	**8**,**11**	**10**,**11**
0.67(24/36)	HTB-10	SK-N-MC	**11**,**11**	11,11	**8**,8	**12**,**12**	**17**,18	**9.3**,**9.3**	**X**,**X**	9,**11**	**10**,10
0.67(24/36)	HTB-46	Caki-1	**11**,12	11,12	**8**,**12**	**12**,**12**	15,**17**	6,8	**X**,**X**	**8**,**11**	**10**,**11**
0.67(24/36)	HTB-77	SK-OV-3	**11**,**11**	**8**,11	13,14	**12**,**12**	**17**,18	9,**9.3**	**X**,**X**	**8**,**11**	**11**,11
0.67(24/36)	JCRB0801	Caki-1	**11**,12	11,12	**8**,**12**	**12**,**12**	15,**17**	6,8	**X**,**X**	**8**,**11**	**10**,**11**
0.67(24/36)	JCRB1158	Yub633	**11**,**11**	**8**,9	10,**12**	9,**12**	**14**,**17**	6,6	**X**,**X**	**8**,**11**	**10**,12
0.67(24/36)	JCRB1166	NCR-G1	**11**,**11**	**8**,**13**	10,**12**	**12**,**12**	15,15	7,7	**X**,**X**	**8**,**11**	**10**,10
0.67(24/36)	RCB1985	Caki-1	**11**,12	11,12	**8**,**12**	**12**,**12**	15,**17**	6,8	**X**,**X**	**8**,**11**	**10**,**11**

[a]Evaluation value (EV) is the ratio between the number of generated peaks cell line A multiplied by 2 and the total number of peaks of cell line A + B. Only the cells with the highest EV values are shown.

3.4.2 Phenotypic characterization indicates BAS cells are highly proliferative, motile, and capable to grow in anchorage-independent fashion

Metaplastic breast carcinomas are often diagnosed as rapidly growing mass (Bian *et al.*, 2016). Moreover, tumour tissues from MBC patients are frequently found to over-express *Ki67*, a marker of cellular proliferation (Song *et al.*, 2013). To assess whether the isolated BAS cell line represents this phenotypic attribute of MBC, I determined the population doubling time, an estimate of proliferation rate of cells. BAS cells showed a very high proliferative capacity, with a population doubling time of approximately 28 hours. Interestingly, BAS cells were found to show even significantly higher proliferation rate than the existing metaplastic HS578T cell line, for which the estimated population doubling time was approximately 49 hours (**Figure 3.1**).

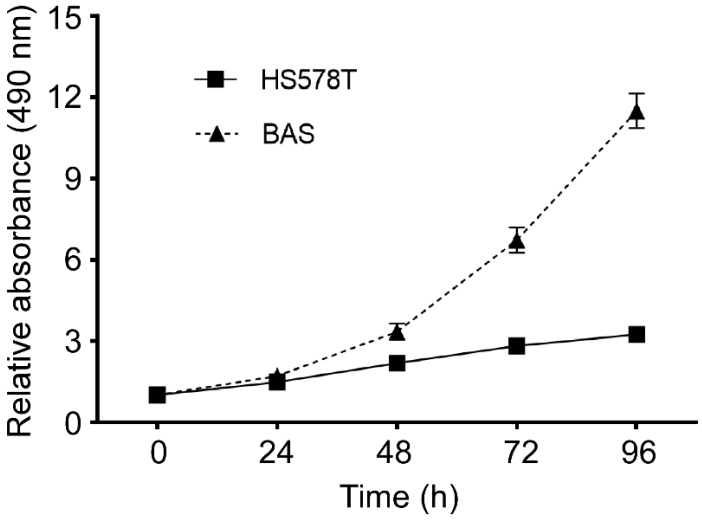


Figure 3.1: Proliferation of HS578T and BAS cells. Cellular proliferation was determined by sulphorhodamine B assay. Cells (2 x 10^3 / well) were seeded in 96-well plates with their appropriate culture medium, fixed at every 24 hours interval, and stained with SRB dye. The optical density (OD) was measured at 490 nm after solubilization of protein bound SRB stain. The relative absorbance was calculated by normalization to the absorbance at zero hour. Data points represent the average ± SD from at least six replicates. The proliferation curves are obtained with GraphPad Prism software. Trendlines of these curves obtained with Microsoft Excel were used to calculate population doubling time.

Although MBCs are usually diagnosed as local disease, the incidence of *de novo* metastatic condition is significantly higher with MBCs than that found with IDCs (Schwartz *et al.*, 2013; Tray, Taff & Adams, 2019). In addition, the risk of developing distal metastasis is almost twice compared to the conventional TNBC (Tray, Taff & Adams, 2019). Importantly, MBCs tend to be inherently chemotherapy refractory in nature and patients with MBCs are usually less responsive to the systemic chemotherapy (Al Sayed *et al.*, 2006; Weigelt *et al.*, 2014). These aggressive behaviours of MBCs, leading to poor prognosis, are suggestive of being caused by EMT and CSC, as accumulated evidence indicated the enrichment of EMT and CSC markers/inducers in tumour tissues of MBCs (Lien *et al.*, 2007; Hennessy *et al.*, 2009; Creighton, Chang & Rosen, 2010; Taube *et al.*, 2010). For this, I aimed to assess motility and anchorage-independent growth capacity, an *in vitro* surrogate of CSC phenotype, of BAS cells.

Assessment of motility by scratch assays indicated that BAS cells were motile, with approximately 21% scratch gap closure observed after 24 hours (**Figure 3.2**). However, BAS cells were not found to be as motile as HS578T cells. In fact, HS578T cells were found to be hyper motile, with complete disappearance of scratch gap only after 24 hours. Additionally, basal-like MDA-MB-231 cells, another triple-negative breast cancer cells, also showed slightly higher motility than the metaplastic breast cancer derived BAS cells. The scratch gap closure observed with MDA-MB-231 cells was approximately 34% after 24 hours.

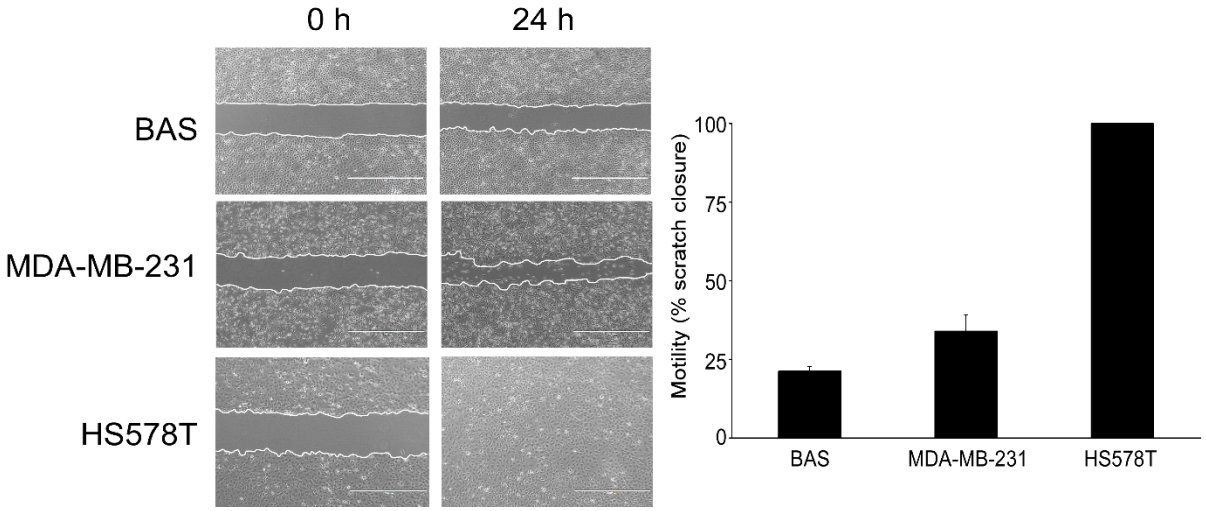


Figure 3.2: Motility of BAS, MDA-MB-231 and HS578T breast cancer cells. Scratch assay was employed to assess the cellular motility. Scratch gap closure were determined after 24 hours from the pictures using Image J software. Pictorial data are representatives of three independent experiments. Numerical data represent the average ± SD of three independent experiments.

Mammosphere assays indicated that BAS cells were capable to form spheres in liquid culture (**Figure 3.3 A**). In comparison with HS578T cells, the mammosphere forming capacity was even more than 4-fold higher with BAS cells (**Figure 3.3 A**). Indeed, the sizes of spheres were also appeared to be larger with BAS cells. Furthermore, growth in soft agar assays demonstrated that the isolated BAS cells formed large colonies (**Figure 3.3 B**). As HS578T cells did not from clones in soft agar, with only few cell groupings much smaller than the clone size cut-off of 100 µm diameter observed (**data shown in Chapter 4 Figure 4.5 E**), I used another triple-negative breast cancer cells CAL51, which has been shown to grow well in soft agar (Asaduzzaman *et al.*, 2017), to see how efficient the BAS cells are in forming clones in soft agar. Interestingly, data showed that the clone forming capacity of BAS cells in soft agar were almost 4-fold higher than that with the CAL51 cells (**Figure 3.3 B**). Thus, metaplastic breast cancer derived BAS cells are capable to grow in anchorage-independent manner.

Overall, metaplastic breast cancer derived BAS cells are highly proliferative and motile, and have anchorage-independent growth capacity.

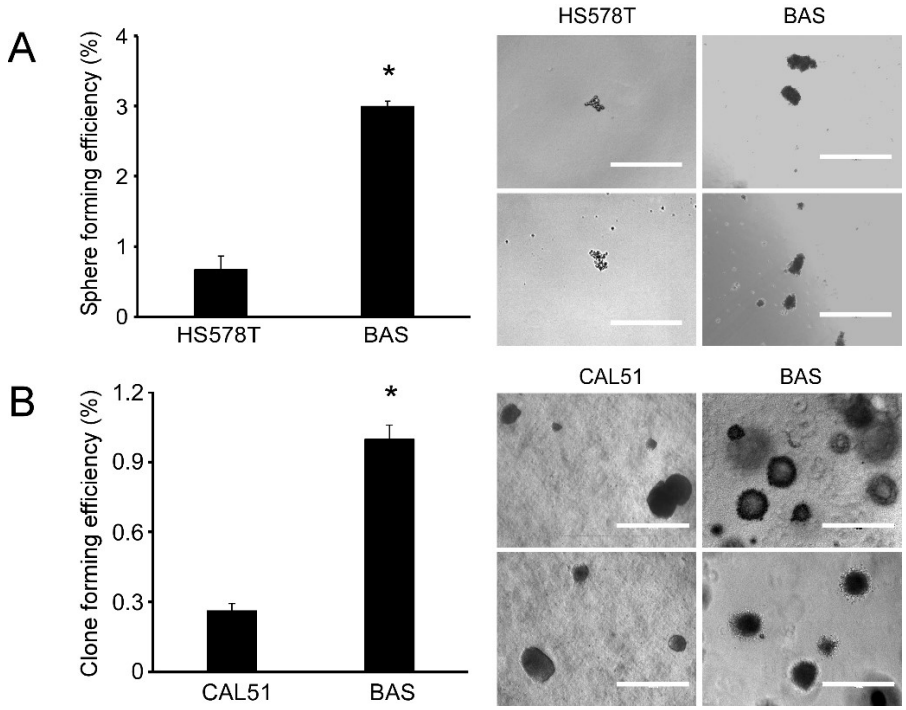


Figure 3.3: BAS cells show anchorage-independent growth capacity. Anchorage independent growth assays, used to assess CSC phenotypes of BAS cells *in vitro*, included mammosphere formation in liquid culture (A) and growth in soft agar (B). A, Mammosphere formation assay, HS578T and BAS cells: Cells (4 x 10^3 / well) were seeded in 6-well low-attachment plates with appropriate culture medium and the spheres were counted after two weeks of culture. B, Soft agar colony formation assay, CAL51 and BAS cells: Cells (2 x 10^4 / well) were seeded in 6-well plates with medium containing soft agar and the formation of colonies was determined after 4 weeks of culture. In all cases, clones or spheres larger than 100 µm in diameter were counted. Clone or sphere forming efficiency calculated relative to the total number of plated cells x100. Pictorial data are representatives of at least three independent experiments. Numerical data represent the average ± SD of three independent experiments. Bar represents 1000 µm. *, $p<0.05$.

3.4.3 BAS cell line resembles MBC subclass 1

As BAS cells represent a novel breast cancer cell line, I compared the expression of key markers in a small panel of breast cancer cell lines. However, a particular attention was given to comparison with the only existing triple-negative metaplastic cell line HS578T. Reassuringly, similar to the parental tumour tissue, BAS cells also lack the expression of oestrogen (*ESR1*), progesterone (*PGR*) and HER-2 (*ERBB2*) receptors expression, thereby represent a triple-negative molecular category, a phenomenon also observed with other basal-

like breast cancer cell lines (CAL51, MDA-MB-231 and HS578T) (**Figure 3.4 A and B**). As expected, BAS cells showed over-expression of integrin β-4 (*ITGB4*), which was used for positive selection during sub-population isolation (**Figure 3.4 A**). Interestingly, programmed death-ligand (*PD-L1*), identified as a biomarker of MBC (Joneja *et al.*, 2017), was found to be expressed in both HS578T and BAS cell lines, except for basal-like MDA-MB-231 and non-tumorigenic MCF-10A cells, which also showed high and very low levels of expression for *PD-L1*, respectively (**Figure 3.4 A**)

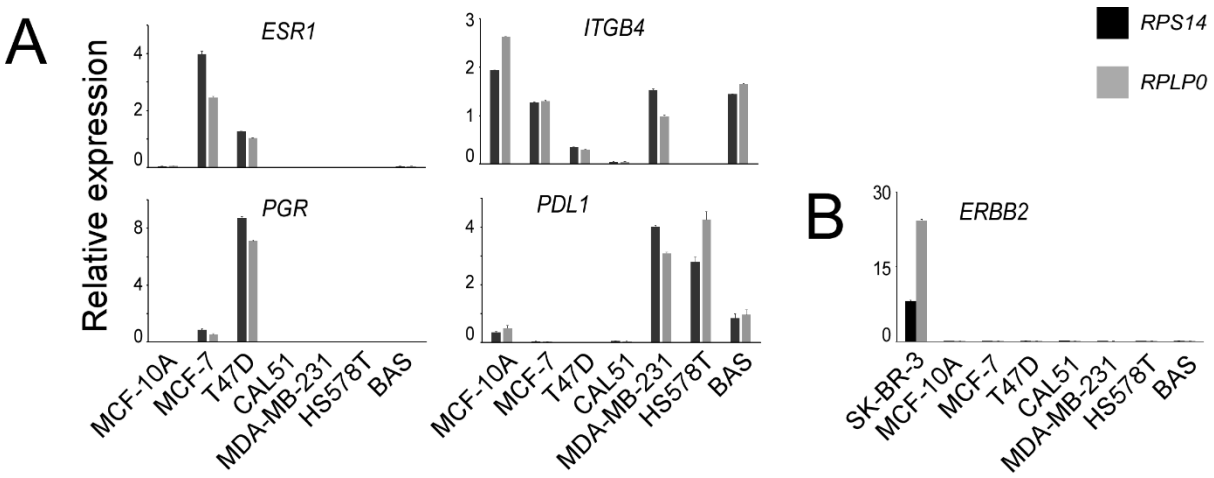


Figure 3.4: BAS cells represent a triple-negative breast cancer molecular subtype. Expression profile of BAS cells and a small panel of breast cancer cell lines, including non-tumorigenic breast epithelial cells (MCF-10A), luminal breast cancer cells (MCF-7 and T47D) and basal-like breast cancer cells (CAL51, MDA-MB-231 and HS578T), determined by quantitative real-time PCR (A). SK-BR-3 cells were included as a positive control for *ERBB2* expression (B). The relative mRNA levels were calculated by normalization to the *RPS14* and *RPLP0* genes. Data represent the average ± SD of three independent experiments.

As MBCs are enriched in EMT and CSC markers (Lien *et al.*, 2007; Hennessy *et al.*, 2009; Taube *et al.*, 2010), interrogation of some these molecular markers indicated that BAS cells expressed EMT and CSC markers to different extents (**Figure 3.5 A and B**). BAS cells, as other TNBC cell lines, did not express luminal epithelial marker E-cadherin, and were negative for the E-cadherin transcriptional activator FOXA1. Moreover, BAS cells showed high expression levels for transcriptional repressors of E-cadherin, including Slug and Twist, like HS578T cells. Although mesenchymal markers N-cadherin and vimentin were found to be expressed in metaplastic HS578T cells and all the triple-negative cell lines, respectively, BAS cells did not show expression for either of these markers. Interestingly, FOXC1, a

potent EMT-related transcription factor and a biomarker for BLBC (Han *et al.*, 2017), was found to be expressed in BAS cells like other TNBC cell lines, particularly metaplastic HS578T and basal-like MDA-MB-231 cells. However, BAS cells showed very low or lack of expression of Snail, Zeb1/2 and *TGFB2* among the EMT markers probed. Although a positive correlation was observed between Slug and vimentin expression in triple-negative CAL51, MDA-MB-231 and HS578T cell lines, the novel triple-negative BAS cells lacked the expression of vimentin, despite being Slug positive. This type of discordance in expression of a particular marker is commonly observed in cell lines, particularly when probed against enough cell lines of same subtype. For example, among the triple-negative basal-like CAL51, MDA-MB-231 and HS578T cells, the mesenchymal marker N-cadherin is expressed only in HS578T cells, although all the cell lines were positive for EMT-related transcription factors, Slug and Zeb1 (**Figure 3.5 A and B**). However, it is important to note that basal-like is the most heterogenous among all subtypes of breast cancer cell lines and thus further subdivided into basal A and B. Vimentin is identified as one of the classifier genes, with highly expressed in basal B cluster of breast cancer cell lines (Neve *et al.*, 2006). Reassuringly, all the triple-negative basal B cell lines (CAL51, MDA-MB-231 and HS578T) showed the expression of vimentin.

Furthermore, BAS cells expressed CSC markers, such as *NANOG* and *POU5F1*, at very higher levels compared to the HS578T cells, correlating with high tumorigenic phenotypes observed in anchorage-independent mammospheres formation assay (**shown in Figure 3.3 A**). Similar to other TNBC cell lines, BAS cells did not express CSC marker *SOX2*, which was found to be exclusively expressed in luminal MCF-7 and T47D breast cancer cells. Off note, *IL6*, encoding the pleiotropic cytokine IL-6, was found to be expressed in BAS cells at a very low level, compared to HS578T cells. Overall, these data indicate BAS cells express molecular markers of EMT and CSC.

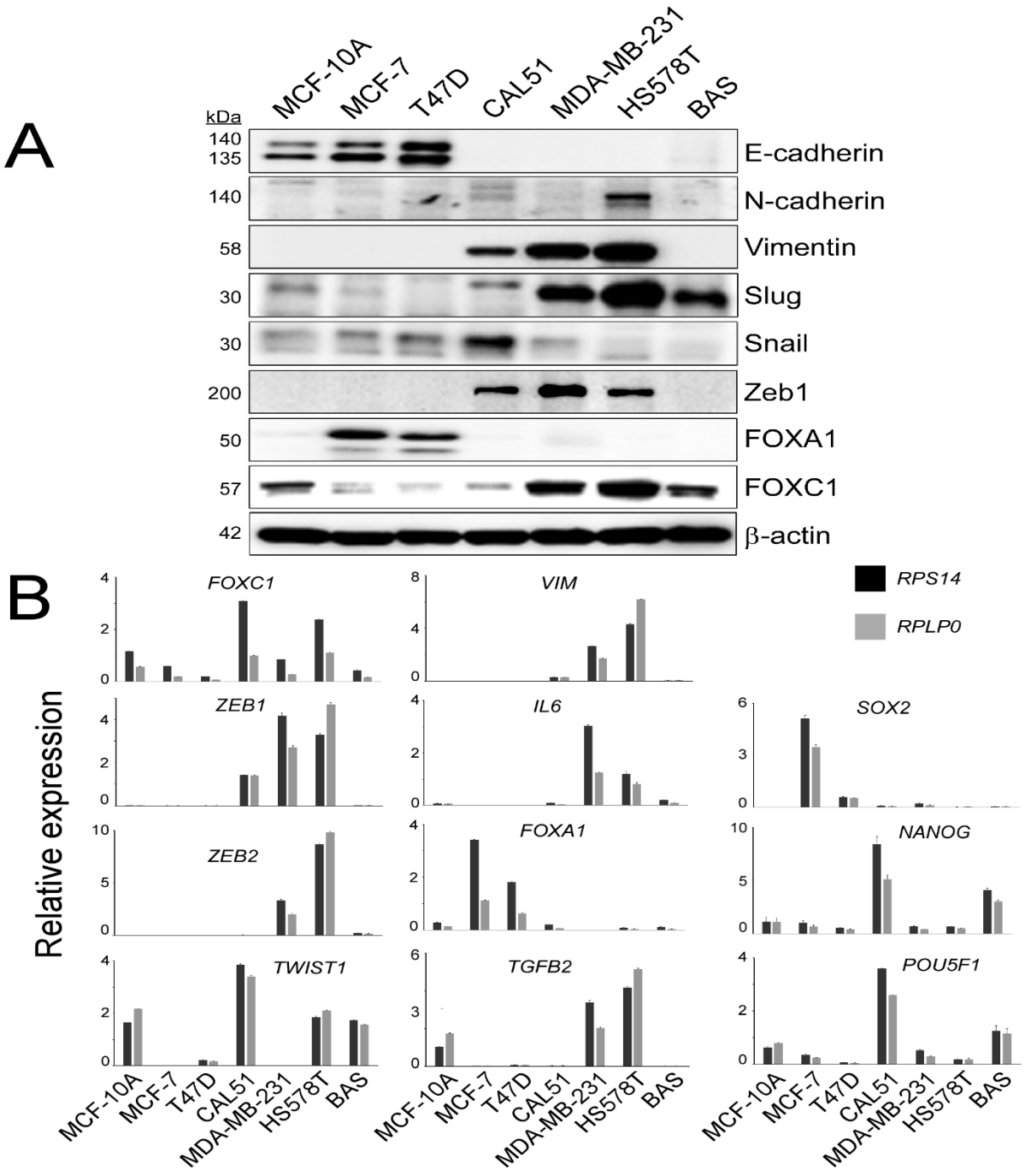


Figure 3.5: BAS cells express molecular markers of EMT and CSC. Expression profile of BAS cells and a small panel of breast cancer cell lines, including non-tumorigenic breast epithelial cells (MCF-10A), luminal breast cancer cells (MCF-7 and T47D) and basal-like breast cancer cells (CAL51, MDA-MB-231 and HS578T). A, Western blot analyses were performed with whole cell lysates and β-actin was used as a control for protein loading. Molecular masses of relevant bands are indicated in kDa. E-cadherin is detected as two bands, 140 kDa precursor and 135 kDa after convertase processing. Data show a representative blot of at least triplicate experiments. B, Quantitative real-time PCR analyses using *RPS14* and *RPLP0* as normalizers. Numerical data represent the average ± SD of three independent experiments.

Importantly, QPCR analyses of discriminator signature genes between two MBC subclasses (Lien *et al.*, 2007), indicated that HS578T cells belong to the subclass 2, whereas BAS cells expression profile resembles to the subclass 1 (**Figure 3.6**). BAS cells showed low or null expression of several markers, including *KCNE4*, *ADAMTS5*, *PDGFA*, *PDGFRA*, *THBS1*, *THBS2*, *EDIL3*, *TIMP3* and *SPARC*, compared to HS578T cells. However, among the discriminator genes probed, *MCAM*, *STAG2* and *SLC25A12* were significantly expressed in BAS cells. Notably, the discriminator gene *ADAMTS5* was exclusively expressed in metaplastic HS578T cells in the small panel of breast cancer cell lines examined.

Taken together, the novel triple-negative metaplastic breast cancer derived BAS cells demonstrated molecular diversity to existing metaplastic HS578T cell line (**Figure 3.7**), resembling MBC subclass 1.

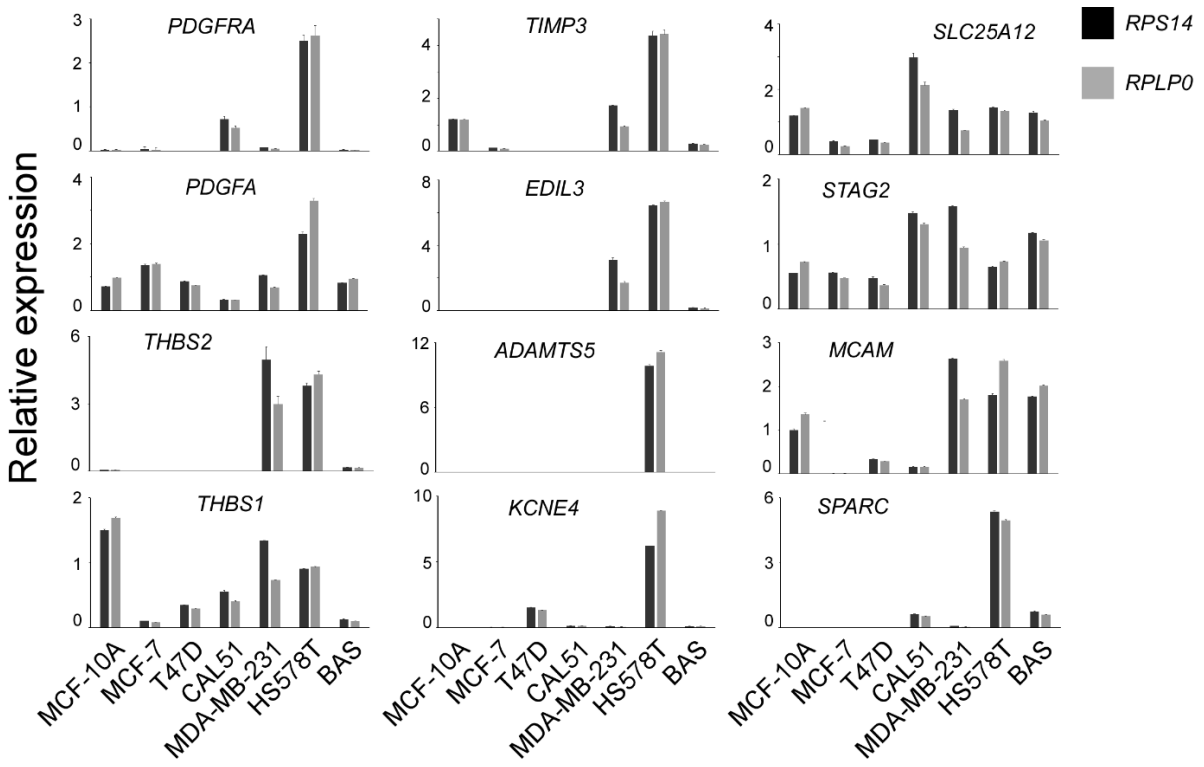


Figure 3.6: Molecular profile of BAS cells resembles MBC subclass 1. Expression of MBC subclasses discriminator genes in BAS cells and a small panel of breast cancer cell lines, including non-tumorigenic breast epithelial cells (MCF-10A), luminal breast cancer cells (MCF-7 and T47D) and basal-like breast cancer cells (CAL51, MDA-MB-231 and HS578T), determined by quantitative real-time PCR. The relative mRNA levels were calculated by normalization to the *RPS14* and *RPLP0* genes. Data represent the average ± SD of three independent experiments.

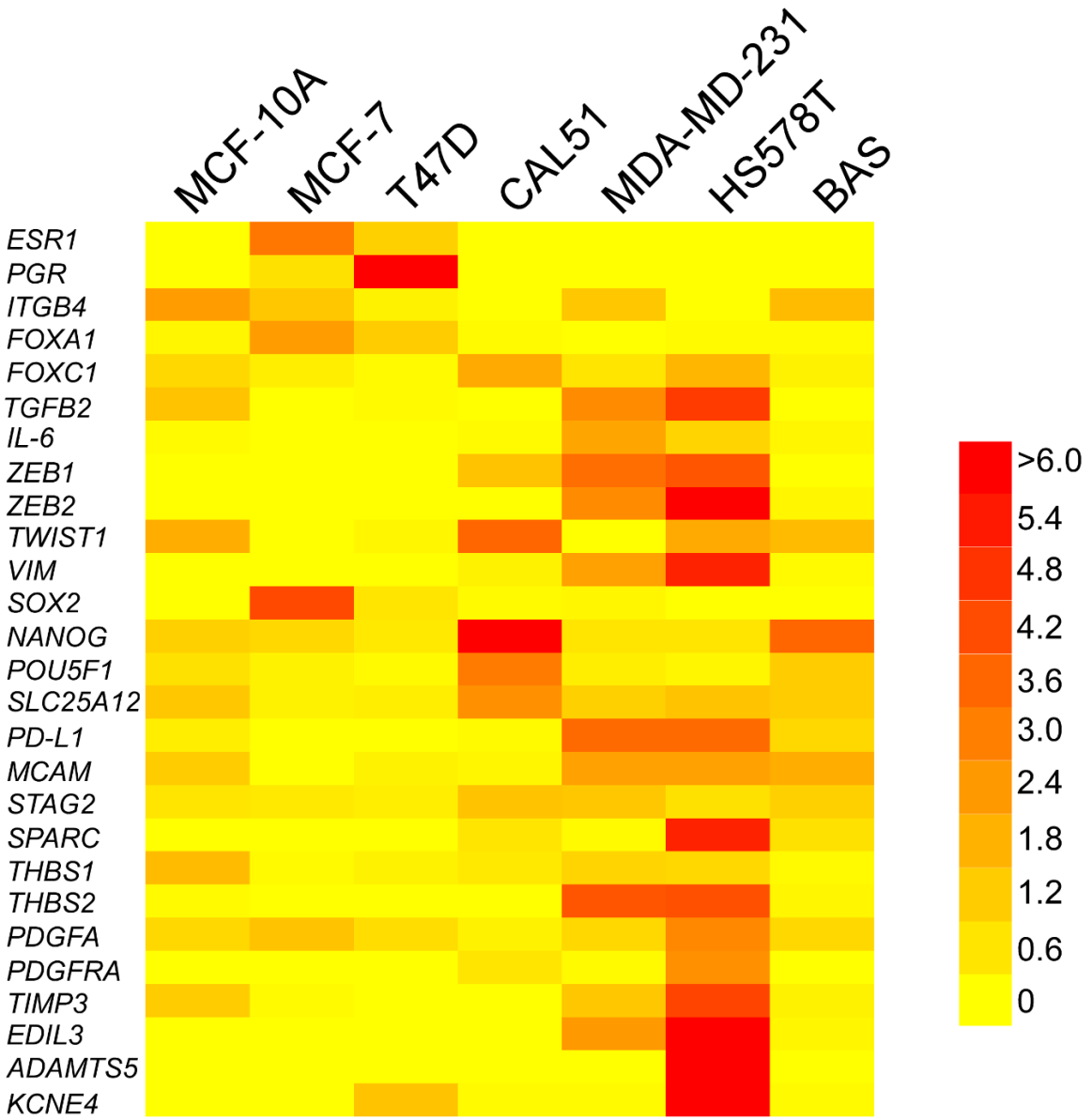


Figure 3.7: Expression profile of metaplastic breast cancer derived BAS cells. Heatmap of expression data generated by real-time quantitative PCR shown in Figure 3.4 A, Figure 3.5 B and Figure 3.6 (average expression using *RPS14* and *RPLP0* as normalizers).

3.4.4 E-cadherin gene promoter methylation status of BAS cells resembles that of MBC patients

MBCs exhibit frequent loss of E-cadherin expression (Taube *et al.*, 2010; Zhang, Toy & Kleer, 2012). Similarly, we have already seen that both metaplastic breast cancer derived HS578T and BAS cells also lacked E-cadherin expression. Lack of E-cadherin is a hallmark of EMT, and breast cancer cells can achieve this by variety of mechanisms, including up-regulation of *CDH1* transcriptional repressors, down-regulation of *CDH1* transcriptional activators, and methylation of *CDH1* promoter (Wong *et al.*, 2018). The current metaplastic breast carcinoma cell line, HS578T, has a highly methylated *CDH1* promoter (Reinhold *et al.*, 2007), but the *CDH1* promoter methylation in MBC has not been studied so far. Here, I compared the methylation profile of 21 well-characterized CpG sites of *CDH1* promoter in a small panel of breast cancer cell line, including BAS cells, reduction mammoplasties from healthy control (n = 3) and clinical samples from MBC patients (n = 11). Overall, the median percentage of methylation in healthy controls was found to be 2.18%, that increased to 4.88% in MBC patients ($p < 0.0001$), although some individual CpG sites in some patients showed values up to 37% (**Figure 3.8 A**). Considering the patients individually, the average percentage methylation of all 21 CpG sites in healthy controls ranged from 1.5 to 3.7, compared to 3.8 to 7.8 in MBC patients (**Figure 3.8 B**). However, this small increase in CpG sites methylation of *CDH1* promoter is very unlikely to be fully responsible for imposing constraint on E-cadherin expression in MBC patients, suggesting that other mechanisms, as seen MBCs enrichment of E-cadherin transcriptional repressors (Hennessy *et al.*, 2009; Taube *et al.*, 2010; Zhang, Toy & Kleer, 2012) or down-regulation of E-cadherin transcriptional activators (Lien *et al.*, 2007; Asaduzzaman *et al.*, 2017), might function together to cause complete silencing of E-cadherin expression in MBC.

TNBC cell lines, CAL51 and MDA-MB-231 showed a very similar methylation status for *CDH1* promoter, with an average percentage of methylation was found to be 8.2 and 9.3, respectively, whereas a dramatic increase in average percentage methylation to 37.2 was observed in HS578T cells **(Figure 3.8 A)**. Notably, some CpG sites in HS578T cells, especially those located in the most proximal region of the promoter showed methylation values as high as 84% (**Figure 3.8 C**), in agreement with the previous findings (Reinhold *et al.*, 2007). In contrast, novel metaplastic breast cancer derived BAS cells showed an average methylation of 1.5%, and no individual CpG site showed values higher than 2.8%, similar to both luminal MCF-7 and T47D cells with 1.8% and 1.7%, respectively (**Figure 3.8 A and**

C). This suggests that the epigenetic process of promoter methylation does not necessarily pose significant constraint on E-cadherin expression in BAS cells, as in the case speculated for patients with MBC. Thus, the methylation status of the *CDH1* promoter in BAS cells resembles more the one found in MBC patients than that from HS578T cells.

Overall, BAS cells represent an additional MBC derived cell line, particularly resembling MBC subclass 1.

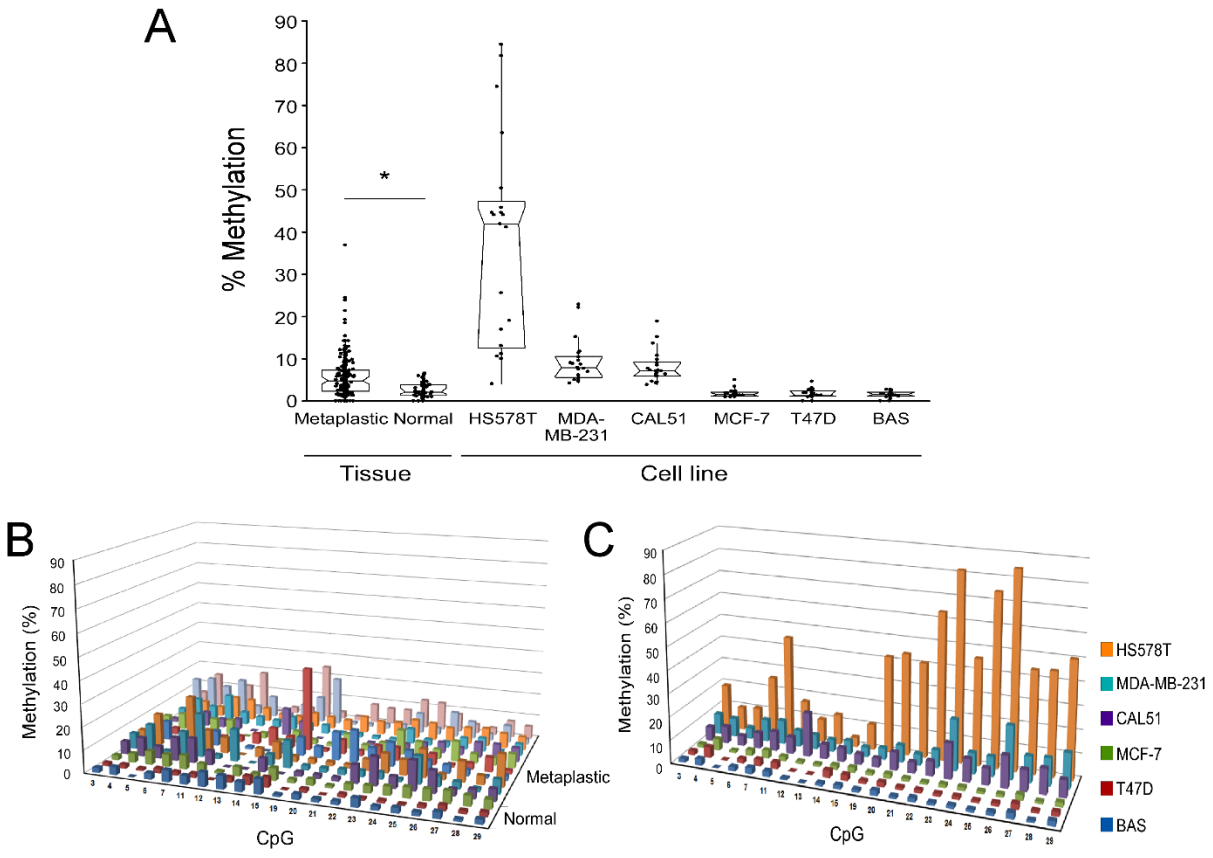


Figure 3.8: Methylation status of E-cadherin gene promoter in MBC patients and a selected panel of breast cancer cell lines. Methylation status at 21 CpGs in the proximal *CDH1* (E-cadherin) promoter was determined after bisulphite conversion and pyrosequencing in DNA isolated from cosmetic reduction mammoplasties (n = 3) and MBC (n = 11) FFPE tissue samples and a small panel of breast cancer cell lines, including luminal breast cancer cells (MCF-7 and T47D), basal-like breast cancer cells (CAL51, MDA-MB-231), and MBC derived cells (HS578T and BAS). A, Box plot representation of the methylation percentage in 21 CpGs in all patients and cell lines analysed. Box plot indicates the median within the box at 95% confidence interval. Data were analysed using the Mann-Whitney test (p<0.0001). B-C, Individual methylation percentage in 21 CpGs of MBC clinical samples (B) and cell lines (C).

3.5 Discussion

Metaplastic breast cancer is an aggressive malignancy associated with poor prognosis (Jung *et al.*, 2010; Song *et al.*, 2013). Although MBCs are almost invariably triple-negative, their genetic profile differs from conventional/non-metaplastic triple-negative breast cancers (Hennessy *et al.*, 2009; Weigelt, Kreike & Reis-Filho, 2009; McQuerry *et al.*, 2019; Djomehri *et al.*, 2020). Moreover, MBCs are themselves a heterogenous group displaying ductal carcinoma admixed with different histologic elements, such as squamous, spindle, osseous, or chondroid cell morphology (Schwartz *et al.*, 2013). Thus, there is a need to establish a series of new cell lines encompassing this diversity *in vitro* to understand the pathobiology of MBC more comprehensively, aiming to develop more specific therapeutic approaches. Here, I present a novel triple-negative metaplastic breast cancer derived cell line, BAS, which shows molecular and phenotypic diversity to the existing triple-negative MBC cells, HS578T.

This novel cell line shows high proliferation, thereby reflecting the typical MBC characteristics of being identified as a rapidly growing mass and over-expression of proliferation marker Ki67 (Song *et al.*, 2013; Bian *et al.*, 2016). Cytologically, MBC is characterized by the admixture of epithelial and mesenchymal components, which are phenotypes potentially related to EMT (Reddy *et al.*, 2020). Some studies indicate MBCs are enriched with EMT and CSC markers, including FOXC1 and TGF-β (Lien *et al.*, 2007; Taube *et al.*, 2010; Zhang, Toy & Kleer, 2012), although this is not confirmed by others (Weigelt, Kreike & Reis-Filho, 2009). Interestingly, metaplastic breast cancer derived BAS cells were found to be motile, despite less than HS578T cells, and thus shows the phenotype acquired through EMT program. Moreover, BAS cells formed mammospheres in liquid culture and clones in soft agar, hence demonstrating an anchorage-independent growth capacity, a key phenotype of cancer stem cells (Weiswald, Bellet & Dangles-Marie, 2015).

Molecular profiling indicated that BAS cells lack the expression of E-cadherin, a hallmark of EMT (Liu *et al.*, 2005; Onder *et al.*, 2008). A similar phenomenon has also been reported previously describing mesenchymal spindle-cell regions in MBC tumours were negative for E-cadherin expression, as identified by immunohistochemical analysis (Asaduzzaman *et al.*, 2017). Lack of E-cadherin expression in BAS cells is further corroborated by the expression of E-cadherin gene transcriptional repressors, Slug and Twist, as well as by absence of FOXA1, a positive regulator of E-cadherin expression. In addition, BAS cells expressed another potent EMT-related transcription factor FOXC1. As FOXC1 expression is a

biomarker for BLBC (Han *et al.*, 2017), this supports the previous report denoting majority of the MBCs belong to the BLBC molecular subtype (Weigelt, Kreike & Reis-Filho, 2009). Furthermore, BAS cells displayed a triple-negative phenotype, which is one of the classic features associated with BLBC subtype (Han *et al.*, 2017). BLBC displays aggressive clinical behaviors and is associated with poor prognosis. Gene expression profiling identified that these tumors express markers that are typically expressed in myoepithelium of normal mammary gland, such as basal cytokeratins (CK5/6, CK14, and CK17), p63, integrin-β4, and epidermal growth factor receptor (EGFR) (Perou *et al.*, 2000; Sørlie *et al.*, 2001; Sarrió *et al.*, 2008). Additionally, BLBC shows the expression signatures related to EMT. For example, these tumors exhibit up-regulation of EMT markers (smooth muscle actin, vimentin, N-cadherin, and cadherin-11), down-regulation of epithelial markers (E-cadherin), and up-regulation of proteins related to ECM remodeling and invasion (SPARC, laminin, and fascin) (Sarrió *et al.*, 2008). Although the diagnostic gold standard for BLBC is the gene expression profiling, different studies used varying diagnostic markers to define BLBC (Elian, Yan & Walter, 2018). Nielsen *et al.* used ER and HER2 negativity, together with positivity for CK5, EGFR and/or c-kit, to identify BLBC, whereas other groups used positive CK5, p63, and P-cadherin expression, in addition to ER and HER2 negativity or solely the positive expression of CK5 and CK14, irrespective of ER and HER2 status (Nielsen *et al.*, 2004; Sarrió *et al.*, 2008; Elian, Yan & Walter, 2018).

In addition to the already described triple-negative phenotype and positivity for FOXC1 expression, BAS cells share with BLBC the expression pattern of some other molecular markers, such as lack of E-cadherin expression, as well as expression of EMT markers, Slug and Twist. Moreover, BAS cells showed high levels of expression for integrin-β4, and low, but detectable, levels of SPARC. These data suggest that BAS cells share some of the molecular features of BLBC, warranting further study to identify whether BAS cells represent a particular BLBC subtype.

Analogous to the phenotypic observation of anchorage-independent growth capacity demonstrating a CSC characteristic, BAS cells showed the expression for CSC molecular markers, *NANOG* and *POU5F1*. Importantly, according to the expression pattern of genes included in discriminatory signature between two MBC morphological subclasses, 1 and 2 (Lien *et al.*, 2007), the novel BAS cells align well with the subclass 1, whereas HS578T cells is more similar to subclass 2. This further confirms that BAS cell line displayed phenotypic

diversity to the existing HS578T cells and thus could be used to address *in vitro* the heterogeneity that resides within MBC.

Methylation status of *CDH1* promoter in BAS cells, as of MBC clinical samples, indicated that this epigenetic process does not contribute significantly or at all to the E-cadherin silencing. This warrants further study to rule out any other epigenetic regulation, such as chromatin constraint imposed by HDAC, behind the absence of E-cadherin in MBC. In addition, genetic alterations, such as chromosomal deletions and somatic mutation in E-cadherin gene, have been identified to play important roles in loss or reduced expression of E-cadherin during tumour progression in several carcinoma types, including invasive lobular carcinoma of the breast (Hirohashi, 1998; Berx *et al.*, 1998). Thus, future work should consider revealing these potential causes of E-cadherin loss in MBC.

In addition to EMT related gene expression signature that I addressed here, MBC displays some classic molecular features, such as high frequency of *TP53* and *PIK3CA* mutations, and *EGFR* gene amplification, among others (Ross *et al.*, 2015; Leo *et al.*, 2016; Reddy *et al.*, 2020). Thus, this initial characterization of novel metaplastic breast cancer derived BAS cells should expand future addressing these molecular alterations. Moreover, future identification of $CD44^{+}/CD24^{-}$ as well as $ALDH^{+}$ populations is important to corroborate the phenotypic and molecular markers related to CSC studied.

In summary I have phenotypically and molecularly characterized a novel metaplastic breast cancer derived cell line. Given the pressing need for more MBC derived cell lines to aid in the characterization as well as identification of potential therapeutic targets for this notorious subtype of breast cancer, BAS cells represent a valuable addition as an *in vitro* tool for investigation.

Chapter 4: FOXC1 is a determinant of MDR phenotype in breast cancer cells

4.1 Introduction

4.1.1 MDR in cancer

Breast cancer is the most frequently diagnosed cancer in women worldwide, although earlier diagnosis and development of targeted therapies have caused significant improvements in mortality rates, especially in developed countries (Autier *et al.*, 2010; Jemal *et al.*, 2011). Traditional stratification of breast cancers into three main groups (ER/PR-positive, HER2-enriched and TNBC) provides an opportunity to determine the therapeutic treatment. The availability of targeted therapies for ER/PR-positive tumours (for example, oestrogen receptor blockers and aromatase inhibitors) and HER2-enriched tumours (for example, monoclonal antibodies such as herceptin or small molecule inhibitors such as lapatinib) give better prognosis with these categories of breast cancers compared to TNBC tumours, for which use of traditional chemotherapeutics (for example, anthracyclines and taxanes) remains only treatment option (Harbeck *et al.*, 2019). In addition to lack of targeted therapy, TNBCs pose a significant treatment problem due to chemotherapy resistance (Nedeljković & Damjanović, 2019).

Interestingly, cancer cells are capable of developing resistance not only to a particular drug or a class of similar drugs, but they can also develop cross-resistance to a variety of mechanistically divergent and structurally different compounds through a process called Multidrug Resistance (MDR). The clinical problem of MDR can be broadly divided into two main types, one acquired during treatment and other intrinsic resistance. Acquired resistance develops in response to a particular treatment such that tumours initially respond well to one type of therapy and once recurred, acquire resistance not only to that therapy, but also to a wide range of drugs with quite different structures as well as modes of action. In contrast, intrinsic resistance pre-exists at the time of diagnosis and tumour cells show resistance to a range of chemotherapeutics due to already presence of resistance mediating factors (Baguley, 2010).

Chemotherapy failure can arise from various reasons. Anticancer drugs given as systemic chemotherapy are subject to multiple steps, including absorption, metabolism, and delivery to target tissues. Any of these steps can be a cause of therapy failure. For example, tumours can

be located in parts of the body poorly penetrated by the drugs or could by protected by local environment such as increased tissue hydrostatic pressure or altered tumour vasculature. Broadly, cellular resistance to chemotherapy can be achieved by three major mechanisms: first, reduced transporters-dependent intracellular uptake of water-soluble drugs such as folate antagonists, cisplatin and nucleoside analogues; second, various cellular changes affecting the capacity of chemotherapeutics to kill the cells, including altered metabolism of drugs, increased repair of DNA damage, alterations in cell cycle and reduced apoptosis; third, increased active transport-mediated efflux of hydrophobic drugs that could otherwise accumulate in the cell by diffusion through plasma membrane (Szakács *et al.*, 2006).

MDR still represents an important clinical problem in cancer therapy. Of these mechanisms described, the one that is most encountered in MDR is the increased efflux of hydrophobic cytotoxic drugs due to upregulation of membrane-embedded drug transporters, known as ABC (ATP-binding cassette) transporters. Several members of ABC-transporter family, including ABCB1, ABCC1 and ABCG2, are found to be involved in MDR. Despite many years of research, no targeted treatments for MDR are clinically available. Although many of the MDR effectors are well characterized, the upstream regulators of these MDR effectors have been less studied. Thus, this offers new avenues for the development of targeted therapy against MDR in cancer (Robey *et al.*, 2018).

4.1.2 FOXC1 and cancer prognosis

Accumulated evidence indicates an elevated FOXC1 expression is associated with poor clinical outcomes in variety of different carcinomas, including breast cancer, hepatocellular carcinoma, NSCLC, colorectal cancer, pancreatic carcinoma, cervical cancer, gastric cancer, melanoma, etc.

Breast cancer

Analysis of different publicly available gene expression microarray datasets of human breast cancer found FOXC1 consistently over-expressed in BLBC. A significant positive correlation is observed between high FOXC1 expression and the BLBC subgroup (Ray *et al.*, 2010). An elevated FOXC1 expression is associated with worse overall survival, with each unit rise of relative FOXC1 mRNA level decreases the overall survival by 35% (Ray *et al.*, 2010). Over-

expression of FOXC1 positively correlates with brain and lung metastasis in breast cancer (Jensen *et al.*, 2015). FOXC1 orchestrates BLBC aggressive phenotypes through interaction with critical signalling pathways, including NF-κB signalling pathway, EGFR induced Ras/ERK and PI3K/AKT signalling pathways, and Hedgehog signalling pathways (Han *et al.*, 2017; Elian, Yan & Walter, 2018). FOXC1 activates the NF-κB signalling pathway in BLBC cells by increasing the NF-κB subunit p65 protein stability. FOXC1 upregulates the expression of Pin1, a peptidyl-prolyl isomerase, which binds physically to p65 in the cytoplasm and thus blocks its association with NF-κB inhibitor IκBα and ubiquitin ligase cytokine signal inhibitor SOCS-1, resulting in inhibition of p65 degradation. P65 is then phosphorylated and translocated into the nucleus where it binds to the DNA and regulates genes expression responsible for cell growth and proliferation (Wang *et al.*, 2012b). Moreover, high propensity of BLBC cells to metastasize to the brain is attributed to the FOXC1-induced activation of NF-κB signalling, leading to the establishment of a favourable microenvironment for the disseminated tumour cells to form macro-metastases in brain (Han *et al.*, 2017). Activation of EGFR by its ligand EGF leads to upregulation of FOXC1 via both Ras/ERK and PI3K/AKT downstream signalling pathways. The upregulated FOXC1 then enhances the expression of c-Myc and Cyclin-D, in which both transcription factors contribute to the proliferation, invasion and migration of BLBC cells (Jin *et al.*, 2014). FOXC1 can directly bind and activate the transcription factor glioma-associated oncogene family zinc finger 2 (GLI2) without any assistance from Smoothened (SMO), thereby leading to SMO-independent activation of Hedgehog signalling. Analysis of breast cancer patient gene expression database identified high FOXC1 expression is strongly correlated with increased Hedgehog pathway-associated genes expression in patients with lower disease-specific survival. Moreover, hyperactivation of Hedgehog signalling has been found to be involved with breast cancer stem cell like properties. Thus, FOXC1 activation of Hedgehog signalling pathways suggests its link to CSC properties of BLBC (Han *et al.*, 2015; Takebe *et al.*, 2015).

Hepatocellular carcinoma

In HCC, FOXC1 expression is associated with shorter overall survival and higher recurrence rates. Cells with FOXC1 over-expression show the characteristics of EMT with increased invasiveness and lung metastasis, whereas its knockdown leads to opposite effects.

Interestingly, FOXC1 transactivates the expression of transcription factor Snail1 (a well-known transcriptional repressor of E-cadherin) leading to down-regulation of E-cadherin and induction of EMT. In addition, FOXC1 transcriptionally regulates the expression of neural precursor cell expressed developmentally down-regulated protein 9 (NEDD9), which promotes HCC cells metastasis (Xia *et al.*, 2013). Another study reported that FOXC1 promotes EMT-mediated microvascular invasion in primary HCC, as patients with microvascular invasion showed significantly higher levels of FOXC1. Down-regulation of FOXC1 in HCC cells led to partial reversal of EMT, with a decreased cell proliferation, migration, and invasion (Xu *et al.*, 2012). Moreover, FOXC1 transactivates the expression of chemokine (C-C motif) ligand 2 (CCL2) and chemokine (C-X-C motif) receptor 1 (CXCR1) in HCC cells, leading to promotion of inflammation and the invasion and metastasis of HCC cells (Huang *et al.*, 2015).

Non-small cell lung cancer

In NSCLC, FOXC1 is highly expressed in cancer compared to non-cancerous tissues. An elevated FOXC1 expression is correlated with poor tumour differentiation and lymph node metastasis. Moreover, FOXC1 expression is identified as an independent prognostic factor in NSCLC and patients with high levels of FOXC1 expression have worst prognosis (Wei *et al.*, 2013). FOXC1 regulates proliferation and invasion of NSCLC cells. Silencing FOXC1 in NSCLC cells down-regulates cell cycle-related protein cyclin D1 and significantly decreases the cell proliferative capacity. Moreover, silencing FOXC1 increases the expression of E-cadherin, leading to reversal of EMT program and consequently inhibition of migration (Chen *et al.*, 2016). Another study reported FOXC1 induction of CSC-like properties in NSCLC; knockdown of FOXC1 in NSCLC cells decreases $CD133^+$ cell population, sphere forming efficiency and tumorigenicity *in vivo*, whereas its overexpression enhances these CSC-like properties. Interestingly, FOXC1 regulates CSC-like properties in NSCLC cells via β-catenin; knockdown of β-catenin in NSCLC cells is found to cause reduction of CSC-like properties induced by FOXC1 over-expression and overexpression of β-catenin leads to reverse the CSC-like properties attenuated by FOXC1 silencing (Cao *et al.*, 2018).

Colorectal cancer

FOXC1 contributes to development and progression of colorectal carcinoma (CRC). High FOXC1 expression is found in the CRC tissues compared to the non-cancerous mucosa and is significantly associated with poor overall survival. FOXC1 promotes CRC cell proliferation by enhancing the Warburg effect. Silencing FOXC1 expression in CRC cells significantly suppresses cell proliferation, induces apoptosis, and reduces their glucose uptake and lactate production, whereas over-expression of FOXC1 leads to enhanced cell viability, reduced apoptosis, and increased glucose consumption and lactate production (Li *et al.*, 2019b). Importantly, FOXC1 upregulation is associated with poor prognosis in CRC; FOXC1 knockdown in CRC cells inhibits cell migration and invasion, while the over-expression of FOXC1 shows the opposite phenotypes (Zhang *et al.*, 2020b). Moreover, FOXC1 is found to be involved in oxaliplatin resistance in CRC (Hsu *et al.*, 2019).

Pancreatic carcinoma

An association between FOXC1 overexpression and poor prognosis is also observed in pancreatic carcinoma. Patients with high levels of FOXC1 expression in pancreatic ductal adenocarcinoma tend to have shorter overall survival than those with low levels. Notably, FOXC1 overexpression significantly correlates with the degree of clinical stage, histological differentiation, and lymph node metastasis (Wang *et al.*, 2013). Furthermore, FOXC1 promotes pancreatic carcinoma growth and metastasis. Silencing FOXC1 expression in pancreatic cancer cells decreases proliferation, inhibits migration and invasion abilities, and reduces anchorage-independent growth of pancreatic cancer cells, whereas FOXC1 overexpression leads to opposite effects. Interestingly, silencing FOXC1 expression in pancreatic cancer cells down-regulates the expression of EMT markers, including Snail, Slug, Zeb, β-catenin, N-cadherin, and vimentin and, in contrast, its over-expression causes up-regulation of these EMT markers, suggesting a role for FOXC1 in regulating the EMT program (Subramani *et al.*, 2018)

Cervical cancer

In human cervical cancer, significantly higher levels of FOXC1 expression are found in cancer tissues and FOXC1 over-expression positively correlates with the lymph node

metastasis as well as poor overall survival. Silencing FOXC1 expression in cervical cancer cells inhibits proliferation and invasion and induces apoptosis (Wang *et al.*, 2018b). At the molecular level, FOXC1 promotes EMT via activation of PI3K/AKT signalling pathways in cervical cancer cells. Silencing FOXC1 in cervical cancer cells leads to a significant decrease in AKT and GSK3β phosphorylation as well as downregulation of cyclin D1. Importantly, FOXC1 silencing causes changes in gene expression characteristics of reversal of EMT program, such as down-regulation of N-cadherin, vimentin, and EMT-related transcription factors, including Snail, Zeb1 and Twist; and up-regulation of E-cadherin. Interestingly, inhibition of PI3K in cervical cancer cells also causes same effects with down-regulation of these EMT-related transcription factors and N-cadherin and up-regulation of E-cadherin (Huang *et al.*, 2017).

Gastric cancer

In gastric cancer, FOXC1 expression is identified as an independent prognostic factor. Patients with high FOXC1 expression are found to have shorter overall survival compared to those with low expression. Moreover, high FOXC1 expression is correlated with lymph node metastasis and distant metastasis (Xu *et al.*, 2014). Another study reported that FOXC1 transactivates the glutathione peroxidase 8 (GPX8) expression in gastric cancer cells, leading to activation of Wnt signalling pathway, which consequently results in increased cell proliferation, migration, and invasion (Chen *et al.*, 2020).

Melanoma

FOXC1 upregulates the expression of macrophage stimulating 1 receptor (MS1R) in melanoma cells and thus, activates the PI3K/AKT pathway, leading to increased cell proliferation, migration, and invasion. FOXC1 is also involved in the tumorigenesis of melanoma cells. Overexpression of FOXC1 increases colony forming efficiency of melanoma cells in soft agar, whereas its knockdown reduces the colony forming efficiency. Importantly, FOXC1 expression can be a prognostic indicator in melanoma. Patients with higher FOXC1 expression are found to be associated with significantly lower distant metastasis free survival than the those with lower FOXC1 expression (Wang *et al.*, 2016a).

4.2 Aim of the chapter

Out of all the associations of FOXC1 has with disparate cancer types, the involvement of FOXC1 in breast cancer pathogenesis, particularly BLBC, is the most elucidated (Elian, Yan & Walter, 2018). BLBC is usually associated with aggressive clinical behaviour and poor prognosis (Wang *et al.*, 2012b), which has been attributed to their intrinsic chemotherapy-refractory properties (Rakha, Reis-Filho & Ellis, 2008). Importantly, FOXC1 is exclusively and consistently over-expressed in BLBC. Taken together, FOXC1 might contribute to the drug resistance phenotype of BLBC. Moreover, FOXC1 has been reported to be a potent EMT inducer in breast cancer (Taube *et al.*, 2010). FOXC1's involvement in EMT induction is suggestive of having its significant contribution in the acquisition of drug resistance in breast cancer.

Recently, FOXC1 has been found to be involved in endocrine therapy resistance in breast cancer. FOXC1 expression is associated with loss or decrease of ER expression in recurrent tumours after initial adjuvant endocrine therapy in breast cancer patients with ER-positive primary tumours, leading to acquire endocrine therapy resistance. The study indicates that FOXC1 competes with GATA binding protein 3 (GATA3) for the same binding regions at the promoter of ER_{α} gene and hence downregulates ER_{α} expression (Yu-Rice *et al.*, 2016). Ectopic over-expression of FOXC1 in luminal breast cancer cells reduces ER_{α} expression, resulting in decreased sensitivity to oestrogen and tamoxifen (Yu-Rice *et al.*, 2016; Wang *et al.*, 2017b). However, FOXC1's implication in conventional chemotherapy resistance in breast cancer has not yet been clearly addressed. Here, I aimed to elucidate the role of FOXC1 on MDR phenotype of breast cancer. For this, I have generated doxorubicin- and paclitaxel-resistant derivatives of both BAS and HS578T cells. In addition, I have modulated FOXC1 expression in breast cancer cells, with luminal MCF-7 breast cancer cells over-expressing FOXC1 and basal-like MDA-MB-231 breast cancer cells down-regulating FOXC1, to assess its impact on drug sensitivity.

4.3 Materials and methods

4.3.1 Generation of drug resistant cell line models

Four drug resistant cell lines have been generated in this study. Parental cell lines used were HS578T and BAS, and clinically relevant chemotherapeutic drugs used were doxorubicin and paclitaxel (Sigma-Aldrich, Poole, UK). For the generation of resistant cells, a pulse strategy was used in an escalating manner as essentially described (Zhou *et al.*, 2014). In brief, drug was added to cell cultures for a short time, typically 3 days, and then cells were left to recover for up to 3 passages before a new drug treatment. Initial exploratory experiments were used to ascertain concentrations of drugs affecting the cells, but not killing the culture in its totality. Next, an escalation phase was used, in which progressively higher drug concentrations were used. Final drug concentration used for the generation of drug resistant derivatives killed 100% of the original naive cell population. The last phase involved establishment of the resistant phenotype by recurrent drug pulses until cells were not affected at all in their morphology and proliferation, thus considered drug resistant. All cells were routinely tested for the presence of mycoplasma using a MycoAlert Mycoplasma Detection Kit (Lonza, Rockland, ME, USA). Overall, the whole process took between 3 and 9 months depending on the drug and cell line. **Table 4.1** indicates some steps in the strategy and final drug concentrations. Drug resistant derivatives of HS578T cells have been described by us (Mahmud *et al.*, 2019). Drug resistant cells were routinely grown in drug free medium with drug treatments every 3-5 passage to maintain the resistant phenotype. A sulphorhodamine B (Sigma-Aldrich, St. Louis, MO, USA) assay was used to screen for drug cytotoxicity as described in **section 2.8.1.**

Table 4.1: Strategy and the concentrations used for generation of drug resistant cell lines

Parental Cell	Drug	Initial range (nM)	Intermediate steps (nM)	Resistant cells[a] (nM)	Maintenance[b] (nM)	Nomenclature of resistant cells
HS578T	Doxorubicin	10-500	25, 50, 75	100	75-100	HS-DOX
	Paclitaxel	5-500	20, 30, 40	50	40-50	HS-TX
BAS	Doxorubicin	10-1000	50, 75, 100	160	100-160	BAS-DOX
	Paclitaxel	1-200	5, 10	20	20	BAS-TX

[a] Final drug concentration in which resistant cells proliferate and which kills 100% of naive cells.

[b] Routine drug concentration used to maintain the drug resistance phenotype. Drug treatment every 3-5 passages.

4.4 Results

4.4.1 Doxorubicin- and paclitaxel-resistant derivatives of metaplastic breast cancer derived cells show a MDR phenotype

The drug resistant cell line models provide us the opportunity not only to identify the novel down-stream effectors of drug resistance, but also their upstream regulators and are therefore important for the initial studies of candidate targets with the goal to reduce the burden of cancer patient mortality (Yagüe *et al.*, 2007; Wang *et al.*, 2017a; Mahmud *et al.*, 2019; Kumar *et al.*, 2021a). In a recent report, we have shown the generation of doxorubicin- and paclitaxel-resistant derivatives from the only available triple-negative MBC derived cell line, HS578T (Mahmud *et al.*, 2019). However, with the changes of drug sources and batches there have been a little variation observed in LD_{50} values, which may be due to minor variation in drug potency. Thus, to maintain the comparative homogeneity here I determined the LD_{50} for these drug resistance derivatives again. Using the same dose-escalating strategy, I have generated the doxorubicin (BAS-DOX) and paclitaxel (BAS-TX) resistant derivatives of our novel triple-negative metaplastic breast cancer derived BAS cells. To identify if any genetic drift happened during the generation of drug resistant derivatives as it is a newly derived cell line, or purity from any unwanted contamination of other cell lines routinely cultured in the lab, I have determined the STR profiles of both drug resistant derivatives. Reassuringly, both the BAS-DOX and BAS-TX cell models maintain the identical STR profile as the parental BAS cells (**Table 4.2**).

Table 4.2: Short-tandem repeat analysis of BAS naïve and drug resistant derivatives

Locus	BAS	BAS-DOX	BAS-TX
AMEL	X, X	X, X	X, X
D13S317	8, 13	8, 13	8, 13
D16S539	12, 12	12, 12	12, 12
CSF1PO	10, 11	10, 11	10, 11
TH01	9.3, 9.3	9.3, 9.3	9.3, 9.3
vWA	14, 17	14, 17	14, 17
D7S820	8, 12	8, 12	8, 12
D5S818	11, 11	11, 11	11, 11
TPOX	8, 11	8, 11	8, 11

As the acquisition of drug resistance is often associated with other phenotypic changes, including cell proliferation rate, the population doubling times of each cell line and their drug resistant derivatives were estimated to ensure the homogeneity in drug treatment period while calculating LD_{50}. Here, the drug treatment period for HS578T cell and its drug resistant derivatives (HS-DOX and HS-TX) was a length of time equivalent to their 1.5 population doubling times, whereas that of for the BAS cell and its drug resistant derivatives (BAS-DOX and BAS-TX) was a length of time corresponding to their two population doubling times (**Table 4.3**). Interestingly, both drug resistant derivatives of HS578T cells were less proliferative than the parental cell line, suggesting that gain of less proliferative phenotype might be a way to avoid effects of cytotoxic agents as essentially described in the model quiescent cells (**Figure 4.1 A and Table 4.3**) (Lage, 2008). The similar phenomenon was observed with BAS-TX cell, which was also less proliferative than BAS cell, while the doxorubicin-resistant derivative, BAS-DOX showed almost the same proliferation rate that of the parental BAS cell (**Figure 4.1 B and Table 4.3**).

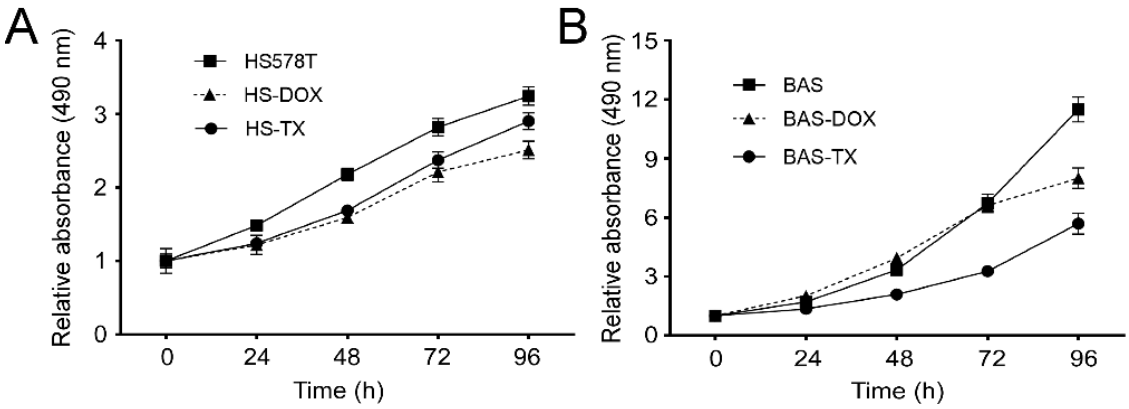


Figure 4.1: Proliferation of metaplastic breast cancer derived cells and their drug resistant derivatives. Cellular proliferation was determined by sulphorhodamine B assay (A, HS578T naïve and drug resistant derivatives, HS-DOX and HS-TX; B, BAS naïve and drug resistant derivatives, BAS-DOX and BAS-TX). Cells (2 x 10^3 / well) seeded in 96-well plates, fixed at every 24 hours interval, and stained with SRB dye. The optical density (OD) was measured at 490 nm after solubilization of protein bound SRB stain. The relative absorbance was calculated by normalization to the absorbance at zero hour. Data points represent the average ± SD from at least six replicates. The proliferation curves are obtained with GraphPad Prism software. Trendlines of these curves obtained with Microsoft Excel were used to calculate population doubling time (**Table 4.3**).

Table 4.3: Population doubling times of parental cells and their drug resistant derivatives

Cell Line	Doubling Times (h)
HS578T	49.1
HS-DOX	69.1
HS-TX	61.7
BAS	27.9
BAS-DOX	24.8
BAS-TX	42.4

Cross resistance/sensitivity was assessed by short-term SRB staining assay using four different conventional chemotherapeutic agents, including doxorubicin, paclitaxel, cisplatin, and 5-fluorouracil (5-FU) (**Figure 4.2 and 4.3**). LD_{50} values indicated that all four drug-resistant derivatives exhibit MDR phenotype with cross resistance to paclitaxel and doxorubicin by the doxorubicin (HS-DOX and BAS-DOX) and paclitaxel (HS-TX and BAS-TX) resistant derivatives, respectively (**Table 4.4**). The estimated cross resistance to paclitaxel in the resistant cells generated with doxorubicin were 9.6-fold for HS-DOX and 15.7-fold for BAS-DOX, and thus BAS-DOX cells showed the higher cross resistance to paclitaxel than the HS-DOX cells. On the other hand, the cross resistance to doxorubicin was higher in HS-TX cells (4.9-fold) than the BAS-TX cells (3.7-fold). Interestingly, the highest resistance to both doxorubicin and paclitaxel was observed in BAS-DOX cells, with the resistance ratios of more than 28-fold and 15.7-fold, respectively. In addition, BAS-DOX cells also showed cross resistance to cisplatin (1.4-fold) and 5-FU (1.5-fold) (**Table 4.4**). Although BAS-TX cells were resistant to 5-FU (2.7-fold), the cells were found to be sensitive to cisplatin (1.8-fold). However, both HS-DOX and HS-TX cells exhibited collateral sensitivity to both cisplatin (2.1-fold and 1.5-fold, respectively) and 5-FU (1.9-fold and 3.4-fold, respectively) (**Table 4.4**), a commonly observed phenomenon in both cellular models and in the clinical settings (Pluchino *et al.*, 2012; Raguz *et al.*, 2013).

Overall, these data clearly indicate that all four drug-resistant derivatives of metaplastic breast cancer derived cells demonstrate a MDR phenotype against both doxorubicin and paclitaxel.

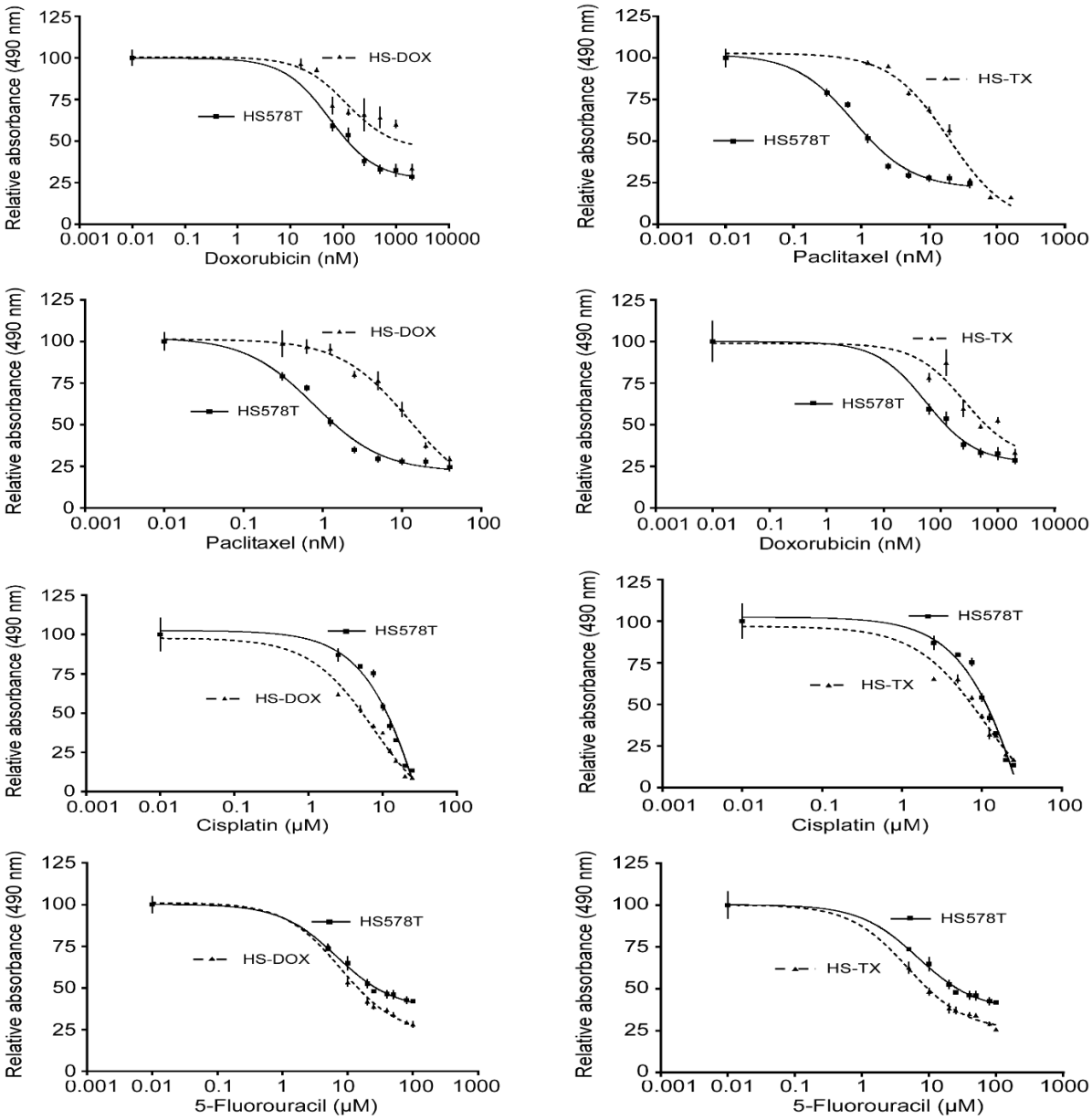


Figure 4.2: Doxorubicin- and paclitaxel-resistant HS578T cells show a MDR phenotype. Drug sensitivity curves were determined by sulphorhodamine B assays. Parental HS578T cells and their drug resistant derivatives, doxorubicin resistant HS-DOX cells (*left panels*) and paclitaxel resistant HS-TX cells (*right panels*), were treated with a range of concentration of four different chemotherapeutics, including doxorubicin, paclitaxel, cisplatin, and 5-fluorouracil. The optical density (OD) was measured at 490 nm after solubilization of protein bound SRB stain. The relative absorbance was calculated by normalization to the untreated control x100. Data points represent the average ± SD from six replicates. The best-fit curves are obtained with GraphPad Prism software. Curves from three independent experiments were used to calculate the LD_{50} values (**Table 4.4**).

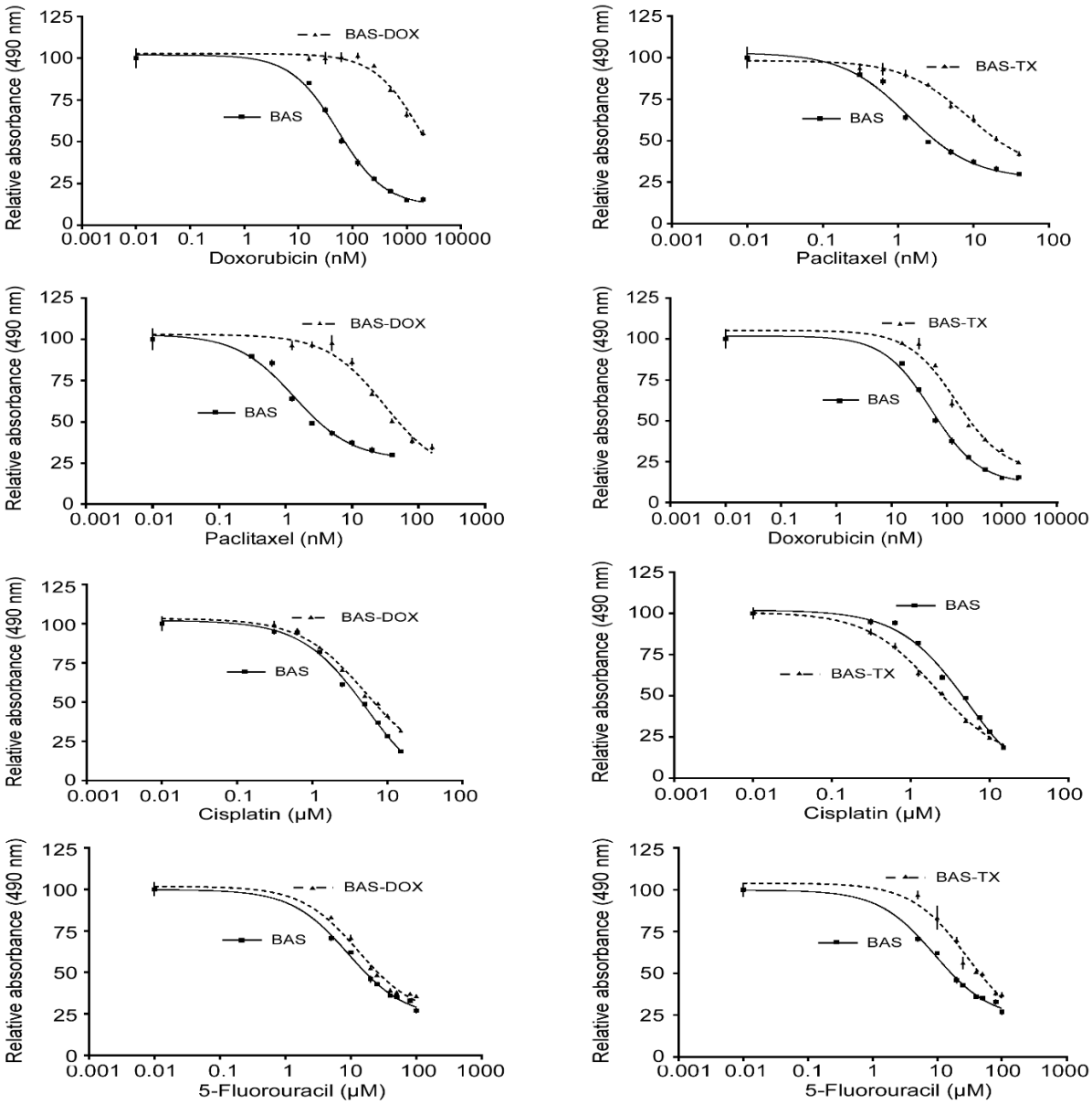


Figure 4.3: Doxorubicin- and paclitaxel-resistant BAS cells show a MDR phenotype. Drug sensitivity curves were determined by sulphorhodamine B assays. Parental BAS cells and their drug resistant derivatives, doxorubicin resistant BAS-DOX cells (*left panels*) and paclitaxel resistant BAS-TX cells (*right panels*) were treated with a range of concentration of four different chemotherapeutics, including doxorubicin, paclitaxel, cisplatin, and 5-fluorouracil. The optical density (OD) was measured at 490 nm after solubilization of protein bound SRB stain. The relative absorbance was calculated by normalization to the untreated control x100. Data points represent the average ± SD from six replicates. The best-fit curves are obtained with GraphPad Prism software. Curves from three independent experiments were used to calculate the LD_{50} values (**Table 4.4**).

Table 4.4: Sensitivity of metaplastic breast cancer derived cell lines to different drugs

Drug	Target/ mode of action	LD_{50}[a] [Resistance ratio][b]					
		HS578T	**HS-DOX**	**HS-TX**	**BAS**	**BAS-DOX**	**BAS-TX**
Doxorubicin	Topoisomerase 2α	119 nM	1188 nM [10]	585 nM [4.9]	70.8 nM	>2000 nM [>28]	263 nM [3.7]
Paclitaxel	Tubulin (microtubule depolymerisation)	1.4 nM	13.5 nM [9.6]	20.7 nM [14.8]	3.2 nM	50.1 nM [15.7]	21.1 nM [6.6]
Cisplatin	DNA crosslinking	11.1 μM	5.2 μM [-2.1]	7.4 μM [-1.5]	4.6 μM	6.5 μM [1.4]	2.6 μM [-1.8]
5-Fluorouracil	Thymidylate synthetase (DNA synthesis)	26.9 μM	14.1 μM [-1.9]	7.9 μM [-3.4]	16.6 μM	25.7 μM [1.5]	44.7 μM [2.7]

[a]All LD_{50} values from drug resistant cells were significant ($P<0.05$) when compared to their corresponding parental cells
[b]Negative resistance ratios indicate that the resistant cell is more sensitive to a particular drug than the parental cell

4.4.2 Upregulation of EMT and CSC markers in metaplastic breast cancer derived MDR cells

As acquisition of drug resistance is often associated with EMT and further development of CSC phenotypes (Shibue & Weinberg, 2017), and FOXC1 is identified as a potent EMT-related transcription factor (Ray *et al.*, 2010; Taube *et al.*, 2010), I interrogated how FOXC1 and other key players in EMT and stemness were modulated in these drug resistant cell models generated. Notably, FOXC1 levels were highly up-regulated in both BAS-DOX and BAS-TX cells compared to the parental BAS cells, with more than 4-fold up-regulation in both MDR BAS cells (**Figure 4.4 A and B)**. However, the levels of FOXC1 expression in both drug resistant derivatives of HS578T were almost the same of that found in parental cells, attributing the fact that HS578T cells express high endogenous levels of FOXC1, which did not increase further in HS-DOX or HS-TX cells (**Figure 4.4 A and B**). RT-QPCR analyses revealed that the expression of many of the EMT and CSC markers were modulated to different extents in drug resistant cells (**Figure 4.4 C**). For instance, both the drug resistant derivatives of BAS cells showed the up-regulation of CSC marker *NANOG*, whereas *POU5F1* and *SOX2*, which are also the CSC markers, were up-regulated in BAS-DOX or BAS-TX, respectively. However, neither drug resistant HS-DOX nor HS-TX cells showed

significant changes in any of the CSC markers studied (**Figure 4.4 C**). Both the drug resistant HS-DOX and HS-TX cells showed up-regulation of EMT-related transcription factor *ZEB2*, whereas only BAS-TX cells exhibited an up-regulation for this transcription factor. Moreover, paclitaxel resistant HS-TX and BAS-TX cells also showed an up-regulation of *ZEB1* and *TWIST1*. Transcription factors *SNAI1* was up-regulated only in HS-TX cells out of all four drug-resistant derivatives. Similarly, only BAS-TX cells showed an up-regulation of mesenchymal marker *VIM* (**Figure 4.4 C**). Importantly, among the EMT and CSC markers studied, there was no up-regulated marker common to all four drug-resistant cells. Overall, metaplastic breast cancer derived MDR cells exhibited up-regulation of different EMT and CSC markers in varying extents, particularly MDR BAS cells showed an up-regulation of transcription factor FOXC1.

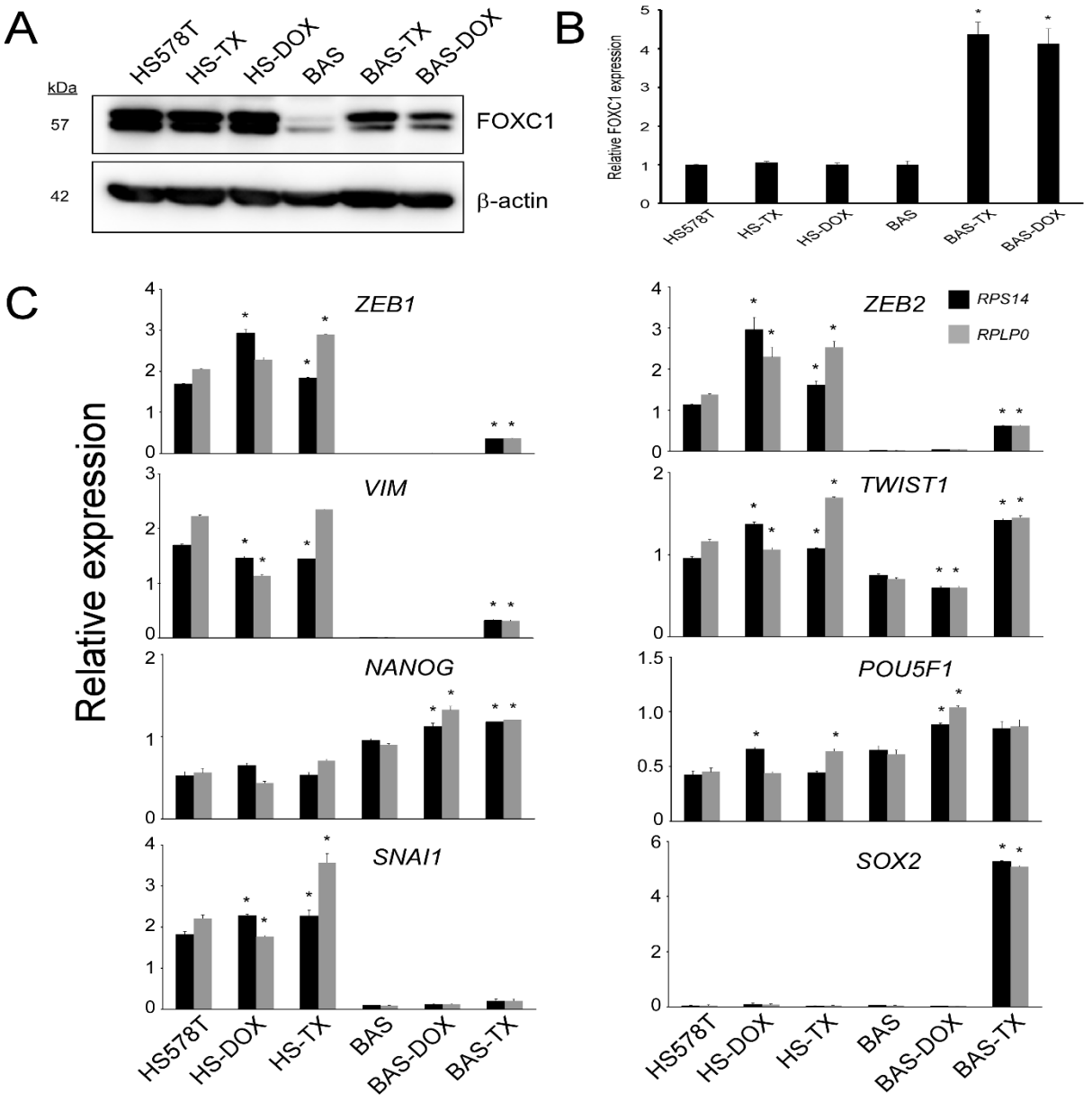


Figure 4.4: Metaplastic breast cancer derived MDR cells show upregulation of different EMT and CSC markers, with significant higher expression of transcription factor FOXC1 in MDR BAS cells. A, Western blot analysis of FOXC1 expression in MBC derived drug resistant cell models. The analysis was performed using whole cell lysates and β-actin was used as a control for protein loading. Molecular masses of relevant bands are indicated in kDa. FOXC1 protein was detected as two bands with molecular masses very close to 57 kDa (top band: phosphorylated FOXC1; bottom band: non-phosphorylated FOXC1). Data show a representative blot of at least triplicate experiments. B, Image quantification of FOXC1 immunoblots obtained with MBC derived drug resistant cell models. FOXC1 signal was normalized to the β-actin signal. The relative FOXC1 expression in drug resistant cells were calculated with respect to their corresponding parental cells. Data represent the average ± SD of three experiments. C, Quantitative real-time PCR analyses of different gene targets. The relative mRNA levels were calculated by normalization to the *RPS14* and *RPLP0* genes. Numerical data represent the average ± SD of three independent experiments. *, $p<0.05$.

4.4.3 Assessment of EMT and CSC phenotypes of metaplastic breast cancer derived MDR cells

As drug resistance is often associated with acquisition of a stem-like phenotype (Asaduzzaman *et al.*, 2017), I aimed to investigate if any changes in the anchorage independent growth capacity, an *in vitro* surrogate of CSC phenotype, in the metaplastic derived drug resistant cell models compared to their corresponding naïve cells. Growth in ultra-low attachment plates indicated an increase in mammosphere formation in both drug resistant HS-DOX and HS-TX cells, but almost equal and a small increase (statistically insignificant) were observed in BAS-DOX or BAS-TX cells, respectively (**Figure 4.5 A and B**). In contrast, growth in soft agar indicated that neither BAS-DOX nor BAS-TX cells did show an increase the anchorage-independent clone formation with respect to parental BAS cells (**Figure 4.5 C**). Indeed, BAS-TX cells showed even lower clone forming capacity in soft agar than BAS cells. A similar phenomenon has been reported and observed here again with another triple-negative breast cancer cell line CAL51 and its doxorubicin-resistant CALDOX derivative (**Figure 4.5 D**) (Raguz *et al.*, 2013). Thus, although drug resistant cells normally have a higher tumorigenic capacity, this is not always the case. It is important to mention that HS578T and its drug resistant derivatives (HS-DOX and HS-TX) did not form clones up to two months in soft agar. These three cell models formed few outgrowths always much smaller than the clone size threshold of 100 μm in diameter (**Figure 4.5 E**).

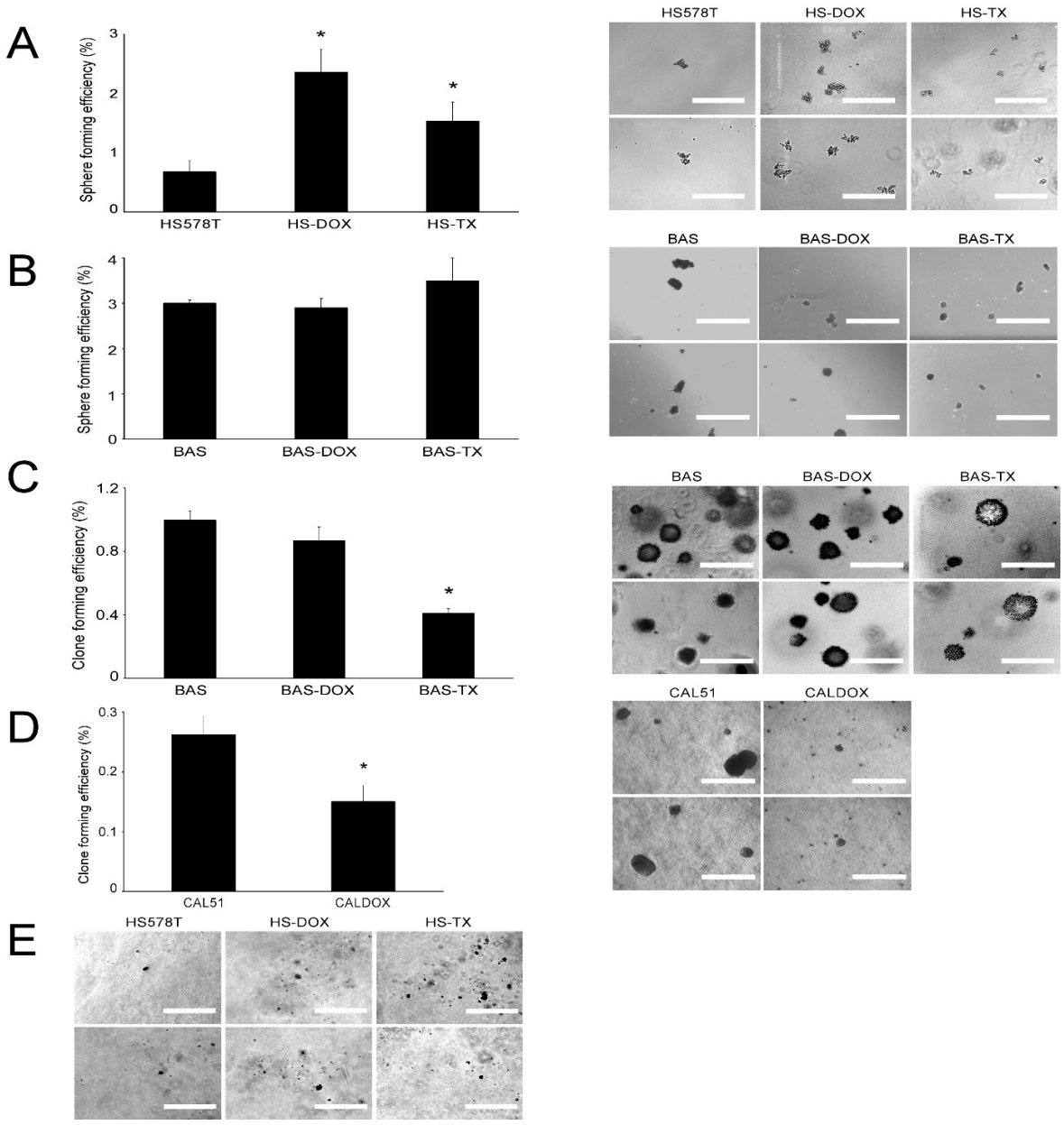


Figure 4.5: Anchorage independence of metaplastic derived and basal-like MDR breast cancer cells. Anchorage independent growth assays, used as *in vitro* surrogates for tumor formation in MDR cells, included mammosphere formation in liquid culture using low-attachment plates (A, B) and colony formation in medium containing soft agar (C-E). Mammosphere assay (A, B): cells (4 x 10^3 / well) were seeded in 6-well low-attachment plates with appropriate culture medium and the spheres were counted after two weeks of culture (A, MDR HS578T cells; B, MDR BAS cells). Soft agar assay (C-E): cells (2 x 10^4 / well) were seeded in 6-well plates with medium containing soft agar and the formation of colonies were determined after 4 weeks (C, MDR BAS cells; D, MDR CALDOX cells) and 8 weeks (E, MDR HS578T cells) of culture. In all cases, clones or spheres larger than 100 µm in diameter were counted. Clone or sphere forming efficiency calculated relative to the total number of plated cells x100. Pictorial data are representatives of at least three independent experiments. Numerical data represent the average ± SD of three independent experiments. Bar represents 1000 µm. *, $p<0.05$.

Furthermore, drug resistance is usually accompanied by phenotypic shift characteristics of EMT, such as an increase in motility, thus making tumour cells more aggressive (Hu *et al.*, 2014b). To assess this hypothesis, a scratch assay was used to determine the cell migratory ability. Drug resistant HS-DOX and HS-TX did not show any further increase in already very high motility observed in parental HS578T cells. All three cell models were found to cause almost complete scratch closure just after 9 hours (**Figure 4.6 A**). Interestingly, both drug resistant BAS-DOX and BAS-TX cells showed significant increase in their motility compared to the parental BAS cells (**Figure 4.6 B**). In fact, almost complete scratch closures were observed with both drug resistant derivatives of BAS cells after 72 hours, whereas there was still significant scratch gap with naïve BAS cells. Overall, an acquisition of MDR phenotype in metaplastic derived BAS cells was associated with an increase in motility.

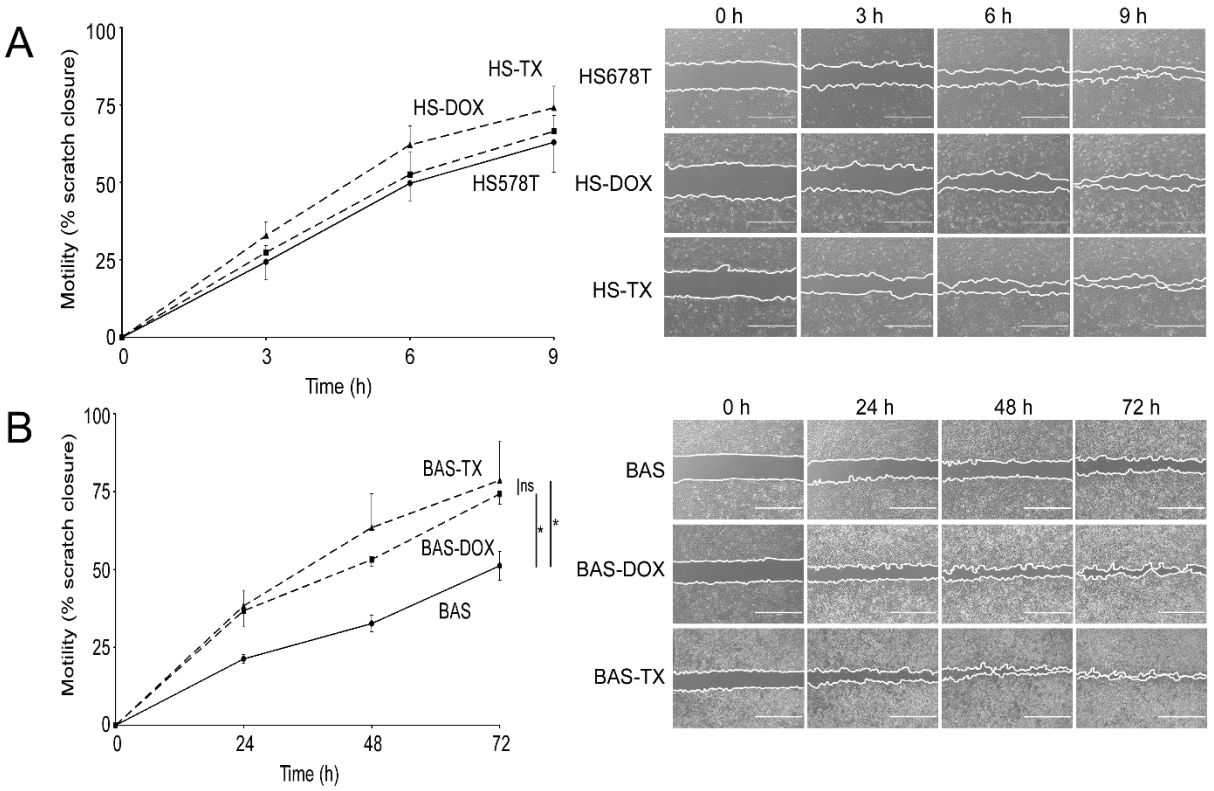


Figure 4.6: Motility of metaplastic breast cancer derived MDR cells. Scratch assays were employed to assess the cellular motility. Scratch gap closure at different time points were determined from the pictures using Image J software. A, Motility of MDR HS578T cells. B, Motility of MDR BAS cells. Pictorial data are representatives of three independent experiments. Numerical data represent the average ± SD of three independent experiments. *, $p<0.05$.

4.4.4 FOXC1 regulates the MDR phenotype in metaplastic derived BAS cells

FOXC1 is a potent EMT inducer in breast cancer and has been found to be correlated with poor clinical outcome in BLBC (Ray *et al.*, 2010; Taube *et al.*, 2010). Moreover, FOXC1 modulates docetaxel and cisplatin sensitivity in NSCLC (Cao *et al.*, 2018) and is an indicator of poor treatment response to anthracycline-based systemic adjuvant chemotherapy in sporadic TNBC (Xu *et al.*, 2017). As FOXC1 was found to be up-regulated in both BAS-DOX and BAS-TX MDR cells, I hypothesized that FOXC1 might be responsible for gain of MDR phenotype. To test this hypothesis, I interrogated whether the experimental down-regulation of FOXC1 expression in these cellular models could lead to re-sensitization to both doxorubicin and paclitaxel. Here, I transiently silenced *FOXC1* mRNA expression by RNA interference, causing approximately 50% and 30% down-regulation of its expression in BAS-DOX and BAS-TX cells, respectively (**Figure 4.7 A**). The drug sensitivity curves from both cell models as obtained from short-term SRB staining assays indicated that the silencing FOXC1 expression caused an increase in sensitivity to both doxorubicin and paclitaxel (**Figure 4.7 B**). LD_{50} values calculated for these cell lines showed that down-regulation of FOXC1 expression in BAS-DOX MDR cells led to increase in sensitivity to doxorubicin approximately 5-fold and to paclitaxel approximately 2-fold, and in BAS-TX MDR cells the increase in sensitivity were 3.9-fold for doxorubicin and 2.6-fold for paclitaxel (**Table 4.5**). Taken together, FOXC1 modulates MDR phenotype in metaplastic derived BAS cells.

Table 4.5: Sensitivity of cells to doxorubicin and paclitaxel after experimental modulation of FOXC1 levels in metaplastic breast cancer derived MDR cells

			LD_{50}[a] (nM) [resistance ratio][b]			
Cell	**Experimental**	**Cell Nomenclature**	**Doxorubicin**		**Paclitaxel**	
BAS-DOX	Transient down-regulation	siGFP	1949.8		64.6	
		siFOXC1	371.5	[-5.2]	33.5	[-1.9]
BAS-TX	Transient down-regulation	siGFP	>250.0		20.2	
		siFOXC1	64.5	[> -3.9]	7.7	[-2.6]

[a]All LD_{50} values from FOXC1-modulated cells were significant ($p<0.05$) when compared to their corresponding control cells

[b]Negative resistance ratios indicate that the cell is more sensitive to a particular drug than the control cell

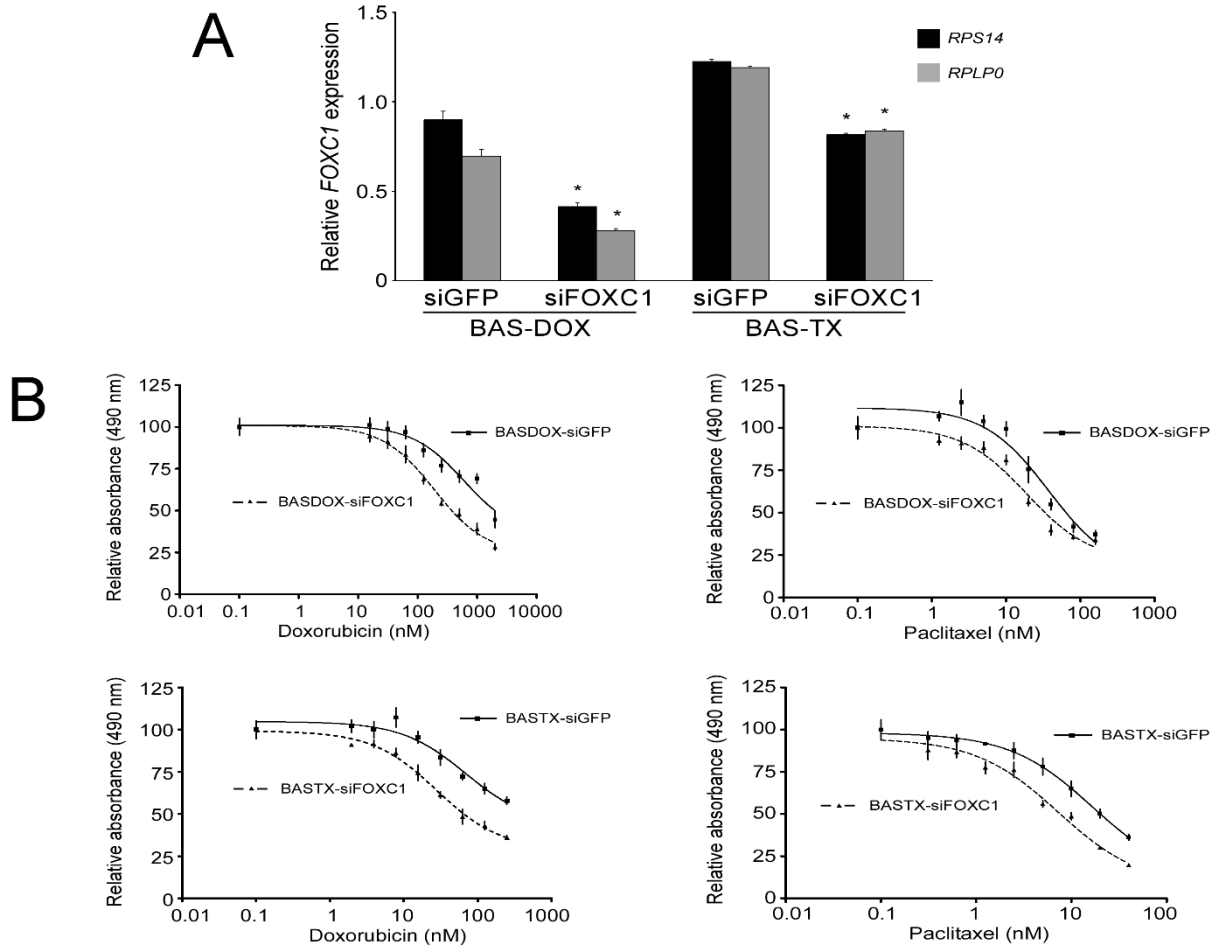


Figure 4.7: Experimental downregulation of FOXC1 leads to re-sensitization of MDR BAS cells to doxorubicin and paclitaxel. A, Down-regulation of FOXC1 expression in BAS-DOX and BAS-TX MDR cells after transient transfection with siRNAs targeting either *FOXC1* or *GFP* (used as a negative control) mRNAs. FOXC1 expression was measured with quantitative real-time PCR and the relative *FOXC1* mRNA levels were calculated by normalization to the *RPS14* and *RPLP0* genes. Data represent the average ± SD of three independent experiments. *, $p<0.05$. B, Drug sensitivity curves determined by sulphorhodamine B assays. BAS-DOX (*top panels*) and BAS-TX (*bottom panels*) MDR cells were treated with a range of concentration of doxorubicin (*left panels*) and paclitaxel (*right panels*) for a length of time corresponding to their two population doubling times. The optical density (OD) was measured at 490 nm after solubilization of protein bound SRB stain. The relative absorbance was calculated by normalization to the untreated control x100. Data points represent the average ± SD from six replicates. The best-fit curves are obtained with GraphPad Prism software. Curves from three independent experiments were used to calculate the LD_{50} values (**Table 4.5**).

4.4.5 Modulation of FOXC1 expression alters doxorubicin and paclitaxel sensitivity in luminal and basal-like breast cancer cells

To ascertain the regulation MDR by FOXC1 was not exclusive to BAS cells, I planned to modulate the FOXC1 expression in other breast cancer cell models to assess potential changes in sensitivity to doxorubicin and paclitaxel. For this, I first assessed FOXC1 expression levels in a small panel of breast cancer cell lines (**Figure 4.8**). As expected, the basal-like MDA-MB-231 and metaplastic HS578T breast cancer cells showed very high levels of FOXC1 expression, whereas very low levels of expression were observed in luminal MCF-7 and T47D breast cancer cells. The triple-negative CAL51 breast cancer cells also showed very low FOXC1 expression and transformed but non-tumorigenic breast epithelial cells, MCF-10A expressed FOXC1 protein at intermediate levels. Therefore, the luminal MCF-7 cells harbouring very low endogenous FOXC1 levels and basal-like MDA-MB-231 cells, which have high levels of FOXC1 expression, were selected for experimental over-expression and down-regulation of FOXC1 expression, respectively.

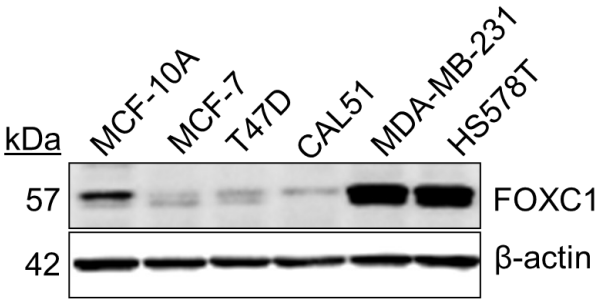


Figure 4.8: Expression of FOXC1 in a selected panel of breast cancer cell lines. Western blot analysis of FOXC1 expression in a small panel of breast cancer cell lines, including non-tumorigenic breast epithelial cells (MCF-10A), luminal breast cancer cells (MCF-7 and T47D) and basal-like breast cancer cells (CAL51, MDA-MB-231 and HS578T). The analysis was performed with whole cell lysates and β-actin was used as a control for protein loading. Molecular masses of relevant bands are indicated in kDa. FOXC1 protein was detected as two bands with molecular masses very close to 57 kDa (top band: phosphorylated FOXC1; bottom band: non-phosphorylated FOXC1). Data show a representative blot of at least triplicate experiments.

MCF-7 cells over-expressing FOXC1 were generated after stable transfection with a FOXC1-expression cassette. After initial screening with cell pools (**Figure 4.9 A**), which showed unsatisfactory levels of FOXC1 over-expression, I opted to isolate individual clones from both empty vector and FOXC1-expression cassette containing cell pools, in an intention to get cell clones with maximum contrast in FOXC1 expression. A total of 11 clones from empty vector cell pool and of 32 clones from FOXC1-expression cell pool were isolated at the beginning, but some of them were lost during scaling-up. All these clones were analysed for expression levels of FOXC1 protein together with their corresponding cell pool (**Figure 4.9 B**). Two empty vector clones (MCF-7-ev-c7 and -c10) showed the lowest endogenous FOXC1 levels, whereas comparatively higher FOXC1 expression were found in five FOXC1-expression clones (MCF-7-FOXC1-c6, -c19, -c22, -c31 and -c32). These clones were further screened together to assess the contrast in FOXC1 expression (**Figure 4.9 C**), and finally one empty vector (MCF-7-ev-c7) and three FOXC1 over-expressing (MCF-7-FOXC1-c6, -c22 and -c31) clones were selected as workhorses for further experiments. On the other hand, after initial attempts to obtain stably transfected MDA-MB-231 cells expressing FOXC1 hairpins to experimentally down-regulate its expression I opted for a transient down-regulation approach, as in MDR BAS cells, using siRNAs. RT-QPCR data indicated a very robust *FOXC1* mRNA down-regulation in MDA-MB-231 cells (more than 75%), compared to siGFP control (**Figure 4.9 D)**.

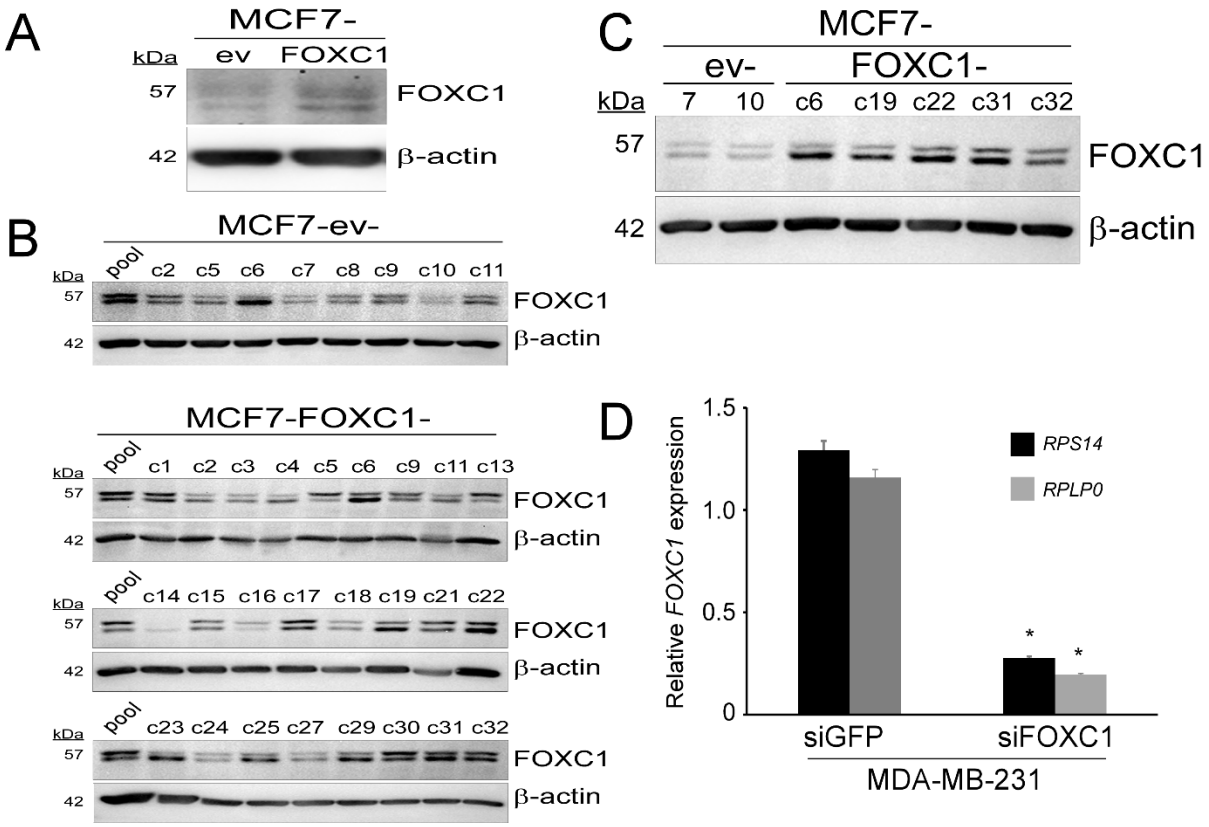


Figure 4.9: Experimental modulation of FOXC1 expression in luminal MCF-7 and basal-like MDA-MB-231 breast cancer cells. MCF-7 cells were stably transfected with a FOXC1 expression vector or empty pcDNA3.1, which was used as a control. Individual clones were isolated from these stably transfected MCF-7 cell pools with empty vector or FOXC1-expression cassette. A, FOXC1 expression in MCF-7 cell pools stably transfected with FOXC1 expression vector, and empty vector control. B, FOXC1 expression in different clonal expands of empty vector or FOXC1-expression cassette containing MCF-7 cells. C, Final contrast screening of FOXC1 expression in selected two MCF-7 cells with empty vector clonal expands control and five MCF-7 cells over-expressing FOXC1 clonal expands. In all cases, FOXC1 expression was determined by western blot analysis. Western blot was performed with whole cell lysate and β-actin was used as a control for protein loading. Molecular masses of relevant bands are indicated in kDa. FOXC1 protein can be detected as two bands with molecular masses very close to 57 kDa (top band: phosphorylated FOXC1; bottom band: non-phosphorylated FOXC1). *ev*, empty vector. Data show a representative blot of at least triplicate experiments. D, Down-regulation of FOXC1 expression in MDA-MB-231 cells after transient transfection with siRNAs targeting either *FOXC1* or *GFP* (used as a negative control) mRNAs. FOXC1 expression was measured 48 hours of post-transfection using quantitative real-time PCR. The relative *FOXC1* mRNA levels were calculated by normalization to the *RPS14* and *RPLP0* genes. Data represent the average ± SD of three independent experiments. *, $p<0.05$.

Doxorubicin and paclitaxel sensitivity of stably transfected MCF-7 cells over-expressing FOXC1 and their empty vector control were estimated by short-term SRB staining assays, with the drug treatment period selected for their corresponding two population doubling times (**Table 4.6**). Population doubling times indicated that all three FOXC1 over-expressing MCF-7 clones acquired a less proliferative phenotype compared to the empty vector, a phenomenon also observed with metaplastic derived MDR cell models, except for BAS-DOX (**Figure 4.10 and Table 4.6**).

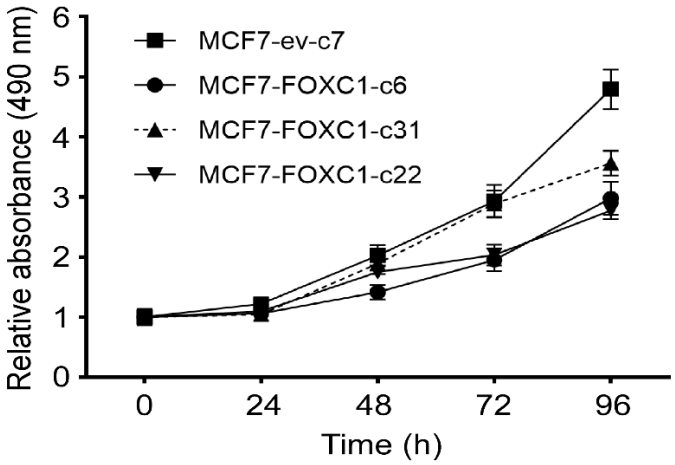


Figure 4.10: Proliferation of stably transfected MCF-7 cells over-expressing FOXC1. Different clonal isolates of MCF-7 cells stably transfected with FOXC1-expression cassette or empty vector (used as a control). Cellular proliferation was determined by sulphorhodamine B assay. Cells (2 x 10^3 / well) seeded in 96-well plates, fixed at every 24 hours interval, and stained with SRB dye. The optical density (OD) was measured at 490 nm after solubilization of protein bound SRB stain. The relative absorbance was calculated by normalization to the absorbance at zero hour. Data points represent the average ± SD from at least six replicates. The proliferation curves are obtained with GraphPad Prism software. Trendlines of these curves obtained with Microsoft Excel were used to calculate population doubling time (**Table 4.6**).

Table 4.6: Population doubling times of different clones of stably transfected MCF-7 cells over-expressing FOXC1 and their empty vector control clone

Cell Line	Doubling Times (h)
MCF7-ev-c7	47
MCF7-FOXC1-c6	70.6
MCF7-FOXC1-c31	54.1
MCF7-FOXC1-c22	67.4

Drug sensitivity curves indicated over-expression of FOXC1 in MCF-7 cells led to increase in resistance to both doxorubicin and paclitaxel (**Figure 4.11 A**). LD_{50} calculations identified all three FOXC1 over-expressing MCF-7 clones showed increase in drug resistance at different extents, more specifically increases in doxorubicin resistance were between 3.7 and 7.9-fold and paclitaxel resistance were between 2.3 and 15-fold (**Table 4.7**) In contrast, silencing FOXC1 in MDA-MB-231 cells increased sensitivity to both drugs, as assessed by both short-term SRB staining and long-term clonogenic assays (**Figure 4.11 B and C**). Short-term drug sensitivity assays estimated down-regulation of FOXC1 in MDA-MB-231 cells led to increases in sensitivity to doxorubicin by at least 1.8-fold and to paclitaxel by 8.7-fold (**Table 4.7**). Long-term clonogenic assays using different concentrations of doxorubicin (3.3-20 nM) and paclitaxel (0.5-4.0 nM) revealed a decrease in drug resistant clones after FOXC1 knock-down in MDA-MB-231 cells, compared to the control (siGFP) (**Figure 4.11 C**). In fact, no surviving clones were observed in MDA-MB-231 cells down-regulating FOXC1 beyond the concentration of 6.7 nM for doxorubicin and of 1.5 nM for paclitaxel, whereas still a significant number of clones up to 10 nM of doxorubicin and 2 nM of paclitaxel were found in control MDA-MB-231 cells (siGFP). The absolute absorbances of solubilized crystal violet stain indicated a significant lowering in the number of drug resistant clones due to FOXC1 silencing at various concentrations of both doxorubicin and paclitaxel (**Figure 4.11 C**). Taken together, these data clearly indicate transcription factor FOXC1 regulates MDR in breast cancer cells.

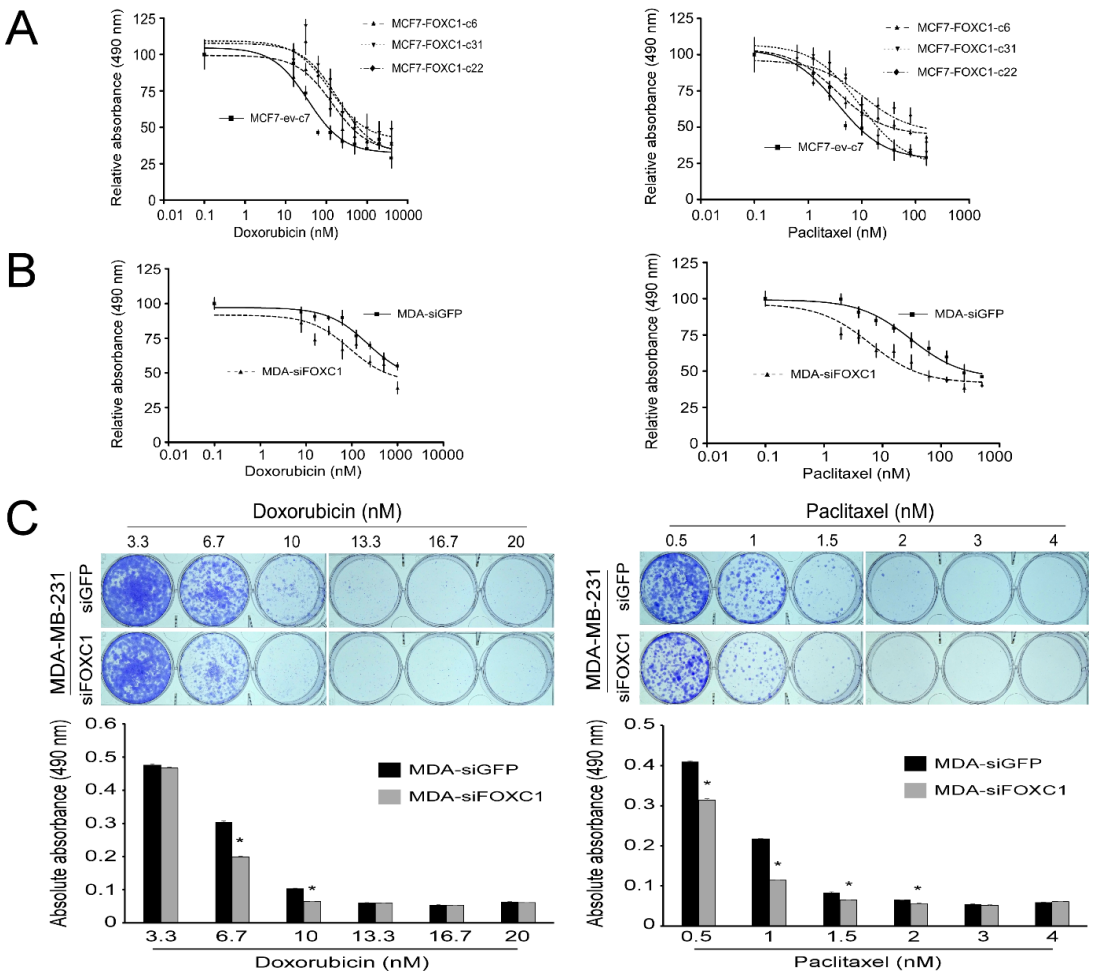


Figure 4.11: Experimental modulation of FOXC1 expression in MCF-7 and MDA-MB-231 cells alters doxorubicin and paclitaxel sensitivity. A, Drug sensitivity curves obtained with doxorubicin and paclitaxel in three different clonal isolates of MCF-7 cells over-expressing FOXC1. B, Drug sensitivity curves for doxorubicin and paclitaxel in MDA-MB-231 cells down-regulating FOXC1. In both cases, drug sensitivity curves were determined by sulphorhodamine B assays. Cells were treated with a range of concentration of doxorubicin (*left panel*) and paclitaxel (*right panel*). For transiently transfected MDA-MB-231 cells silencing FOXC1, cells were transfected in 6-well plates for 24 hours and then seeded in 96-well plates, followed by drug treatment for 72 hours. The optical density (OD) was measured at 490 nm after solubilization of protein bound SRB stain. The relative absorbance was calculated by normalization to the untreated control x100. Data points represent the average ± SD from six replicates. The best-fit curves are obtained with GraphPad Prism software. Curves from three independent experiments were used to calculate the LD_{50} values (**Table 4.7**). C, Long-term resistance of MDA-MB-231 cells down-regulating FOXC1 to doxorubicin and paclitaxel. Cells were transfected in 6-well plates for 24 hours, seeded again in 6-well plates (5 x 10^3 cells / well), treated with an initial 3-day pulse of doxorubicin, and paclitaxel, and resistant clones were allowed to grow for 14 days before crystal violet staining. The optical density (OD) of solubilized crystal violet stain was measured at 490 nm. Pictorial data show a representative picture of at least three independent experiments. Numerical data represent average ± SD of three independent experiments. *, $p<0.05$.

Table 4.7: Sensitivity of cells to doxorubicin and paclitaxel after experimental modulation of FOXC1 levels in MCF-7 and MDA-MB-231 cells

			LD_{50}[a] (nM) [resistance ratio][b]			
Cell	**Experimental**	**Cell Nomenclature**	**Doxorubicin**		**Paclitaxel**	
MCF-7	Stable overexpression	MCF7-ev-c7	109.6		8.5	
		MCF7-FOXC1-c6	407.4	[3.7]	33.9	[4.0]
		MCF7-FOXC1-c31	861.0	[7.9]	19.5	[2.3]
		MCF7-FOXC1-c22	609.5	[5.6]	127.4	[15.0]
MDA-MB-231	Transient down-regulation	siGFP	>1000.0		301.9	
		siFOXC1	562.3	[> -1.8]	34.6	[-8.7]

[a]All LD_{50} values from FOXC1-modulated cells were significant ($p<0.05$) when compared to their corresponding control cells
[b]Negative resistance ratios indicate that the cell is more sensitive to a particular drug than the control cell

4.4.6 FOXC1 regulates anchorage independence in breast cancer cells

As FOXC1 proves to be an important regulator of MDR, I wanted to assess further whether modulation of its expression was associated with others aggressive cancer cells characteristics, such as increases in anchorage independence or motility. Formation of mammospheres in liquid culture showed that over-expression of FOXC1 in luminal MCF-7 breast cancer cells significantly increased the anchorage-independent growth capacity, with more than twice to thrice sphere forming efficiency in two FOXC1 over-expressing clones, compared to the empty vector control (**Figure 4.12 A**). Similarly, growth in soft agar also indicated up-regulation of FOXC1 in MCF-7 cells led to increase in cloning efficiency, with almost 7-fold increase in one FOXC1 over-expressing clone, with respect to empty vector control (**Figure 4.12 B**). Thus, over-expression of FOXC1 in MCF-7 cells increased anchorage-independence, an important phenotype of cancer stem cells. Molecular profiling by RT-QPCR analysis also demonstrated that several stem cells markers, including *NANOG*, *SOX2*, *POU5F1* and *ABCG2*, and EMT markers, such as *ZEB1* and *SNAI1* were significantly up-regulated in the all three FOXC1 over-expressing MCF-7 clones, except for EMT marker *SNAI2*, which was markedly down-regulated. Off note, anti-apoptotic *BCL2* was up-regulated in two out of three FOXC1 over-expressing clones, suggesting a possible role of FOXC1 in apoptosis evasion (**Figure 4.12 C**).

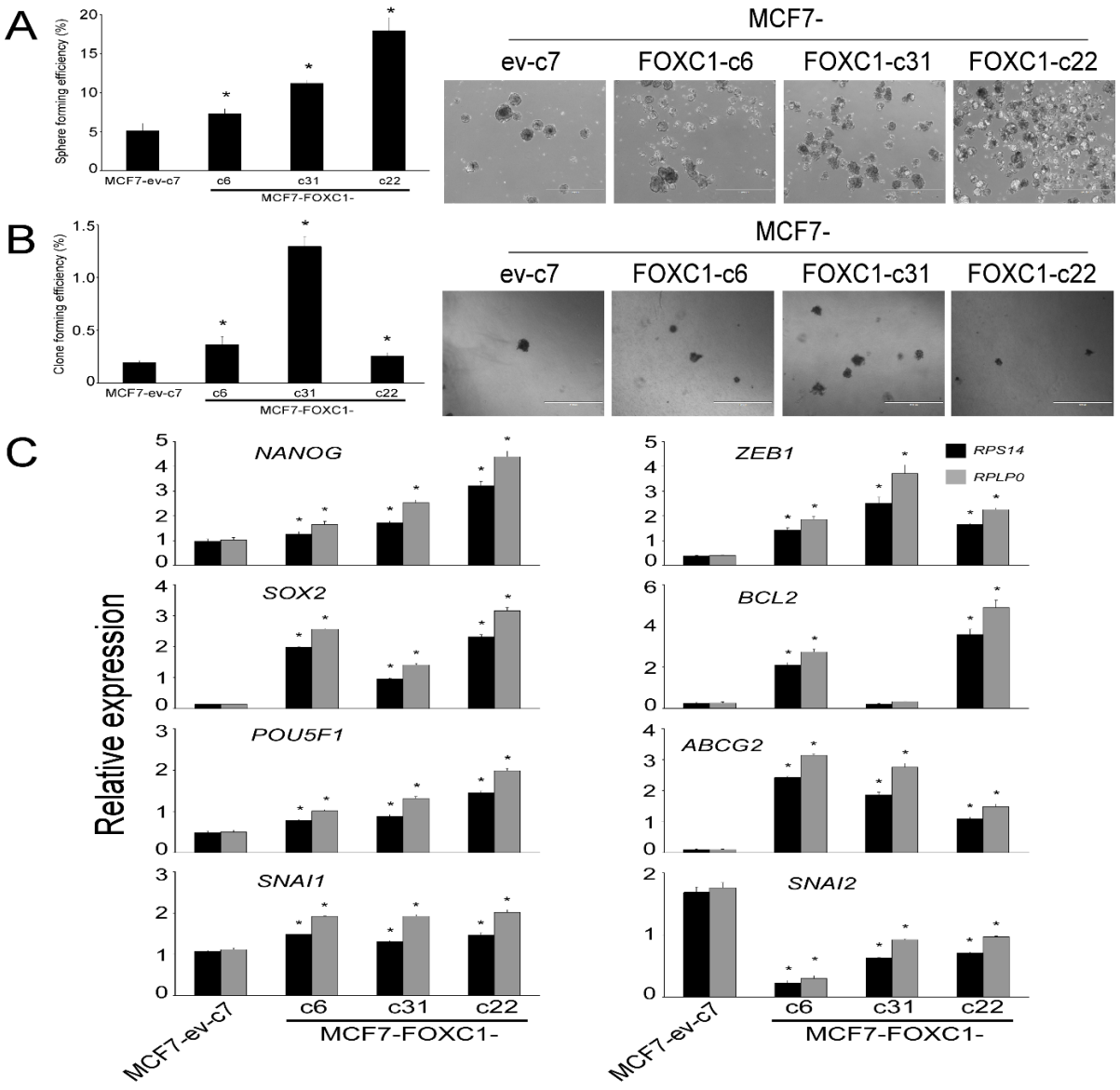


Figure 4.12: FOXC1 over-expression in luminal MCF-7 breast cancer cells increases anchorage independence. Anchorage independent growth assays, used to assess CSC phenotypes of three clonal isolates of MCF-7 cells over-expressing FOXC1 *in vitro*, included mammosphere formation in liquid culture (A) and growth in soft agar (B). A, Mammosphere formation assay: Cells (4 x 10^3 / well) were seeded in 6-well low-attachment plates with appropriate culture medium and the spheres were counted after two weeks of culture. B, Soft agar colony formation assay: Cells (2 x 10^4 / well) were seeded in 6-well plates with medium containing soft agar and the formation of colonies was determined after 4 weeks of culture. In all cases, clones or spheres larger than 100 µm in diameter were counted. Clone or sphere forming efficiency calculated relative to the total number of plated cells x100. Pictorial data are representatives of at least three independent experiments. Numerical data represent the average ± SD of three independent experiments. Bar represents 1000 µm. C, Quantitative real-time PCR analyses of some well-known EMT, CSC and anti-apoptotic marker genes expression. The relative mRNA levels were calculated by normalization to the *RPS14* and *RPLP0* genes. Data represent the average ± SD of three independent experiments. *, $p<0.05$.

On the other hand, *in vitro* scratch assays showed that FOXC1 over-expression in MCF-7 cells did not increase their motility, with one clone even showed decreased motility than the empty vector control, probably due to clonal variation (**Figure 4.13 A**). Moreover, FOXC1 over-expression did not alter the expression of adherens junction protein E-cadherin, explaining a possible cause why cellular motility in these FOXC1 over-expressed cells remained unaffected (**Figure 4.13 B**).

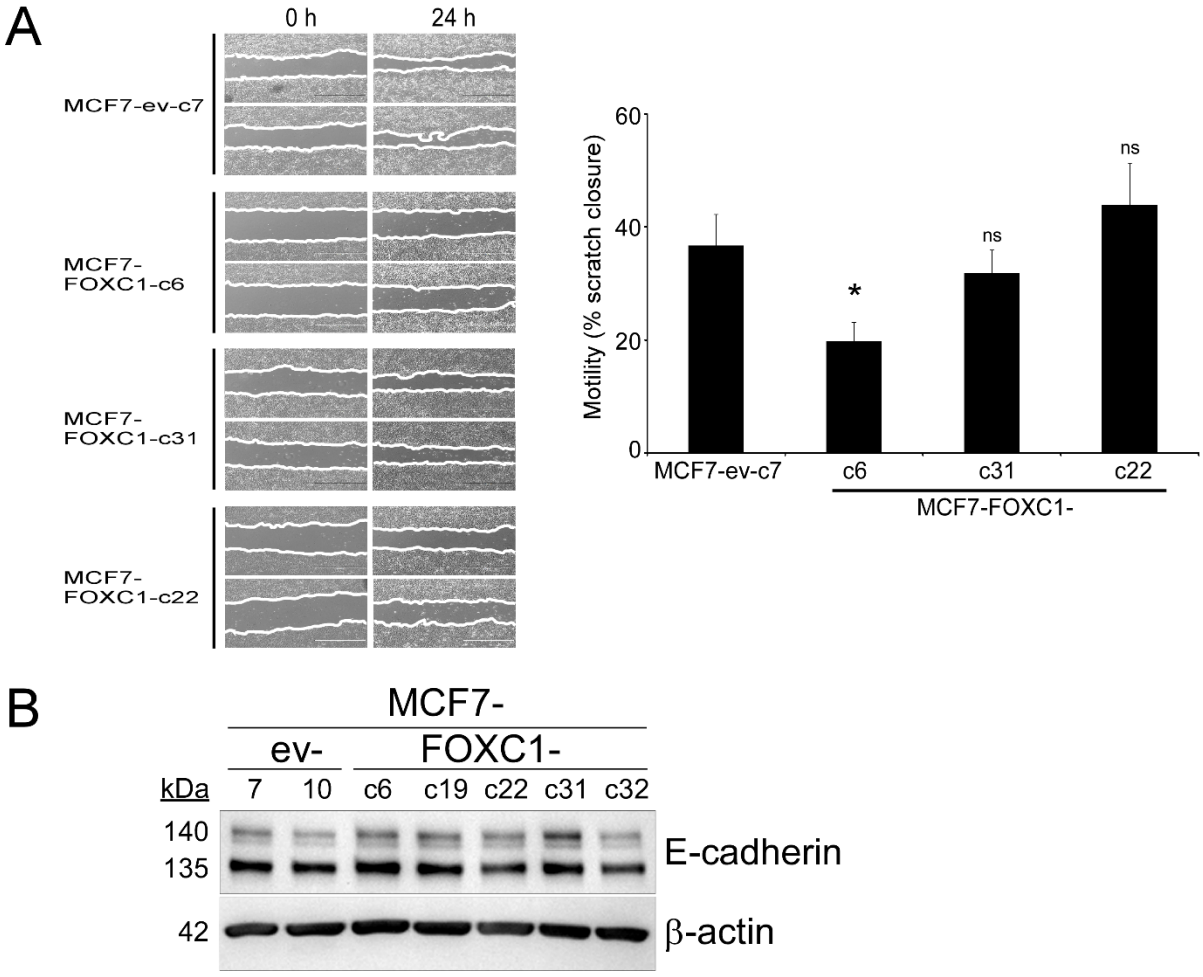


Figure 4.13: FOXC1 over-expression in MCF-7 cells does not alter motility. A, Scratch assay was employed to assess the cellular motility of MCF-7 clones overexpressing FOXC1. Scratch gap closure was determined after 24 hours from the pictures using Image J software. Pictorial data are representatives of three independent experiments. Numerical data represent the average ± SD of three independent experiments. Bar represents 1000 µm. B, E-cadherin expression in FOXC1 over-expressing MCF-7 clones determined by western blot using whole cell lysate. β-actin was used as a control for protein loading. Molecular masses of relevant bands are indicated in kDa. E-cadherin is detected as two bands, 140 kDa precursor and 135 kDa after convertase processing. Data show a representative blot of at least triplicate experiments. *ev*, empty vector. *, $p<0.05$; *ns*, not significant.

Silencing FOXC1 in basal-like MDA-MB-231 breast cancer cells led to a significant decrease in anchorage-independent growth capacity, with approximately 35% reduction in mammosphere forming efficiency in liquid culture, compared to control (siGFP) (**Figure 4.14 A**). In line with this phenotypic alteration, RT-QPCR data also indicated down-regulation of stem cell marker *SOX2* (approximately 60%) and EMT markers *SNAI1* and *SNAI2* (both approximately 30%). Interestingly, *TGFB2*, which encodes an isoform of EMT-related cytokine TGF-β, was down-regulated in response to FOXC1 silencing in MDA-MB-231 cells (**Figure 4.14 B**). However, among the different markers probed, expression of some of the EMT markers, such as *ZEB1*, *ZEB2* and *VIM*, and CSC markers, such as *NANOG* and *ABCG2*, were not altered due to FOXC1 silencing, and one CSC marker *POU5F1* was even slightly elevated (**Figure 4.14 B**).

Overall, these data clearly indicate that FOXC1 regulates anchorage independence in breast cancer cells, suggesting that FOXC1's involvement in the regulation of MDR in breast cancer might be through modulating stemness, further bolstering the CSC theory of chemotherapy resistance.

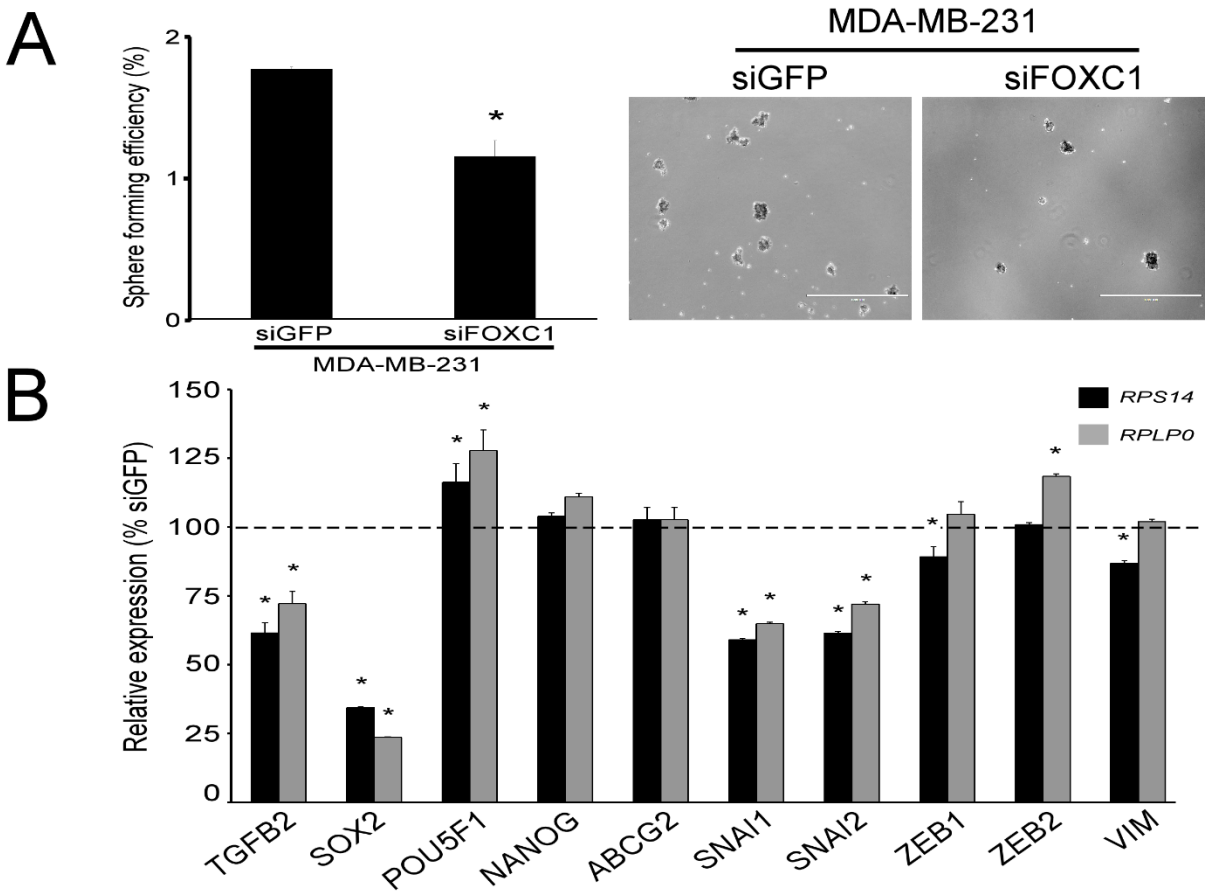


Figure 4.14: FOXC1 silencing in basal-like MDA-MB-231 cells decrease anchorage independence. A, Mammosphere formation in liquid culture was used to assess the anchorage independent growth, a phenotype of CSC. Cells were transfected in 6-well plates with siRNAs targeting FOXC1 or GFP (used as negative control) for 24 hours, seeded (4 x 10^3 cells / well) in 6-well low-attachment plates with appropriate culture medium and the spheres larger than 100 µm in diameter were counted after two weeks of culture. Sphere forming efficiency calculated relative to the total number of plated cells x100. Pictorial data are representatives of at least three independent experiments. Numerical data represent the average ± SD of three independent experiments. Bar represents 1000 µm. B, Quantitative real-time PCR analyses of some well-known EMT and CSC marker genes expression. The mRNAs levels were normalized to the *RPS14* and *RPLP0* genes. The relative expression of each gene after siFOXC1 transfection were calculated with respect to siGFP control (dashed line). Data represent the average ± SD of three independent experiments. *, $p<0.05$.

4.5 Discussion

The aggressive clinical behaviour of MBC poses a significant treatment challenge and gives patients a bad prognosis (Schwartz *et al.*, 2013; Weigelt *et al.*, 2014). Despite questionable efficacy, the standard systemic chemotherapy treatment for MBCs in use today is the same as for conventional TNBCs (Jung *et al.*, 2010; Chen *et al.*, 2011). Moreover, lack of targeted therapies, as with other TNBCs, and intrinsic or acquired resistance to traditional chemotherapeutics create added burdens (Schwartz *et al.*, 2013). Thus, a better understanding of MBC pathobiology, particularly related to chemotherapeutics resistance, is of paramount importance to identify novel therapeutic targets, leading to improved patient survival. In this chapter, I demonstrate that transcription factor FOXC1 contributes to multi-drug resistance in breast cancer cells, with a particular attention to MBC derived cells.

In an effort to better understand the molecular and phenotypic alteration associated with acquisition of chemotherapeutics resistance, I have generated drug resistant derivatives of MBC derived cell lines. Drug sensitivity data presented with four commonly used chemotherapeutics indicate that these MBC derived drug resistant cellular models, although multi-drug resistant, exhibit different patterns of sensitivity/resistance. Although both doxorubicin- and paclitaxel-resistant cells show cross-resistance to paclitaxel and doxorubicin, respectively, they are found to exhibit collateral sensitivity to either cisplatin, 5-FU, or both, except for BAS-DOX cells, which also show resistance to both cisplatin and 5-FU. This phenomenon of collateral sensitivity has also been reported previously with variety of drug resistant cells (Raguz *et al.*, 2013), particularly when tested against enough drugs, and it offers a promising therapeutic avenue (Hall, Handley & Gottesman, 2009; Pluchino *et al.*, 2012). Analogous to indigenous heterogeneity, as HS578T and BAS cells resemble MBC sub-classes 2 and 1, respectively, an acquisition of MDR phenotype in these cells is accompanied by diverse phenotypic alterations. HS578T MDR cells show an increased anchorage independence, but no change in their already very high motility. In contrast, BAS MDR cells exhibit an increased motility, whereas no variation in already high anchorage-independent growth capacity.

Whilst metaplastic HS578T cells acquire MDR, at least in part, via up-regulation of aldo-keto reductases (Mahmud *et al.*, 2019), acquisition of MDR in metaplastic derived BAS cells is mediated by FOXC1. Both BAS MDR cells show up-regulated FOXC1 levels, although it is not observed in the HS578T MDR cells, probably due to already very high endogenous levels in parental cells. Silencing FOXC1 expression in both BAS MDR cells significantly increases

their doxorubicin and paclitaxel sensitivities. In agreement to the current findings, FOXC1 over-expression has been reported to be correlated with poor response to anthracycline-based chemotherapy in patients with sporadic TNBCs (Xu *et al.*, 2017). In one study involving two breast cancer patients' datasets revealed that FOXC1 expression is a predictor of breast cancer clinical outcome, and patients with high FOXC1 expression in their tumours show a poorer survival (Taube *et al.*, 2010). Moreover, *FOXC1* promoter hypermethylation, which causes epigenetic silencing of its expression, is associated with improved survival in locally advanced breast cancer patients treated with doxorubicin (Dejeux *et al.*, 2010). Moreover, BLBC, an aggressive form of triple-negative breast cancer subtype associated with high metastatic tendency and poor prognosis, shows over-expression of FOXC1 (Lee *et al.*, 2020). Basal-like MDA-MB-468 breast cancer cells resistant to FEM (5-FU, Epirubicin and Mitomycin C), a regimen used to treat metastatic disease, exhibit an up-regulation of FOXC1 expression (Tkocz *et al.*, 2012).

FOXC1 is involved in various signalling pathways related to disease progression and aggressive clinical features in several different carcinomas, particularly BLBC (Han *et al.*, 2017; Elian, Yan & Walter, 2018). This warrants further studies to identify down-stream effectors of FOXC1 responsible for MDR in metaplastic breast cancer derived cells. A study shows that FOXC1 increases the stability of p65/RelA protein BLBC cells, leading to activation of NF-κB signalling. Pharmacological inhibition of NF-κB attenuates FOXC1-induced increased cellular proliferation, migration, and invasion in MDA-MB-231 cells (Wang *et al.*, 2012b). Importantly, NF-κB has been reported to promote chemotherapy resistance in several different cancer cells, including breast cancer, pancreatic cancer, colon cancer and Hodgkin disease (Bentires-Alj *et al.*, 2003; Arlt *et al.*, 2003; Tapia *et al.*, 2007). Inhibition of NF-κB pathway in breast cancer BT-474 cells increases their sensitivity to doxorubicin (Tapia *et al.*, 2007). A recent report identifies that doxorubicin resistant both MCF-7 and MDA-MB-231 breast cancer cells shows higher NF-κB subunit p65 activity. Inhibition of NF-κB (p65) significantly sensitizes these resistant cells to doxorubicin. Moreover, experimental over-expression of NF-κB (p65) in MDA-MB-231 cells confers resistance to doxorubicin, together with up-regulation of ABCB1 (also known as P-glycoprotein), an efflux pump involved in MDR (Abdin *et al.*, 2021). Furthermore, human colon cancer HCT15 cells also down-regulate the expression of ABCB1 upon NF-κB inhibition (Bentires-Alj *et al.*, 2003). These data points suggest that the FOXC1-mediated MDR phenotype in MBC derived cells might be through increased NF-κB activity.

An acquisition of drug resistance is often associated with EMT and further development of stem-like phenotypes. This phenomenon of interplay between EMT, CSC and drug resistance has been described using minimally transformed primary human mammary epithelial cells (Mani *et al.*, 2008; Onder *et al.*, 2008; Zhou *et al.*, 2014). E-cadherin is recognised as a key molecule regulating these processes in epithelial cells. However, its role in regulating EMT has been questioned, as a study reported that ectopic expression of E-cadherin in breast cancer cell lines with EMT phenotype and molecular expression neither reverses the phenotype, nor alters the markers expression, highlighting loss of E-cadherin is not mandatory for EMT induction, at least in some cell lines (Hollestelle *et al.*, 2013). Importantly, a regulation of these three processes independent of E-cadherin is well studied in TNBC cells. For instance, although experimental over-expression of *CDH1* transcriptional activator EP300 in some TNBC cells results in E-cadherin expression, together with decrease in drug resistance and CSC characteristics (Asaduzzaman *et al.*, 2017), in other cells, such as HS578T, up-regulation of EP300 does not trigger E-cadherin expression, attributed to its promoter hypermethylation, but increases EMT and CSC phenotypes, and chemoresistance (Mahmud *et al.*, 2019). The data presented here clearly indicates FOXC1 regulates MDR, in addition to metaplastic derived BAS cells, in luminal MCF-7 and basal-like MDA-MB-231 cells. Moreover, FOXC1 promotes anchorage independence in these cells. Interestingly, E-cadherin expression in MCF-7 cells remains un-altered upon experimental FOXC1 over-expression, suggesting that FOXC1 functions either down-stream of E-cadherin or via different signalling pathways in regulating these processes. Similarly, FOXC1 over-expression in MCF-7 cells does not increase their motility, an EMT phenotype. Loss of E-cadherin in MCF-7 cells leads to an increase in motility and drug resistance (Zhou *et al.*, 2014), whereas FOXC1 over-expression results in increased drug resistance only, further supporting the notion of different FOXC1-mediated MDR regulatory mechanism independent of E-cadherin in epithelial cells.

FOXC1-induced promotion of anchorage independence in breast cancer cells suggests its role in the maintenance CSC phenotype, in agreement to the previous report demonstrating FOXC1 is involved in the SMO-independent activation of Hedgehog signalling pathway that establishes stem-like characteristics in BLBC cells (Han *et al.*, 2015). FOXC1' involvement in the activation of Hedgehog signalling could consequently explain the role of this transcription factor in mediating MDR, as this originally developmental signalling pathway contributes to the acquisition of chemotherapy resistance in several carcinoma types,

including ovarian cancer, colorectal cancer, oral squamous cell carcinoma, and acute myeloid leukemia (Kumar *et al.*, 2021b). Interestingly, activation of Hedgehog signalling confers chemoresistance in these cancer cells through the ABC transporters, such as ABCB1, ABCC1, or ABCG2 (Chen, Bieber & Teng, 2014; Huang *et al.*, 2019; Zhang *et al.*, 2020a; Po *et al.*, 2020; Lu *et al.*, 2020). This leads to hypothesize that FOXC1 might exploit Hedgehog signalling pathway to promote MDR in breast cancer cells, although in the cells studied here, this would be in an ABC transporter-independent manner.

Additionally, the data presented here indicates that FOXC1 regulates, either directly or indirectly, expression of *SOX2*, a transcription factor that plays an important role in the maintenance of stem cell phenotype, among others. A study shows that down-regulation of SOX2 by a neddylation inhibitor small-molecule MLN4942 re-sensitizes the tamoxifen resistant MCF-7 breast cancer cells to the endocrine therapy (Yin *et al.*, 2019). However, this study did not address the sensitivity towards conventional chemotherapeutics upon SOX2 down-regulation. Another study indicated that wedelolactone, a naturally occurring compound, delivered as encapsulated nanoparticles causes down-regulation of SOX2 and ABCG2, leading to increased sensitivity of breast cancer stem cells to paclitaxel (Das *et al.*, 2019). These reports suggest that inhibition of SOX2 could attenuate FOXC1-induced chemoresistance in breast cancer cells, thus warranting further studies to identify whether SOX2 functions as an MDR effector down-stream of FOXC1.

In summary FOXC1 contributes to the MDR in breast cancer cells, particularly in metaplastic breast cancer derived cells. Thus, future identification of up- and down-stream molecules of FOXC1 controlling MDR is of utmost importance to unveil more targets for development of new therapeutics to combat the chemotherapy resistance phenomenon in breast cancer.

Chapter 5: TGF-β regulates MDR phenotype in metaplastic breast cancer derived cells

5.1 Introduction

5.1.1 Whole transcriptome expression analysis and profiling

Gene expression profiling, using DNA microarray or other techniques of functional genomics, allow analysis of expression of thousands of genes in parallel. Analysis of expression levels of genes in different physiological conditions both in cultured cells and tissues finds regulatory expression patterns and thereby helps to understand intricate molecular networks that cross communicate both in health and disease. This offers versatile applications in the field of molecular medicine, particularly in the study of genetic alterations involved in the disease progression as well as identifying potential targets for drug candidate development and diagnostics (Celis *et al.*, 2000).

In oncology, transcriptome profiling to assess gene expression patterns on a large-scale in tumours or cell line models has potential uses in the discovery of new chemotherapeutics. Gene expression profile may allow tumours in the same disease to be separated into different subtypes with distinct pathways utilization. Molecular signatures involving these pathways separating one subtype from another can be potential targets for chemotherapeutics development (Sausville & Holbeck, 2004). For example, gene expression profiling of an activated B cell type of lymphoma identifies expression of genes responsible for NF-κB signalling pathway activation, suggesting molecules related to this pathway can be potential targets in developing new therapies for this category of diffuse large B cell lymphoma (Davis *et al.*, 2001). Moreover, analysis of changes in signature genes expression of a disease after exposure of mammalian cell line models to a novel compound has been used as a potential strategy for drug development. Alternatively, changes in gene expression pattern can be correlated with the degree of cytotoxic effect of candidate drug leads, thereby identifying the mechanism or pathway involved in drug action that could help further to develop analogues (Sausville & Holbeck, 2004).

Furthermore, transcriptomic profiling has been used extensively to identify gene expression signatures related to phenotypes after modulation of expression of a marker gene. For example, genome-wide expression profiling using a breast cancer cellular model identified EP300-regulated gene expression signatures involved in EMT, stemness and drug resistance

(Asaduzzaman *et al.*, 2017). In another study using a different breast cancer cellular model, transcriptomic profiling identified EP300-regulated genes *AKR1C1-3* as effectors of stemness and drug resistance, and their pharmacological inhibition alters doxorubicin and paclitaxel sensitivity, thereby suggesting a new therapeutic option to tackle chemotherapeutic resistance (Mahmud *et al.*, 2019).

5.2 Aim of the chapter

I have already described in the previous chapter FOXC1 as a potential regulator of MDR in MBC derived cells. Development of new therapeutic modalities to overcome chemotherapeutic resistance requires deeper understanding of crosstalk of complex molecular mechanisms or pathways involved. There have been evidences of multiple signalling pathways involved in the chemotherapeutic resistance in conventional TNBC, including TGF-β, Wnt/β-catenin, Notch, Hedgehog, TNF-α/NF-κB, and RTK signalling pathways (Nedeljković & Damjanović, 2019). However, gene expression signatures identifying the key molecules or pathways responsible for the chemotherapy resistance in MBC cells have not been studied. The metaplastic breast cancer derived drug resistant cellular models generated provide the opportunity to identify not only potential effectors, but also upstream regulators of drug resistance. Here, I aimed to perform genome-wide expression analysis of MBC derived doxorubicin- and paclitaxel-resistant cell line models to identify different gene expression signatures of drug resistance. Finally, I aimed to screen a potential candidate target from the MDR expression signature for the development of novel therapy to overcome chemotherapy resistance, particularly in MBC.

5.3 Materials and methods

5.3.1 Whole transcriptome expression array

Genome-wide expression analysis was performed with Clariom S GeneChip Whole Transcript (WT) expression arrays using WT PLUS reagent kit (Thermo Fisher Scientific) (**Table 5.1**). The amplified and biotinylated sense-strand DNA targets were generated from total RNA following the manufacturer's instructions. This technique does not require an up-front selection or enrichment step for RNA. The entire length of RNA, including both poly(A) and non-poly(A), was primed using reverse transcription priming method. The schematic diagram of whole process is shown in **Figure 5.1**. Some steps required different thermal conditions, as described in the GeneChip WT PLUS reagent kit manual (**Table 5.2)**.

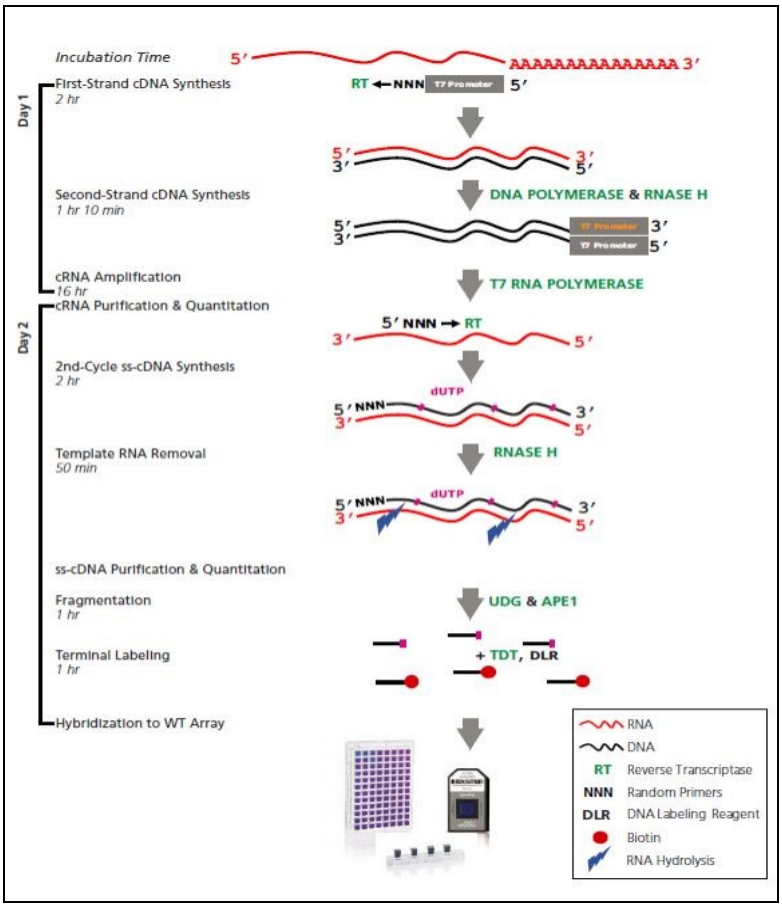


Figure 5.1: Schematic representation of steps involved in the whole transcriptome expression array. The method involves multiple steps to generate sense-strand of DNA from total RNA followed by labeling and subsequent hybridization to the array (The figure is taken from GeneChip WT PLUS reagent kit manual target preparation for GeneChip Whole Transcript (WT) expression arrays of Thermo Fisher Scientific).

Table 5.1: GeneChip WT PLUS reagent kit contents and storage

Component	10-Reaction Kit for Manual use (P/N 902280)	Storage
WT Amplification Kit Module 1		
First-Strand Enzyme	11 µL	-20^{0}C
First-Strand Buffer	44 µL	-20^{0}C
Second-Strand Enzyme	22 µL	-20^{0}C
Second-Strand Buffer	198 µL	-20^{0}C
IVT Enzyme	66 µL	-20^{0}C
IVT Buffer	264 µL	-20^{0}C
Control RNA (1 mg/mL HeLa total RNA)	5 µL	-20^{0}C
Second-Cycle Primers	44 µL	-20^{0}C
Second-Cycle ss-cDNA Enzyme	44 µL	-20^{0}C
Second-Cycle ss-cDNA Buffer	88 µL	-20^{0}C
RNase H	44 µL	-20^{0}C
Nuclease-free water	2 x 1.0 mL	any temp
WT Amplification Kit Module 2		
Purification Beads	2.2 mL	4^{0}C [a]
GeneChip Poly-A RNA Control Kit		
Poly-A Control Stock	16 µL	-20^{0}C
Poly-A Control Dil Buffer	3.8 mL	-20^{0}C
GeneChip WT Terminal Labeling Kit		
10X cDNA Fragmentation Buffer	48 µL	-20^{0}C
UDG, 10 U/µL	10 µL	-20^{0}C
APE 1, 1000 U/µL	10 µL	-20^{0}C
5X TdT Buffer	120 µL	-20^{0}C
TdT, 30 U/µL	20 µL	-20^{0}C
DNA Labeling Reagent, 5mM	10 µL	-20^{0}C
RNase-free Water	825 µL	any temp [a]
GeneChip Hybridization Control Kit		
20X Hybridization Controls	450 µL	-20^{0}C
3 nM Control Oligo B2	150 µL	-20^{0}C

[a]No freezing

Table 5.2: Thermal cycler programs for whole transcriptome expression array

Program	Heated Lid Temp	Alternate Protocol [a]	Step 1	Step 2	Step 3	Step 4	Volume
First-Strand cDNA Synthesis	42^0C	105^0C	25^0C, 60 min	42^0C, 60 min	4^0C, 2 min		10 µL
Second-Strand cDNA Synthesis	RT or disable	Lid open	16^0C, 60 min	65^0C, 10 min	4^0C, 2 min		30 µL
In Vitro Transcription cRNA Synthesis	40^0C	40^0C oven	40^0C, 16 hr	4^0C, hold			60 µL
Second-Cycle Primers-cRNA Annealing	70^0C	105^0C	70^0C, 5 min	25^0C, 5 min	4^0C, 2 min		28 µL
Second-Cycle ss-cDNA Synthesis	70^0C	105^0C	25^0C, 10 min	42^0C, 90 min	70^0C, 10 min	4^0C, hold	40 µL
RNA Hydrolysis	70^0C	105^0C	37^0C, 45 min	95^0C, 5 min	4^0C, hold		44 µL
Fragmentation	93^0C	105^0C	37^0C, 60 min	93^0C, 2 min	4^0C, hold		48 µL
Labeling	70^0C	105^0C	37^0C, 60 min	70^0C, 10 min	4^0C, hold		60 µL
Hybridization Control	65^0C	105^0C	65^0C, 5 min				variable
Hybridization Cocktail	99^0C	105^0C	95^0C or 99^0C, 5 min	45^0C, 5 min			Variable

[a]For thermal cycler that lack a programmable heated lid

5.3.2 Preparation of total RNA

Extraction of RNA from cell lines

Total RNA was extracted from HS578T and BAS cell lines and their drug resistant derivatives to paclitaxel and doxorubicin following the procedure described in **section 2.6.1**. The procedure for the generation of drug resistant cell lines is described in **section 4.3.1**. All the necessary precautions were taken to avoid cross contamination as well as possible contamination with RNAase from environment. RNA was isolated from four biological replicates for the parental cell lines and from three biological replicates for each drug resistant cells. The description of the samples used is further described in the **Table 5.3**.

Table 5.3: Description of the samples used for the whole transcriptome expression analysis

HS578T parental and its drug resistant derivatives			BAS parental and its drug resistant derivatives		
Sample ID	**Sample Name**	**Sample type**	**Sample ID**	**Sample Name**	**Sample type**
1	HS-WT1	PARENTAL	11	BAS-WT1	PARENTAL
2	HS-WT2		12	BAS-WT2	
3	HS-WT3		13	BAS-WT3	
4	HS-WT4		14	BAS-WT4	
5	HS-TX1	PACLITAXEL RESISTANT	15	BAS-TX1	PACLITAXEL RESISTANT
6	HS-TX2		16	BAS-TX2	
7	HS-TX3		17	BAS-TX3	
8	HS-DOX1	DOXORUBICIN RESISTANT	18	BAS-DOX1	DOXORUBICIN RESISTANT
9	HS-DOX2		19	BAS-DOX2	
10	HS-DOX3		20	BAS-DOX3	

Determination of RNA quantity, quality, and integrity

The quantification of total RNA extracted was performed using a NanoDrop ND1000 (Thermo Fisher Scientific). As the efficiency of RNA sample amplification depends on the quality of RNA, which should be free from contaminating proteins, DNA, phenol, ethanol and salts, A260/A280 ratios were measured to determine RNA quality, with an acceptable range of 1.7 to 2.1. Another important component of RNA quality is the integrity of the RNA sample, which is determined as proportion of full-length RNA. RNA integrity was evaluated by the RNA Integrity Number (RIN) and the separation and visibility of conspicuous bands of *18S* and *28S* ribosomal RNA (rRNA) in electropherograms, as well as the ratio of two rRNA [28S/18S] bands using a Bioanalyzer (Agilent). For full-length mRNA, the maximum possible RIN value is 10 and the ratio of band intensities of 28S/18S rRNA is approximately 2. Only samples surpassing the minimal quality threshold (RIN > 8.0) were used in the subsequent steps. The details of these parameters as measured by the Bioanalyzer are described in **Table 5.4 and Figure 5.2**.

Table 5.4: Quality control (QC) parameters of extracted total RNA samples used for the whole transcriptome expression array

Sample ID	Sample Name	A260/A280 Ratio	RIN	rRNA Ratio [28S/18S]
1	HS-WT1	2.00	10	2.1
2	HS-WT2	2.06	10	2.1
3	HS-WT3	2.05	10	2.2
4	HS-WT4	1.99	10	2.2
5	HS-TX1	2.05	10	2.2
6	HS-TX2	2.07	10	2.1
7	HS-TX3	2.08	10	2.3
8	HS-DOX1	2.06	10	2.4
9	HS-DOX2	2.06	10	2.4
10	HS-DOX3	2.06	10	2.5
11	BAS-WT1	2.04	10	2.5
12	BAS-WT2	2.04	10	2.5
13	BAS-WT3	1.98	10	2.3
14	BAS-WT4	2.05	10	2.4
15	BAS-TX1	2.06	10	2.2
16	BAS-TX2	2.06	10	2.2
17	BAS-TX3	2.05	10	2.3
18	BAS-DOX1	2.07	10	2.4
19	BAS-DOX2	2.07	10	2.6
20	BAS-DOX3	2.07	10	2.6

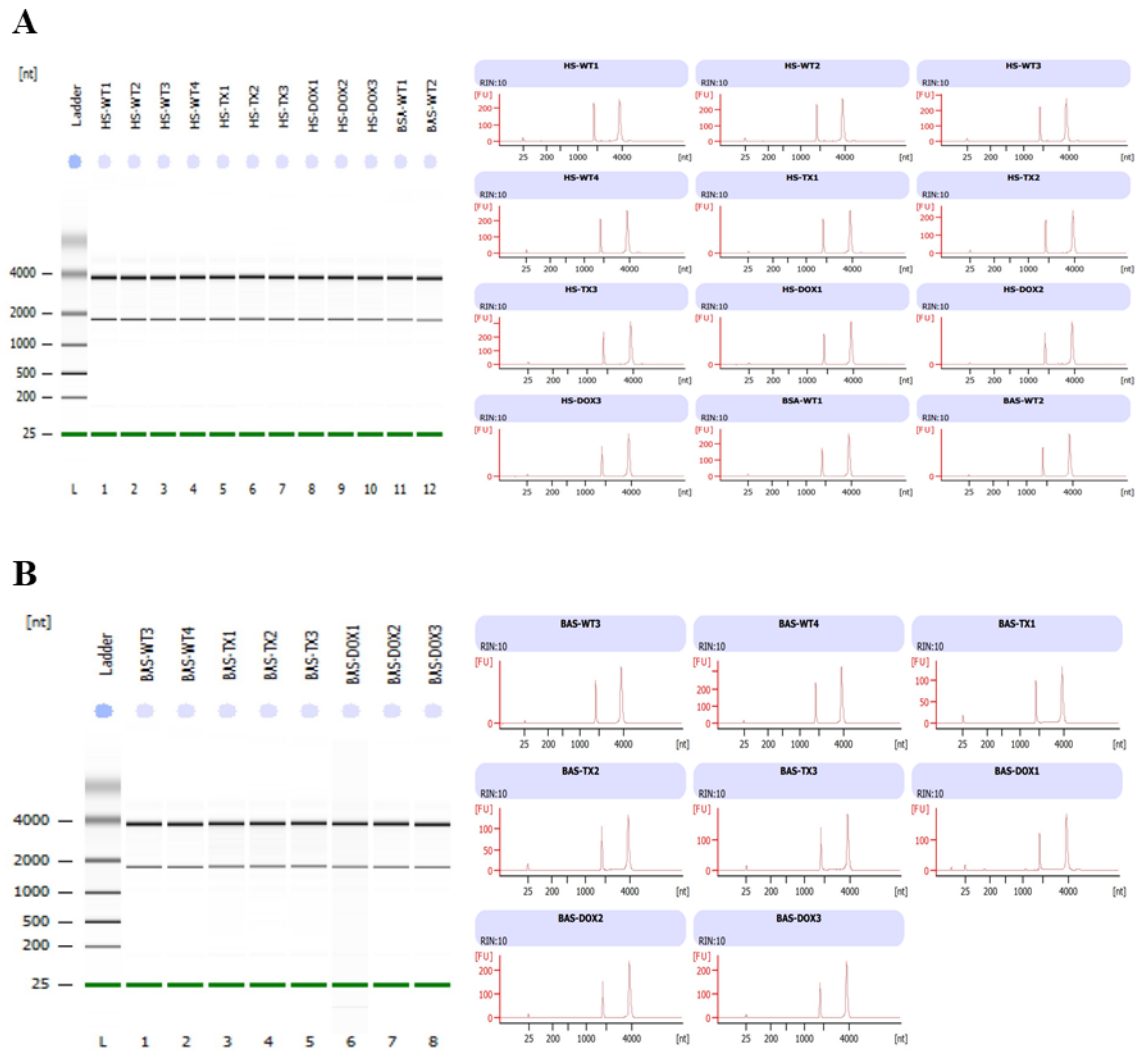


Figure 5.2: Integrity analysis of RNA samples used in the whole transcriptome expression array. Gel electrophoresis (*left*) and electropherogram (*right*) of RNA samples. As there are only twelve wells in the Agilent 2100 Bioanalyzer when using the nano chip, the samples were run separately in two different chips with the 12 samples in one chip (A) and the remaining 8 samples in another chip (B). The gel electrophoresis and electropherogram data indicate that the *28S* and *18S* rRNAs were resolved clearly into two discrete bands. The ratios of band intensities of 28S/18S rRNAs were in the range of 2.1-2.6, which is highly satisfactory indicating full-length mRNA. All samples showed RIN values of 10, the maximum possible value for full-length mRNA.

5.3.3 Preparation of total RNA/ poly-A RNA control mixture

The total RNA input for each reaction was set to 250 ng. Firstly, the poly-A spike controls, exogenous positive controls for monitoring the entire target preparation and the labeling process independently, were prepared. An appropriate dilution of poly-A control stock for 250 ng RNA input was made with the Poly-A Control Dil Buffer following the serial dilution process described in **Table 5.5**. Then, 2 µL of poly-A controls (4^{th} dilution) was added to the total RNA sample, and the final volume was adjusted to 5 µL following **Table 5.6**.

Table 5.5: Serial dilution of poly-A control stock

Total RNA Input Amount	**Serial Dilution**				**Volume of 4^{th} Dilution Added to the Total RNA**
	1^{st} Dilution	**2^{nd} Dilution**	**3^{rd} Dilution**	**4^{th} Dilution**	
250 ng	1:20	1: 50	1: 50	1:4	2 µL

Table 5.6: Preparation of total RNA/Poly-A RNA control mixture

Component	**Volume/Reaction**
Total RNA Sample	Variable
Diluted Poly-A RNA controls (4^{th} Dilution)	2 µL
Nuclease-free Water	Variable
Total Volume	**5 µL**

5.3.4 Synthesis of first-strand cDNA

This is basically reverse transcription reaction where total RNA of each sample is primed separately to synthesize single-stranded cDNA with the primers that produce T7 promoter sequence at the 5′ end. Firstly, first-strand master mix was prepared considering the total sample with 5% overage following the manufacturer's protocol described in **Table 5.7**. Then, 5 µL of total RNA/ Poly-A control mixture of each sample were added to each 5 µL aliquot of first-strand master mix with a final reaction volume of 10 µL. Following the thermal cycler program provided in the GeneChip WT PLUS kit manual described in **Table 5.2**, the first-strand cDNAs were synthesized in a thermal cycler.

Table 5.7: Preparation of first-strand master mix

Component	Volume/Reaction
First-Strand Buffer	4 µL
First-Strand Enzyme	1 µL
Total Volume	**5 µL**

5.3.5 Synthesis of second-strand cDNA

In this procedure, a second-strand cDNA complementary to the first-strand cDNA of each sample was synthesized to produce doubled-stranded cDNA, which acts as a template for *in vitro* transcription. Here two enzymes, namely RNase H and DNA polymerase, work simultaneously to degrade the RNA and synthesize second-strand cDNA, respectively. Following the manufacturer's protocol, the second-strand master mix was prepared for all the samples with 5% overage (**Table 5.8**). Then, 20 µL of the second-strand master mix was added to each (10 µL) first-strand cDNA sample for a final reaction volume of 30 µL and mixed thoroughly. After incubation in a thermal cycler following the thermal program described in **Table 5.2**, the second-strand cDNAs were synthesized.

Table 5.8: Preparation of second-strand master mix

Component	Volume/Reaction
Second-Strand Buffer	18 µL
Second-Strand Enzyme	2 µL
Total Volume	**20 µL**

5.3.6 Synthesis of cRNA by *in vitro* transcription

The synthesis and amplification of antisense RNA (complementary RNA or cRNA) was carried out by *in vitro* transcription (IVT) method using second-strand cDNA as a template with T7 RNA polymerase. This method of RNA synthesis is developed based on original T7 *in vitro* transcription technology known as the Eberwine or RT-IVT method (Van Gelder *et al.*, 1990). Firstly, the IVT master mixed was prepared following the manufacturer's protocol with the components described in **Table 5.9**. At room temperature, 30 µL of the IVT master mix were added to each (30 µL) second-strand cDNA sample for a final reaction volume of 60 µL and mixed thoroughly by gently vortexing. The reaction mixtures were then incubated

in accordance with the thermal cycler program provided in the GeneChip WT PLUS kit manual described in **Table 5.2** to synthesize cRNA.

Table 5.9: Preparation of IVT master mix

Component	Volume/Reaction
IVT Buffer	24 µL
IVT Enzyme	6 µL
Total Volume	**30 µL**

5.3.7 Purification and quantitation of cRNA

The complementary RNA (cRNA) free from all the impurities (enzymes, salts, inorganic phosphates, and unincorporated nucleotides) is used for the synthesis of second-cycle single-stranded cDNA. The purification was carried out by binding of cRNA with the purification beads followed by washing with 80% ethanol thrice and then air dried. The bound cRNA of each sample was then eluted with 27 µL of preheated (65^0C) nuclease-free water. All the steps were carried out following the manufacturer's protocol described in the GeneChip WT PLUS kit manual.

The concentration of the purified cRNA was determined by measuring absorbance at 260 nm using a NanoDrop spectrophotometer. As the initial concentrations of all the samples were greater than 3000 ng/µL, each sample was diluted with nuclease-free water at a ratio of 1:1. The concentration of the diluted cRNA samples were then determined. The details of concentration of each sample and yield obtained are shown in **Table 5.10**.

Table 5.10: Assessment of cRNA yield

Sample ID	Sample Name	cRNA Conc. (ng/µL)	Dilution Factor	Total Amount of cRNA (µg)
1	HS-WT1	2111.5	2	114.021
2	HS-WT2	2236	2	120.744
3	HS-WT3	2061	2	111.294
4	HS-WT4	2330.5	2	125.847
5	HS-TX1	2203	2	118.962
6	HS-TX2	2229	2	120.366
7	HS-TX3	2061.5	2	111.321
8	HS-DOX1	2130.5	2	115.047
9	HS-DOX2	1734	2	93.636
10	HS-DOX3	1742.5	2	94.095
11	BAS-WT1	2154	2	116.316
12	BAS-WT2	1913.5	2	103.329
13	BAS-WT3	2187	2	118.098
14	BAS-WT4	2024	2	109.296
15	BAS-TX1	2065.5	2	111.537
16	BAS-TX2	1970.5	2	106.407
17	BAS-TX3	2282	2	123.228
18	BAS-DOX1	2089.5	2	112.833
19	BAS-DOX2	2172	2	117.288
20	BAS-DOX3	2086.5	2	112.671

5.3.8 Synthesis of second-cycle single-stranded cDNA

In this step, the purified anti-sense RNA (cRNA) is used as template to synthesize the sense-strand cDNA by the reverse transcription using second-cycle primers. The sense-strand cDNA contains dUTP at a fixed ratio relative to dTTP. The cRNA input for the synthesis of second-cycle single-stranded cDNA synthesis was 15 µg. Following the manufacturer's protocol provided, the required amount of cRNA of each sample and second-cycle primers mix were prepared with the final volume adjusted to 28 µL using nuclease-free water (**Table 5.11**). The mixes were then incubated as per the thermal cycler program described in **Table 5.2**. Afterward, the second-cycle ss-cDNA master mix for total samples with 5% overage was prepared according to the procedure provided with the component described in **Table 5.12**. On ice, 12 µL of the second-cycle ss-cDNA master mix was added to each (28 µL) cRNA/second-cycle primers sample for a final reaction volume of 40 µL. The reaction

mixtures were then incubated in the thermal cycler following the thermal cycler program provided in the GeneChip WT PLUS kit manual described in **Table 5.2** to synthesize second-cycle ss-cDNA.

Table 5.11: Preparation of cRNA and second-cycle primers mix

Component	Volume/Reaction
cRNA Sample (15 µg)	Variable
Nuclease-free Water	Variable
Second-Cycle Primers	4 µL
Total Volume	**28 µL**

Table 5.12: Preparation of second-cycle ss-cDNA master mix

Component	Volume/Reaction
Second-Cycle ss-cDNA Buffer	8 µL
Second-Cycle ss-cDNA Enzyme	4 µL
Total Volume	**12 µL**

5.3.9 Hydrolysis of RNA using RNase H

The cRNA template was hydrolyzed using RNase H to get the single-stranded cDNA. In brief, 4 µL of the RNase H was added to each (40 µL) of the second-cycle ss-DNA sample for a final reaction volume of 44 µL following the manufacturer's protocol and then incubated in the thermal cycler maintaining the thermal conditions noted in the thermal cycler programs provided in the GeneChip WT PLUS kit manual described in **Table 5.2**. Finally, 11 µL of nuclease-free water was added to each (44 µL) hydrolyzed second-cycle ss-cDNA sample for a final reaction volume of 55 µL and proceeded to the purification step.

5.3.10 Purification and quantitation of second-cycle single-stranded cDNA

The synthesized second-cycle single-stranded cDNA was purified after hydrolysis of template cRNA to remove enzymes, salts, and unincorporated dNTPs. Briefly, each ss-cDNA sample was bound to the purification beads. The purification beads were then washed with 80% ethanol thrice followed by air drying. Finally, ss-cDNA of each sample was eluted with

the 30 µL of the preheated (65^0C) nuclease-free water. All the steps of purification process were carried out following the protocol described in the GeneChip WT PLUS kit manual. The purified ss-cDNA was used for fragmentation and labeling. Before proceeding to these steps, the concentration of each purified ss-cDNA was determined by measuring the absorbance at 260 nm using a NanoDrop spectrophotometer. The concentration and yield obtained for each sample is shown in **Table 5.13**.

Table 5.13: Assessment of yield of ss-cDNA

Sample ID	Sample Name	ss-cDNA Conc. (ng/µL)	Total Amount of ss-cDNA (µg)
1	HS-WT1	506	15.18
2	HS-WT2	526	15.78
3	HS-WT3	437	13.11
4	HS-WT4	555	16.65
5	HS-TX1	513	15.39
6	HS-TX2	525	15.75
7	HS-TX3	459	13.77
8	HS-DOX1	468	14.04
9	HS-DOX2	486	14.58
10	HS-DOX3	394	11.82
11	BAS-WT1	469	14.07
12	BAS-WT2	414	12.42
13	BAS-WT3	488	14.64
14	BAS-WT4	447	13.41
15	BAS-TX1	524	15.72
16	BAS-TX2	476	14.28
17	BAS-TX3	508	15.24
18	BAS-DOX1	437	13.11
19	BAS-DOX2	458	13.74
20	BAS-DOX3	461	13.83

5.3.11 Fragmentation and labeling of single-stranded cDNA

The fragmentation of the each purified ss-cDNA was performed using two enzymes, uracil-DNA glycosylase (UDG) and apurinic/apyrimidinic endonuclease 1 (APE 1), in order to break the DNA strand at the unnatural dUTP residues. The fragmented cDNA of each sample was then labeled by terminal deoxynucleotidyl transferase (TdT) using the biotin tagged proprietary DNA labeling reagent. The input of single-stranded cDNA for fragmentation and

labeling was 5.5 µg. In short, the volume required for each 5.5 µg of ss-cDNA sample was taken and adjusted to volume 31.2 µL with the nuclease-free water maintaining the temperature condition. On ice, the fragmentation master mix was then prepared with the components mentioned in **Table 5.14** and 16.8 µL of the fragmentation master mix was added to each (31.2 µL) purified ss-cDNA sample for a final reaction volume of 48 µL. The reaction mixtures were then incubated following the thermal cycler program in the manufacturer's protocol described in **Table 5.2**. The size analysis of the each fragmented ss-cDNA sample was done as a quality control parameter using a Bioanalyzer (**Figure 5.3**).

For labeling, 45 µL of each fragmented ss-cDNA sample was mixed with 15 µL of labeling master mix, prepared with the components described in **Table 5.15**, for a final reaction volume of 60 µL. The reaction mixtures were then incubated in a thermal cycler using the labeling program provided with the protocol described in **Table 5.2**. All the steps of fragmentation and labeling were performed following the protocol described in the GeneChip WT PLUS kit manual. The fragmented and labeled ss-cDNA were then ready for WT array hybridization.

Table 5.14: Preparation of fragmentation master mix

Component	Volume/Reaction
Nuclease-free water	10 µL
10x cDNA Fragmentation Buffer	4.8 µL
UDG, 10 U/µL	1 µL
APE 1, 1,000 U/µL	1 µL
Total Volume	**16.8 µL**

Table 5.15: Preparation of labeling master mix

Component	Volume/Reaction
5X TdT Buffer	12 µL
DNA Labeling Reagent, 5mM	1 µL
TdT, 30 U/µL	2 µL
Total Volume	**15 µL**

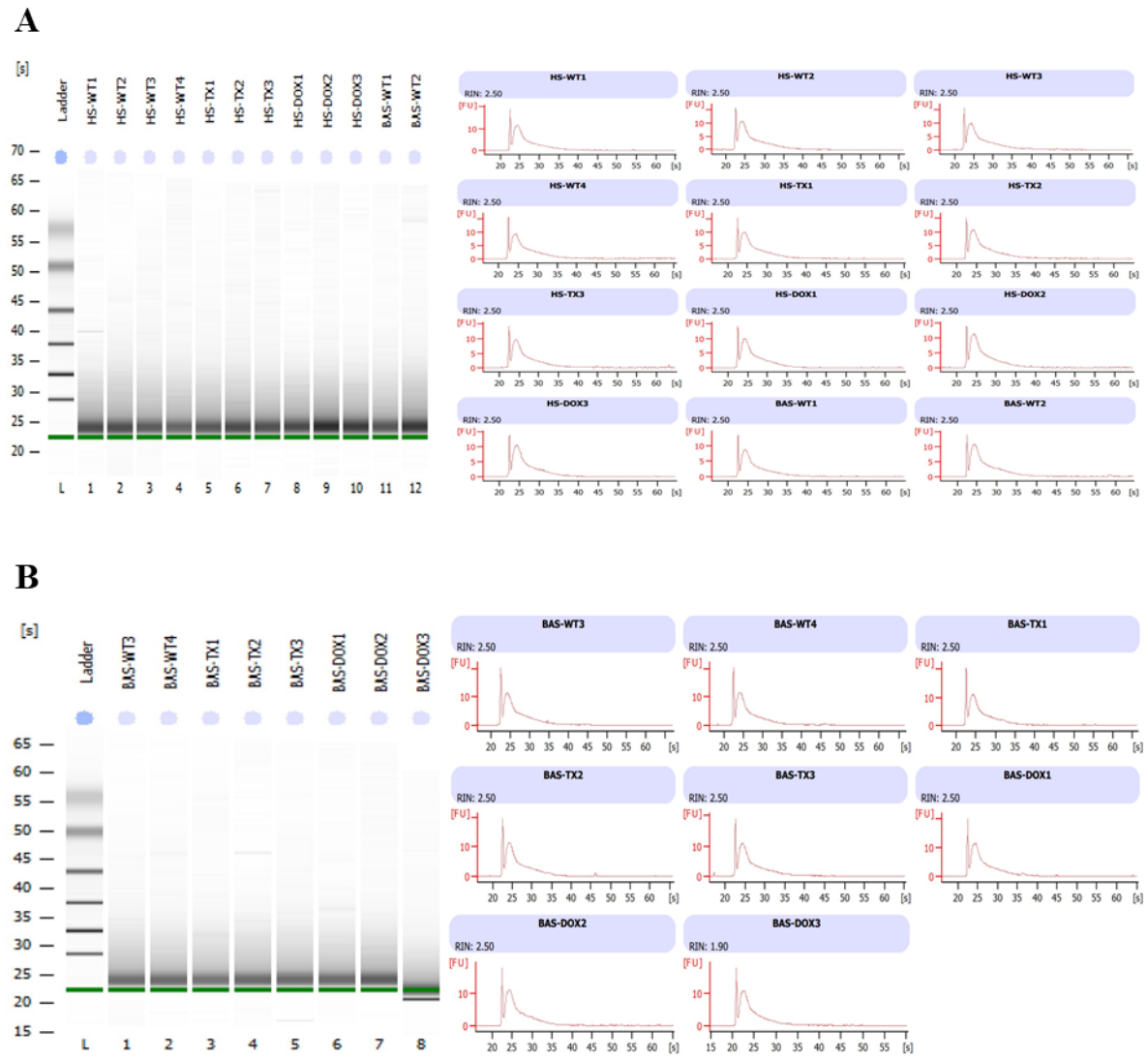


Figure 5.3: Size analysis of fragmented ss-cDNA. Gel electrophoresis (*left*) and electropherogram (*right*) of fragmentated ss-cDNA samples. As there are twelve wells in the Agilent 2100 Bioanalyzer when using the nano chip, the samples were run separately in two different chips with the 12 samples in one chip (A) and the remaining 8 samples in another chip (B). The integrity number of all the samples were 2.5, except BAS-DOX3 in which case it was 1.90, indicating satisfactory fragmentation of each ss-cDNA sample falling within the recommended size distribution limit of 40-70 nt.

5.3.12 Cartridge array hybridization

For hybridization, Clariom S human arrays (Thermo Fisher Scientific) were used (**Figure 5.4**). Briefly, each array was labeled with the name of the sample that will be hybridized, and the sample and the array information were registered into AGCC. The 20X hybridization controls were heated for 5 minutes at 65^0C in a thermal cycler using the hybridization control

program described in **Table 5.2**. The hybridization master mix, appropriate for Clariom S Human array i.e. 169 or 400-format, was prepared for all the samples plus 10% overage with the components mentioned **Table 5.16**, following the prescribed protocol. The hybridization cocktail for 169 or 400-format array prepared by adding hybridization master mix to each fragmentated and biotin-labeled ss-cDNA (**Table 5.17**) and then incubated following the hybridization cocktail program provided in the manufacturer's protocol described in **Table 5.2**. The appropriate amount of each hybridization cocktail sample for 169 or 400-format array (80 µL) was injected into the specific array as registered into AGCC. The arrays were then incubated for 16 hours in the hybridization oven (GeneChip Hybridization Oven 645, P/N 00-0331, Thermo Fisher), which had already been set to temperature 45^0C and RPM 60 according to the manufacturer's protocol.

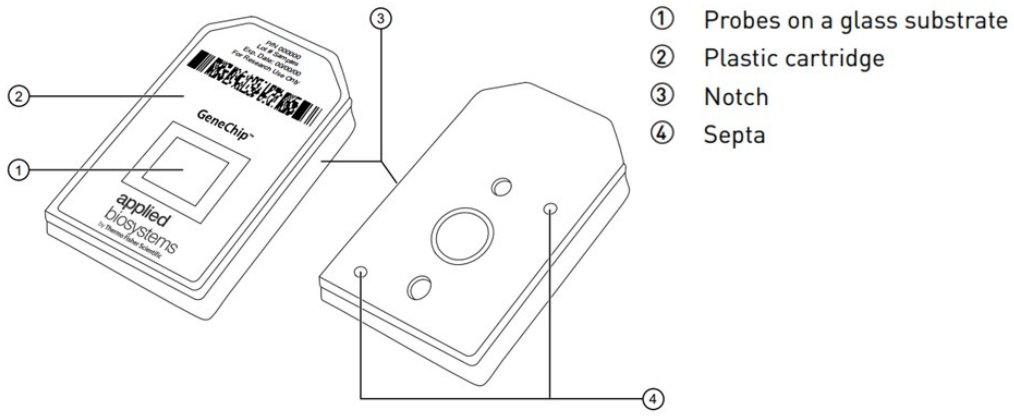


Figure 5.4: Cartridge array. (The figure is taken from whole transcript 169- and 400-format arrays product information sheet, Pub. no. 703133, Rev. 8, Applied Biosystems by Thermo Fisher Scientific)

Table 5.16: Preparation of hybridization master mix for a single reaction

Component	169 or 400-Format	Final Concentration
Fragmented and Labeled ss-cDNA	**2.3 µg**	**23 ng/µL**
Control Oligo B2 (3 nM)	1.7 µL	50 pM
20X Hybridization Controls (*bioB, bioC, bioD, cre*)	5 µL	1.5, 5, 25, and 100 pM respectively
2X Hybridization Mix	50 µL	1X
DMSO	7 µL	7%
Nuclease-free Water	9.3 µL	
Total Volume	**73 µL**	

Table 5.17: Preparation of hybridization cocktail

Component	169 or 400-Format
Hybridization Master Mix	73 µL
Fragmented and Labeled ss-cDNA	27 µL
Total Volume	**100 µL**

5.3.13 Array washing, staining and scanning

All the steps of washing and staining were carried out according to the GeneChip Fluidics Station 450 User Guide AGCC (P/N 08-0295), the GeneChip Expression Wash, Stain, and Scan User Guide for Cartridge Arrays (P/N 702731) using the fluidic protocol recommended for 169 or 400-format array (FS450_0007). Finally, scanning of all the arrays was performed using a GeneChip Scanner 3000 7G System (Thermo Fisher Scientific) according to the manufacturer's instructions.

All the steps of target preparation, array hybridization, washing, staining, and scanning were performed by myself at the Nottingham Arabidopsis Stock Centre (NASC), School of Biosciences, University of Nottingham.

5.3.14 Analysis of array data

Data were acquired as CEL files. Raw CEL files were normalized using RMA background correction with quantile normalization, log base 2 transformation and mean probe-set summarization with adjustment for GC content. The principal component analysis (PCA) revealed the all the arrays were of good quality with the replicates from a given sample clustered together without any outliers (**Figure 5.5)**. Differentially expressed genes were considered significant if p-value with FDR ≤ 0.05 and fold-change >2 or < -2. Microarray data were deposited at the NCBI Gene Expression Omnibus (GEO) (http://ncbi.nlm.nih.gov/geo/) under accession number GSE144113.

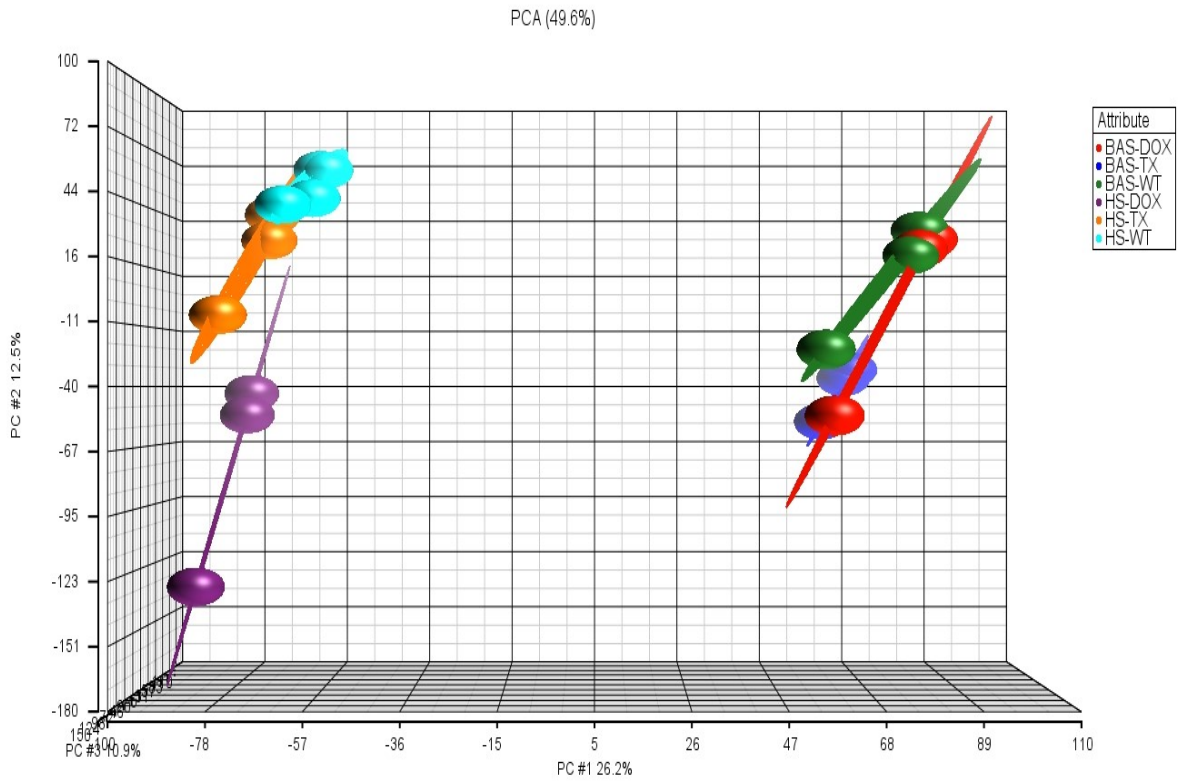


Figure 5.5: Principal component analysis (PCA). PCA plot depicting gene expression patterns of all the samples, comprising replicates of parental HS578T and BAS cells, and their doxorubicin- and paclitaxel-resistant derivatives (HS-DOX and BAS-DOX, and HS-TX and BAS-TX, respectively).

5.3.15 Methodological considerations for the generation of gene expression signatures

The raw data from CEL files were extracted into Excel files in which expression of levels of genes in each drug resistant cell were compared to their corresponding parental cells resulting in a list of differentially expressed genes with their expression values in fold difference for each drug resistant cell model (HS-DOX, HS-TX, BAS-DOX and BAS-TX). This list includes by default a defined cut-off value of >2 for up-regulated and <-2 for down-regulated genes. These individual gene expression signatures were then used to identify common gene expression signatures in respect to drug or cell line involved. Identification of genes whose expression changed in a similar way (that is, both either up-regulated or down-regulated) across the cell lines after made resistant to a particular drug gave rise to doxorubicin-resistant signature (HS578T and BAS cells resistant to doxorubicin) and paclitaxel-resistant signature (HS578T and BAS cells resistant to paclitaxel). Technically, this was achieved through

isolating both either up-regulated or down-regulated gene duplicates between the HS-DOX and BAS-DOX or HS-TX and BAS-TX signatures. Similarly, multidrug resistance gene expression signatures were obtained by identification of common differentially expression up- and down-regulated genes between doxorubicin- and paclitaxel-resistant derivatives of each metaplastic derived cell line. Thus, recognition of both either up- or down-regulated gene duplicates between HS-DOX and HS-TX gene expression signatures resulted in a HS578T cells MDR gene expression signature and the same between BAS-DOX and BAS-TX gene expression signatures yielded to a BAS cells MDR gene expression signature. The average fold expression for each gene was then calculated in all four common signatures to identify the most up-regulated and down-regulated genes.

5.4 Results

5.4.1 MBC derived cells drug resistance gene expression signatures

As the acquisition of drug resistance involves multiple molecular mechanisms or pathways (Lage, 2008; Nedeljković & Damjanović, 2019), I aimed to investigate changes in gene expression associated with drug resistance in MBC derived cell models. Genome-wide transcriptome analyses of doxorubicin- and paclitaxel-resistant derivatives of both metaplastic derived HS578T (HS-DOX and HS-TX) and BAS (BAS-DOX and BAS-TX) cells, with their corresponding parental cells as control, resulted in an identification of over 2 x 10^4 differentially expressed genes in each drug resistant cell model. Filtering these raw data with the threshold set for fold expression greater than 2 (up-regulated genes) and lower than -2 (down-regulated genes) led to identification of significant differentially expressed genes sets representing individual gene expression signatures for HS-DOX, HS-TX, BAS-DOX and BAS-TX cells (**Table 5.18-5.21**). These signatures included 550 up-regulated and 745 down-regulated genes for HS-DOX cells; 114 up-regulated and 63 down-regulated genes for HS-TX cells; 46 up-regulated and 57 down-regulated genes for BAS-DOX cells; and 777 up-regulated and 455 down-regulated genes for BAS-TX cells (**Figure 5.6**).

However, a particular focus was given to the identification of gene expression signatures common for doxorubicin, and paclitaxel resistance across the cell lines, as well as MDR signatures (that is, resistance to both doxorubicin and paclitaxel) for each MBC derived cell line (HS578T and BAS cells). The doxorubicin and paclitaxel resistance gene expression signatures, which represent genes with a similar pattern of expression in resistant cells generated by exposure to each drug in both cells, included a total of 13 (9 up-regulated and 4 down-regulated genes) and 26 (24 up-regulated and 2 down-regulated genes) differentially expressed genes, respectively (**Table 5.22-5.23 and Figure 5.6**). Similarly, a MDR gene expression signature for HS578T cells, representing similar changes in gene expression in both drug resistant HS-DOX and HS-TX cells, comprised 86 differentially expressed genes (52 upregulated and 34 down-regulated genes) (**Table 5.24 and Figure 5.6**). Equally, a MDR gene expression signature was obtained for BAS cells, showing the genes with a similar pattern of expression in both drug resistant BAS-DOX and BAS-TX cells, and this signature included a total of 42 differentially expressed genes (14 up-regulated and 28 down-regulated genes) (**Table 5.25 and Figure 5.6**). Interestingly, no traditional effector of multi-drug resistance was identified in MDR gene expression signatures for both metaplastic derived

HS578T and BAS cells. *ABCB1*, an efflux pump involved in MDR, was slightly up-regulated only in doxorubicin resistant HS-DOX and BAS-DOX cells (2.1-fold and 2.7-fold, respectively). BAS cells MDR gene expression signature was characterized by a significant up-regulation of *TGFB2*, a gene encoding an isoform of well-known EMT inducer cytokine TGF-β. Importantly, there was no signature associated with MDR common to all four MBC derived drug-resistant cells, suggesting that metaplastic derived HS578T and BAS cells acquire MDR phenotype via modulation of expression of different set of genes.

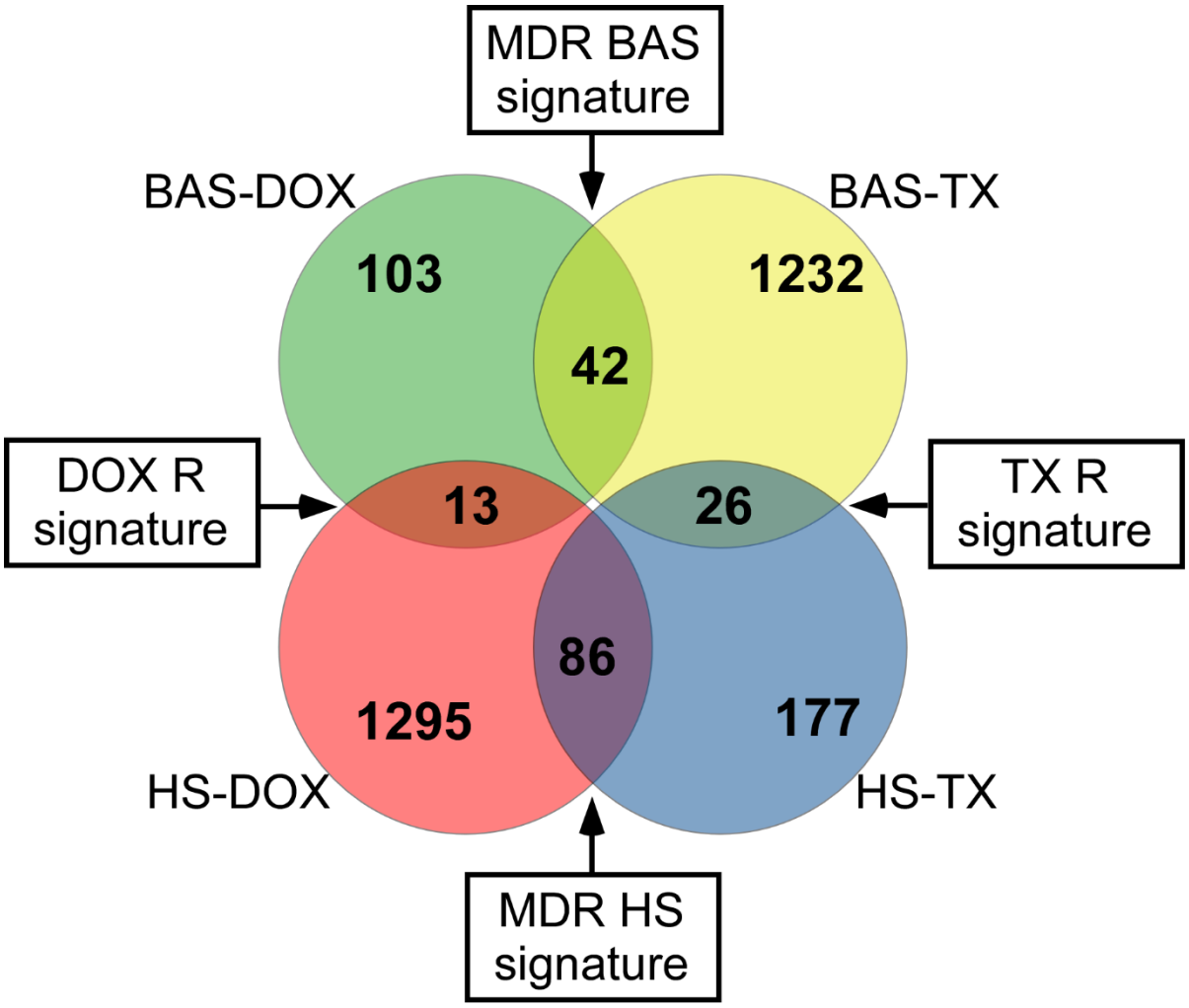


Figure 5.6: Number of differentially regulated genes in each MBC derived drug resistant cell and signature. Genome-wide expression profile of doxorubicin- and paclitaxel-resistant derivatives of metaplastic derived HS578T (HS-DOX and HS-TX) and BAS (BAS-DOX and BAS-TX) cells, compared to their corresponding parental cells, were used to determine the specific signatures.

Table 5.18: Most differentially regulated genes in HS-DOX resistant cells

Gene Symbol	Description	Fold expression[a]
SLC14A1	solute carrier family 14 member 1 (Kidd blood group)	94.5
NPFFR2	neuropeptide FF receptor 2	25.7
MGP	matrix Gla protein	22.7
SPP1	secreted phosphoprotein 1	20.7
GABARAPL1	GABA type A receptor associated protein like 1	18.5
CDH12	cadherin 12	17.2
RHOXF2	Rhox homeobox family member 2	17.0
CST4	cystatin S	16.4
MCTP1	multiple C2 and transmembrane domain containing 1	15.3
RHOXF2B	Rhox homeobox family member 2B	15.2
EDN1	endothelin 1	-8.3
MEST	mesoderm specific transcript	-10.1
LY6E	lymphocyte antigen 6 family member E	-10.2
NRG1	neuregulin 1	-11.2
MYH10	myosin heavy chain 10	-13.2
SLC24A3	solute carrier family 24 member 3	-13.4
ACTG2	actin γ2, smooth muscle	-16.0
ACTA2	actin α2, smooth muscle	-16.6
GPR15	G protein-coupled receptor 15	-20.2
ABI3BP	ABI family member 3 binding protein	-24.5

[a]Positive expression values denote up-regulation and negative expression values denote down-regulation respect to HS578T cells

Table 5.19: Most differentially regulated genes in HS-TX resistant cells

Gene Symbol	Description	Fold expression[a]
CDH12	cadherin 12	7.2
ACKR3	atypical chemokine receptor 3	7.1
CRISPLD1	cysteine rich secretory protein LCCL domain containing 1	6.1
IL1B	interleukin 1β	6.1
CDH8	cadherin 8	5.7
TMPRSS15	transmembrane serine protease 15	5.6
MXRA5	matrix remodeling associated 5	5.1
CNN1	calponin 1	4.9
GASK1B	Golgi associated kinase 1B	4.6
KCNMB1	potassium calcium-activated channel subfamily M regulatory β subunit 1	4.6
GAGE1	G antigen 1	-3.6
GAGE12C	G antigen 12C	-3.7
KRT17	keratin 17	-3.8
GAGE12I	G antigen 12I	-3.8
CREG1	cellular repressor of E1A stimulated genes 1	-3.9
GAGE4	G antigen 4	-4.1
GAGE12D	G antigen 12D	-4.1
GAGE12G	G antigen 12G	-4.1
GAGE12H	G antigen 12H	-4.1
NCAM1	neural cell adhesion molecule 1	-9.8

[a]Positive expression values denote up-regulation and negative expression values denote down-regulation respect to HS578T cells

Table 5.20: Most differentially regulated genes in BAS-DOX resistant cells

Gene Symbol	Description	Fold expression[a]
CCL20	C-C motif chemokine ligand 20	4.2
LEPR	leptin receptor	4.0
PADI3	peptidyl arginine deiminase 3	3.7
SEMA3A	semaphorin 3A	3.7
RNF128	ring finger protein 128	3.6
BRINP3	BMP/retinoic acid inducible neural specific 3	3.3
ADGRF1	adhesion G protein-coupled receptor F1	2.9
TSPAN7	tetraspanin 7	2.9
ABCB1	ATP binding cassette subfamily B member 1	2.7
ANKRD22	ankyrin repeat domain 22	2.6
LRIG1	leucine rich repeats and immunoglobulin like domains 1	2.6
BCAM	basal cell adhesion molecule	-3.7
CDR1	cerebellar degeneration related protein 1	-4.0
GJB2	gap junction protein β2	-4.0
TGM2	transglutaminase 2	-4.2
PDPN	podoplanin	-5.7
KLK5	kallikrein related peptidase 5	-5.7
CHGB	chromogranin B	-5.8
MFAP5	microfibril associated protein 5	-6.4
MEST	mesoderm specific transcript	-6.5
SNRPN	small nuclear ribonucleoprotein polypeptide N	-34.9

[a]Positive expression values denote up-regulation and negative expression values denote down-regulation respect to BAS cells

Table 5.21: Most differentially regulated genes in BAS-TX resistant cells

Gene Symbol	Description	Fold expression[a]
EDIL3	EGF like repeats and discoidin domains 3	84.1
IGFBP7	insulin like growth factor binding protein 7	79.4
TFPI	tissue factor pathway inhibitor	62.8
CLDN1	claudin 1	50.3
ANKRD1	ankyrin repeat domain 1	41.8
SPRY1	sprouty RTK signaling antagonist 1	38.4
SAA2	serum amyloid A2	35.0
PPARGC1A	PPARG coactivator 1α	32.3
GRIA4	glutamate ionotropic receptor AMPA type subunit 4	31.3
NEGR1	neuronal growth regulator 1	30.8
APOD	apolipoprotein D	27.0
RERG	RAS like estrogen regulated growth inhibitor	24.8
ADAM22	ADAM metallopeptidase domain 22	24.2
SRGN	serglycin	24.0
MGP	matrix Gla protein	23.3
TGFB2	transforming growth factor β2	22.0
IGFBP3	insulin like growth factor binding protein 3	22.0
SAA1	serum amyloid A1	19.4
CARD16	caspase recruitment domain family member 16	19.1
SVEP1	sushi, von Willebrand factor type A, EGF and pentraxin domain containing 1	17.7
FBLN1	fibulin 1	17.2
ADM	adrenomedullin	16.5
PLXDC2	plexin domain containing 2	16.4
CPVL	carboxypeptidase vitellogenic like	16.3
SLC46A3	solute carrier family 46 member 3	16.0
CASP1	caspase 1	15.7
ESRP1	epithelial splicing regulatory protein 1	-16.6
FAM83B	family with sequence similarity 83 member B	-18.3
IL1B	interleukin 1β	-18.7
RAB25	RAB25, member RAS oncogene family	-19.0
MPZL2	myelin protein zero like 2	-20.7
S100A14	S100 calcium binding protein A14	-20.8
KRT6C	keratin 6C	-20.9
KRT6A	keratin 6A	-26.6
TP63	tumor protein p63	-42.6
PDPN	podoplanin	-44.5

[a]Positive expression values denote up-regulation and negative expression values denote down-regulation respect to BAS cells

Table 5.22: Differentially regulated genes common between HS-DOX and BAS-DOX resistant cells

Gene Symbol	Description	HS-DOX	BAS-DOX
IL1A	interleukin 1α	6.9[a]	2.0
LEPR	leptin receptor	2.8	4.0
SEMA3A	semaphorin 3A	2.7	3.7
TMC7	transmembrane channel like 7	3.8	2.0
PCYT1B	phosphate cytidylyltransferase 1, choline, β	2.6	2.2
ABCB1	ATP binding cassette subfamily B member 1	2.1	2.7
KLHL13	kelch like family member 13	2.4	2.1
FANK1	fibronectin type III and ankyrin repeat domains 1	2.3	2.1
MAP2	microtubule associated protein 2	2.2	2.0
LOXL1	lysyl oxidase like 1	-2.1	-2.4
KIAA1549L	KIAA1549 like	-2.4	-2.6
TP53I11	tumor protein p53 inducible protein 11	-2.9	-2.3
MEST	mesoderm specific transcript	-10.1	-6.5

[a]Positive expression values denote up-regulation and negative expression values denote down-regulation respect to drug sensitive cells

Table 5.23: Differentially regulated genes common between HS-TX and BAS-TX resistant cells

Gene Symbol	Description	HS-TX	BAS-TX
MGP	matrix Gla protein	4.4[a]	23.3
RERG	RAS like estrogen regulated growth inhibitor	2.1	24.8
CARD16	caspase recruitment domain family member 16	2.4	19.1
PLXDC2	plexin domain containing 2	2.3	16.4
ACTA2	actin α2, smooth muscle	2.1	8.1
ACKR3	atypical chemokine receptor 3	7.1	2.0
MXRA5	matrix remodeling associated 5	5.1	3.1
BGN	biglycan	2.4	5.7
GABARAPL1	GABA type A receptor associated protein like 1	2.4	4.9
ARHGAP24	Rho GTPase activating protein 24	2.4	4.9
GASK1B	Golgi associated kinase 1B	4.6	2.3
VGLL3	vestigial like family member 3	2.1	4.4
KITLG	KIT ligand	2.2	3.9
ICAM1	intercellular adhesion molecule 1	2.2	3.7
NPR3	natriuretic peptide receptor 3	3.0	2.8
BDNF	brain derived neurotrophic factor	2.2	3.5
CCL2	C-C motif chemokine ligand 2	2.9	2.5
GAREM1	GRB2 associated regulator of MAPK1 subtype 1	3.1	2.3
PLCB1	phospholipase C β1	3.3	2.1
SYT11	synaptotagmin 11	3.1	2.0
DMD	dystrophin	2.2	2.6
ARMCX2	armadillo repeat containing X-linked 2	2.5	2.3
ARHGAP20	Rho GTPase activating protein 20	2.4	2.0
SLC7A2	solute carrier family 7 member 2	2.2	2.1
CCNG2	cyclin G2	-2.2	-2.6
KRT17	keratin 17	-3.8	-2.7

[a]Positive expression values denote up-regulation and negative expression values denote down-regulation respect to drug sensitive cells

Table 5.24: Differentially regulated genes common between HS-DOX and HS-TX resistant cells

Gene Symbol	Description	HS-DOX	HS-TX
MGP	matrix Gla protein	22.7 [a]	4.4
CDH12	cadherin 12	17.2	7.2
CRISPLD1	cysteine rich secretory protein LCCL domain containing 1	14.9	6.1
GABARAPL1	GABA type A receptor associated protein like 1	18.5	2.4
MXRA5	matrix remodeling associated 5	15.1	5.1
CST1	cystatin SN	15.1	2.1
IL1B	interleukin 1β	10.8	6.1
SELL	selectin L	11.7	3.3
ACKR3	atypical chemokine receptor 3	7.8	7.1
KLHL4	kelch like family member 4	9.8	2.8
CCND2	cyclin D2	6.1	4.3
FAM198B	family with sequence similarity 198 member B	5.2	4.6
CT83	cancer/testis antigen 83	4.6	3.7
FYB	FYN binding protein	5.3	2.7
NFIA	nuclear factor I A	5.6	2.4
PLCB1	phospholipase C β1	4.6	3.3
TMPRSS15	transmembrane protease, serine 15	2.2	5.6
APOL1	apolipoprotein L1	5.0	2.8
RERG	RAS like estrogen regulated growth inhibitor	5.6	2.1
CREB5	cAMP responsive element binding protein 5	4.5	3.2
TNFAIP6	TNFα induced protein 6	5.1	2.4
ARHGAP24	Rho GTPase activating protein 24	4.9	2.4
CCL2	C-C motif chemokine ligand 2	4.3	2.9
STRA6	stimulated by retinoic acid 6	4.0	3.2
ABCA1	ATP binding cassette subfamily A member 1	4.7	2.4
PAGE2B	PAGE family member 2B	4.9	2.1
PTGS2	prostaglandin-endoperoxide synthase 2	2.7	4.2
PAPSS2	3'-phosphoadenosine 5'-phosphosulfate synthase 2	4.9	2.1
MYEOV	myeloma overexpressed	3.2	3.1
RAB36	RAB36, member RAS oncogene family	4.2	2.1
CARD16	caspase recruitment domain family member 16	3.8	2.4
WDR72	WD repeat domain 72	2.1	4.0
RAC2	rac family small GTPase 2	3.4	2.4
PKIB	protein kinase (cAMP-dependent, catalytic) inhibitor β	3.6	2.2
LCP1	lymphocyte cytosolic protein 1	2.8	2.7
FLRT3	fibronectin leucine rich transmembrane protein 3	3.2	2.3
TGM2	transglutaminase 2	3.3	2.1
PAGE2	PAGE family member 2	3.0	2.3
GAREM1	GRB2 associated regulator of MAPK1 subtype 1	2.1	3.1
TNFRSF11B	TNF receptor superfamily member 11b	2.8	2.2
TRPC4	transient receptor potential cation channel subfamily C member 4	2.4	2.6
ARMCX2	armadillo repeat containing, X-linked 2	2.4	2.5
FZD8	frizzled class receptor 8	2.5	2.2

[a]Positive expression values denote up-regulation and negative expression values denote down-regulation respect to HS578T cells

Table 5.24: Differentially regulated genes common between HS-DOX and HS-TX resistant cells (Contd.)

Gene Symbol	Description	HS-DOX	HS-TX
LMO2	LIM domain only 2	2.3[a]	2.4
F2RL1	F2R like trypsin receptor 1	2.3	2.3
KITLG	KIT ligand	2.3	2.2
SRPX2	sushi repeat containing protein, X-linked 2	2.0	2.4
ERG	ETS transcription factor ERG	2.1	2.3
PTGIS	prostaglandin I2 synthase	2.1	2.3
FIBIN	fin bud initiation factor homolog (zebrafish)	2.1	2.2
C7	complement C7	2.2	2.1
MSRB2	methionine sulfoxide reductase B2	2.0	2.1
TAF11	TATA-box binding protein associated factor 11	-2.1	-2.0
CPM	carboxypeptidase M	-2.2	-2.0
HMCES	5-hydroxymethylcytosine (hmC) binding, ES cell-specific	-2.4	-2.1
SNRNP48	small nuclear ribonucleoprotein U11/U12 subunit 48	-2.5	-2.1
RPP40	ribonuclease P/MRP subunit p40	-2.7	-2.0
GCNT2	glucosaminyl (N-acetyl) transferase 2, I-branching enzyme	-2.4	-2.5
CENPA	centromere protein A	-2.9	-2.1
GEN1	Holliday junction 5' flap endonuclease	-2.7	-2.4
FZD7	frizzled class receptor 7	-3.1	-2.4
MMP13	matrix metallopeptidase 13	-2.9	-2.6
PLAU	plasminogen activator, urokinase	-2.7	-2.8
RUNX2	runt related transcription factor 2	-3.3	-2.3
TNFSF10	tumor necrosis factor superfamily member 10	-3.3	-2.5
BNIP3	BCL2 interacting protein 3	-3.8	-2.1
PSG5	pregnancy specific β-1-glycoprotein 5	-3.5	-2.8
GAGE10	G antigen 10	-3.6	-2.7
POLH	DNA polymerase η	-4.5	-2.2
CDKN3	cyclin dependent kinase inhibitor 3	-4.6	-2.1
GAGE2B	G antigen 2B	-3.9	-2.9
OLFML3	olfactomedin like 3	-4.1	-2.9
GAGE1	G antigen 1	-4.3	-3.6
MICB	MHC class I polypeptide-related sequence B	-5.2	-2.8
KRT17	keratin 17	-4.5	-3.8
GAGE2D	G antigen 2D	-4.9	-3.5
GAGE12F	G antigen 12F	-5.3	-3.2
GAGE12C	G antigen 12C	-4.9	-3.7
KIFC1	kinesin family member C1	-7.7	-2.0
SDC1	syndecan 1	-7.8	-2.0
EDN1	endothelin 1	-8.3	-2.2
GAGE4	G antigen 4	-7.0	-4.1
GAGE12I	G antigen 12I	-7.3	-3.8
GAGE12D	G antigen 12D	-7.2	-4.1
GAGE12G	G antigen 12G	-7.2	-4.1
GAGE12H	G antigen 12H	-7.2	-4.1

[a]Positive expression values denote up-regulation and negative expression values denote down-regulation respect to HS578T cells

Table 5.25: Differentially regulated genes common between BAS-DOX and BAS-TX resistant cells

Gene Symbol	Description	BAS-DOX	BAS-TX
TGFB2	transforming growth factor β2	2.3[a]	22.0
CLYBL	citrate lyase β-like	2.1	10.7
LRIG1	leucine rich repeats and immunoglobulin like domains 1	2.6	9.1
SLC25A40	solute carrier family 25 member 40	2.1	9.3
LEPR	leptin receptor	4.0	6.0
TSPAN7	tetraspanin 7	2.9	6.2
PADI3	peptidyl arginine deiminase 3	2.9	5.9
ADAM12	ADAM metallopeptidase domain 12	2.0	6.4
TTLL7	tubulin tyrosine ligase like 7	2.2	6.2
CACNA2D1	calcium voltage-gated channel auxiliary subunit α2 δ1	2.5	5.4
MAP2	microtubule associated protein 2	2.0	5.2
ROR1	receptor tyrosine kinase like orphan receptor 1	2.2	3.0
IFNE	interferon epsilon	2.4	2.5
RHOF	ras homolog family member F, filopodia associated	-2.0	-2.1
NTM	neurotrimin	-2.0	-2.4
STMN3	stathmin 3	-2.1	-2.6
IGFBP6	insulin like growth factor binding protein 6	-2.0	-2.7
AQP3	aquaporin 3	-2.2	-2.5
CDH11	cadherin 11	-2.5	-2.2
HES7	hes family bHLH transcription factor 7	-2.3	-2.8
SLC16A9	solute carrier family 16 member 9	-2.6	-2.5
TP53I11	tumor protein p53 inducible protein 11	-2.3	-3.0
CTSV	cathepsin V	-2.2	-3.4
CDH4	cadherin 4	-2.6	-3.2
BID	BH3 interacting domain death agonist	-3.6	-2.6
TGM2	transglutaminase 2	-4.2	-2.6
XG	Xg blood group	-3.6	-4.2
KCNG1	potassium voltage-gated channel modifier subfamily G member 1	-3.2	-5.1
BCAM	basal cell adhesion molecule	-3.7	-4.7
FAM110C	family with sequence similarity 110 member C	-2.5	-5.9
MEST	mesoderm specific transcript	-6.5	-3.0
GJB2	gap junction protein β2	-4.0	-5.7
CHGB	chromogranin B	-5.8	-4.2
MCF2	MCF.2 cell line derived transforming sequence	-2.5	-8.5
ATP8A2	ATPase phospholipid transporting 8A2	-2.9	-9.5
MFAP5	microfibrillar associated protein 5	-6.4	-9.7
NTSR1	neurotensin receptor 1	-2.5	-13.8
PLTP	phospholipid transfer protein	-2.3	-14.7
KLK5	kallikrein related peptidase 5	-5.7	-14.7
KRT6A	keratin 6A	-2.1	-26.6
PDPN	podoplanin	-5.7	-44.5

[a]Positive expression values denote up-regulation and negative expression values denote down-regulation respect to BAS cells

5.4.2 Metaplastic derived HS578T and BAS cells acquire a MDR phenotype via common cancer hallmarks

Cancer hallmarks show the biological capabilities acquired by the cancer cells during the multistep development of tumours (Hanahan & Weinberg, 2011). Identification of cancer hallmarks is important for cancer research, and the participatory genes in cancer hallmarks are likely to be cancer drivers (Yu, Huang & Zhou, 2019) and thus provide essential information about targets identification for new chemotherapeutics development as well as overcoming drug resistance. To obtain a clear functional picture of each drug resistant gene expression signature (doxorubicin resistance, paclitaxel resistance, HS578T cells MDR, and BAS cells MDR signatures), I interrogated the molecular signature database hallmark gene set collection (Liberzon *et al.*, 2015). The gene set enrichment analysis (GSEA) of each signature genes involvement in relevant hallmarks identified several statistically significant key cancer hallmarks (**Figure 5.7**). Both HS578T and BAS cells MDR gene signatures showed common hallmarks such as EMT and apoptosis, among others (**Figure 5.7 A and B**). Paclitaxel resistance gene signature was found to be involved with EMT, TNFα-NF-κB signalling, inflammatory response and hypoxia hallmarks (**Figure 5.7 C**), although doxorubicin resistance gene signature did not show any statistically significant hallmarks probably due to its small number of genes. Thus, metaplastic derived HS578T and BAS cells acquire MDR phenotype via common hallmarks, although different individual genes.

The key hallmarks were then investigated for individual genes involved from GSEA of each drug resistance signature. Many genes were found to be overlapped with those in the molecular signature database hallmark gene set collection (Liberzon *et al.*, 2015) and involved in different hallmarks (**Table 5.26-5.28**).

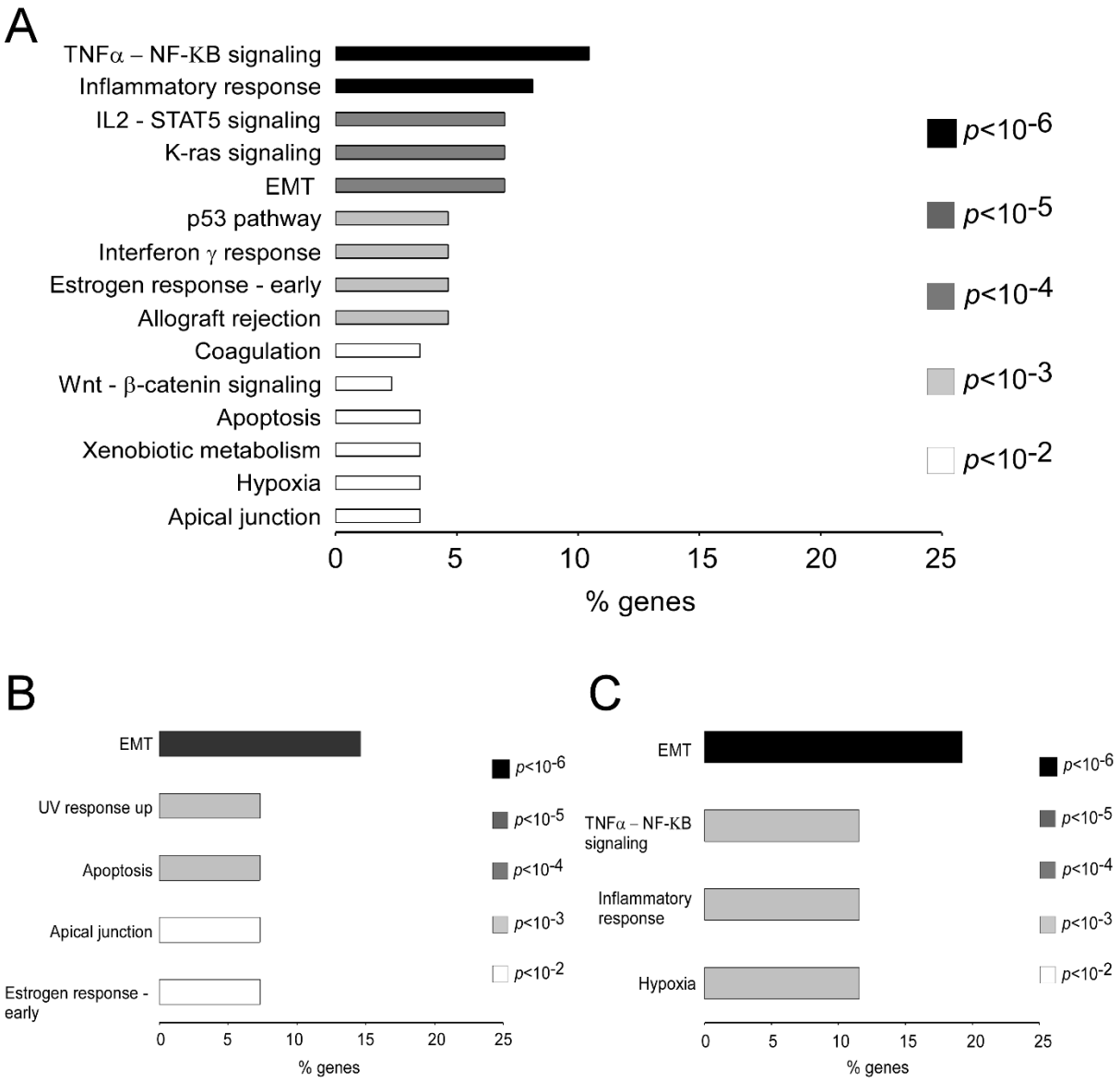


Figure 5.7: A similar set of hallmarks define the signatures associated with metaplastic breast cancer derived MDR cells. Gene expression signatures obtained from the genome-wide expression profiling of metaplastic breast cancer derived drug resistant cells (**Table 5.22-5.25**) were compared to the molecular signature database hallmark gene set collection to identify the involvement of genes in each signature with the key cancer hallmarks. A, Hallmarks in HS578T MDR signature. B, Hallmarks in BAS MDR signatures. C, Hallmarks in paclitaxel resistance signature. Length of histogram bar is proportional to the percentage of genes in the signature (x-axis) associated with a particular hallmark (indicated to the left). Hallmarks are ordered by significance, with the highest significant values on top.

Table 5.26: Gene/gene set overlap matrix for HS578T MDR gene expression signature

Entrez gene ID	Gene symbol	TNFα-NFκB signalling	Inflammatory response	IL2-STAT5 signalling	EMT	K-ras signalling up	Allograft rejection	Estrogen response early	Interferon γ response	p53 pathway	Coagulation	Wnt-β-catenin signalling	Apoptosis	Apical junction	Hypoxia	Xenobiotic metabolism
3553	*IL1B*	■	■			■	■						■			
6347	*CCL2*	■	■				■		■							
7130	*TNFAIP6*	■	■						■							
19	*ABCA1*	■	■													
1906	*EDN1*	■	■													
5743	*PTGS2*	■				■			■							
5328	*PLAU*	■				■					■					
2150	*F2RL1*	■				■										
57007	*ACKR3*	■													■	
8743	*TNFSF10*		■	■					■				■			
6402	*SELL*		■	■												
7052	*TGM2*			■	■			■							■	
894	*CCND2*			■		■	■			■		■	■			
2151	*F2RL2*			■							■					
23710	*GABARAPL1*			■												■
6382	*SDC1*				■					■						
8325	*FZD8*				■							■				
4982	*TNFRSF11B*				■									■		
25878	*MXRA5*				■											
4256	*MGP*				■											
3936	*LCP1*					■										
2533	*FYB1*						■							■		
9060	*PAPSS2*							■								■
4277	*MICB*							■								
56944	*OLFML3*							■								
5429	*POLH*									■						
3872	*KRT17*									■						
22921	*MSRB2*										■					
5880	*RAC2*													■		
2651	*GCNT2*														■	■

Table 5.27: Gene/gene set overlap matrix for BAS MDR gene expression signature

Entrez gene ID	Gene Symbol	EMT	UV response up	Apoptosis	Apical junction	Estrogen response early
1009	*CDH11*	■			■	
7052	*TGM2*	■				■
4232	*MEST*	■				
8038	*ADAM12*	■				
50863	*NTM*	■				
8076	*MFAP5*	■				
637	*BID*		■	■		
360	*AQP3*		■			■
1515	*CTSV*		■			
7042	*TGFB2*			■		
3489	*IGFBP6*			■		
54509	*RHOF*				■	
1002	*CDH4*				■	
26018	*LRIG1*					■

Table 5.28: Gene/gene set overlap matrix for paclitaxel resistance gene expression signature

Entrez gene ID	Gene symbol	EMT	Hypoxia	Inflammatory response	TNFα-NFκB signalling
633	*BGN*	■	■		
627	*BDNF*	■			
25878	*MXRA5*	■			
4256	*MGP*	■			
59	*ACTA2*	■			
57007	*ACKR3*		■		■
901	*CCNG2*		■		
3383	*ICAM1*			■	■
6347	*CCL2*			■	■
6542	*SLC7A2*			■	

5.4.3 Inhibition of TGF-β pathway re-sensitizes MDR BAS cells to doxorubicin and paclitaxel

Genome-wide expression analysis identified *TGFB2* as one of the most up-regulated genes in MDR BAS cells (2.3-fold in BAS-DOX and 22-fold in BAS-TX resistant cells). Reassuringly, RT-QPCR analysis confirmed up-regulation of *TGFB2* in BAS-DOX or BAS-TX cells (**Figure 5.8 A**). *TGFB2* encodes an isoform of TGF-β, a cytokine found to play pivotal roles in promoting tumour growth and cancer cell invasion, metastatic dissemination, and distal metastasis (Massagué, 2008). Interestingly, a study shows that treatment with TGF-β in Namru murine mammary gland cells leads to up-regulation of *Foxc1* mRNA levels via SMAD-dependent pathway (Hopkins, Coatham & Berry, 2017). To ascertain the roles of TGF-β pathway in acquisition of chemotherapeutic resistance in MDR BAS cells, I used an inhibitor of type I TGF-β receptor (TβR-I), galunisertib, which is in clinical trials for several different cancers, including pancreatic cancer, glioblastoma, and hepatocellular carcinoma (Akhurst & Hata, 2012; Herbertz *et al.*, 2015). Reassuringly, galunisertib treatment in both BAS-DOX and BAS-TX cells was found to cause down-regulation of FOXC1, both at mRNA (**Figure 5.8 B**) and protein levels (**Figure 5.8 C**). Importantly, galunisertib treatment (at the concentrations non-toxic to cells, 5-10 μM) led to increase in sensitivity to doxorubicin (by approximately 35-40%) and to paclitaxel (by approximately 25%) in BAS-DOX and BAS-TX resistant cells, respectively (**Figure 5.8 D and E**). Thus, inhibition of the TGF-β pathway in MDR BAS cells led to increase in drug sensitivity, with down-regulation of FOXC1, an MDR regulator in metaplastic breast cancer derived BAS cells that I have identified in **chapter 4**.

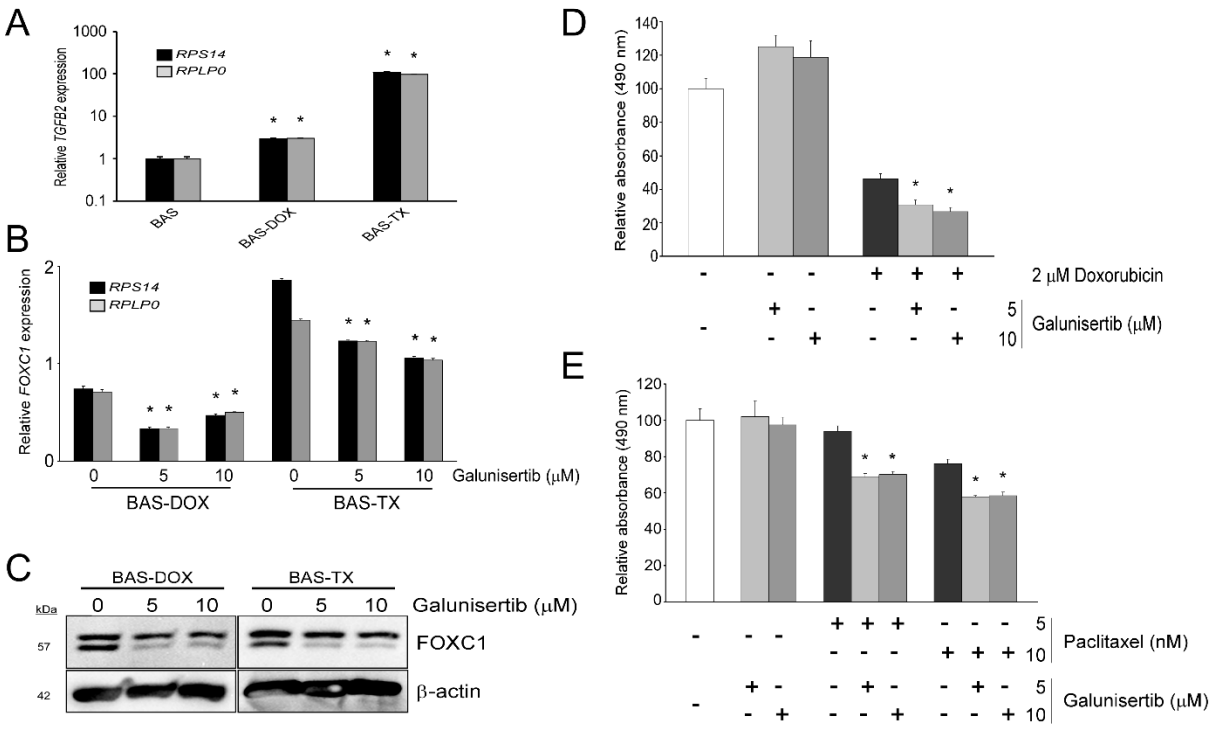


Figure 5.8: Galunisertib re-sensitizes metaplastic breast cancer derived drug resistant cells to doxorubicin and paclitaxel. A, Quantitative real-time PCR analysis of *TGFB2* expression in BAS-DOX and BAS-TX drug resistant cells. The mRNA levels were normalized to the *RPS14* and *RPLP0* genes. The relative expression was calculated with respect to parental BAS cells. B, Quantitative real-time PCR analysis of FOXC1 expression in BAS-DOX and BAS-TX drug resistant cells after treatment with galunisertib for 5 days. The relative mRNA levels were calculated by normalization to the *RPS14* and *RPLP0* genes. C, Western blot analysis of FOXC1 expression in BAS-DOX and BAS-TX drug resistant cells after treatment with galunisertib for 5 days. The analysis was performed with whole cell lysates and β-actin was used as a control for protein loading. Molecular masses of relevant bands are indicated in kDa. FOXC1 protein can be detected as two bands with molecular masses very close to 57 kDa (top band: phosphorylated FOXC1; bottom band: non-phosphorylated FOXC1). D-E, Drug sensitivity determined by sulphorhodamine B assays of BAS-DOX (D) and BAS-TX (E) drug resistant cells treated with doxorubicin, paclitaxel, and galunisertib. The galunisertib treatment was for 5 days. Doxorubicin and paclitaxel treatment was for 3 days, starting at day 2. The optical density (OD) was measured at 490 nm after solubilization of protein bound sulphorhodamine B stain. The relative absorbance was calculated by normalization to the respective control x100. Pictorial data show representatives of at least triplicate independent experiments. Numerical data represent the average ± SD of three independent experiments (* P<0.05).

5.4.4 Inhibition of TGF-β pathways reduces motility of MDR BAS cells

As TGF-β is a well-known EMT inducer and found to be involved in stemness (Shirakihara *et al.*, 2011; Mani *et al.*, 2008), I aimed to assess if any changes in cellular motility, a phenotype arising in cells undergoing EMT, and anchorage-independent growth capacity, an *in vitro* surrogate for stemness and phenotype of CSCs, due to inhibition of TGF-β pathway in both MDR BAS cells (BAS-DOX and BAS-TX cells). Scratch assays for cellular motility *in vitro* indicated the galunisertib treatment led to a robust decrease in motility of both BAS-DOX and BAS-TX cells (**Figure 5.9 A**). In fact, a very small closure of scratch gap (only approximately 20-30%) was observed with galunisertib treatment (5-10 μM) in both BAS-DOX and BAS-TX drug resistant cells after 72 hours, whereas there was almost complete closure of scratch gap (approximately 80%) with these drug resistant cells in absence of galunisertib. This suggests that inhibition of TGF-β pathway in metaplastic breast cancer derived MDR cells strongly affects their motility. In line with this phenotypic alteration, QPCR analyses indicated significant down-regulation of EMT-related transcription factors in both BAS-DOX and BAS-TX drug resistant cells after galunisertib treatment (**Figure 5.9 B**). The transcription factors *ZEB1* and *ZEB2* were down-regulated in both BAS-DOX and BAS-TX cells, although *SNAI1* and *SNAI2* were only down-regulated in BAS-DOX cells. Interestingly, mesenchymal marker *VIM* was down-regulated in both BAS-DOX and BAS-TX cells with galunisertib treatment. However, galunisertib treatment did not cause decrease in anchorage-independent growth capacity as observed in the mammosphere forming ability in liquid culture using ultra-low attachment plates. Indeed, both BAS-DOX and BAS-TX cells showed a small increase in mammosphere forming capacity with galunisertib treatment (**Figure 5.9 C**). Similarly, interrogation of CSC markers by QPCR analyses revealed their up-regulation in BAS-DOX and BAS-TX cells after galunisertib treatment. The CSC marker *POU5F1* was up-regulated in both BAS-DOX and BAS-TX cells, although *NONOG* and *SOX2* were only up-regulated in BAS-TX cells (**Figure 5.9 B**). Overall, inhibition of TGF-β pathway in metaplastic breast cancer derived MDR cells by galunisertib treatment led to down-regulation of EMT molecular markers and decrease in motility, a phenotype acquired by EMT, but to an increase in anchorage independence.

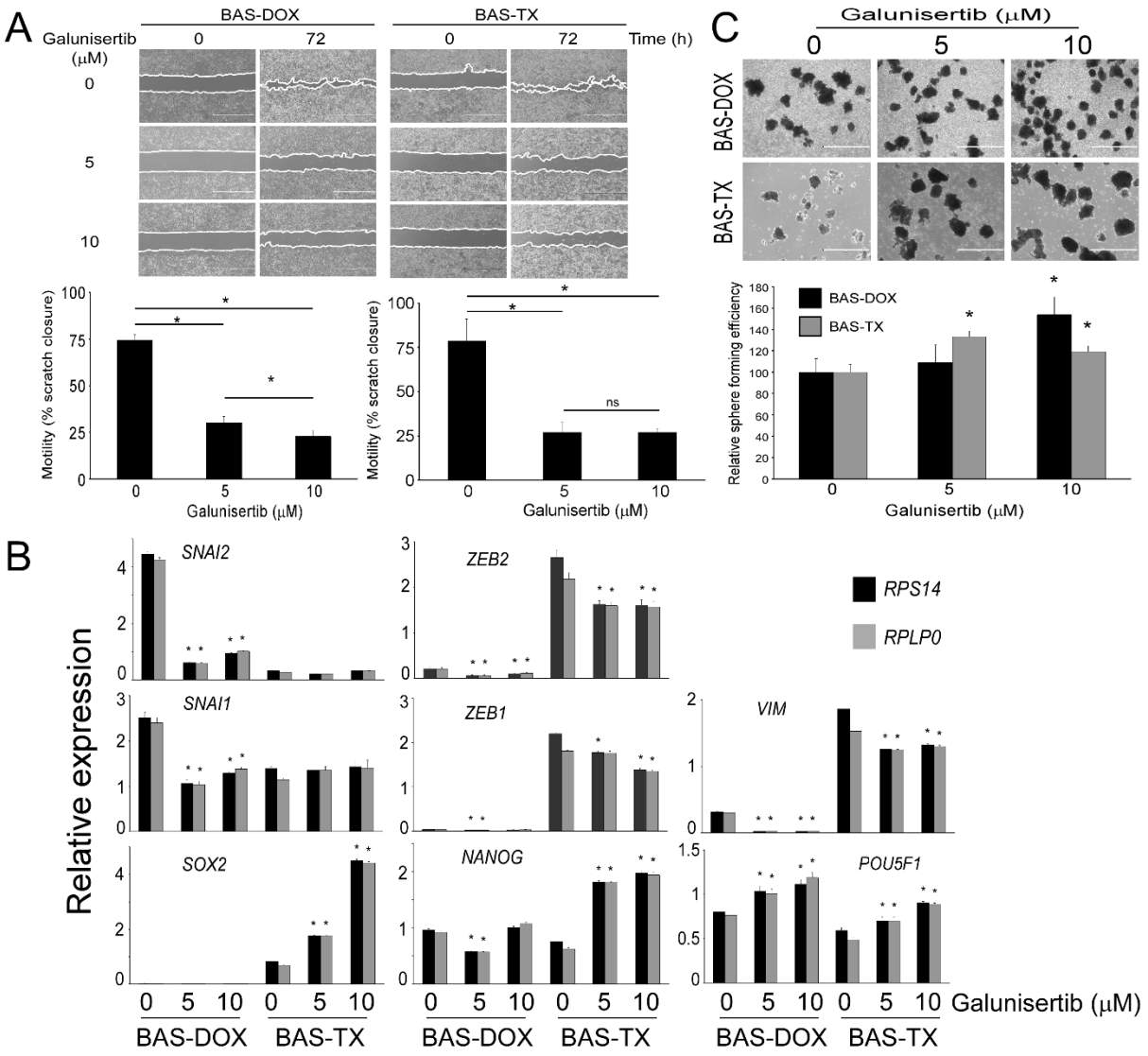


Figure 5.9: Galunisertib inhibits motility of metaplastic breast cancer derived MDR cells. A, Scratch assay was employed to assess the motility of BAS-DOX and BAS-TX drug resistant cells. Cells were pre-treated with galunisertib for 48 hours before the plates were scratched. Scratch gap closure after 72 hours, always in the presence of inhibitor, were determined from the pictures using Image J software. Control cells were always inhibitor-free. B, Quantitative real-time PCR analyses of selected EMT and CSC markers in BAS-DOX and BAS-TX cells after treatment with galunisertib for 5 days. The relative mRNA levels were calculated by normalization to the *RPS14* and *RPLP0* genes. C, Mammosphere formation in liquid culture was used to assess the anchorage independent growth, a phenotype of CSCs, of BAS-DOX and BAS-TX cells. Cells (4 x 10^3 / well) were seeded in 6-well low-attachment plates with appropriate culture medium and the spheres larger than 100 μm in diameter were counted after two weeks of culture with continuous presence of galunisertib. The relative sphere forming efficiency calculated by normalization to the inhibitor-free control x100. Pictorial data are representatives of at least three independent experiments. Numerical data represent the average ± SD of three independent experiments (* P<0.05). Bar represents 1000 μm.

5.5 Discussion

5.5.1 MDR phenotype in metaplastic breast cancer derived cells is multi-factorial

MDR poses a significant treatment challenge in the management of cancer patients, and is classified into two broad types, one acquired during treatment and other intrinsic resistance (Baguley, 2010). Cellular model of drug resistance provides us the opportunity not only to identify the down-stream effectors of chemotherapy resistance, but also their up-stream regulators. With genome-wide expression analyses of doxorubicin- and paclitaxel-resistant derivatives of two MBC derived cell lines, I have identified gene expression signatures common for doxorubicin, and paclitaxel resistance across the cell lines, as well as MDR signatures (that is, involved in resistance to both doxorubicin and paclitaxel) for each MBC derived cell line.

Doxorubicin resistance signature for MBC derived cells includes many genes reported to be involved in poor prognosis and chemotherapy resistance in several different carcinomas, including different subtypes of breast cancer. Among the upregulated genes, *IL1A* has been reported to be associated with poor prognosis in breast cancer (Snoussi *et al.*, 2005). Moreover, *IL1A* is associated with chemotherapy resistance in HER2-overexppressed breast cancer (Liu *et al.*, 2018b) and cisplatin resistance in gastric carcinoma (Xuan & Wang, 2017). *LEPR* promotes EMT and stemness in TNBC cells (Zheng *et al.*, 2013) and collaborates with *IL1A* to promote tumour growth and cachexia as evidenced in a luminal breast cancer xenograft model (Kumar *et al.*, 2003). The P-glycoprotein membrane transporter, *ABCB1*, is responsible for cross resistance to many different chemotherapeutics, including doxorubicin, paclitaxel, 5-FU, and carboplatin, in breast cancer cells (Oba, Izumi & Ito, 2016; Tang *et al.*, 2015). However, it is important to note that *ABCB1* was only up-regulated by 2.1-fold and 2.7-fold in doxorubicin resistant derivatives of HS578T and BAS cells, respectively. Moreover, *ABCB1* mRNA is subjected to translational regulation as a consequence of a stem loop in its 5'-end region (Randle *et al.*, 2007), suggesting that these small changes in mRNA expression levels in the drug resistant cells are less likely to produce a physiological drug efflux, as a potential cause of chemotherapeutic resistance. On the other hand, *TP53I11*, a down-regulated gene in doxorubicin resistance signature, is a tumour suppressor and a negative regulator of EMT and metastasis in breast cancer cells (Xiao *et al.*, 2019).

Similarly, accumulated evidence indicated that many up-regulated genes in the paclitaxel resistance signature for MBC derived cells are involved in EMT, drug resistance and poor

prognosis in disparate cancer types. *MGP* and *PLXDC2* are also up-regulated in paclitaxel resistant ovarian carcinoma (Sterzyńska *et al.*, 2018; Wang & Li, 2018). Moreover, MGP is reported to be a potential prognostic marker in breast cancer, with higher expression in patients with worse prognosis (Yoshimura *et al.*, 2009). *MXRA5* has been considered as a drug resistant genetic signature in epithelial ovarian carcinoma (Hyter *et al.*, 2018). Interestingly, higher expression of *ACTA2, ACKR3, GABARAPL1, ICAM1*, and *BDNF* genes is associated with poor prognosis in breast cancer (Nurmik *et al.*, 2020; Fan *et al.*, 2018; Ran *et al.*, 2017; Schröder *et al.*, 2011; Patani, Jiang & Mokbel, 2011). In addition, *ACKR3* is a biomarker of anti-androgen therapy resistance in prostate cancer (Li *et al.*, 2019c) and *ICAM1* expression correlates with MDR phenotype in multiple myeloma (Schmidmaier *et al.*, 2006). *BGN* is involved with chemotherapy resistance in colon cancer by activating *NF-kB* (Liu *et al.*, 2018a) and its higher expression is associated with poor prognosis in prostate cancer (Jacobsen *et al.*, 2017) as well as in oesophageal squamous cell carcinoma (Zhu *et al.*, 2013). *CCL2* promotes breast cancer metastasis (Kitamura *et al.*, 2015) and is a key contributor to cabazitaxel resistance in prostate cancer cells (Natsagdorj *et al.*, 2019) and to docetaxel resistance in lung cancer cells (Wang *et al.*, 2018c). Up-regulation of *PLCB1* is associated with proliferation and poor prognosis in hepatocellular carcinoma (Li *et al.*, 2016b) and with metastatic relapse in breast cancer (Sengelaub *et al.*, 2016). Among the downregulated genes in paclitaxel resistance signature, *CCNG2* is a negative regulator cancer aggressiveness, as expression of this gene inhibits EMT induction by disrupting Wnt/β-catenin signalling pathway in epithelial ovarian carcinoma (Bernaudo *et al.*, 2016). Moreover, low expression of *CCNG2* is found to be associated with poor prognosis in breast cancer (Zimmermann *et al.*, 2016).

Interestingly, several up-regulated genes in the MDR signature for HS578T cells, including *GABARAPL1, CST1, IL1B, SELL, ACKR3* and *FYB*, are involved in progression and metastasis of different subtypes of breast carcinoma (Ran *et al.*, 2017; Dai *et al.*, 2017; Tulotta & Ottewell, 2018; Natoni, Macauley & O'Dwyer, 2016; Neves *et al.*, 2019; Song *et al.*, 2020). A homologue of *CRISPLD1* is associated with prostate cancer progression (Gibbs, Roelants & O'Bryan, 2008). *MGP* and *ACKR3* have already been described to be responsible for chemotherapy resistant in ovarian and prostate cancers, respectively. A high number of different G-antigens were down-regulated in both drug resistant HS578T cells, indicating that they might help to avoid immune attack, as their over-expression elicits a cellular and humoral immune response (Gjerstorff & Ditzel, 2008). Moreover, downregulation of *SDC1* is

responsible for EMT and its expression after chemotherapy correlates with favourable prognosis in oral cancer (Orosco *et al.*, 2007). *BNIP3*, a proapoptotic gene, is down-regulated in pancreatic cancer causing poor response to gemcitabine (Akada *et al.*, 2005) and its over-expression reverses oxaliplatin resistance in colon carcinoma cells (Wang *et al.*, 2012c).

The MDR phenotype in BAS cells is acquired by modulation of expression of a completely different set of genes to the one found with HS578T cells. Many differentially regulated genes in MDR signatures for BAS cells have direct or inferred roles in disease progression and drug resistance in a variety of carcinomas. For instance, *TGFB2* is a well-known inducer of EMT and also up-regulated in resistant ovarian carcinoma (Shirakihara *et al.*, 2011; Januchowski *et al.*, 2014). *CACNA2D1* is associated with drug resistant in small-cell lung carcinoma (Yu *et al.*, 2018), whereas *TSPAN7* expression is associated with poor prognosis in NSCLC and promotes lung cancer cells proliferation and migration (Wang *et al.*, 2018d). *ADAM12* promotes stemness in claudin low subtype of breast cancer (Duhachek-Muggy *et al.*, 2017). Among the down-regulated genes, *KLK5* and *CHG* are found to function as tumour suppressor in breast and pancreatic neuroendocrine cancers, respectively (Avgeris *et al.*, 2011; Pampalakis *et al.*, 2014; Weisbrod *et al.*, 2013). Additionally, *BID* is an activator of apoptotic cell death and its low expression has been found to be related to chemotherapy resistance (García-Aranda, Pérez-Ruiz & Redondo, 2018).

Traditionally, the MDR phenotype has been associated with up-regulation of ABC transporters, such as ABCB1, ABCC1 and ABCG2 (Robey *et al.*, 2018), although several other mechanisms, such as inhibition of apoptotic death or increased DNA damage repair, also play an important role (Holohan *et al.*, 2013). Whilst *ABCA1* was up-regulated by 4.7-fold and 2.4-fold in doxorubicin- and paclitaxel-resistant derivatives of HS578T cells, respectively, this ABC-transporter is involved in cholesterol efflux and not in the export of drugs (Nagao, Tomioka & Ueda, 2011). Moreover, *ABCA1* mRNA levels do not always accurately predict the protein levels, as the overall correlation between mRNA and protein levels has been found to be very low (R^2= 0.199), owing to post-translation regulation affecting protein expression and function (Wellington *et al.*, 2002; Kang, Singaraja & Hayden, 2010; Yokoyama *et al.*, 2012). Overall, no traditional effectors of multidrug resistance were present in the current MDR signatures for both HS578T and BAS cells, rather multiple genes involved in cancer progression, poor survival, and drug resistance, suggesting that the MDR phenotype in these MBC derived cells is more likely to be multifactorial.

5.5.2 EMT contributes to the MDR phenotype in metaplastic breast carcinoma

Although MDR phenotype in two metaplastic breast cancer derived cell lines is achieved via modulation of completely a different set of key molecules, GSEA indicates that both cells share some hallmarks related to aggressive cancer cell properties. EMT and apoptosis are two key cancer hallmarks involved in acquisition of MDR in both MBC derived cells, although HS578T cells showed involvement of others cancer hallmarks, including TNFα-NF-κB, Wnt-β-catenin, K-ras signalling, and hypoxia. EMT is the fundamental process responsible for gaining aggressive cellular traits, such as invasion and migration abilities, and contributes to the further development of stem cell-like phenotypes and acquisition of chemotherapeutic resistance (Asaduzzaman *et al.*, 2017). The pro-inflammatory cytokine TNFα plays important roles in many steps of tumorigenesis, including proliferation, invasion, angiogenesis, and metastasis (Wu & Zhou, 2010). The signalling cascade initiated by TNFα allows nuclear translocation of free NF-κB, leading to induction of expression of many EMT-related transcription factors (Min *et al.*, 2008). Wnt-β-catenin signalling pathway is also involved in EMT induction, stemness, metastatic growth, and acquisition of drug resistance in variety of carcinomas (Wang & Zhou, 2011; Heidel *et al.*, 2012; Wu *et al.*, 2012; Nedeljković & Damjanović, 2019). Oncogenic KRAS can activate EMT program and thus contributes to the cancer initiation, progression, metastasis, and therapy resistance in multiple cancers (Arner, Du & Brekken, 2019). Hypoxia, either by direct hypoxia inducible factor-1 alpha (HIF-1α) signalling or its crosstalk with the NF-κB or Wnt-β-catenin signalling pathway, promotes EMT and invasion of cancer cells (Lei *et al.*, 2015). Overall, the hallmark EMT, induced by enrichment of its directly contributing molecules or via multiple other signalling crosstalk, plays a vital role in the acquisition of MDR phenotype in MBC.

5.5.3 Inhibition of TGF-β pathway re-sensitizes MDR BAS cells and decreases their motility

The cytokine TGF-β is a potent EMT inducer (Massagué, 2008; Heldin, Landström & Moustakas, 2009). In carcinoma, the invasive front of the tumour is enriched with TGF-β and other cytokines, suggesting their possible roles in EMT induction as the cells in that location demonstrate the features characteristics of EMT (Massagué, 2008). Additionally, TGF-β interacts with stromal cells to induce secretion of chemokines that cause EMT induction and counteract the tumour suppressive effects of TGF-β exerted in the premalignant state (Bierie

& Moses, 2006). Importantly, an up-regulation of TGF-β is observed in MBC (Lien *et al.*, 2007; Taube *et al.*, 2010), and inhibition of TGF-β leads to improved chemotherapy response in TNBC (Bhola *et al.*, 2013). This suggests that TGF-β inhibitors may be a potential therapy for certain types of MBC (Xiao *et al.*, 2017; Yam, Mani & Moulder, 2017). Here, I demonstrate that TGF-β2 (*TGFB2*) regulates MDR in metaplastic breast cancer derived cells, as pharmacological inhibition of this pathway leads to down-regulation of transcription factor FOXC1 and re-sensitization of BAS MDR cells to doxorubicin and paclitaxel. This suggests that FOXC1 acts down-stream of *TGFB2* in MDR regulation, in agreement to previous report describing an elevation *Foxc1* mRNA in Namru murine mammary gland cells upon TGF-β treatment (Hopkins, Coatham & Berry, 2017).

TGF-β can promote EMT via both SMAD-dependent and SMAD-independent signalling pathways (Massagué, 2008; Heldin, Landström & Moustakas, 2009). TGF-β/SMAD signalling axis induces the expression EMT-related transcription factors, such as Snail1, Snail2, Zeb1 and Zeb2, as well as a mesenchymal marker vimentin (Morita, Mayanagi & Sobue, 2007; Thuault *et al.*, 2008; Smith *et al.*, 2009; Heldin, Landström & Moustakas, 2009). Moreover, crosstalk of this signalling with Notch signalling pathways also induces EMT (Heldin, Landström & Moustakas, 2009). In the SMAD-independent pathway, TGF-β type II receptor (TβR-II) phosphorylate polarity complex protein Par6, leading to disassembly of cell junction complexes and subsequently EMT induction (Ozdamar *et al.*, 2005). Interestingly, inhibition of TGF-β pathways in metaplastic breast cancer derived MDR cells down-regulate EMT-related transcription factors, in agreement with the signalling effects mentioned in regulating EMT. Moreover, a mesenchymal marker *VIM* is also down-regulated upon TGF-β pathway inhibition. Therefore, inhibition of TGF-β pathway prevents EMT induction.

The involvement of TGF-β in EMT could consequently suggest its role in the development of metastatic disease. In hepatocellular carcinoma, TGF-β induces platelet-derived growth factor (PDGF) signalling, which promote proliferation and migration of neoplastic hepatocytes (Fischer *et al.*, 2007). Similarly, TGF-β induces expression of periostin in prostate cancer cells, resulting in induction of EMT and thus increased cellular migration and invasion (Hu *et al.*, 2015). In breast cancer, higher levels of secreted TGF-β1 were found in the advancing edges of the primary tumour than its centre and, notably, metastatic tumour expresses significantly higher levels of both intra- and extra-cellular TGF-β1 compared to the primary tumour tissue, reflecting the role of TGF-β1 in metastatic disease progression (Dalal, Keown

& Greenberg, 1993). Interestingly, TGF-β in the tumour microenvironment primes cancer cells for distal metastasis (Massagué, 2008). TGF-β in the primary tumour microenvironment induces the departing cancer cells to express another cytokine, angiopoietin-like 4 (*ANGPTL4*), which helps disrupting the pulmonary capillary walls by the cancer cells and thereby seeding for lung metastases. Blocking TGF-β signalling substantially reduces the ability of human breast cancer cells to produce lung metastases in nude mice (Padua *et al.*, 2008). Once micro-metastases have developed, the local production of TGF-β facilitates environment to produce macro-metastases (Massagué, 2008). These data suggest that the upregulated TGF-β in doxorubicin- and paclitaxel-resistant derivatives of BAS cells might be responsible for their increased motility, an EMT phenotype prerequisite for metastatic dissemination. Experimental evidence by inhibiting TGF-β pathway in both MDR BAS cells proved this hypothesis, with a robust decrease in cellular motility. Thus, TGF-β pathway plays a vital role in MBC derived cells to gain EMT associated aggressive cellular phenotype.

Although several studies reported the involvement of TGF-β in the development of CSC phenotype (Shipitsin *et al.*, 2007; Mani *et al.*, 2008), inhibition of TGF-β pathways in MDR BAS cells did not cause decrease in anchorage-independent growth capacity, an *in vitro* surrogate for CSC phenotype, as measured by mammosphere formation in liquid culture. Indeed, a small increase in sphere forming efficiency was observed with both cells, although doxorubicin-resistant BAS cells did not show an increase with lower concentration of TGF-β inhibitor that caused alteration of other phenotypes, such as drug sensitivity and motility. This warrants further experimental evidence to unravel the mechanisms linking TGF-β and CSC in these MBC derived cellular models. Growth in soft agar assay, another *in vitro* assessment of anchorage-independence, could not be carried out due to technical limitation with TGF-β inhibitor for such long-term experiment. Therefore, extensive molecular and phenotypic characterization by stably silencing *TGFB2* in MDR BAS cells is required to elucidate the role of this cytokine in the regulation of CSCs.

Overall, inhibition of TGF-β pathway re-sensitizes MBC derived doxorubicin- and paclitaxel-resistant cells and decreases their motility, suggesting that this could be a potential treatment avenue against this aggressive category of breast cancer.

Chapter 6: MiRs regulate chemoresistance in metaplastic breast carcinoma

6.1 Introduction

6.1.1 MiRs in chemotherapy resistance in breast cancer

The involvement of miRs in regulating EMT and development of CSC phenotype may suggest a role in drug resistance in cancers, particularly in breast cancer. A large body of evidence indicates that miRs play vital roles in acquisition of drug resistance in breast cancer. For example, a study showed that acquired resistance to doxorubicin in luminal MCF-7 cells is correlated with the loss of miR-200c. Interestingly, restoration of miR-200c re-sensitized the resistant cells to doxorubicin by inhibiting Akt signalling pathway via up-regulation of E-cadherin and PTEN (Chen *et al.*, 2013). In contrast, up-regulation of miR-29a contributes to the doxorubicin resistance in luminal MCF-7 cells. Inhibition of up-regulated miR-29a in doxorubicin-resistant MCF-7 cells increases their drug sensitivity, whereas expression of miR-29a mimic renders the sensitive MCF-7 cells resistant to doxorubicin (Shen *et al.*, 2016). Another miR found to contribute to the doxorubicin resistance in breast cancer cells is miR-222. Breast cancer MCF-7 cells resistant to doxorubicin shows an up-regulation of miR-222. Upregulation of this miR causes down-regulation of pro-apoptotic protein Bim, resulting in reduced drug induced apoptosis and hence, acquired resistance to chemotherapy. Inhibition of miR-222 increases the sensitivity of drug resistant cells to doxorubicin (Dai *et al.*, 2019). Another study showed that miR-200 family (miR-200b and miR-200c) is down-regulated in endocrine-resistant breast cancer MCF-7 cells. These miR-200 family members contribute to the development of drug resistance, as over-expression of miR-200b and miR-200c re-sensitized the cells to tamoxifen and fulvestrant (Manavalan *et al.*, 2013). MiR-125b confers chemotherapy resistance in breast cancer cells. A study showed that Snail-induced activation of Wnt-β-catenin signalling pathway in breast cancer cells leads to over-expression of miR-125b, which causes enrichment of CSC population and inhibition apoptosis via down-regulation of Bak1, resulting in acquisition of chemotherapy resistance (Liu *et al.*, 2013). Another study reported that a higher circulating miR-125b expression level in blood serum is correlated with the poor therapeutic response in breast cancer patients. Interestingly, analysis of surgical specimens after neoadjuvant chemotherapy indicated less effects of chemotherapy, measured as the presence of higher proliferating cells percentage and lower apoptotic cells percentage, in patients with higher miR-125b expression (Wang *et al.*, 2012a).

MiR-452 is involved with resistance to docetaxel. Breast cancer MCF-7 cells resistant to docetaxel is found to over-express miR-452. Experimental modulation of its expression alters the sensitivity to the drug (Hu *et al.*, 2014a). Down-regulation of miR-451 is observed in breast cancer tissue and in paclitaxel resistant breast cancer SK-BR-3 and MCF-7 cells. MiR-451 causes down-regulation of β-catenin and hence, negatively regulates the expression of two Wnt-β-catenin signalling transcriptional targets, cyclin D1 and c-Myc, resulting in induction of cell cycle arrest and promotion of apoptosis (Wang *et al.*, 2017c). MiR-567 is reported to be involved in resistance to transtuzumab, a drug commonly used to treat HER2-positive breast cancer. Breast cancer patients resistant to transtuzumab found to have significant down-regulation of miR-567 expression, compared to the responding patients. An over-expression of miR-567 in transtuzumab resistant breast cancer SK-BR-3 and BT474 cells, in which miR-567 is significantly down-regulated, reverses their resistance phenotype, whereas inhibition of miR-567 confers transtuzumab resistance to the sensitive cells (Han *et al.*, 2020).

Several miRs regulate the expression of different ABC-transporters and thus play an important role in MDR in breast cancer. MiR-326 is found to be down-regulated in breast cancer and its expression is negatively correlated with the ABCC1 expression (also known as multidrug resistance associated protein 1, MRP1). Ectopic expression of miR-326 in MDR breast cancer MCF-7 cells down-regulates the ABCC1 expression and re-sensitizes the cells to cytotoxic agents, such as etoposide and doxorubicin (Liang *et al.*, 2010). MiR-181a is involved in mitoxantrone resistance in breast cancer cells via negatively regulating ABCG2 expression (commonly known as breast cancer resistance protein, BCRP). Breast cancer MCF-7 cells resistant mitoxantrone show a significant down-regulation of miR-181a expression. Over-expression of miR-181a in mitoxantrone resistant cells down-regulates ABCG2 expression and re-sensitizes the cells to mitoxantrone, whereas miR-181a inhibition in mitoxantrone sensitive cells decreases their sensitivity by up-regulating ABCG2 expression (Jiao *et al.*, 2013). Another miR involved in acquired resistance to mitoxantrone in breast cancer cells via negatively regulating ABCG2 expression is miR-487a. A study showed that miR-487a expression is significantly down-regulated in mitoxantrone resistant breast cancer MCF-7 cells and its ectopic expression in these cells reverses the resistance phenotype by down-regulating ABCG2 expression. Additionally, miR-487a inhibition up-regulates ABCG2 expression and consequently renders the sensitive MCF-7 cells resistant to mitoxantrone (Ma *et al.*, 2013). Furthermore, miR-302S family, which includes miR-302a,

miR-302b, miR-302c and miR-302d, also cooperatively represses ABCG2 expression in breast cancer MCF-7 cells and thus increases their chemotherapeutic sensitivity (Wang *et al.*, 2016b). Another study shows that miR-302S family plays an important role in regulating ABCB1 expression (P-glycoprotein, P-gp) and thus determines the chemotherapeutics sensitivity. Doxorubicin resistant breast cancer MCF-7 cells over-expressing ABCB1 show a significant down-regulation of miR-302S expression. Over-expression of miR-302S family in breast cancer cells cooperatively represses ABCB1 expression via inhibition of ERK signalling pathway and increases their sensitivity to doxorubicin, paclitaxel, and etoposide (Zhao *et al.*, 2016).

Using breast cancer cellular models, several reports have been published from our lab demonstrating a novel EMT/CSC/drug resistance regulatory axis controlled by the miRs. For example, miR-106b~25 cluster was found to be involved in the EMT and drug resistance phenotype in breast carcinoma. Three miRs of this cluster (miR-106b, miR-93 and miR-25) negatively regulate EP300, a transcription activator of E-cadherin, by directly targeting its mRNA. This ultimately results in down-regulation of E-cadherin expression and subsequent induction of EMT, leading to increased cell migration and invasion abilities and resistance to doxorubicin and γ-radiation (Zhou *et al.*, 2014). Moreover, using a minimally transformed mammary epithelial cell model, our lab has also reported that this miR cluster is involved in apoptosis evasion and regulates ABC transporter P-glycoprotein-independent multidrug resistant (MDR) phenotype, potentially via down-regulating EP300 (Hu *et al.*, 2016a). Another miR reported from our lab regulating MDR in breast cancer is miR-218. This miR is involved in the acquisition of chemotherapeutics resistance in breast cancer via negative regulation of survivin expression by directly targeting its mRNA and leading to evasion from apoptosis (Hu, Xu & Yagüe, 2015). Again, collaboratively our lab demonstrated that miR-205 enhances the sensitivity of breast cancer cells to chemotherapeutics by suppressing the expression of both FGF2 and VEGFA (Hu *et al.*, 2016b).

Therefore, targeting miRs could offer new treatment modalities in cancer therapy aiming at restoring the chemotherapeutics sensitivity of drug-resistant tumours in breast cancer.

6.2 Aim of the chapter

MBCs are inherently chemotherapeutic resistant (Al Sayed *et al.*, 2006; Weigelt *et al.*, 2014). The distinct molecular expression of MBC with enrichment of EMT and CSC markers contributes to their chemoresistance (Lien *et al.*, 2007; Hennessy *et al.*, 2009; Taube *et al.*, 2010). Moreover, we have already seen that the acquired resistance to doxorubicin and paclitaxel in MBC derived cells involved alteration of multiple pathways. Importantly, TGF-β-FOXC1 regulatory axis was identified to play an important role in the acquisition of MDR in a novel metaplastic breast cancer derived cell line, BAS. Interestingly, miRs offer another layer of control of gene expression and have been identified to be involved in regulating EMT and CSC, two key phenomena associated with chemotherapeutic resistance (Wang *et al.*, 2010). Several miRs have been found to play vital roles in chemoresistance in a variety of carcinomas, including breast cancer (Yang *et al.*, 2008; Zhou *et al.*, 2010; Kutanzi *et al.*, 2011; Zhou *et al.*, 2014; Hu *et al.*, 2016a). However, miR expression profiling identifying key miRs responsible for chemotherapy resistance in MBC has not been studied so far. Here, I aimed to identify if any role of miR in drug resistance in MBC. For this, I attempted to-

1. identify miR expression signatures for MBC derived cells.
2. analyse miR expression profile of doxorubicin- and paclitaxel-resistant derivatives of both HS578T and BAS cells to ascertain whether there were miRs responsible for MDR in metaplastic breast cancer derived cells.
3. analyse miR expression profile of breast cancer clinical samples, including MBC.

6.3 Materials and methods

6.3.1 MicroRNA (miR) expression analysis

MiR expression analysis was performed with GeneChip miRNA arrays (Applied Biosystems, Thermo Fisher Scientific) using a FlashTag Biotin HSR Labeling Kit (**Table 6.1**). Probes were prepared by labeling total RNA following the manufacturer's instructions. The process involves two steps, a brief tailing reaction followed by ligation of the biotinylated signal molecule to the target RNA sample (**Figure 6.1**). This provides a fast, simple, accurate, highly sensitive and reproducible method for miR analysis. The high sensitivity of FlashTag Biotin HSR is due to proprietary 3DNA dendrimer, a branched structure of single and double stranded DNA conjugated with numerous labels, signal amplification technology.

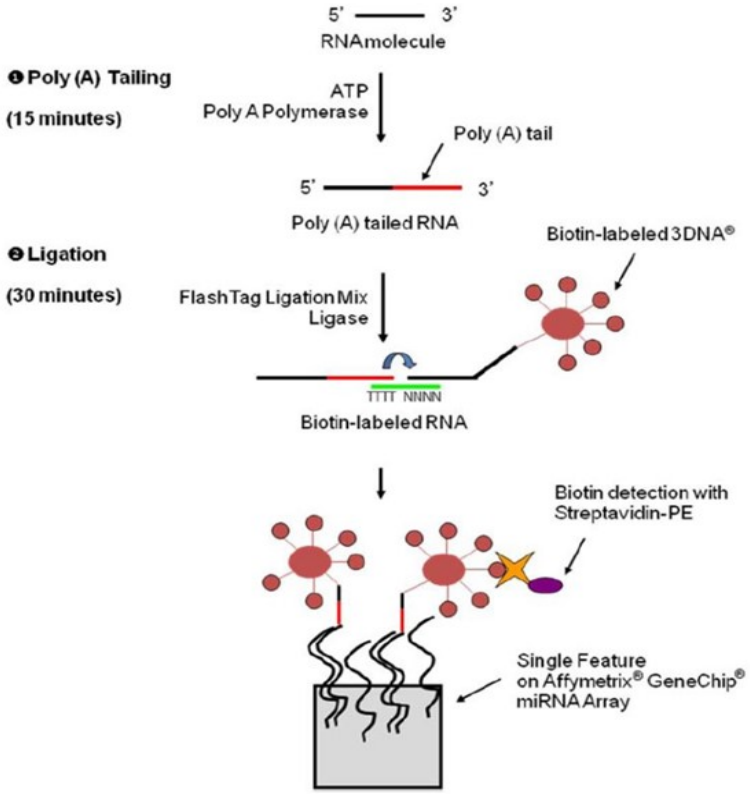


Figure 6.1: Schematic representation of FlashTag Biotin HSR RNA labeling for analysis by GeneChip miRNA arrays. (The figure is taken from the manual of FlashTag Biotin HSR RNA Labeling kit for GeneChip miRNA arrays from Applied Biosystems, Thermo Fisher Scientific)

Table 6.1: FlashTag Biotin HSR RNA labeling kit reagents and storage conditions, 10 rxn (P/N 901910)

Vial	Component	Storage	Handling
1	10X Reaction Buffer	-20^{0}C	Thaw at room temperature, vortex, and briefly microfuge.
2	25 mM $MnCl_2$	-20^{0}C	Thaw at room temperature, vortex, and briefly microfuge.
3	ATP Mix	-20^{0}C	Thaw on ice, microfuge if necessary, and keep on ice at all times.
4	PAP Enzyme	-20^{0}C	Remove from freezer just prior to use, and briefly microfuge. Keep on ice at all times. Do not vortex.
5	5X FlashTag Biotin HSR Ligation Mix	-20^{0}C	Thaw at room temperature, vortex, and briefly microfuge.
6	T4 DNA Ligase	-20^{0}C	Remove from freezer just prior to use, and briefly microfuge. Keep on ice at all times. Do not vortex.
7	HSR Stop Solution	-20^{0}C	Thaw at room temperature, vortex, and briefly microfuge.
8	RNA Spike Control Oligos	-20^{0}C	Thaw on ice, microfuge if necessary, and keep on ice at all times.
9	ELOSA Spotting Oligos	-20^{0}C	Thaw at room temperature, vortex, and briefly microfuge.
10	ELOSA Positive Control	-20^{0}C	Thaw on ice, microfuge if necessary, and keep on ice at all times.
11	Nuclease-Free Water	-20^{0}C	Thaw at room temperature, vortex, and briefly microfuge.
12	27.5% Formamide	-20^{0}C	Thaw at room temperature, vortex, and briefly microfuge.

6.3.2 Total RNA isolation and quantitation

Isolation of total RNA from cell lines

For miR expression analysis in cell lines, total RNA was isolated using a miRCURY RNA isolation kit (Exiqon, Qiagen). A small panel of cells comprising primary mammary epithelial cells (HMEC), non-tumorigenic (MCF-10A) and breast cancer cell lines (MCF-7, MDA-MB-231, HS578T and BAS), and drug resistant derivatives of HS578T and BAS, were used for the analysis. Cells (except HMEC) grown in 25 cm^2 culture flask at a confluence of 80-90% were harvested following standard protocols. Normal human mammary epithelial cells

(HMECs) from three different donors were obtained as frozen vials from Breast Cancer Tissue Bank, UK and expanded in HuMEC Ready Medium (Gibco, Thermo Fisher Scientific) in 25 cm^2 dishes until cells reached 80% confluency. Cells were trypsinized following the standard procedure, pooled, washed twice with cold PBS and processed for RNA extraction. Cells' pellet obtained for each sample was lysed with 350 µL of lysis solution by vortexing for 15 seconds. The lysate was then passed through 20G needle attached to a syringe for at least five times to break down the genomic DNA. Next, 200 µL of 100% ethanol was added to the lysate and mixed by vortexing for 10 seconds and loaded onto the column assembled with the collection tube and centrifuged for 1 minute at >3,500 x *g*. The flow-through was discarded, and the spin column was reassembled with its collection tube. The column was washed with 400 µL of wash solution thrice by centrifugation at 14,000 x *g* for 1 minute, following the manufacturer's instructions. The column was spun for another 2 minutes to thoroughly dry the resin. The collection tube was then discarded, and column was assembled into a fresh 1.7 mL elution tube provided with the kit. Finally, RNA was eluted with 50 µL of elution buffer by centrifugation at 200 x *g* for 2 minutes, followed by 14,000 x *g* for 1 minute, according to the manufacturer's protocol. The concentration of the isolated RNA was determined using a NanoDrop ND1000 spectrophotometer (Thermo Fisher Scientific). A260/A280 ratio was used as quality control (QC) parameter to determine the purity of isolated RNA. All the samples were stored at -80^{0}C until further manipulation. The description of the cell lines used are further described in **Table 6.2**.

Table 6.2: Description of the cell lines used for miR expression analysis

Sample ID	Sample Name	Conc. (ng/µL)	A260/A280 Ratio	Sample Type
1	HMEC	170.9	2.06	Primary Cell
2	MCF-10A	1130.3	2.08	Naïve
3	MCF-7	158.1	2.05	
4	MDA-MB-231	858.9	2.08	
5	HS578T	1046.5	2.09	
6	BAS	572.0	2.08	
7	HS-TX	363.0	2.03	Paclitaxel Resistant
8	BAS-TX	715.8	2.05	
9	HS-DOX	531.4	2.00	Doxorubicin Resistant
10	BAS-DOX	537.4	2.06	

Isolation total RNA from clinical FFPE samples

For miR expression analysis in clinical FFPE samples, total RNA was isolated using miRNeasy FFPE Kit (QIAGEN) with a prior deparaffinization step, following the manufacturer's instructions. Clinical samples (n=23) from previous studies (Asaduzzaman *et al.*, 2017; Mahmud *et al.*, 2019) were used, comprising normal breast tissue both from tissues with non-tumoral morphological abnormalities (Normal-MA) and cosmetic reduction mammoplasties (Normal-CRM), non-cancerous tumours (Benign), invasive ductal carcinoma (IDC), invasive lobular carcinoma (ILC), and MBC (Metaplastic). Four 10-µm thick sections were used per sample in a single 2 mL microcentrifuge tube. Next, 320 µL Deparaffinization Solution was added, vortexed vigorously for 10 seconds, and centrifuged briefly. The samples were incubated at 56^0C for 3 minutes, then allowed to cool at room temperature followed by addition of 240 µL Buffer PKD and mixed by vortexing. After centrifugation (11,000 x *g*) for 1 minute, the lower, clear phase was mixed with 10 µL proteinase K. The samples were then incubated at 56^0C for 15 minutes followed by incubation again at 80^0C for 15 minutes. The lower, clear phase was taken into a new 2 mL microcentrifuge tube, followed by incubation on ice for 3 minutes and centrifugation (20,000 x *g*) for 15 minutes. The supernatant was transferred to a new microcentrifuge tube and mixed with 25 µL DNase Booster Buffer and 10 µL DNase I stock solution, followed by brief centrifugation and incubation at room temperature for 15 minutes. The lysate was then mixed thoroughly with 500 µL Buffer RBC. Next, the sample was mixed with 1750 µL ethanol (100%), and transferred immediately (700 µL) to an RNeasy MinElute spin column fitted in a 2 mL collection tube and centrifuged at ≥8000 x *g* for 15 seconds. The flow-through was discarded, and the spin column was reassembled with its collection tube. This process of binding total RNA, including miRs, to the column was repeated until the entire sample had passed through the RNeasy MinElute spin column. The spin column was washed with 500 µL Buffer RPE twice by centrifugation at ≥8000 x *g* for 15 seconds (first washing) or 2 minutes (second washing), following the manufacturer's instructions. The column was centrifuged again at a full speed, keeping the lid of the spin column open, for 5 minutes with a new 2 mL collection tube. The collection tube with the flow-through was discarded, and the spin column was placed in a new 1.5 mL collection tube. Finally, total RNA, including miR, was eluted with 20 µL RNase-free water by applying directly to the spin column membrane followed by centrifugation at full speed for 1 minute. The concentration of the isolated RNA was determined using a NanoDrop ND1000 spectrophotometer (Thermo Fisher Scientific).

A260/A280 ratio was used as quality control (QC) parameter to determine the purity of isolated RNA. All the samples were stored at -80^{0}C until further manipulation. The description of the clinical samples used are further described in **Table 6.3.**

Table 6.3: Description of the clinical samples used for miR expression analysis

Sample ID	Sample Name	Conc. (ng/µL)	A260/A280 Ratio	Sample Type
1	Normal MA 1	197	2.02	
2	Normal MA 2	33	1.98	
3	Normal CRM 3	32	1.87	Normal (n=5)
4	Normal CRM 4	94	1.94	
5	Normal CRM 5	118	1.88	
6	Benign 1	2600	1.99	
7	Benign 2	635	1.90	Benign (n=3)
8	Benign 3	1781	1.98	
9	Invasive_Ductal 1	177	2.01	
10	Invasive_Ductal 2	231	1.99	
11	Invasive_Ductal 3	1240	1.99	IDC (n=5)
12	Invasive_Ductal 4	949	2.01	
13	Invasive_Ductal 5	47	1.73	
14	Invasive_Lobular 1	168	1.94	
15	Invasive_Lobular 2	1432	1.94	
16	Invasive_Lobular 3	323	1.81	ILC (n=5)
17	Invasive_Lobular 4	299	1.86	
18	Invasive_Lobular 5	755	1.94	
19	Metaplastic 1	184	1.84	
20	Metaplastic 2	1531	1.83	
21	Metaplastic 3	361	1.74	Metaplastic (n=5)
22	Metaplastic 4	62	1.67	
23	Metaplastic 5	41	1.92	

6.3.3 FlashTag Biotin HSR RNA labeling

Poly (A) tailing

Starting with total RNA sample, the RNA input used for FlashTag Biotin HSR labeling for miRNA 100 format arrays (GeneChip miRNA 4.0 array) was 1000 ng for cell lines and 250 ng for clinical samples due to their low yield. Following the manufacturer's protocol

provided, the required amount of each RNA sample was taken, and adjusted to volume 8 µL with nuclease-free water (**Table 6.4**). On ice, 2 µL of RNA spike control oligos was added to each (8 µL) RNA sample for a reaction volume of 10 µL. The ATP mix was diluted as recommended for total RNA samples (1:500) with 1 mM Tris, and the poly A tailing master mix was prepared for all the sample plus 10% overage with the components described in **Table 6.5**, following the manufacturer's instructions. Then, 5 µL of poly A tailing master mix was added to each (10 µL) RNA/spike control oligo, for a reaction volume of 15 µL. After gentle mixing and centrifugation, the reaction mixtures were incubated in a heat block at 37^0C for 15 minutes.

Table 6.4: RNA input for FlashTag Biotin HSR labeling

Component	Volume/Reaction
Total RNA Sample[a] (250-1000 ng)	Variable
Nuclease-free Water	Variable
Total Volume	**8 µL**

[a]250 ng for clinical samples and 1000 ng for cell lines

Table 6.5: Preparation of poly A tailing master mix

Component	Volume/miRNA Array
10X Reaction Buffer	1.5 µL
25 mM $MnCl_2$	1.5 µL
Diluted ATP Mix (1:500)	1.0 µL
PAP Enzyme	1.0 µL
Total Volume	**5 µL**

FlashTag Biotin HSR ligation

The 15 µL of each tailed RNA sample was briefly centrifuged. On ice, 4 µL of 5X FlashTag Biotin HSR Ligation Mix were added to each sample, for a reaction volume of 19 µL. Then, 2 µL of T4 DNA Ligase were added to each sample. After gentle mixing and centrifugation, the reaction mixtures were incubated at 25^0C (room temperature) for 30 minutes. Finally, the reaction was stopped by adding 2.5 µL of HSR Stop Solution to each ligated sample followed by mixing and centrifugation. The biotin-labeled RNA samples were stored at -20^0C prior to hybridization on GeneChip miRNA arrays.

6.3.4 Cartridge array hybridization

For hybridization, GeneChip miRNA 4.0 arrays (Applied Biosystems, Thermo Fisher Scientific) were used (**Figure 6.2**). Briefly, arrays were labeled with the name of the sample to be hybridized, and the sample and array information were registered into AGCC. The arrays were then allowed to equilibrate to room temperature for 10-15 minutes. After thawing, the 20X Eukaryotic Hybridization Controls (*bioB, bioC, bioD* and *cre* from GeneChip Eukaryotic Hybridization Control Kit) were heated for 5 minutes at 65^0C. The hybridization master mix, appropriate for GeneChip miRNA 4.0 array (100-format array), were prepared for all the samples plus 10% overage with the components described in **Table 6.6**, following the manufacturer's instructions. The hybridization cocktail for 100-format array was then prepared by adding 110.5 µL of hybridization master mix to each (21.5 µL) biotin-labeled sample for a final volume of 132 µL (**Table 6.7**). The hybridization cocktail was then incubated at 99^0C for 5 minutes, followed by 45^0C for 5 minutes. The volume of each hybridized cocktail appropriate for 100-format array (130 µL) was injected into the specific array as registered into AGCC, following the manufacturer's instruction. The arrays were then incubated for 16 to 18 hours in the hybridization oven (GeneChip Hybridization Oven 645), which has already been set to temperature 48^0C and RPM 60 according to the protocol provided by the manufacturer.

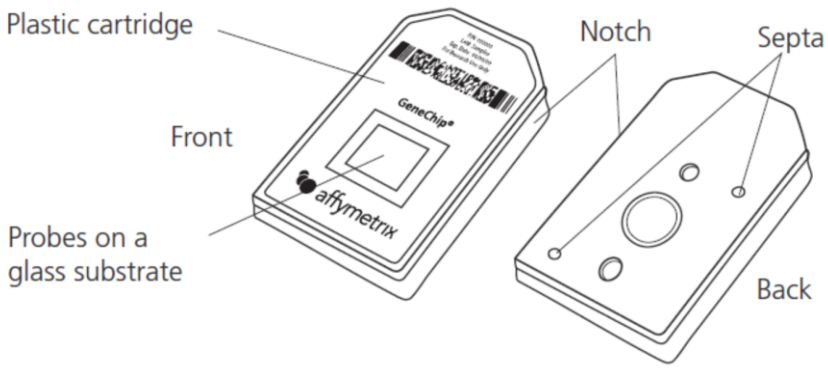


Figure 6.2: GeneChip cartridge array for miR. (The figure is taken from the manual of FlashTag Biotin HSR RNA Labeling kit for GeneChip miRNA arrays from Applied Biosystems, Thermo Fisher Scientific)

Table 6.6: Preparation of hybridization master mix for GeneChip miRNA 4.0 array (for a single reaction)

Component	Volume for a 100 Format Array (miRNA 3.0 and later designs)
2X Hybridization Mix	66 µL
27.5% Formamide	19.2 µL
DMSO	12.8 µL
20X Hybridization Controls	6.6 µL
Control Oligo B2, 3nM	2.2 µL
Nuclease-free Water	3.7 µL
Total Volume	**110.5 µL**

Table 6.7: Preparation of hybridization cocktail for GeneChip miRNA 4.0 array

Component	100 Format Array (miRNA 3.0 and later designs)
Biotin-labeled Sample	21.5 µL
Hybridization Master Mix	110.5 µL
Total Volume	**132 µL**

6.3.5 Array washing, staining, and scanning

All the steps of array washing, and staining were performed following the GeneChip Expression Wash, Stain, and Scan User Guide for Cartridge Arrays (P/N 702731) with the GeneChip Fluidics Station 450 using an appropriate fluidics protocol recommended for 100-format array (FS450_0002). Finally, scanning of all the arrays were done following Command Console User Guide (P/N 702569) using GeneChip Scanner 3000 7G (Thermo Fisher Scientific).

Array hybridization, washing, staining, and scanning were performed at the Genomic Centre, King's College London, for clinical samples, and at the China Tianjin Breast Cancer Prevention, Treatment and Research Center, Tianjin Medical University Cancer Institute and Hospital, National Clinical Research Center of Cancer, Tianjin, PR China.

6.3.6 Analysis of array data

Data were acquired as CEL files. RMA-normalized expression was calculated from raw CEL files using R tool ‘oligo’ (Carvalho & Irizarry, 2010), and data filtered for human annotation only. Differentially expressed miRs were considered significant if p-value with FDR ≤ 0.05 and fold-change >2 or < -2. KEGG (Kyoto Encyclopaedia of Genes and Genomes) pathway analyses were carried out using DIANA-miRPath v3.0 (Vlachos *et al.*, 2015) and heatmaps were generated with ‘gplots’ R package. Microarray data were deposited at the NCBI Gene Expression Omnibus (GEO) (http://ncbi.nlm.nih.gov/geo/) under accession numbers GSE144445 for cell lines and GSE144534 for clinical samples.

6.4 Results

6.4.1 Metaplastic breast cancer derived cells show distinct miR expression signatures

Given the distinct genetic architecture enriched with EMT and CSC markers contributing to the intrinsic chemo-refractory nature of MBC (Lien *et al.*, 2007; Hennessy *et al.*, 2009; Taube *et al.*, 2010), I aimed to identify if there were miRs differentially expressed in MBC derived cells. For this, I determined the miR expression profile in a small panel of breast cancer cell lines, including metaplastic derived HS578T and BAS cells, and primary human mammary epithelial cells. As expected, hierarchical clustering showed both MBC derived HS578T and BAS cells grouped together. Four interesting miR expression clusters were identified, showing the miRs exclusively down-regulated in both MBC derived cells (cluster 1), and up-regulated in BAS (cluster 2), HS578T (cluster 4) and both cells (cluster 3) (**Figure 6.3 and Table 6.8-6.11**). Thus, these clusters represent individual miR expression signatures for HS578T (cluster 4) and BAS cells (cluster 2), as well as signatures common for both MBC derived cells (cluster 1: down-regulated miRs and cluster 3: up-regulated miRs).

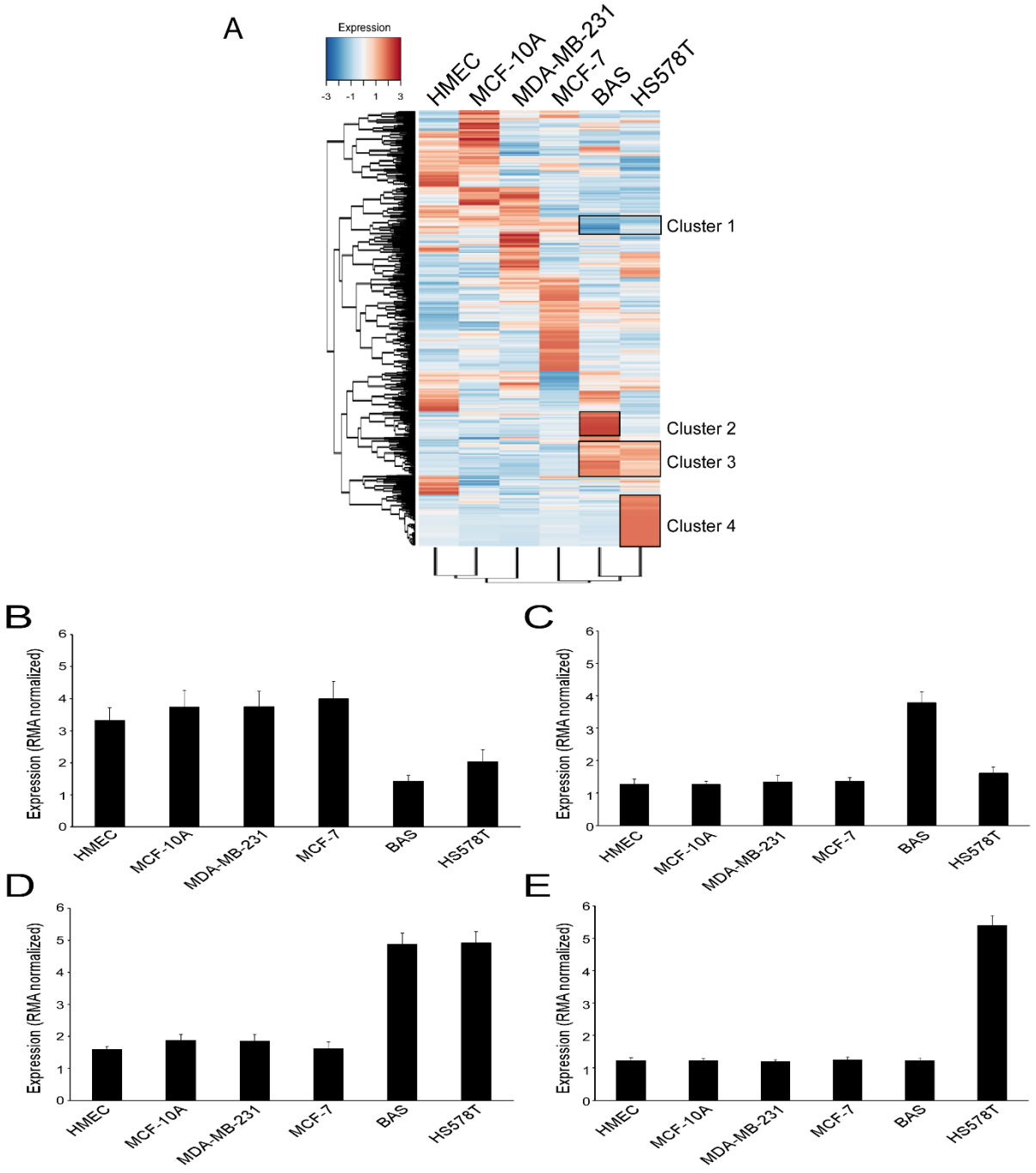


Figure 6.3: Identification of the MBC derived cells miR expression signatures. A, Hierarchical clustering of small RNA expression obtained with the GeneChip miRNA 4.0 Array in a small panel of breast cancer cell lines, including non-tumorigenic breast epithelial cells (MCF-10A), luminal breast cancer cells (MCF-7), basal-like breast cancer cells (MDA-MB-231), and MBC derived cells (HS578T and BAS), and primary human mammary epithelial cells (HMEC). Clusters exclusive to MBC derived cells are indicated. B-E, GeneChip miRNA 4.0 Array RMA normalized average expression values ± SD in cluster 1 (B), cluster 2 (C), cluster 3 (D) and cluster 4 (E).

Table 6.8: MiRs down-regulated (RMA normalised expression values) in both MBC derived HS578T and BAS cells (Cluster 1)

Transcript	HMEC	MCF-10A	MCF-7	MDA-MB-231	HS578T	BAS
hsa-miR-376c-5p	1.61	1.09	1.15	1.51	0.91	0.74
hsa-mir-4635	1.70	1.29	1.18	1.39	1.07	0.68
hsa-miR-5004-5p	2.80	2.66	2.80	2.76	0.97	1.14
hsa-miR-4725-3p	1.55	1.28	2.20	1.34	1.38	0.74
hsa-miR-6726-5p	1.71	1.56	1.63	2.12	1.41	0.85
hsa-miR-4742-5p	2.29	3.24	2.70	2.56	1.14	1.13
hsa-mir-3910-1	2.04	2.35	2.89	2.76	1.49	0.95
hsa-mir-3910-2	2.04	2.35	2.89	2.76	1.49	0.95
hsa-miR-5681a	2.03	1.51	1.90	1.75	1.64	0.91
hsa-miR-4720-5p	5.21	6.97	5.65	6.06	1.25	1.44
hsa-miR-3921	4.12	5.15	7.16	5.11	1.25	1.63
hsa-miR-6820-5p	2.72	2.17	2.96	2.57	1.80	1.32
hsa-miR-1263	3.98	5.77	5.04	5.05	2.00	1.19
hsa-miR-1298-3p	4.14	5.30	5.90	5.75	1.45	1.86
hsa-miR-628-5p	5.05	5.80	4.86	5.96	1.82	2.10
hsa-miR-23b-5p	6.26	5.37	6.50	5.95	6.43	3.03
hsa-miR-3178	7.35	9.58	10.50	8.44	7.09	3.57

Table 6.9: MiRs up-regulated (RMA normalised expression values) in BAS cells (Cluster 2)

Transcript	HMEC	MCF-10A	MCF-7	MDA-MB-231	HS578T	BAS
hsa-miR-708-5p	0.93	1.64	2.13	1.77	1.90	9.74
hsa-miR-92a-1-5p	5.37	2.29	3.86	5.85	5.44	7.79
hsa-miR-543	1.11	0.83	0.93	0.80	2.88	5.95
hsa-miR-487a-3p	0.84	0.95	0.87	0.75	2.68	5.60
hsa-miR-1185-1-3p	1.51	1.08	1.22	0.89	3.37	5.38
hsa-miR-205-3p	1.35	1.86	0.71	1.25	1.04	4.60
hsa-miR-409-5p	1.16	1.00	0.92	0.97	1.13	4.51
hsa-miR-1910-3p	1.89	3.15	2.73	2.34	2.03	4.38
hsa-miR-495-3p	1.31	1.18	1.07	0.80	1.13	4.18
hsa-miR-654-3p	0.98	0.91	1.11	0.79	1.14	4.07
hsa-miR-376c-3p	1.28	1.07	1.63	0.92	1.01	3.97
hsa-miR-323a-5p	1.12	1.36	1.50	1.02	1.28	3.74
hsa-mir-205	1.71	1.42	0.74	1.00	0.83	3.24
hsa-miR-323a-3p	1.22	1.49	1.00	0.65	0.87	3.13
hsa-miR-376a-3p	0.82	0.86	1.07	0.86	0.84	3.06
hsa-mir-31	1.20	1.27	1.02	0.68	1.30	3.01
hsa-miR-668-3p	1.21	0.91	1.47	1.48	1.72	2.87
hsa-mir-139	1.29	0.75	1.93	2.67	2.03	2.83
hsa-miR-412-5p	0.91	0.78	1.19	1.06	1.16	2.77
hsa-miR-411-5p	0.87	1.07	0.94	0.93	0.96	2.67
hsa-mir-487a	0.98	1.02	1.15	0.94	1.10	2.66
hsa-miR-670-5p	1.14	1.63	1.17	2.07	1.60	2.48
hsa-miR-299-5p	0.75	1.14	1.18	1.19	1.29	2.46
hsa-miR-329-3p	0.78	1.02	0.91	0.89	1.16	2.39
hsa-mir-92a-1	1.04	1.16	0.96	1.25	1.31	2.31
hsa-miR-487a-5p	0.97	1.19	1.19	1.07	1.22	2.22
hsa-mir-494	0.95	0.89	1.78	1.33	1.55	2.06
hsa-miR-7-5p	0.91	1.41	1.49	1.44	1.14	1.89

Table 6.10: MiRs up-regulated (RMA normalised expression values) in both MBC derived HS578T and BAS cells (Cluster 3)

Transcript	HMEC	MCF-10A	MCF-7	MDA-MB-231	HS578T	BAS
hsa-miR-615-3p	2.83	4.94	5.61	2.63	8.10	7.08
hsa-miR-1972	3.27	3.80	5.45	3.57	6.58	6.48
hsa-miR-1296-5p	2.56	4.65	3.54	4.90	6.12	5.65
hsa-miR-134-5p	3.27	2.70	1.39	4.50	7.60	6.63
hsa-miR-127-3p	2.22	1.87	1.11	2.88	8.15	8.09
hsa-miR-769-3p	1.93	4.20	1.17	3.91	5.93	4.79
hsa-miR-1292-5p	2.30	3.74	3.61	3.06	3.89	4.87
hsa-miR-432-5p	1.11	0.88	1.10	1.57	7.91	7.91
hsa-miR-409-3p	1.65	1.32	1.21	0.88	7.16	8.08
hsa-miR-935	1.21	0.96	1.91	1.69	8.29	6.19
hsa-miR-601	2.59	2.20	1.18	3.78	5.17	4.94
hsa-miR-196a-5p	1.82	1.75	0.88	1.06	6.62	7.37
hsa-miR-379-5p	1.92	1.05	1.48	1.08	6.56	7.19
hsa-miR-382-5p	1.50	1.40	1.48	1.08	6.46	7.00
hsa-miR-487b-3p	1.71	1.10	0.74	1.00	6.25	6.97
hsa-miR-7152-3p	2.23	1.45	2.47	2.41	4.82	3.88
hsa-miR-433-3p	0.93	1.23	1.18	1.10	6.12	6.39
hsa-miR-485-3p	1.35	1.20	1.21	1.25	5.29	6.52
hsa-miR-769-5p	2.19	2.39	0.95	2.50	4.98	3.43
hsa-miR-370-3p	1.07	1.60	1.48	1.19	5.60	5.00
hsa-miR-195-3p	1.29	1.77	1.25	1.65	3.88	3.00
hsa-miR-431-5p	0.87	0.84	0.88	0.77	3.74	5.52
hsa-miR-1306-3p	1.23	2.29	1.22	2.06	2.61	3.11
hsa-miR-1185-2-3p	1.28	1.51	1.30	1.02	3.37	3.89
hsa-miR-5088-5p	1.42	1.95	1.17	1.62	3.20	2.66
hsa-miR-493-3p	0.85	0.98	1.31	0.99	3.91	3.69
hsa-miR-485-5p	1.16	1.50	1.15	0.81	3.80	3.22
hsa-miR-654-5p	0.96	1.09	1.19	0.97	3.18	3.54
hsa-miR-7844-5p	1.05	1.60	1.63	1.73	2.63	2.28
hsa-miR-4299	1.19	1.72	1.03	1.65	2.34	2.65
hsa-miR-337-5p	0.70	0.94	0.98	0.93	2.07	3.03
hsa-mir-543	0.84	1.13	1.27	1.01	1.29	1.85
hsa-miR-3661	0.82	1.18	0.73	0.96	2.06	1.63
hsa-mir-487b	0.74	0.81	0.77	0.90	1.53	1.40

Table 6.11: MiRs up-regulated (RMA normalised expression values) in HS578T cells (Cluster 4)

Transcript	HMEC	MCF-10A	MCF-7	MDA-MB-231	HS578T	BAS
hsa-miR-145-5p	3.67	1.04	0.70	1.08	13.25	0.88
hsa-miR-143-3p	2.57	1.30	1.30	1.05	11.22	0.98
hsa-miR-214-3p	1.93	1.63	1.26	1.47	10.03	1.93
hsa-miR-512-3p	1.39	1.22	1.22	1.00	8.28	1.34
hsa-miR-498	1.67	1.60	1.93	1.78	8.20	2.01
hsa-miR-199a-3p	1.34	0.94	0.71	0.99	8.14	0.92
hsa-miR-199b-3p	1.34	0.94	0.71	0.99	8.14	0.92
hsa-miR-195-5p	3.09	3.10	4.13	3.72	8.12	3.86
hsa-miR-1323	3.04	2.42	2.92	2.90	7.90	1.94
hsa-miR-516b-5p	1.09	1.07	1.23	1.05	7.53	1.00
hsa-miR-155-5p	3.21	1.05	1.28	1.08	7.23	1.95
hsa-miR-199a-5p	0.98	0.98	1.18	1.02	7.19	0.81
hsa-miR-517a-3p	0.73	0.68	1.01	0.68	6.88	1.34
hsa-miR-517b-3p	0.73	0.68	1.01	0.68	6.88	1.34
hsa-miR-519c-5p	0.74	1.05	0.78	1.07	6.70	0.83
hsa-miR-523-5p	0.74	1.05	0.78	1.07	6.70	0.83
hsa-miR-518e-5p	0.74	1.05	0.78	1.07	6.70	0.83
hsa-miR-522-5p	0.74	1.05	0.78	1.07	6.70	0.83
hsa-miR-519a-5p	0.74	1.05	0.78	1.07	6.70	0.83
hsa-miR-519b-5p	0.74	1.05	0.78	1.07	6.70	0.83
hsa-mir-3160-1	1.11	0.88	1.11	0.89	6.60	1.05
hsa-miR-767-5p	0.80	0.93	0.64	0.98	6.50	0.98
hsa-miR-105-5p	1.05	0.93	1.12	1.07	6.27	0.87
hsa-miR-525-5p	1.14	0.94	1.19	0.96	6.09	0.79
hsa-miR-371a-5p	1.51	1.77	1.39	1.83	6.01	1.40
hsa-miR-497-5p	1.05	1.05	1.42	1.12	5.86	1.31
hsa-miR-526b-5p	0.75	0.97	0.93	0.96	5.65	0.96
hsa-miR-526a	1.06	1.00	1.19	1.02	5.52	0.88
hsa-miR-520c-5p	1.06	1.00	1.19	1.02	5.52	0.88
hsa-miR-518d-5p	1.06	1.00	1.19	1.02	5.52	0.88
hsa-miR-520g-3p	0.75	0.78	0.72	0.68	5.11	0.80
hsa-miR-1281	2.01	2.08	3.22	2.61	5.09	2.95
hsa-miR-143-5p	0.73	1.68	0.85	0.78	4.95	1.14
hsa-miR-518f-5p	1.00	0.98	0.83	0.90	4.81	1.08
hsa-miR-373-3p	1.28	1.01	1.63	0.99	4.72	1.07
hsa-miR-520d-3p	1.05	1.20	0.97	1.14	4.70	1.16
hsa-miR-4793-5p	1.17	1.60	1.14	2.08	4.56	1.77
hsa-miR-3187-3p	1.50	2.67	1.63	1.63	4.54	2.92
hsa-mir-519b	0.91	0.94	1.10	1.19	4.50	0.80

Table 6.11: MiRs up-regulated (RMA normalised expression values) in HS578T cells (Cluster 4) (Contd.)

Transcript	HMEC	MCF-10A	MCF-7	MDA-MB-231	HS578T	BAS
hsa-miR-518b	0.74	1.00	1.09	0.82	4.34	0.98
hsa-miR-7706	1.60	2.50	2.06	1.44	3.86	1.41
hsa-miR-512-5p	0.98	0.85	0.82	0.75	3.74	0.80
hsa-miR-6872-5p	1.59	1.76	2.62	1.90	3.67	1.81
hsa-miR-887-3p	0.63	0.91	0.86	0.79	3.57	0.89
hsa-mir-525	0.98	1.14	1.21	1.05	3.57	1.07
hsa-mir-520c	1.03	0.89	1.41	0.71	3.48	1.23
hsa-mir-522	1.06	1.08	0.89	1.19	3.48	1.23
hsa-miR-518c-5p	1.23	0.80	0.97	0.71	3.35	0.93
hsa-miR-1306-5p	1.45	1.47	1.58	1.40	3.28	1.40
hsa-miR-6856-5p	1.42	1.90	1.58	1.84	3.06	1.21
hsa-miR-520a-5p	1.16	0.75	0.95	0.85	2.66	0.88
hsa-miR-206	1.03	1.27	1.49	1.41	2.63	1.50
hsa-mir-1231	1.08	1.11	1.34	1.15	2.17	1.17
hsa-mir-214	0.87	1.26	1.26	0.95	2.08	1.23
hsa-miR-5092	0.93	1.33	0.87	0.94	2.07	0.88
hsa-miR-3192-5p	0.79	1.20	1.15	1.10	1.64	0.98
hsa-mir-3160-2	0.73	0.79	1.19	0.83	1.58	1.05
hsa-miR-639	0.73	1.16	0.93	1.06	1.55	1.12
hsa-miR-8088	0.68	0.98	0.95	1.00	1.40	0.98

6.4.2 MiR expression profiles of MBC derived cells identify an enrichment of TGF-β signalling pathway

As miRs are involved in the regulation of gene expression, pathways enriched with targets of miRs visualize their functional picture. Pathway analysis (Vlachos *et al.*, 2015) indicated that all four miR expression signatures included miRs involved in proteoglycans in cancer, a pathway associated with tumour growth and metastasis (**Figure 6.4**). In addition, the common up-regulated signatures for both MBC derived cells (cluster 3) included miRs associated with TGF-β, Hippo, Rap1, Ras, mTOR signalling and pluripotency of stem cells, among others (**Figure 6.4 C**). Although individual miR signatures for HS578T (cluster 4) and BAS cells (cluster 2) are unique to each cell model, they seem to regulate many common pathways, such as TGF-β, Hippo, ErbB signalling, proteoglycans in cancer and pluripotency stem cells, obviously via different set of miRs (**Figure 6.4 D and B**). Importantly, all the up-

regulated signatures of clusters 2-4 included miRs associated with TGF-β signalling, Hippo signalling and pluripotency of stem cells.

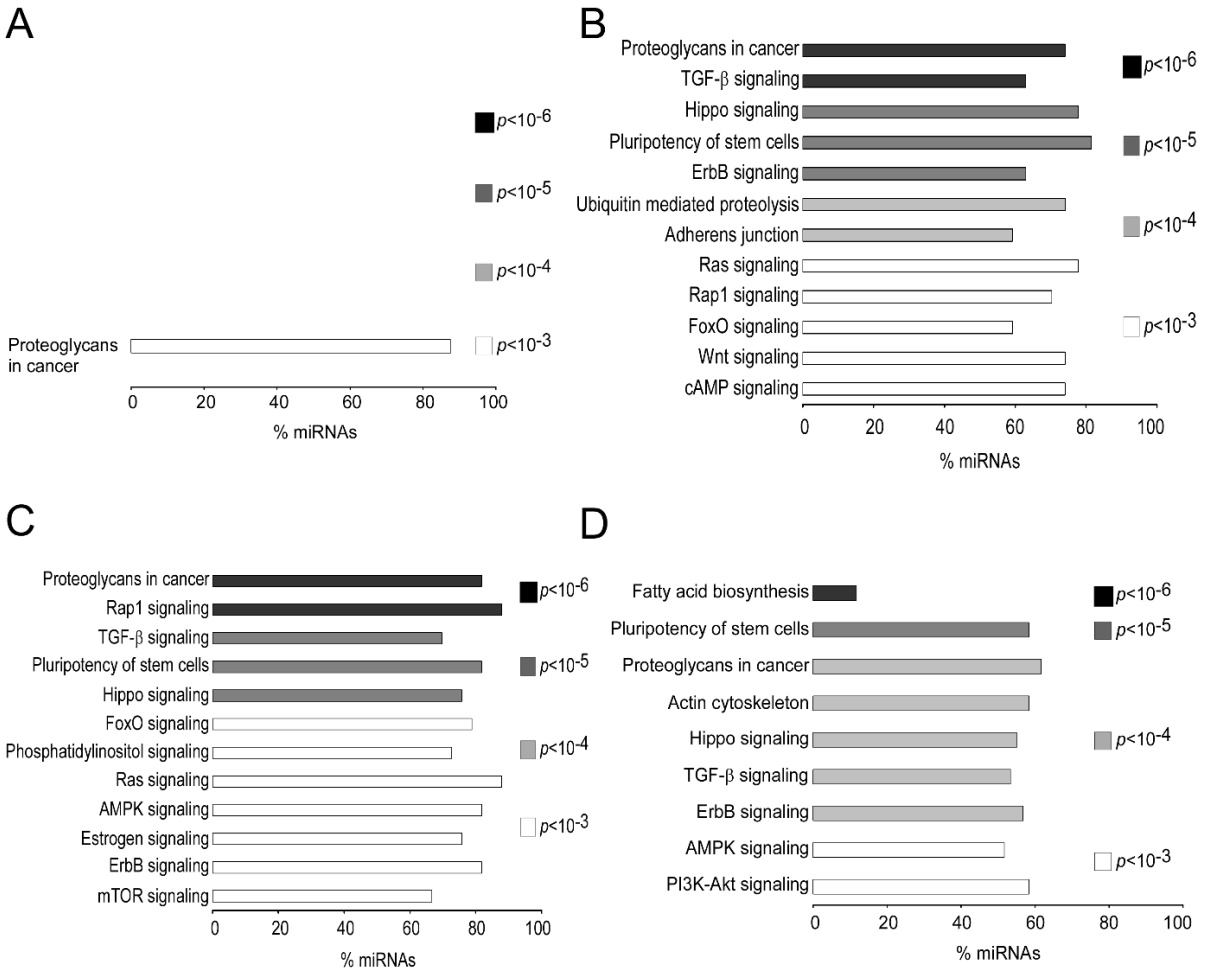


Figure 6.4: MiR expression profile analysis highlights TGF-β signalling pathway in MBC derived cells. Identification of the pathways enriched with targets of miRs from cluster 1 (A), cluster 2 (B), cluster 3 (C) and cluster 4 (D) described in **Table 6.8-6.11** using DIANA-miRPath v3.0 online software suite for miR functional analysis. Most significant pathways were selected at a *p*-value inferior to 0.001. Length of histogram bar is proportional to the percentage of miRs in the signature (x-axis) associated with a particular pathway (indicated to the left). Pathways are ordered by significance, with the highest significant values on top.

6.4.3 MBC derived cells drug resistance miR expression signatures

MiRs represent another layer on regulating gene expression and have been identified to be involved in drug resistance in a variety of carcinomas (Yang *et al.*, 2008; Zhou *et al.*, 2010; Kutanzi *et al.*, 2011; Zhou *et al.*, 2014; Hu *et al.*, 2016a). To ascertain whether there were miRs responsible for MDR in metaplastic breast cancer derived cells, I performed miR expression profiling of doxorubicin- and paclitaxel-resistant derivatives of both metaplastic derived HS578T (HS-DOX and HS-TX) and BAS (BAS-DOX and BAS-TX) cells, with their corresponding parental cells as control. Filtering raw data with the threshold set for fold expression led to identification of miR expression signatures for each of the drug resistant HS-DOX, HS-TX, BAS-DOX and BAS-TX cells (**Table 6.12-6.15**).

Next, miR expression data were categorized in a same way as with the gene expression to identify miR signatures common for doxorubicin and paclitaxel resistance across the cell lines, as well as a MDR signature (that is, resistance to both doxorubicin and paclitaxel) for each MBC derived cell line. The doxorubicin and paclitaxel resistance miR expression signatures, which show miRs with a similar pattern of expression in resistant cells generated by exposure to each drug in both cells, included a total of 23 (3 up-regulated and 20 down-regulated miRs) and 9 (6 up-regulated and 3 down-regulated miRs) differentially expressed miRs, respectively (**Table 6.16-6.17**). Similarly, a MDR miR expression signature for HS578T cells, representing similar changes in miR expression in both drug resistant HS-DOX and HS-TX cells, comprised 9 differentially expressed miRs (4 up-regulated and 5 down-regulated miRs) (**Table 6.18**). Equally, a MDR miR expression signature was obtained for BAS cells, showing miRs with a similar pattern of expression in both drug resistant BAS-DOX and BAS-TX cells, and this signature included 49 differentially expressed miRs (11 up-regulated and 38 down-regulated miRs) (**Table 6.19**). Interestingly, BAS cells MDR miR expression signature showed down-regulation of miR-495-3p (5.1-fold in BAS-DOX and 6.1-fold in BAS-TX cells), a miR targeting both *TGFB2* and *FOXC1* (Welten *et al.*, 2017; Xu *et al.*, 2016), regulators of MDR phenotype in MBC derived BAS cells. As in the case of gene expression signature, there was no common MDR miR signature shared for all four drug-resistant cells, although reducing the threshold for fold expression from 2 to 1.5 showed up-regulation of miR-5004-5p and down-regulation of miR-505-3p, miR-487b and miR-337-5p (**Table 6.20**). This suggests once more that HS578T and BAS cells acquire MDR phenotype via modulation of a different set of key molecules in each cell.

Table 6.12: Most differentially regulated miRs in HS-DOX resistant cells

miRNA	**Fold expression**[a]
hsa-miR-3937	3.9
hsa-miR-3180	3.8
hsa-miR-31-3p	3.3
hsa-miR-1231	3.2
hsa-miR-4674	3.2
hsa-miR-4776-2	3.1
hsa-miR-4673	2.8
hsa-miR-612	2.8
hsa-miR-7106-5p	2.8
hsa-miR-6886-3p	2.8
hsa-miR-4634	2.7
hsa-miR-431-5p	-4.3
hsa-miR-519c-5p	-4.3
hsa-miR-523-5p	-4.3
hsa-miR-518e-5p	-4.3
hsa-miR-522-5p	-4.3
hsa-miR-519a-5p	-4.3
hsa-miR-519b-5p	-4.3
hsa-miR-485-5p	-4.3
hsa-miR-518b	-4.4
hsa-miR-433-3p	-4.5
hsa-miR-409-3p	-4.7
hsa-miR-382-5p	-4.7
hsa-miR-370-3p	-5.2
hsa-miR-432-5p	-5.9
hsa-miR-379-5p	-6.0
hsa-miR-525-5p	-6.4

[a]Positive expression values denote up-regulation and negative expression values denote down-regulation respect to HS578T cells

Table 6.13: Most differentially regulated miRs in HS-TX resistant cells

miRNA	**Fold expression**[a]
hsa-miR-518e-3p	5.5
hsa-miR-372-3p	4.4
hsa-miR-515-3p	4.1
hsa-miR-523-3p	3.7
hsa-miR-524-5p	3.5
hsa-miR-516b-2	3.5
hsa-miR-516a-1	3.4
hsa-miR-516a-2	3.4
hsa-miR-518a-3p	3.2
hsa-miR-516a-5p	3.0
hsa-miR-517-5p	3.0
hsa-miR-517c-3p	3.0
hsa-miR-520c-3p	3.0
hsa-miR-4688	-2.2
hsa-miR-2276-3p	-2.2
hsa-miR-6738-5p	-2.2
hsa-miR-183-3p	-2.3
hsa-miR-3663-5p	-2.3
hsa-miR-6856-5p	-2.3
hsa-miR-6872-5p	-2.5
hsa-miR-3200-3p	-2.5
hsa-miR-1226-3p	-2.7
hsa-miR-6823-5p	-4.4

[a]Positive expression values denote up-regulation and negative expression values denote down-regulation respect to HS578T cells

Table 6.14: Most differentially regulated miRs in BAS-DOX resistant cells

miRNA	**Fold expression**[a]
hsa-miR-34c-5p	4.4
hsa-miR-34c-3p	4.1
hsa-miR-6068	4.0
hsa-miR-3910-1	3.6
hsa-miR-3910-2	3.6
hsa-miR-1263	3.5
hsa-miR-3921	3.3
hsa-miR-548x-3p	3.1
hsa-miR-3188	3.0
hsa-miR-1296-3p	2.7
hsa-miR-6789	2.6
hsa-miR-487b-3p	-4.6
hsa-miR-382-5p	-4.6
hsa-miR-485-3p	-4.6
hsa-miR-409-5p	-5.0
hsa-miR-495-3p	-5.1
hsa-miR-379-5p	-5.3
hsa-miR-433-3p	-5.6
hsa-miR-431-5p	-6.1
hsa-miR-487a-3p	-6.1
hsa-miR-543	-6.6

[a]Positive expression values denote up-regulation and negative expression values denote down-regulation respect to BAS cells

Table 6.15: Most differentially regulated miRs in BAS-TX resistant cells

miRNA	**Fold expression**[a]
hsa-miR-548x-3p	5.5
hsa-miR-1263	5.2
hsa-miR-451a	5.1
hsa-miR-202-5p	4.5
hsa-miR-3921	4.1
hsa-miR-603	3.9
hsa-miR-4720-5p	3.9
hsa-miR-3910-1	3.9
hsa-mirR-3910-2	3.9
hsa-miR-548ae	3.7
hsa-miR-3908	3.4
hsa-miR-1185-1-3p	-5.4
hsa-miR-487b-3p	-5.5
hsa-miR-409-3p	-5.7
hsa-miR-495-3p	-6.1
hsa-miR-370-3p	-6.2
hsa-miR-487a-3p	-6.4
hsa-miR-432-5p	-6.5
hsa-miR-543	-6.5
hsa-miR-935	-6.5
hsa-miR-379-5p	-6.6
hsa-miR-433-3p	-7.3

[a]Positive expression values denote up-regulation and negative expression values denote down-regulation respect to BAS cells

Table 6.16: Differentially regulated miRs common between HS-DOX and BAS-DOX resistant cells

miRNA	**HS-DOX**	**BAS-DOX**
hsa-miR-4674	3.2[a]	2.3
hsa-miR-3621	2.5	2.5
hsa-miR-4634	2.7	2.3
hsa-miR-505-3p	-2.0	-2.1
hsa-miR-381-3p	-2.4	-2.1
hsa-let-7a-2-3p	-2.3	-2.6
hsa-miR-337-5p	-2.0	-3.6
hsa-miR-1185-2-3p	-2.6	-2.5
hsa-miR-493-3p	-3.9	-2.5
hsa-miR-1185-1-3p	-2.6	-4.0
hsa-miR-432-5p	-5.9	-2.2
hsa-miR-485-3p	-2.5	-4.6
hsa-miR-487a-3p	-2.3	-6.1
hsa-miR-370-3p	-5.2	-2.8
hsa-miR-485-5p	-4.3	-3.3
hsa-miR-409-3p	-4.7	-3.2
hsa-miR-543	-2.7	-6.6
hsa-miR-654-5p	-3.5	-4.4
hsa-miR-487b-3p	-3.5	-4.6
hsa-miR-382-5p	-4.7	-4.6
hsa-miR-433-3p	-4.5	-5.6
hsa-miR-431-5p	-4.3	-6.1
hsa-miR-379-5p	-6.0	-5.3

[a]Positive expression values denote up-regulation and negative expression values denote down-regulation respect to drug sensitive cells

Table 6.17: Differentially regulated miRs common between HS-TX and BAS-TX resistant cells

miRNA	HS-TX	BAS-TX	Average fold change
hsa-miR-1298-3p	1.6[a]	3.3	2.5[b]
hsa-miR-3908	1.6	3.4	2.5
hsa-miR-5004-5p	1.9	2.8	2.4
hsa-miR-337-3p	1.9	2.8	2.3
hsa-miR-517c-3p	3.0	1.6	2.3
hsa-miR-450b-5p	1.7	2.4	2.0
has-miR-487b	-2.0	-2.4	-2.2
hsa-miR-505-3p	-1.9	-2.7	-2.2
hsa-miR-337-5p	-1.6	-3.8	-2.3

[a]Positive expression values denote up-regulation and negative expression values denote down-regulation respect to drug sensitive cells

[b]List includes miRs with a threshold of +/- 1.5-fold in individual signatures but a threshold of +/- 2-fold in the average of both signatures

Table 6.18: Differentially regulated miRs common between HS-DOX and HS-TX resistant cells

miRNA	HS-DOX	HS-TX
hsa-miR-31-3p	3.3[a]	2.7
hsa-miR-4776-2	3.1	2.3
hsa-miR-6886-3p	2.8	2.5
hsa-miR-1231	3.2	2.0
hsa-miR-2276-3p	-2.1	-2.2
hsa-miR-6872-5p	-2.0	-2.5
hsa-miR-487b	-2.5	-2.0
hsa-miR-6856-5p	-2.5	-2.3
hsa-miR-3663-5p	-2.5	-2.3

[a]Positive expression values denote up-regulation and negative expression values denote down-regulation respect to HS578T cells

Table 6.19: Differentially regulated miRs common between BAS-DOX and BAS-TX resistant cells

miRNA	BAS-DOX	BAS-TX
hsa-miR-1263	3.5[a]	5.2
hsa-miR-548x-3p	3.1	5.5
hsa-miR-3921	3.3	4.1
hsa-mir-3910-1	3.6	3.9
hsa-mir-3910-2	3.6	3.9
hsa-miR-603	2.1	3.9
hsa-miR-6068	4.0	2.1
hsa-mir-3908	1.9	3.4
hsa-miR-628-5p	2.2	3.1
hsa-miR-6856-5p	2.2	2.8
hsa-miR-5094	2.2	2.0
hsa-miR-6754-5p	-2.2	-2.0
hsa-miR-412-5p	-2.3	-2.1
hsa-miR-758-5p	-2.6	-2.0
hsa-miR-505-3p	-2.1	-2.7
hsa-miR-19a-3p	-2.9	-2.2
hsa-miR-411-5p	-2.2	-2.8
hsa-mir-487a	-2.5	-2.4
hsa-miR-299-5p	-2.3	-2.7
hsa-miR-329-3p	-2.5	-2.6
hsa-miR-29b-3p	-2.6	-2.8
hsa-miR-323a-3p	-2.9	-2.5
hsa-miR-148a-3p	-2.3	-3.3
hsa-miR-323a-5p	-2.9	-2.8
hsa-miR-1185-2-3p	-2.5	-3.5
hsa-miR-29c-3p	-3.6	-2.6
hsa-miR-485-5p	-3.3	-3.0
hsa-miR-654-3p	-2.7	-3.8
hsa-miR-493-3p	-2.5	-5.0
hsa-miR-432-5p	-2.2	-6.5
hsa-miR-126-3p	-3.6	-3.2
hsa-miR-203a	-2.7	-4.8
hsa-miR-337-5p	-3.6	-3.8

[a]Positive expression values denote up-regulation and negative expression values denote down-regulation respect to BAS cells

Table 6.19: Differentially regulated miRs common between BAS-DOX and BAS-TX resistant cells (Contd.)

miRNA	BAS-DOX	BAS-TX
hsa-miR-376a-3p	-4.0[a]	-3.6
hsa-miR-370-3p	-2.8	-6.2
hsa-miR-382-5p	-4.6	-3.3
hsa-miR-409-3p	-3.2	-5.7
hsa-miR-409-5p	-5.0	-3.6
hsa-miR-376c-3p	-4.3	-4.6
hsa-miR-654-5p	-4.4	-4.6
hsa-miR-1185-1-3p	-4.0	-5.4
hsa-miR-485-3p	-4.6	-4.9
hsa-miR-487b-3p	-4.6	-5.5
hsa-miR-495-3p	-5.1	-6.1
hsa-miR-431-5p	-6.1	-5.2
hsa-miR-379-5p	-5.3	-6.6
hsa-miR-487a-3p	-6.1	-6.4
hsa-miR-433-3p	-5.6	-7.3
hsa-miR-543	-6.6	-6.5

[a]Positive expression values denote up-regulation and negative expression values denote down-regulation respect to BAS cells

Table 6.20: Differentially regulated miRs common to all signatures

miRNA	HS-DOX	BAS-DOX	HS-TX	BAS-TX	Average fold change
hsa-miR-5004-5p	2.1[a]	1.5	1.9	2.8	2.1[b]
hsa-miR-505-3p	-2.0	-2.1	-1.9	-2.7	-2.2
hsa-miR-487b	-2.5	-1.9	-2.0	-2.4	-2.2
hsa-miR-337-5p	-2.0	-3.6	-1.6	-3.8	-2.8

[a]Positive expression values denote up-regulation and negative expression values denote down-regulation respect to drug sensitive cells

[b]List includes miRs with a threshold of +/- 1.5-fold in individual signatures but a threshold of +/- 2-fold in the average of the four signatures

6.4.4 Metaplastic derived HS578T and BAS cells acquire chemotherapeutics resistance via pathways related to aggressive cellular phenotypes

Acquisition of chemotherapy resistance involves the modulation of a complex network of signalling pathways (Lage, 2008; Delou *et al.*, 2019; Nedeljković & Damjanović, 2019). Accumulated evidence indicates that miRs are involved in the regulation of various signalling pathways (Wang *et al.*, 2010; Du & Shim, 2016). Identification of the pathways enriched with targets of a certain miR or multiple miRs is the key to understanding their regulatory roles. To functionally characterize each drug resistance miR expression signature (doxorubicin resistance, paclitaxel resistance, HS578T cells MDR, and BAS cells MDR signatures) obtained, I interrogated the DIANA-miRPath v3.0, an online software suite for miR functional analysis (Vlachos *et al.*, 2015). The doxorubicin resistance miR expression signature included miRs associated with pathways related to extracellular matrix-regulated tumour progression and metastasis (proteoglycans in cancer and adherens junction), EMT (TGF-β, Ras and Rap1 signalling) and stemness (pluripotency of stem cells and hippo signalling), among others (**Figure 6.5 A**). MiRs in the paclitaxel resistance miR expression signature were identified to be involved in EMT (Wnt signalling) and pluripotency of stem cells (**Figure 6.5 B**). Interestingly, pathway analysis indicated that miRs in both HS578T and BAS cells MDR miR expression signatures involved in pathways related to cancer hallmark EMT. HS578T cells MDR miR expression signature included miRs associated with Wnt signalling, a signalling pathway involved in EMT induction (Wang & Zhou, 2011) (**Figure 6.5 C**). MiRs in BAS cells MDR miR expression signature were found to be involved in EMT (TGF-β, Ras, Rap1 and PI3K-AKT signalling), stemness (pluripotency of stem cells and hippo signalling) and ECM-regulated tumour growth and metastasis (proteoglycans in cancer, adherens junction and focal adhesion), among others (**Figure 6.5 D**). Overall, the metaplastic breast cancer derived drug resistant cells differentially expressed miRs involved in aggressive cellular phenotypes, such as EMT and stemness.

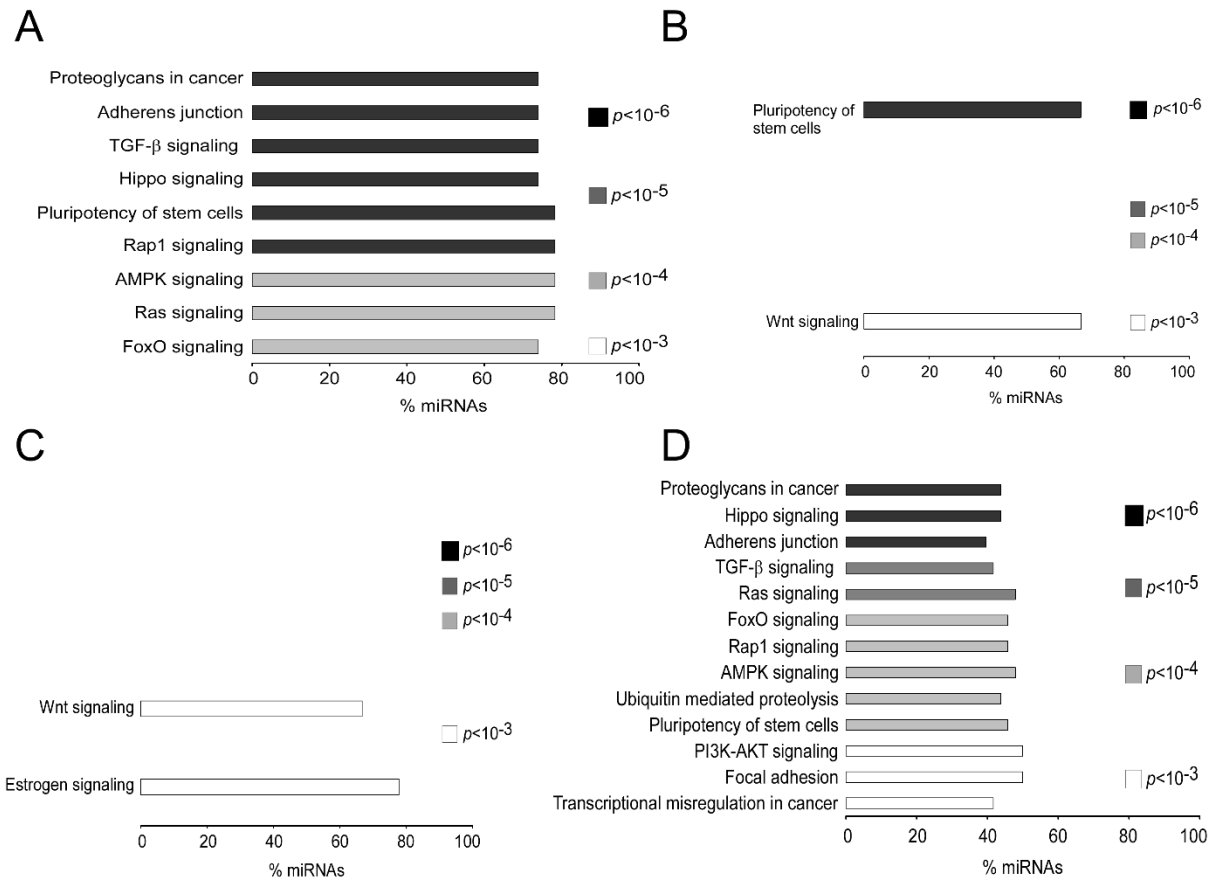


Figure 6.5: Pathways associated with chemotherapeutics resistance in MBC derived cells. Pathway identification was performed using DIANA-miRPath v3.0 online software suite for miR functional analysis from the miR expression signatures obtained with miR expression profiling of metaplastic breast cancer derived drug resistant cells (**Table 6.16-6.19**). A, Pathways enriched with targets of miRs from doxorubicin resistance signature. B, Pathways enriched with targets of miRs from paclitaxel resistance signature. C, Pathways enriched with targets of miRs from HS578T cells MDR signature. D, Pathways enriched with targets of miRs from BAS cells MDR signature. Most significant pathways were selected at a *p*-value inferior to 0.001. Length of histogram bar is proportional to the percentage of miRs in the signature (x-axis) associated with a particular pathway (indicated to the left). Pathways are ordered by significance, with the highest significant values on top.

6.4.5 MiR-495-3p regulates *FOXC1* and *TGFB2* expression in BAS cells

We have already seen the TGF-β-FOXC1 axis regulating MDR phenotype in MBC derived BAS cells. Doxorubicin- and paclitaxel-resistant BAS cells (BAS-DOX and BAS-TX, respectively) showed an up-regulation of both FOXC1 and *TGFB2*. Interestingly, miR expression array analysis identified down-regulation of miR-495-3p, which targets both *FOXC1* and *TGFB2* (Xu *et al.*, 2016; Welten *et al.*, 2017; Elian, Yan & Walter, 2018), in BAS-DOX (5.1-fold) and BAS-TX (6.1-fold) cells (**Table 6.19**). To ascertain whether modulation of miR-495-3p expression alters *FOXC1* and *TGFB2* expression, I transiently transfected BAS MDR cells (BAS-DOX and BAS-TX) and parental BAS cells with miR-495-3p mimic and miR-495-3p inhibitor, respectively. Reassuringly, *FOXC1* and *TGFB2* expression levels decreased in both BAS-DOX and BAS-TX MDR cells upon transfection with miR-495-3p mimic (**Figure 6.6 A and B**). In addition, *ROR1*, another miR-495-3p target (Vlachos *et al.*, 2015) upregulated in both BAS-DOX and BAS-TX cells (**Table 5.25 in chapter 5 and Figure 6.6 C**), was also down-regulated in both MDR cells transfected with miR-495-3p mimic. Furthermore, interrogation of some common EMT and CSC markers revealed that both BAS-DOX and BAS-TX MDR cells transfected with miR-495-3p mimic showed down-regulation of EMT marker *SNAI2* (although EMT marker *ZEB1* was also down-regulated in BAS-TX cells), and CSC markers, *NANOG* and *POU5F1* (**Figure 6.6 A and B**). Conversely, *FOXC1*, *TGFB2* and *ROR1* expression was up-regulated in BAS cells transfected with miR-495-3p inhibitor. Moreover, BAS cells upon transfection with miR-495-3p inhibitor also showed up-regulation of several EMT markers, including *SNAI1*, *SNAI2* and *ZEB2*, and CSC markers, such as *NANOG* and *POU5F1* (**Figure 6.6 D**).

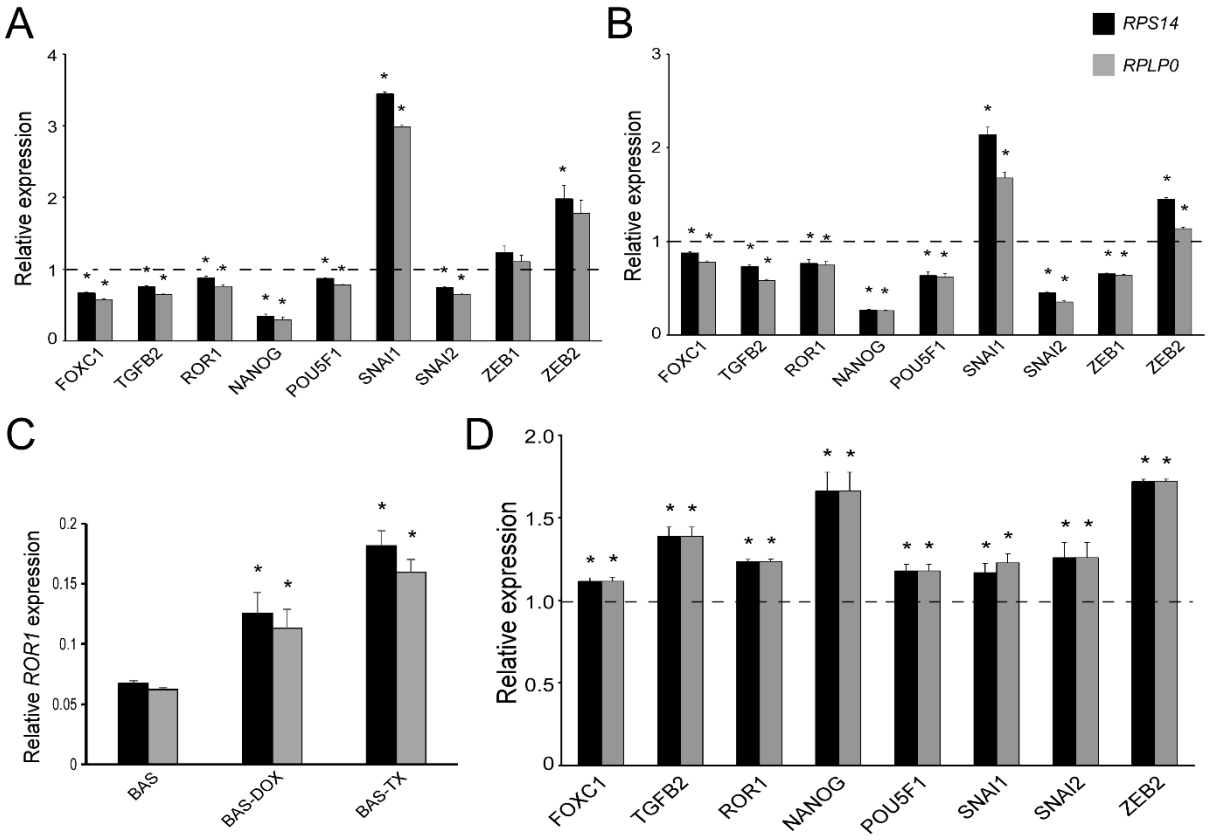


Figure 6.6: Experimental modulation of miR-495-3p alters *FOXC1* and *TGFB2* expression in BAS cells. A-B, Expression of miR-495-3p targets and some well-known EMT and CSC markers after transfection with miR-495-3p mimic in BAS-DOX (A) and BAS-TX (B) MDR cells. C, Expression of *ROR1* in BAS-DOX and BAS-TX MDR cells. D, Expression of miR-495-3p targets and some well-known EMT and CSC markers in naïve BAS cells transfected with miR-495-3p inhibitor. In all cases the gene expression was measured using quantitative real-time PCR. The mRNAs levels were normalized to the *RPS14* and *RPLP0* genes. The relative expression of each gene after transfection with miR-495-3p mimic or inhibitor were calculated with respect to their expression obtained after transfection with corresponding negative control (dashed lines). Data represent the average ± SD of three independent experiments. *, $p<0.05$.

6.4.6 MiR-495-3p regulates MDR phenotype in BAS cells

As we have seen miR-495-3p negatively regulates *FOXC1* and *TGFB2* expression, I aimed to determine whether experimental modulation of its expression would affect MDR phenotype in BAS cells. Drug sensitivity analyses indicated that BAS cells transfected with miR-495-3p inhibitor, which caused an up-regulation of both *FOXC1* and *TGFB2*, showed an increased resistance to both doxorubicin and paclitaxel. In contrast, both BAS-DOX and BAS-TX

MDR cells transfected with miR-495-3p mimic, which caused a down-regulation of both *FOXC1* and *TGFB2*, showed a decrease in doxorubicin and paclitaxel resistance (**Figure 6.7**). Thus, miR-495-3p regulates MDR phenotype in MBC derived BAS cells via targeting both *FOXC1* and *TGFB2* mRNAs.

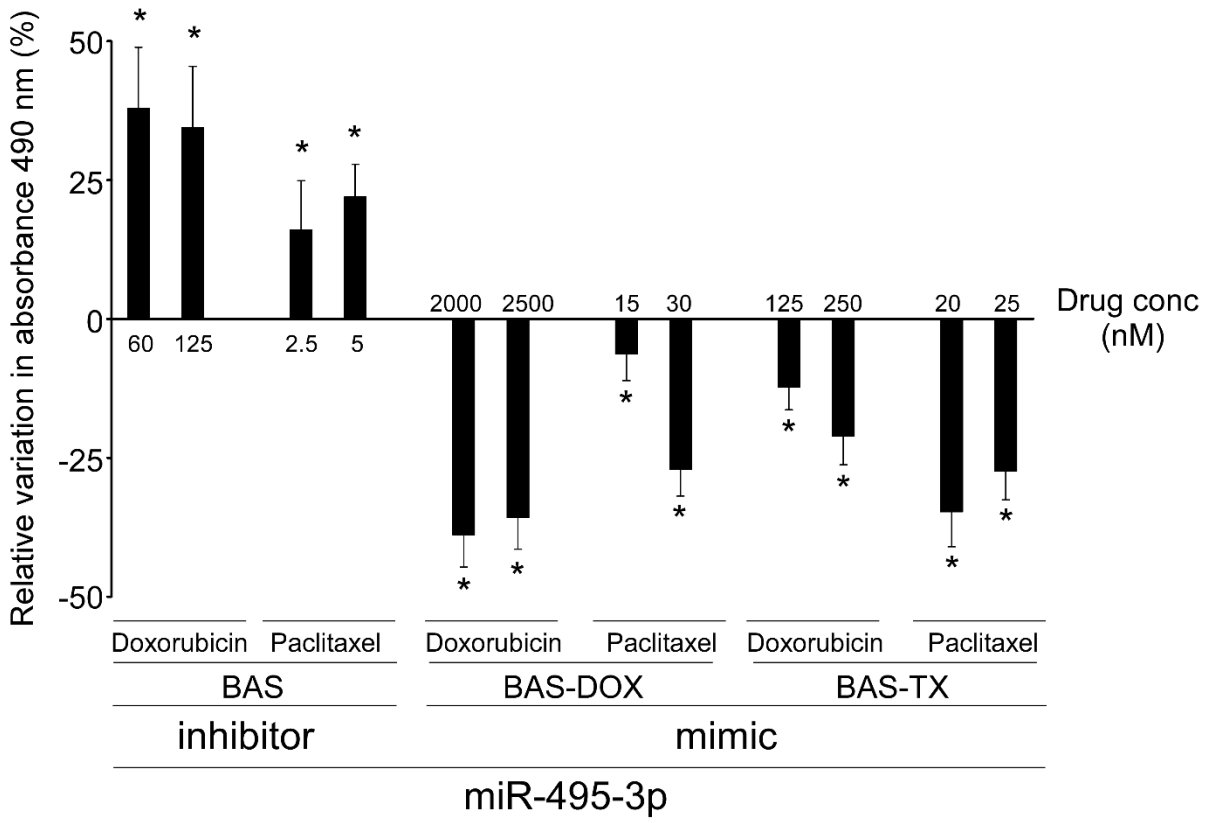


Figure 6.7: Experimental modulation of miR-495-3p expression in BAS cells and their drug resistant derivatives (BAS-DOX and BAS-TX MDR cells) alters doxorubicin and paclitaxel sensitivity. Doxorubicin and paclitaxel sensitivity of BAS naïve and MDR cells transfected with miR-495-3p inhibitor and mimic, respectively, was determined by sulphorhodamine B assays. Cells were transfected in 6-well plates for 24 hours and then seeded in 96-well plates (2 x 10^3 cells / well), followed by drug treatment for 72 hours. The optical density (OD) was measured at 490 nm after solubilization of protein bound SRB stain. Relative variation was calculated after normalization to the respective miR-495-3p inhibitor or mimic negative control (Positive values denote increase in drug resistance; negative values denote increase in drug sensitivity). Data represent the average ± SD of three independent experiments. *, $p<0.05$.

6.4.7 MiR expression analysis of different breast cancer subtypes

In cancer, normal biological processes are dysregulated due to the acquisition of capabilities termed as cancer hallmarks (Hanahan & Weinberg, 2011). As miRs can target many genes involved in biological processes, such as development, cellular proliferation, differentiation, apoptosis, and signal transduction, aberrant miR expression plays vital roles in dysregulation of these biological processes during development of human malignancies (Ruan, Fang & Ouyang, 2009; Kutanzi *et al.*, 2011). Several studies have associated miRs with many aspects of cancer, including disease progression, metastasis, and acquisition of chemotherapeutic resistance (Kutanzi *et al.*, 2011). To assess the aberration in miR expression in breast cancer, I aimed to investigate miR expression profile of different breast cancer subtypes, including metaplastic breast carcinoma. For this, miR expression profiling was performed using a small panel of breast clinical samples, comprising normal breast tissues both from tissues with non-tumoral morphological abnormalities (Normal-MA, n = 2) and cosmetic reduction mammoplasties (Normal-CRM, n = 3), non-cancerous tumours (Benign, n = 3), invasive ductal carcinoma (IDC, n = 5), invasive lobular carcinoma (ILC, n = 5), and MBC (Metaplastic, n = 5).

Principal component analysis (PCA) showed that one sample each from invasive ductal carcinoma (Invasive_Ductal 5) and metaplastic breast carcinoma (Metaplastic 2) did not cluster with their respective group (**Figure 6.8 A**). These two samples were considered as outliers and discarded from further analysis. Hierarchical clustering showed that the expression pattern of normal breast tissues with non-tumoral morphological abnormalities (Normal-MA) was completely different from that of cosmetic reduction mammoplasties of normal tissues (Normal-CRM) (**Figure 6.8 B**). Therefore, only cosmetic reduction mammoplasties of normal breast tissues were considered as a healthy control group for subsequent analysis. Although there were no miR expression signatures unique to each group, four interesting miR expression clusters were identified, showing a population of miRs differentially expressed across the breast cancer subtypes (**Figure 6.8 B**). Cluster 1 comprised miRs down-regulated in both invasive ductal and invasive lobular carcinomas (**Figure 6.8 C**). MiRs in cluster 2 were up-regulated in benign tumours and invasive ductal carcinoma, but down-regulated in MBC (**Figure 6.8 D**). Interestingly, cluster 3 showed a population of miRs down-regulated in benign tumours, invasive ductal carcinoma, and MBC, whereas miRs in cluster 4 were up-regulated in these three categories (**Figure 6.8 E and F**). Considering only

MBC subtype, miRs in both clusters 2 and 3 were down-regulated in MBC, whereas cluster 4 showed the miRs up-regulated in MBC. Invasive lobular carcinoma showed a similar miR expression pattern to that of normal tissue, except for miRs in cluster 1 which were extensively down-regulated.

Pathway analysis (Vlachos *et al.*, 2015) indicated all four miR expression clusters included miRs involved in ECM-mediated signalling pathways regulating tumour growth and metastasis, such as proteoglycans in cancers, focal adhesion, adherens junction, or ECM-receptor interaction (**Figure 6.9**). In addition, miRs in cluster 3 were found to be involved in EMT (TGF-β, Rap1, Wnt, PI3K-AKT, RAS and MAPK signalling) and stemness (Hippo signalling) (**Figure 6.9 C**). Equally, cluster 4 also included miRs involved in EMT (Ras and MAPK signalling) and stemness (Hippo signalling) (**Figure 6.9 D**).

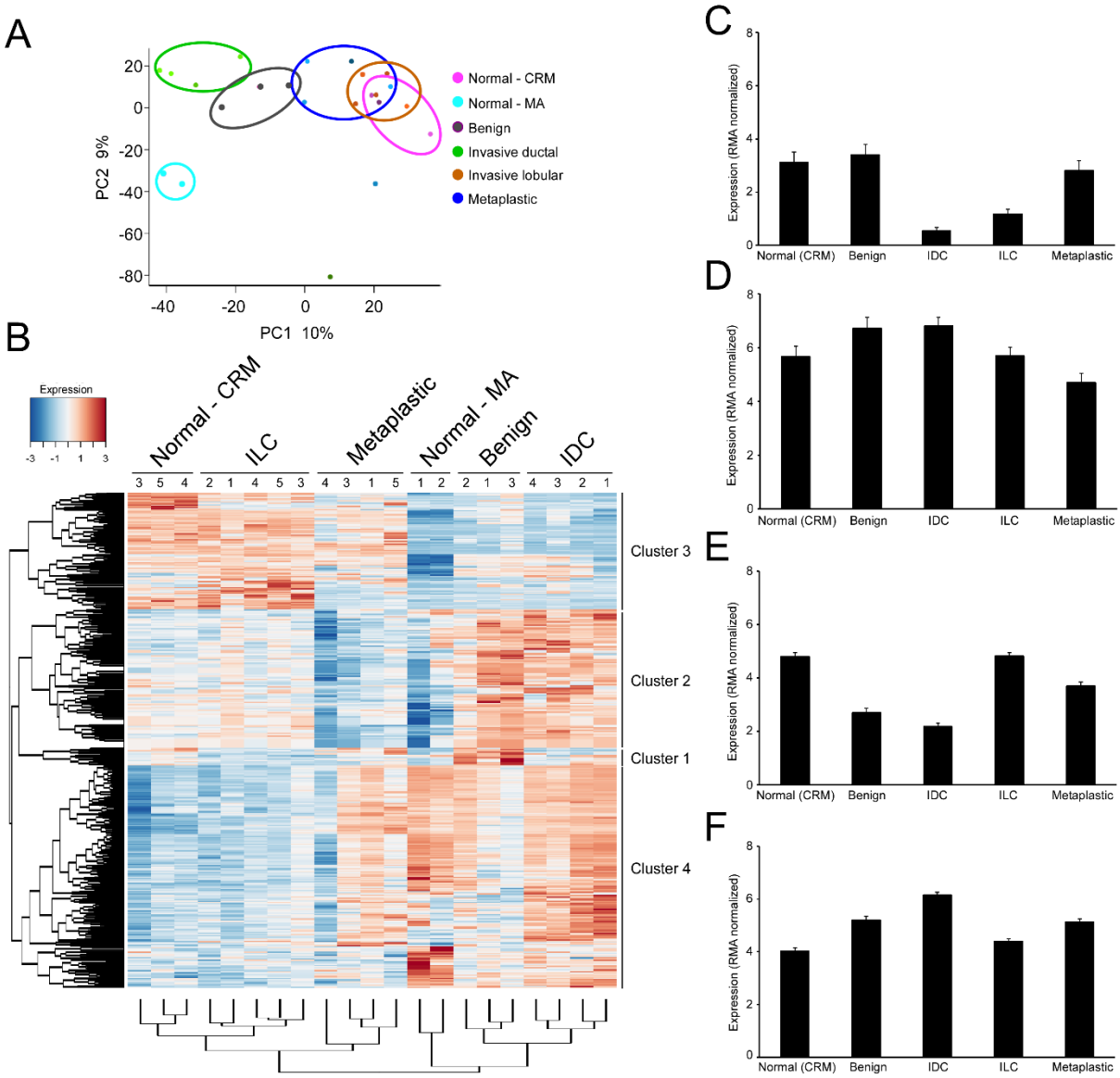


Figure 6.8: MiR expression profiling of different subtypes of breast cancer. Small RNA expression was obtained with GeneChip miRNA 4.0 Array in a small panel of breast clinical samples, including normal breast tissues with non-tumoral morphological abnormalities (Normal-MA, *n* = 2), cosmetic reduction mammoplasties of normal breast tissues (Normal-CRM, *n* = 3), non-cancerous tumours (Benign, *n* = 3), invasive ductal carcinoma (IDC, *n* = 5), invasive lobular carcinoma (ILC, *n* = 5), and MBC (Metaplastic, *n* = 5). A, Principal component analysis (PCA) plot depicting miR expression patterns of all the samples. B, Hierarchical clustering of small RNA expression of all the samples after removing two as outliers (one of each from IDC and MBC). Clusters showing the differential expression of miRs in different breast cancer subtypes are indicated. C-F, GeneChip miRNA 4.0 Array RMA normalized average expression values ± SE in cluster 1 (C), cluster 2 (D), cluster 3 (E) and cluster 4 (F).

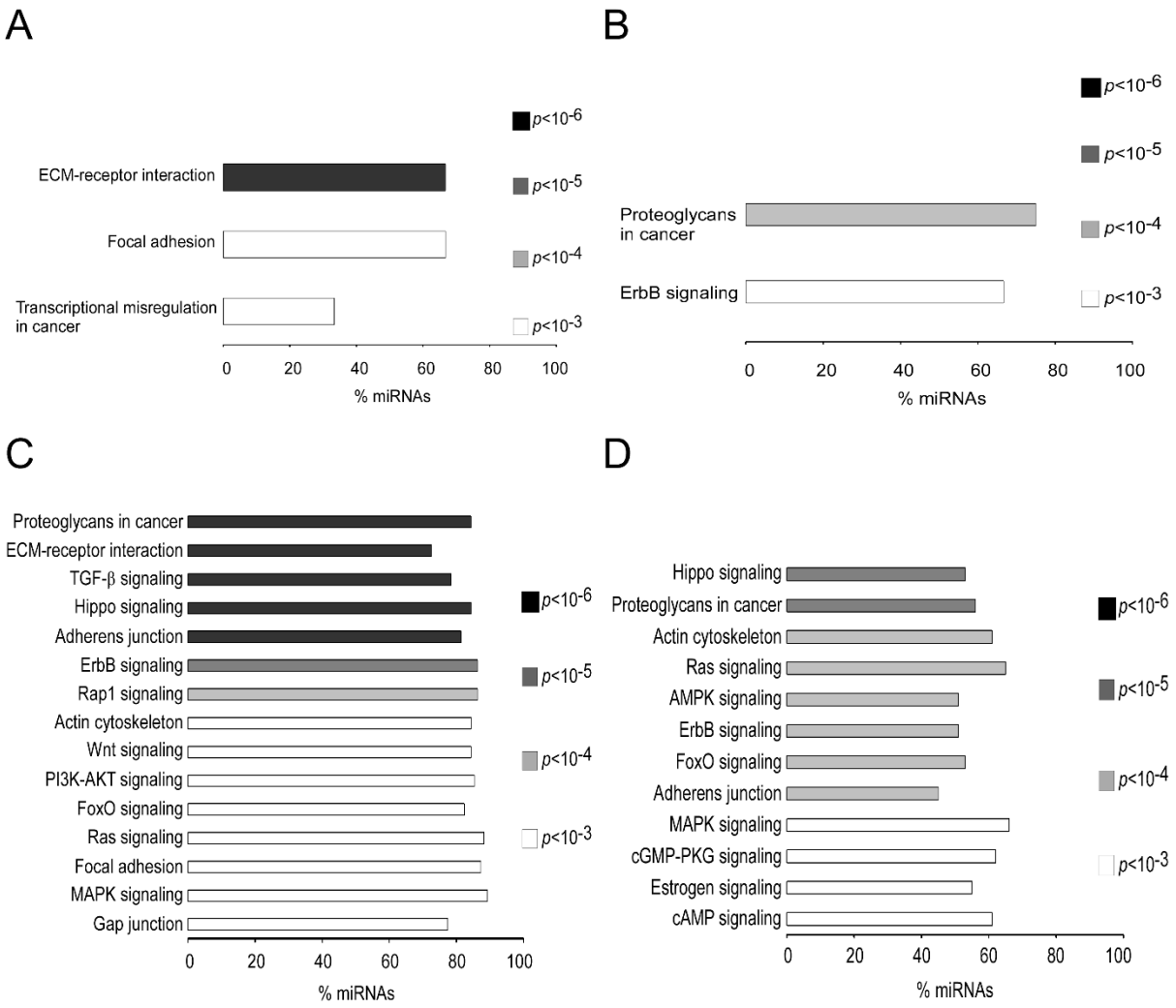


Figure 6.9: MiR expression profile analysis highlights pathways associated with breast cancer. Pathway identification was performed using DIANA-miRPath v3.0 online software suite for miR functional analysis from the miR expression clusters (**Figure 6.8 B**) obtained with miR expression profiling of a small panel of breast cancer clinical samples. A, Pathways enriched with targets of miRs from cluster 1. B, Pathways enriched with targets of miRs from cluster 2. C, Pathways enriched with targets of miRs from cluster 3. D, Pathways enriched with targets of miRs from cluster 4. Most significant pathways were selected at a *p*-value inferior to 0.001. Length of histogram bar is proportional to the percentage of miRs in the signature (x-axis) associated with a particular pathway (indicated to the left). Pathways are ordered by significance, with the highest significant values on top.

6.4.8 Discriminatory miR expression signature between MBC and IDC

MBC is characterized by the coexistence of ductal carcinomatous component with the transdifferentiated sarcomatous component in the same tumour (Lien *et al.*, 2007). Interestingly, MBCs differ from conventional IDC in several clinical and pathological aspects, including relatively large tumour size at diagnosis (Bian *et al.*, 2016), less frequent axillary nodal involvement of similar tumour size (Park *et al.*, 2010; Schwartz *et al.*, 2013; Tray, Taff & Adams, 2019), higher incidence of triple-negative molecular subtype (Park *et al.*, 2010; Jung *et al.*, 2010). Moreover, this morphological subtype of breast cancer is associated with poorer prognosis than the conventional IDC (Song *et al.*, 2013). A study recognized MBC as a genetically discrete breast cancer subtype distinct from the conventional ductal carcinoma of the breast and identified genes differentially expressed in MBC relative to ductal carcinoma. This discriminating gene expression signature included 208 genes, with 87 genes up-regulated and 121 genes down-regulated in MBC (Lien *et al.*, 2007). As the miRs represent another layer on regulation of gene expression, the discriminating miR expression profile between MBC and ductal carcinoma of the breast, particularly IDC, would be crucial to understand the pathobiology of MBC. For this, I aimed to identify miRs differentially expressed in MBC relative to IDC from the miR expression data obtained with a small panel of breast cancer clinical samples, including both IDC and MBC (**Figure 6.8 B**). Filtering these raw data with the threshold set for fold expression greater than 5 (up-regulated miRs) and lower than -5 (down-regulated miRs) led to identification of most differentially expressed miRs in MBC, with respect to IDC. This discriminating miR expression signature between MBC and IDC included 25 miRs, with 23 miRs up-regulated and 2 miRs down-regulated in MBC (**Table 6.21**). Interestingly, miR-200c-3p, a member of miR-200 family, was significantly down-regulated in MBC, compared to IDC. Previous reports identified that down-regulation of this miR contributes to the paclitaxel resistance in breast cancer MCF-7 cells (Chen *et al.*, 2018a) and to the cisplatin resistance in gastric cancer cells (Li *et al.*, 2019a). Moreover, miR-200c negatively regulates EMT, as well as supresses CSC-like phenotypes in different cancers, including breast cancer (Mutlu *et al.*, 2016). Pathway analysis (Vlachos *et al.*, 2015) indicated that many miRs in this signature involved in pathways related to ECM-regulated tumour growth and metastasis (ECM-receptor interaction, proteoglycans in cancer and focal adhesion), EMT (TGF-β, PI3K-AKT, Ras, MAPK and Wnt signalling) and stemness (pluripotency of stem cells and hippo signalling) (**Figure 6.10**).

Table 6.21: Most differentially regulated miRs between metaplastic and IDC

Transcript	Metaplastic vs IDC[a]
hsa-miR-1271-5p	15.7
hsa-miR-199a-5p	13.9
hsa-miR-143-3p	11.8
hsa-miR-199a-3p	11.4
hsa-miR-199b-3p	11.4
hsa-miR-127-3p	11.2
hsa-miR-15a-5p	10.3
hsa-miR-152-3p	9.9
hsa-miR-15b-5p	9.6
hsa-miR-195-5p	9.5
hsa-miR-221-3p	8.5
hsa-miR-497-5p	8.1
hsa-miR-27a-3p	8.0
hsa-miR-28-3p	7.1
hsa-miR-151a-3p	6.9
hsa-miR-27b-3p	6.6
hsa-let-7i-5p	6.5
hsa-miR-222-3p	6.4
hsa-let-7g-5p	5.9
hsa-miR-34a-5p	5.7
hsa-miR-21-5p	5.6
hsa-let-7f-5p	5.5
hsa-miR-22-3p	5.4
hsa-miR-200c-3p	-5.9
hsa-mir-8075	-6.3

[a]Fold difference of RMA normalized expression values (cut-off at +/- 5). Positive values indicate up-regulation whereas negative values indicate down-regulation in metaplastic breast cancer

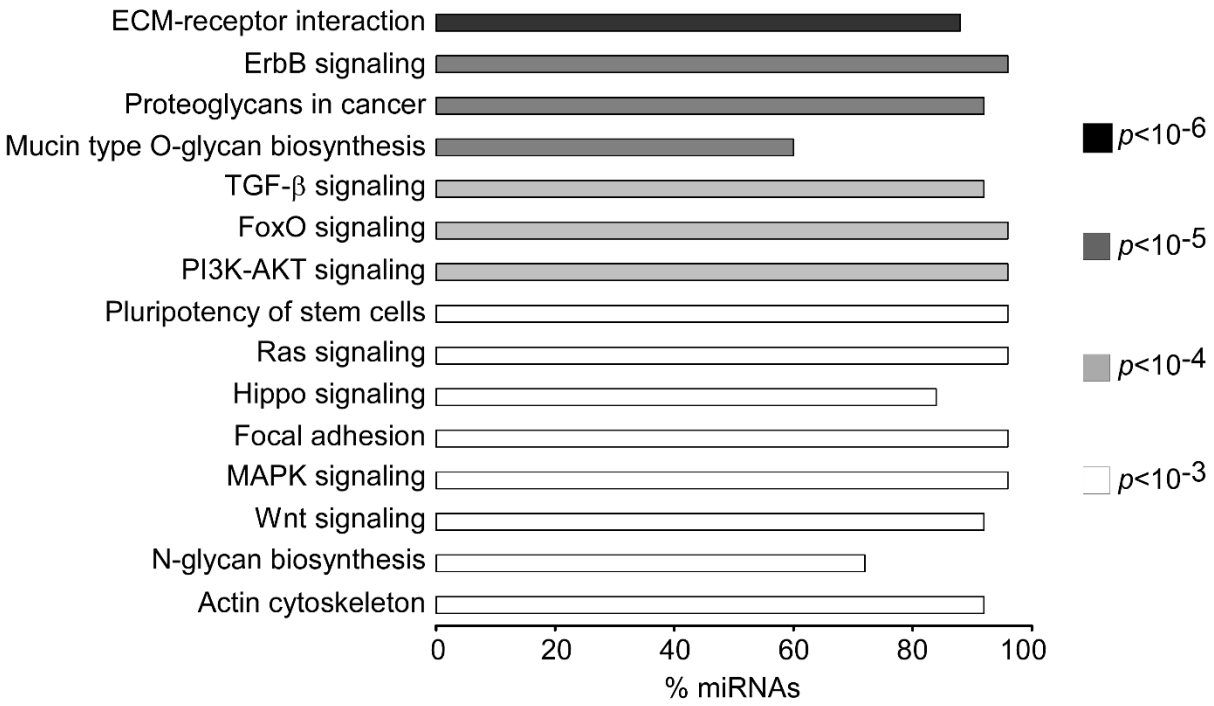


Figure 6.10: Pathways associated with discriminating miR expression signature between MBC and IDC. Identification of the pathways enriched with targets of miRs from discriminating signature between MBC and IDC (**Table 6.21**) was performed using DIANA-miRPath v3.0 online software suite for miR functional analysis. Most significant pathways were selected at a *p*-value inferior to 0.001. Length of histogram bar is proportional to the percentage of miRs in the signature (x-axis) associated with a particular pathway (indicated to the left). Pathways are ordered by significance, with the highest significant values on top.

6.4.9 Assessment of resemblance of miRs differentially regulated in breast cancer subtypes to cell lines

As miR expression profiles analysis of breast cancer clinical samples identified four miR expression clusters, each showing a population of miRs differentially regulated across the breast cancer subtypes, including IDC, ILC and MBC (**Figure 6.8 B**), I aimed to identify their expression pattern in a small panel of breast cancer cell lines, including metaplastic breast cancer derived HS578T and BAS cells. For this, miRs in each cluster were further analysed with respect to their expression in breast cancer cell lines (**Figure 6.11**). Although not analogous to the expression pattern seen in clinical samples, both metaplastic breast cancer derived HS578T and BAS cells showed the upregulation for probes in cluster 1, compared to the normal human mammary epithelial cells (HMEC) (**Figure 6.11 A**). Cluster 2, which is represented by miRs down-regulated in MBC and up-regulated in IDC, was highly expressed in luminal MCF-7 cells. All the basal-like MDA-MB-231, HS578T and BAS cells showed identical expression pattern for these miRs to the HMEC (**Figure 6.11 B**). Clusters 3 and 4 gave more ambiguous results, as the cell lines had a fair number of probes up- and down-regulated across the panel (**Figure 6.11 C and D**).

Importantly, the novel metaplastic derived BAS cells showed a comparable expression pattern to the existing metaplastic HS578T cells across all the miR expression clusters for clinical samples. However, neither of these MBC derived cells did show clear alignment with miR expression pattern obtained with metaplastic breast cancer clinical samples. This may be due to the few clinical samples used in this very preliminary study, which did not yield any distinct miR expression clusters unique to MBC that could be used to compare the resemblance between MBC derived cell lines and the clinical samples. In addition, metaplastic breast cancer is highly heterogenous (Weigelt *et al.*, 2014; Reddy *et al.*, 2020) and thus it would be necessary to subdivide metaplastic samples in either subclasses 1 and 2 (Lien *et al.*, 2007), or in WHO sub-classes (Schwartz *et al.*, 2013). Due to the rarity of this form of breast cancer, this is a task that was out of the scope of this small prospective study and will require a much larger effort.

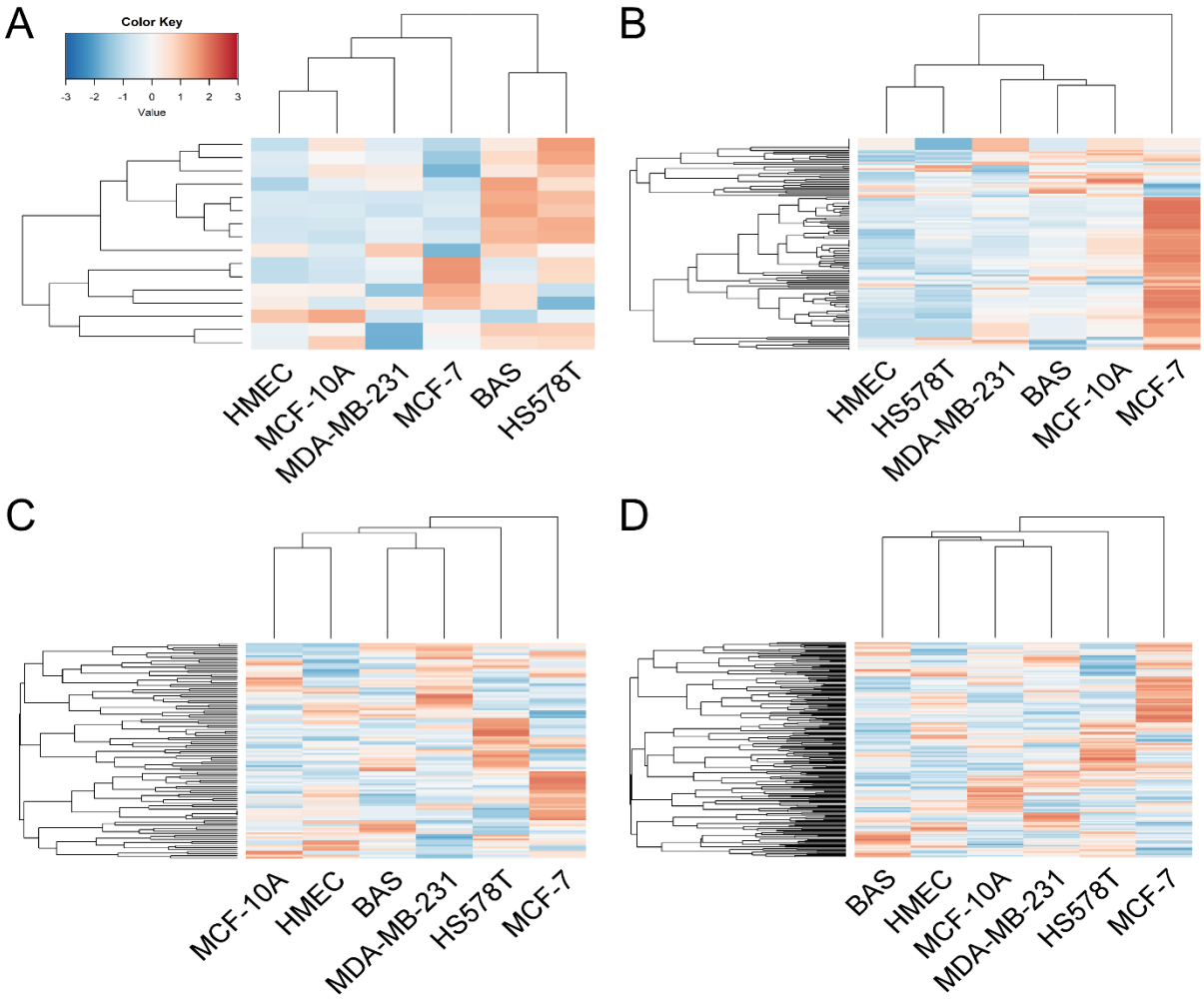


Figure 6.11: Analysis of miR expression resemblance between breast cancer clinical samples and cell lines. Significantly differential probes identified as clusters 1-4 with GeneChip miRNA 4.0 Array in a small panel of breast cancer clinical samples (**Figure 6.8 B**) were analyzed for their expression in breast cancer cell lines, including non-tumorigenic breast epithelial cells (MCF-10A), luminal breast cancer cells (MCF-7), basal-like breast cancer cells (MDA-MB-231) and MBC derived cells (HS578T and BAS cells), and primary human mammary epithelial cells (HMEC). A, Expression of probes from cluster 1. B, Expression of probes from cluster 2. C, Expression of probes from cluster 3. D, Expression of probes from cluster 4.

6.5 Discussion

The distinct clinicopathological features of MBC characterized by their aggressive and chemo-resistant behaviours is attributed to the enrichment of EMT and CSC markers (Lien *et al.*, 2007; Hennessy *et al.*, 2009; Taube *et al.*, 2010). MiR are involved in the regulation of a variety of cellular processes, including chemotherapeutic resistance, EMT and CSC (Wang *et al.*, 2010). For instance, miR-106b~25 cluster, which includes miR-106b, miR-93 and miR-25, targets EP300 and regulates these three phenotypes in minimally transformed mammary epithelial cells. Ectopic expression of this miR cluster causes down-regulation of E-cadherin by directly targeting its transcriptional activator EP300, leading to increased cell migration and invasion abilities, enhancement of anchorage independence, as well as increased doxorubicin resistance (Zhou *et al.*, 2014). In this chapter I have investigated the role of miRs in the acquisition of chemotherapy resistance in MBC. MiR expression profiling in a small panel of breast cancer cell lines and primary human mammary epithelial cells identified distinct miR expression clusters for MBC derived cells, showing a population of miRs differentially regulated (up- or down-regulated) in MBC derived cell lines. These clusters included miR involved in signalling pathways related to EMT and stemness, such as TGF-β, Ras, Rap1, Hippo signalling and pluripotency of stem cells (Wu *et al.*, 2019; Nedeljković & Damjanović, 2019; Cao *et al.*, 2020). As EMT and CSC phenotypes are functionally correlated with the acquisition of chemotherapy resistance (Asaduzzaman *et al.*, 2017), this suggests a possible role of these miRs in the intrinsic chemo-refractory nature of MBC. In addition, miR expression clusters exclusive for each metaplastic breast cancer derived cell line could be discriminatory miR expression signatures between two MBC subclasses, like the discriminatory gene signature (Lien *et al.*, 2007), as we have already seen that HS578T and BAS cells resemble MBC subclasses 2 and 1, respectively, according to their expression profiles of discriminator genes (**Chapter 3**).

In an effort to identify miRs potentially related to the acquired chemotherapy resistance in MBC derived cells, I performed miR expression profiling of doxorubicin- and paclitaxel-resistant derivatives of both HS578T and BAS cells. Interestingly, analysis of these expression data led to identification of miR expression signatures common for doxorubicin, and paclitaxel resistance across the cell lines, as well as MDR (that is, resistance to both doxorubicin and paclitaxel) signature for each MBC derived cell line. These signatures include many miRs already reported to have clinical relevance in a variety of carcinomas, including different subtypes of breast cancer. Interestingly, several miRs in the doxorubicin

resistance signature for MBC derived cells are found to be involved in drug resistance, metastasis, and poor prognosis. For example, down-regulation of miR-409-3p confers oxaliplatin resistance in colon cancer cells (Tan *et al.*, 2016a). MiR-370-3p is down-regulated in temozolomide-resistant glioblastoma multiforme cells and its over-expression restores the drug sensitivity (Gao, Chen & Liu, 2016). MiR-381-3p acts as a negative regulator cellular proliferation and metastasis in cervical cancer by targeting fibroblast growth factor-7 (Shang *et al.*, 2019). Moreover, miR-409-3p, miR-370-3p and miR-381-3p are also found to be significantly down-regulated in the relapsed diffuse large B-cell lymphoma (DLBCL) and their over-expression in DLBCL cells increases sensitivity to doxorubicin and rituximab, the key components in the standard treatment regimen (also known as R-CHOP) (Leivonen *et al.*, 2017). MiR-485-5p is a negative regulator of EMT and its over-expression increases cisplatin sensitivity in oral squamous cell carcinoma (Lin *et al.*, 2017). Low expression levels of miR-487a-3p in pancreatic carcinoma correlate with high metastatic disease rate and poor prognosis (Zhou *et al.*, 2020). MiR-654-5p functions as a tumour suppressor and is down-regulated in aggressive ovarian serous carcinoma (Majem *et al.*, 2019).

Similarly, paclitaxel resistance miR expression signature for MBC derived cells includes many miRs reported to be involved in aggressive disease status and chemotherapeutic resistance. For example, miR-505-3p is also reported to be down-regulated in doxorubicin resistant luminal breast cancer cells (Yoshioka *et al.*, 2011; Hu *et al.*, 2018). Moreover, miR-505-3p is a predictive marker for prostate cancer bone metastasis and is significantly down-regulated in bone metastatic tissues of prostate cancer. MiR-505-3p negatively regulates the activity of TGF-β signalling by targeting its down-stream effectors SMAD2 and SMAD3 (Tang *et al.*, 2019). MiR-5004-3p is also up-regulated in paclitaxel resistant prostate cancer cells (Li *et al.*, 2016a).

Accumulated evidence indicates several miRs in the MDR signature for each metaplastic breast cancer derived cell line are involved in disease progression, metastasis, and drug resistance in disparate carcinoma types. Among the HS578T cells MDR miR expression signature, miR-487b is a negative regulator of metastasis in colorectal cancer (Hata *et al.*, 2017). Another miR in this signature, miR-31-3p is identified as a predictive biomarker in the selection of patients with colorectal cancer for anti-EGFR therapy. Patients with low expression levels of miR-31-3p show better overall response rate to anti-EGFR monoclonal antibody cetuximab (Anandappa *et al.*, 2019). On the other hand, BAS cells MDR miR expression signature also includes some tumour suppressors in breast cancer (miR-379-5p

and miR-431-5p) (Khan *et al.*, 2013; Wang *et al.*, 2020), negative regulators EMT-migration-invasion (miR-431-5p and miR-485-3p) (Kong *et al.*, 2018; Lou *et al.*, 2016), TGF-β signalling regulators (miR-376c-3p, miR-433-3p, and miR-495-3p) (Liu *et al.*, 2014; Li *et al.*, 2013; Welten *et al.*, 2017) and drug resistance regulators (miR-379-5p, miR-382-5p and miR-495-3p) (Guo *et al.*, 2010; Yao *et al.*, 2019; Wei *et al.*, 2017).

Interrogation of the functional relevance of drug resistance miR expression signatures by pathways analysis revealed that the MDR phenotype in both metaplastic breast cancer derived cells is associated with cancer hallmark EMT, although via different signalling pathways. This reinforces once more the data shown in Chapter 5 using genome-wide expression profile analysis and points towards EMT as an important process during the acquisition of MDR in metaplastic breast carcinoma.

As we have already seen the TGF-β-FOXC1 axis regulating MDR in MBC derived BAS cells, with up-regulation of both *TGFB2* and FOXC1, a particular focus was given to the identification of miRs targeting both MDR regulators. Here, I demonstrate that miR-495-3p, which targets both *TGFB2* and *FOXC1* (Welten *et al.*, 2017; Xu *et al.*, 2016), is down-regulated in BAS MDR cells and its experimental modulation leads to changes in expression of both target genes and alteration of the MDR phenotype. This suggests that miR-495-3p negatively regulates MDR phenotype in metaplastic breast cancer derived cells by targeting both *TGFB2* and *FOXC1*. Interestingly, several studies have also reported the involvement of miR-495-3p in EMT, disease progression and drug resistance in different types of carcinomas. In melanoma, low miR-495-3p expression is associated with poor prognosis. Moreover, an elevated expression of miR-495-3p in melanoma cells suppresses EMT (Ma, Duan & Hao, 2020). MiR-495-3p is down-regulated in osteosarcoma and its over-expression in osteosarcoma cells inhibited their proliferation, migration, and invasion abilities, reflecting the role of miR-495-3p as a tumour suppressor (Zhao *et al.*, 2019). In gastric cancer, miR-495-3p also functions as a tumour suppressor (Eun *et al.*, 2018). Additionally, miR-495-3p expression inhibits MDR in gastric cancer cells and patients with low levels of miR-495-3p found to have poor prognosis (Chen *et al.*, 2018b).

MiR expression profiling of metaplastic breast carcinoma is poorly studied, probably due to most studies pool them within the TNBC molecular subtype. Here, I performed miR expression profiling of breast tumours, including invasive ductal carcinoma, invasive lobular carcinoma and metaplastic breast carcinoma, and normal breast tissues. Although no miR

expression signature was obtained unique to each of the breast cancer subtype, probably due to very small sample size in each group, many miRs associated with aggressive cellular phenotypes, such as EMT and stemness, were dysregulated in different subtypes of breast cancer. This warrants further extensive studies with a larger sample size of metaplastic breast cancer.

As MBCs show poorer prognosis and chemotherapy response than the conventional IDC (Song *et al.*, 2013; Schwartz *et al.*, 2013), I interrogated the miRs differentially expressed in MBC relative to IDC. Interestingly, despite using a very small cohort, miR-200c-3p was found to be significantly down-regulated in MBC, in agreement to previous reports of miR-200 family down-regulation in MBC (Gregory *et al.*, 2008; Castilla *et al.*, 2012). Several upregulated miRs in MBC are reported to be involved in chemotherapy resistance in disparate cancer types, including breast cancer. For instance, miR-222-3p confers doxorubicin resistance in colon cancer cells (Wang *et al.*, 2019); miR-221-3p and miR-27a-3p confers doxorubicin resistance in luminal breast cancer MCF-7 cells (Pan *et al.*, 2020; Zhu *et al.*, 2020) and miR-21-5p promotes paclitaxel resistance in breast cancer MCF-7 and MDA-MB-231 cells (Tao, Wu & Zhang, 2019). Moreover, miR-15a-5p and let-7f-5p contribute to chemoresistance in acute myeloid leukaemia and colorectal carcinoma, respectively (Vandewalle *et al.*, 2021; Tie *et al.*, 2018). MiR-34a-5p promotes MDR in osteosarcoma cells (Pu *et al.*, 2017). In addition, functional analysis indicated many differentially expressed miRs in MBC involves in EMT, stemness and disease progression. Therefore, the discriminatory miR expression signature between MBC and IDC could explain the intrinsic chemo-refractory behaviour of MBC.

Chapter 7: FOXA1 regulates chemoresistance in breast cancer cells

7.1 Introduction

7.1.1 Role of FOXA1 in cancer

Breast cancer is molecularly classified into five major subtypes: luminal A, luminal B, basal-like, HER2-enriched, and normal-like (Perou *et al.*, 2000). Both luminal subtypes A and B tumors are positive for estrogen receptor (ER)-α, with subtype A expressing it at higher levels (Sørlie *et al.*, 2001). Interestingly, all ER-positive and a subset of ER-negative tumors express FOXA1 (Bernardo *et al.*, 2013). In ER-positive tumors, FOXA1 functions as a pioneer factor, priming the chromatin for subsequent ER binding to its response elements, resulting in estrogen-induced gene expression (Carroll *et al.*, 2005; Carroll & Brown, 2006). Consistent with this notion, about half of estrogen-induced genes also have binding sites for FOXA1 (Carroll *et al.*, 2005), suggesting that co-expression of FOXA1 and ER is required for optimal expression. Thus, FOXA1 expression may make ER-positive tumors addicted to the estrogen-dependent signaling pathways related to survival and proliferation, creating a favorable environment for endocrine therapies, such as tamoxifen (Badve *et al.*, 2007). While the endocrine therapy is largely successful in the prolongation of disease-free and overall survival, more than half of the breast cancer patients with metastatic tumors do not respond to the therapy, and almost all metastatic patients initially responding to the endocrine therapy ultimately relapse due to acquired resistance (Ring & Dowsett, 2004; Brodie & Sabnis, 2011). One of the key mechanisms underlying endocrine resistance in ER-positive tumors is the ligand-independent ER activation triggered by cross-talk with growth factor receptor pathways, leading to reprogramming of ER transcriptional activity (Massarweh *et al.*, 2008; Fu *et al.*, 2014). FOXA1 facilitates this reprogrammed ER transcriptional activity in tamoxifen-resistant breast cancer cells and thus, ultimately contributes to the development of endocrine resistance in ER-positive breast cancer (Hurtado *et al.*, 2011). A study reveals that endocrine-resistant breast cancer cells show up-regulation of IL8, as one of the most dysregulated genes. Interestingly, FOXA1 overexpression in ER-positive breast cancer cells leads to up-regulation of IL8, resulting in increased cellular proliferation, invasion, and endocrine resistance (Fu *et al.*, 2016). Another study demonstrates high levels of FOXA1 and ER co-expression in endocrine-resistant metastatic tumors, highlighting an altered function of FOXA1 in ER-positive breast cancer metastasis and therapy resistance (Ross-Innes *et al.*,

2012). In endometrial cancer, metastatic lesions express significantly higher levels of FOXA1 than the primary tumors, although high FOXA1 expression in primary tumors is associated with good prognosis (Tangen *et al.*, 2014).

In prostate cancer, FOXA1 function is quite controversial, as its expression level has been found to be correlated with either good or bad prognosis depending on the patient group. Some reports claim high FOXA1 levels correlate with worse prognosis (Gerhardt *et al.*, 2012), while other reports demonstrate low FOXA1 expression is associated with poor clinical outcome (Wang *et al.*, 2011). A study shows that FOXA1 promotes cellular proliferation through AR-dependent pathway and inhibits motility and EMT via AR-independent mechanism. Concordantly, a switch in FOXA1 expression is observed in prostate cancer, with an initial slight up-regulation in primary tumors favoring cellular proliferation, but a significant down-regulation once the disease primes to enter metastatic stage, which requires cellular motility and EMT induction (Jin *et al.*, 2013). However, several studies show high levels of FOXA1 expression in metastatic and castration-resistant prostate cancer (Robinson *et al.*, 2014).

Therefore, these contradictory findings emphasize the importance of studying the functions of FOXA1 further to explore its potential as a therapeutic target in ER-positive breast cancer.

7.2 Aim of the chapter

FOXA1, together with EP300 and RUNX1, plays an important role in promoting expression of E-cadherin (Liu *et al.*, 2005), which, in turn, causes inhibition of cellular ability to undergo an EMT and initiate metastatic dissemination (Onder *et al.*, 2008; Shibue & Weinberg, 2017). EMT enables cancer cells to gain stem cell-like properties, and these processes are associated with disease progression (Hanahan & Weinberg, 2011). In breast cancer, several studies indicated FOXA1 expression is involved in maintaining a less aggressive cellular phenotype and is associated with good prognosis (Liu *et al.*, 2005; Bernardo *et al.*, 2013; Badve *et al.*, 2007). Contradicting this, other reports have associated FOXA1 expression with endocrine therapy resistance in ER-positive breast cancer (Hurtado *et al.*, 2011; Ross-Innes *et al.*, 2012; Fu *et al.*, 2016). However, the role of FOXA1 in chemotherapy response has not yet been studied. Here, I aimed to identify any association of FOXA1 with conventional chemotherapy response in breast cancer. For this, I have experimentally modulated FOXA1 expression in breast cancer cells, with luminal MCF-7 and T47D cells each down-regulating FOXA1 and basal-like MDA-MB-231 cells over-expressing FOXA1, to assess its impact on drug sensitivity.

7.3 Results

7.3.1 Modulation of FOXA1 expression in breast cancer cellular models

To identity if any changes in chemotherapeutic sensitivity due to altered FOXA1 levels, I aimed to experimentally modulate FOXA1 expression in breast cancer cells. For this, I first assessed the expression levels of FOXA1 in a small panel of breast cancer cell lines (**Figure 7.1**). As expected, both luminal MCF-7 and T47D breast cancer cells showed very high levels of FOXA1 expression. In contrast, basal-like CAL51 and HS578T breast cancer cells were null for FOXA1 expression and MDA-MB-231, another basal-like breast cancer cell line, showed a faint signal in immunoblot, indicating a very low level of FOXA1 expression. The transformed but non-tumorigenic breast epithelial cells, MCF-10A also showed a very low FOXA1 expression, as indicated by a faint signal in the immunoblot. Reassuringly, a positive correlation was noticed between FOXA1 and E-cadherin expression (**Figure 7.1**), in agreement to the report showing FOXA1 is a transcriptional activator of *CDH1*, the gene encoding E-cadherin (Liu *et al.*, 2005). Both the luminal MCF-7 and T47D cells showed very high levels of E-cadherin expression, whereas all three basal-like cells were negative for E-cadherin expression. In addition, MCF-10A cells showed an intermediate level of E-cadherin expression. The absence of E-cadherin expression in MDA-MB-231 cells despite very low, but detectable, levels of FOXA1 is attributed to the methylation of *CDH1* promoter, probably causing a closed chromatin conformation of *CDH1* locus in MDA-MB-231 cells (Reinhold *et al.*, 2007). Overall, both luminal MCF-7 and T47D cells, each harboring an elevated endogenous FOXA1 expression, were selected for FOXA1 down-regulation, and the basal-like MDA-MB-231 cells, with very low FOXA1 level, were selected for ectopic over-expression of FOXA1.

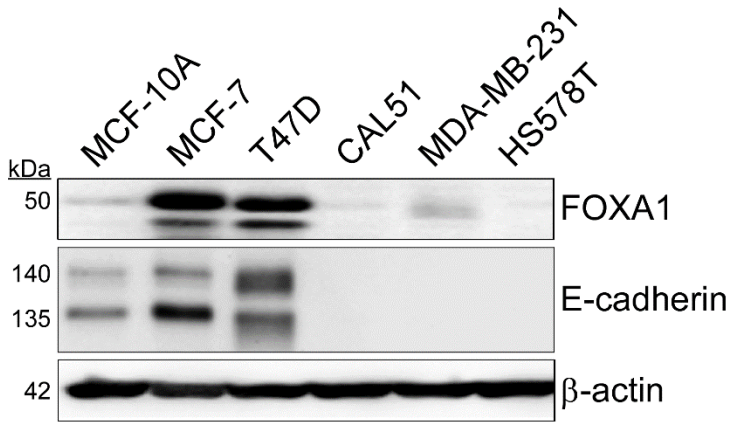


Figure 7.1: Expression of FOXA1 and E-cadherin in a selected panel of breast cancer cell lines. Western blot analysis of FOXA1 and E-cadherin expression in a small panel of breast cancer cell lines, including non-tumorigenic breast epithelial cells (MCF-10A), luminal breast cancer cells (MCF-7 and T47D) and basal-like breast cancer cells (CAL51, MDA-MB-231 and HS578T). The analysis was performed with whole cell lysates and β-actin was used as a control for protein loading. Molecular masses of relevant bands are indicated in kDa. E-cadherin was detected as two bands, 140 kDa precursor and 135 kDa after convertase processing. Data show a representative blot of at least triplicate experiments.

MCF-7 and T47D cells stably down-regulating FOXA1 were generated upon transfection with a lentivirus driving the expression of hairpins targeting *FOXA1* mRNA or empty lentivector control. T47D cells stably expressing six different hairpins individually showed down-regulation of FOXA1 at varying extents, compared to the empty lentivector control (**Figure 7.2 A**). Immunoblot image quantification identified that the T47D cells expressing hairpins sh6 and sh4 showed a down-regulation of FOXA1 by approximately 90% and 65%, respectively. Thus, cells transfected with lentivector stably expressing these two hairpins, named as T47D-shFOXA1(6) and T47D-shFOXA1(4), respectively, were selected for further studies. Equally, MCF-7 cells transfected with lentivector expressing the same six hairpins targeting *FOXA1* mRNA showed down-regulation FOXA1 at different levels, compared to the empty lentivector control (**Figure 7.2 B**). However, extents of FOXA1 down-regulation in six different cell pools, as determined by immunoblot image quantification, were not satisfactory for further functional studies. For this, I opted to isolate individual clones from the cell pools with two best hairpins, sh3 and sh6, in an intention to get clonal expands with satisfactory levels of FOXA1 down-regulation. A total of 16 clones from hairpin 3 expressing pool and of 12 clones from hairpin 6 expressing pool were isolated. Immunoblot analysis of

these clonal expands indicated that clone 6 from cells pool generated with hairpin 3 and clone 8 from cells pool generated with hairpin 6 (hereby named as MCF7-shFOXA1(3)-c6 and MCF7-shFOXA1(6)-c8, respectively) showed a down-regulation of FOXA1 by approximately 60% and 50%, respectively (**Figure 7.2 C-E**). These two clones of MCF-7 cells stably down-regulating FOXA1 were selected for further studies. On the other hand, MDA-MB-231 cells stably over-expressing FOXA1 were generated after transfection with a FOXA1-expression cassette. Immunoblot analysis indicated that the stably transfected MDA-MB-231 cells showed an up-regulation of FOXA1 expression by approximately 3-fold, compared to the empty vector control (**Figure 7.2 F**).

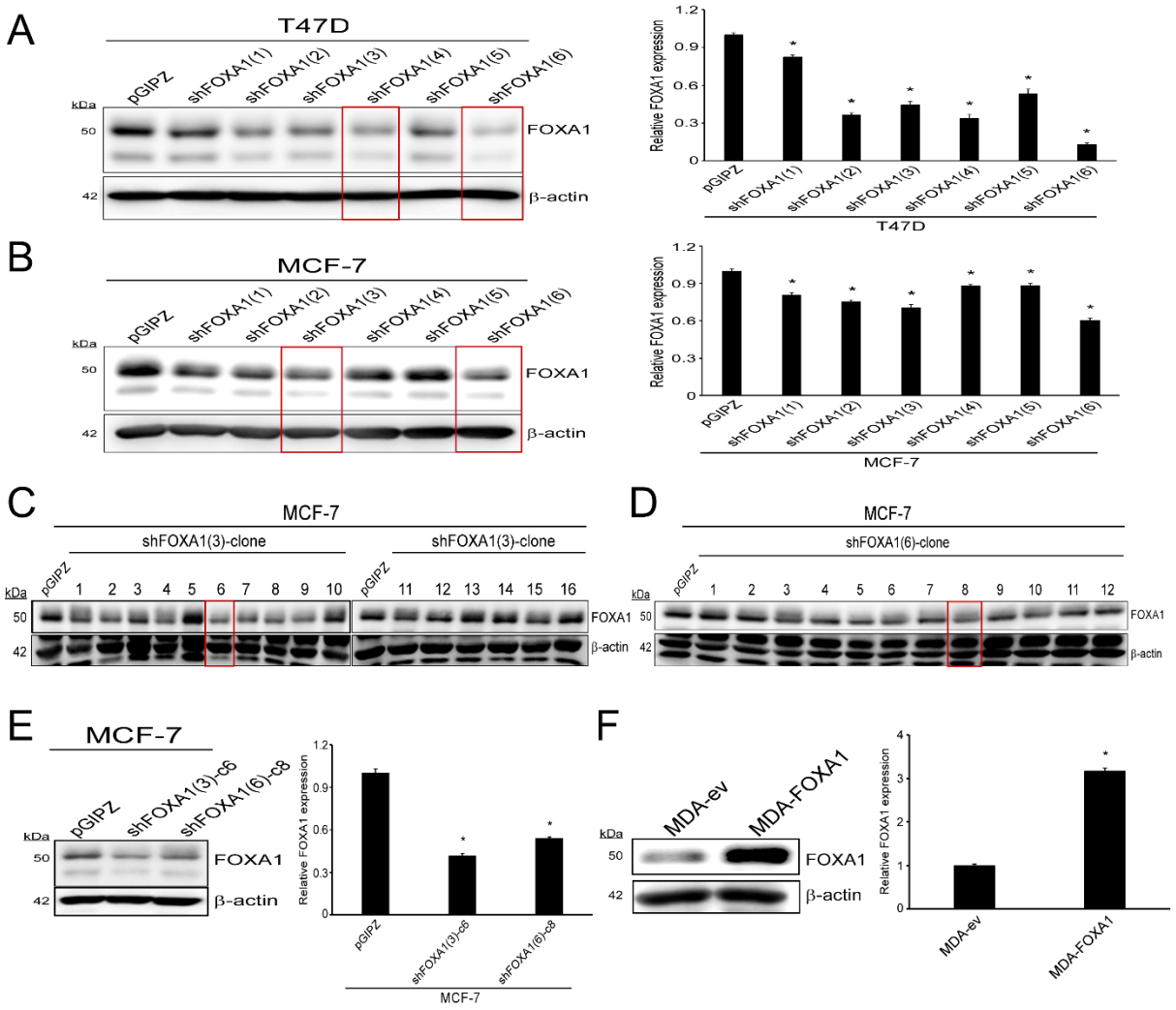


Figure 7.2: Experimental modulation of FOXA1 expression in breast cancer cells. Luminal MCF-7 and T47D breast cancer cells were stably transfected with a lentivector expressing six different small hairpins individually (shFOXA1(1) to shFOXA1(6)) targeting *FOXA1* mRNA. Empty lentivector pGIPZ was used as a negative control. A, FOXA1 expression in stably transfected T47D cell pools. B, FOXA1 expression in stably transfected MCF-7 cell pools. C-D, FOXA1 expression in different clonal expands of MCF-7 transfected pools expressing hairpins sh3 (C) and sh6 (D). E, Selection of two stably transfected MCF-7 clones with the most FOXA1 down-regulation. F, FOXA1 expression in basal-like MDA-MB-231 breast cancer cells stably transfected with FOXA1-expression vector or empty pcDNA3.1 (ev), which was used as a control. In all cases, FOXA1 expression was determined by western blot analysis. Western blot was performed with whole cell lysate and β-actin was used as a control for protein loading. Molecular masses of relevant bands are indicated in kDa. Image quantification of immunoblots were performed with Image J software. FOXA1 signal was normalized to the β-actin signal. The relative FOXA1 expression was calculated with respect to the corresponding control. Numerical data represent the average ± SD of three experiments. Pictorial data show a representative blot of at least triplicate experiments. *, $p<0.05$ of comparisons to vector controls.

7.3.2 Modulation of FOXA1 expression does not alter E-cadherin levels in breast cancer cells

As FOXA1 is identified as a one of the transcription activators of *CDH1* (Liu *et al.*, 2005), it was expected that modulation of FOXA1 expression in breast cancer cells would affect E-cadherin levels. However, down-regulation of FOXA1 in both luminal MCF-7 and T47D breast cancer cells did not cause decrease in E-cadherin expression (**Figure 7.3**). Indeed, one MCF-7 clone stably down-regulating FOXA1 did show a slight up-regulation of E-cadherin expression (**Figure 7.3 A**). Although some hairpins in T47D cells showed a decrease in E-cadherin levels, this was only up to approximately 10% (**Figure 7.3 B**).

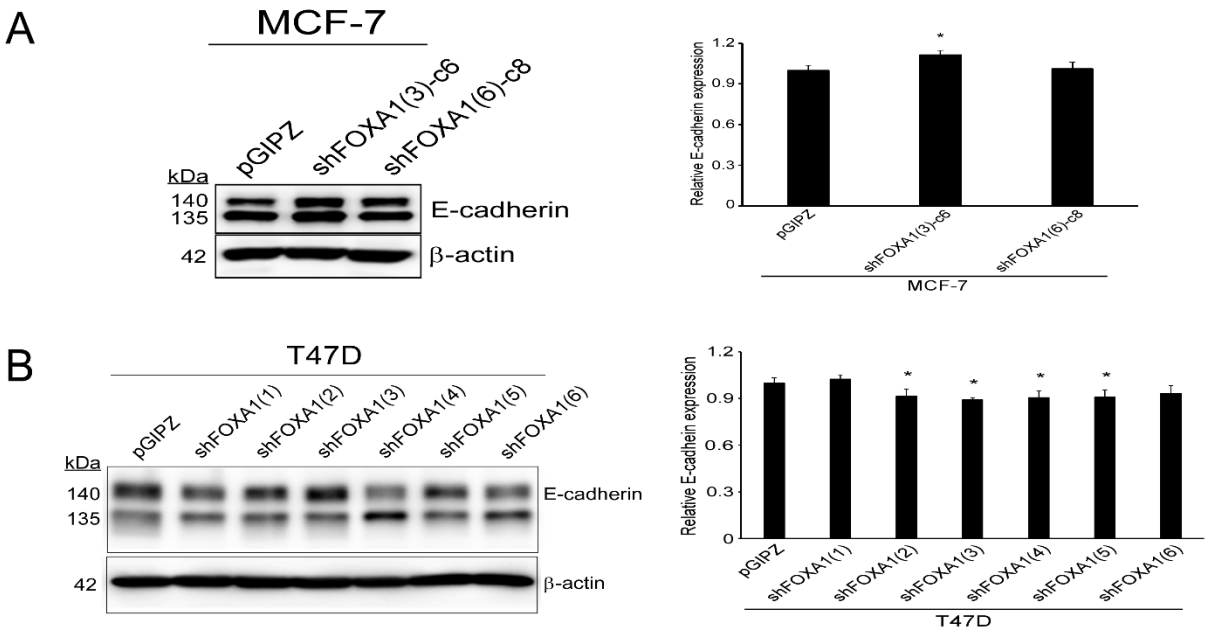


Figure 7.3: E-cadherin expression remains unaffected upon FOXA1 knock-down in MCF-7 and T47D cells. E-cadherin expression in FOXA1 down-regulating MCF-7 (A) and T47D (B) cells was determined by western blot analysis using whole cell lysate. β-actin was used as a control for protein loading. Molecular masses of relevant bands are indicated in kDa. E-cadherin was detected as two bands, 140 kDa precursor and 135 kDa after convertase processing. Image quantification of immunoblots were performed with Image J software. E-cadherin signal was normalized to the β-actin signal. The relative E-cadherin expression was calculated with respect to the corresponding control. Numerical data represent the average ± SD of three experiments. Pictorial data show a representative blot of at least triplicate experiments. *, $p<0.05$ of comparisons to empty vector controls.

To explore whether any compensatory mechanism operated behind the lack of E-cadherin down-regulation, I assessed the expression of other two transcription activators of E-cadherin gene, *EP300* and *RUNX1*, in both MCF-7 and T47D cells down-regulating FOXA1. Interestingly, RT-QPCR analyses indicated an up-regulation of *EP300* and *RUNX1* in both cells, suggesting that the lack of E-cadherin down-regulation upon FOXA1 knock-down might be due to compensation with an up-regulation of these two transcription activators (**Figure 7.4 A**).

Equally, an overexpression of FOXA1 in basal-like MDA-MB-231 cells did not cause an up-regulation of practically null E-cadherin levels at either mRNA or protein levels. As hypermethylation of *CDH1* locus and chromatin constraints imposed by HDAC play an important role in non-expression of E-cadherin in MDA-MB-231 cells (Liu *et al.*, 2005; Reinhold *et al.*, 2007), I aimed to explore whether demethylation of *CDH1* promoter or relief from chromatin constraint could make FOXA1 capable of inducing E-cadherin expression. For this, MDA-MB-231 cells over-expressing FOXA1 were treated with DNA demethylating agent AzaC or HDAC inhibitor trichostatin A (TSA). Interestingly, DNA demethylation did not trigger expression of E-cadherin even in the presence of up-regulated FOXA1 in MDA-MB-231 cells, although it induced the transcription of *ESR1*, a positive control used for azaC treatment (Ferguson *et al.*, 1997) (**Figure 7.4 B**). Although HDAC inhibition apparently indicated activation of *CDH1* transcription, the relative levels of *CDH1* mRNA in TSA treated MDA-MB-231 cells over-expressing FOXA1 or carrying empty vector construct were extremely low, compared to the transcript level in MCF7 cells, a positive control for E-cadherin expression (**Figure 7.4 C**). Importantly, FOXA1 overexpression in MDA-MB-231 cells did not cause any further activation of *CDH1* transcription upon HDAC inhibition. Overall, FOXA1 was unable to trigger E-cadherin expression even after *CDH1* promoter demethylation and removal of HDAC constraint. Furthermore, interrogation of expression of transcriptional repressors of E-cadherin revealed that MDA-MB-231 cells overexpressing FOXA1 showed a slight up-regulation of *ZEB1*, although *ZEB2* and *SNAI1* remained unaltered and *SNAI2* was even slightly down-regulated (**Figure 7.4 D**). However, this small increase in transcription factor *ZEB1* expression is very unlikely to be fully responsible for the lack of E-cadherin expression in FOXA1 over-expressed MDA-MB-231 cells, suggesting that a deep hierarchy exists regulating expression of E-cadherin. Importantly, these cellular models generated represent good systems for studying the phenotypes regulated by FOXA1 independently of E-cadherin.

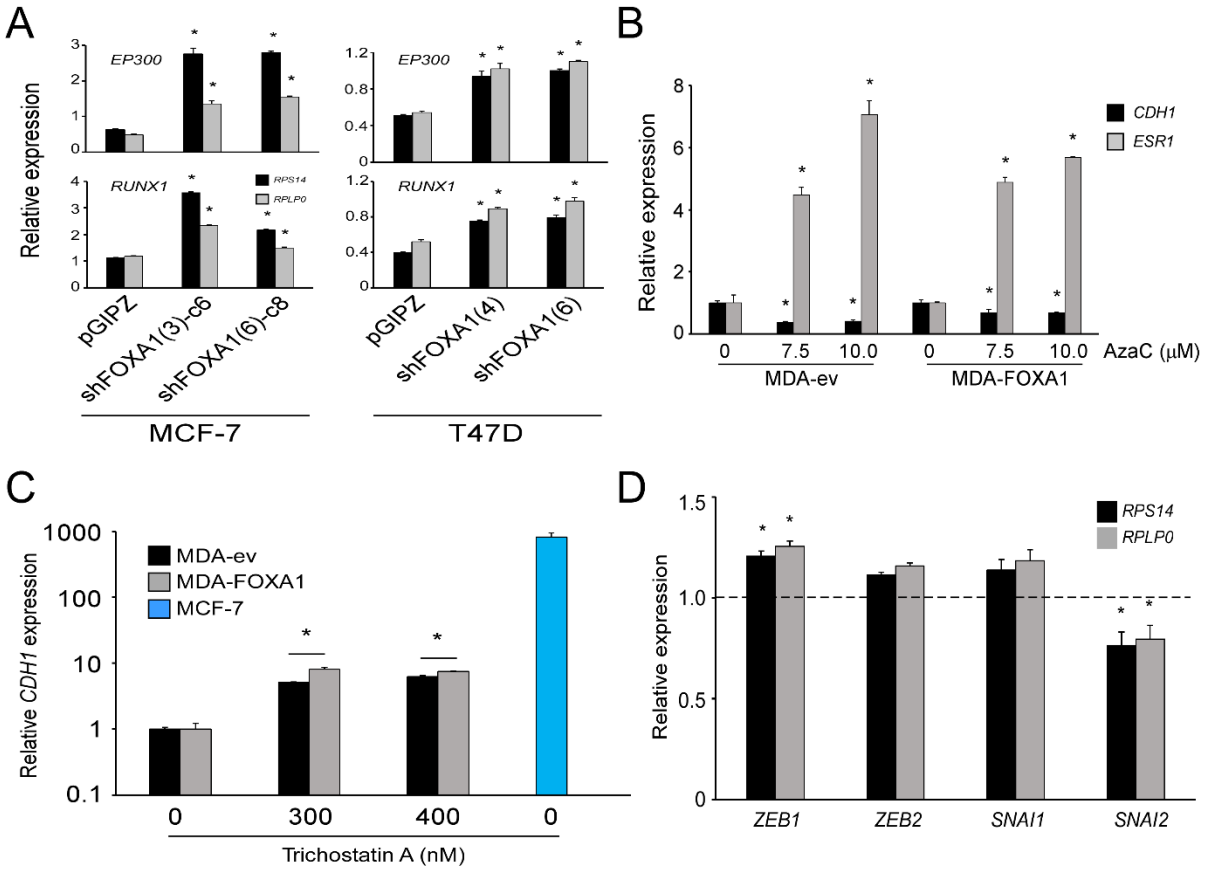


Figure 7.4: Transcriptional regulation analysis of E-cadherin gene in FOXA1-modulated breast cancer cells. A, FOXA1 down-regulation led to up-regulation of *CDH1* transcriptional activators, *EP300* and *RUNX1*. Quantitative real-time PCR analyses of *EP300* (*top panels*) and *RUNX1* (*bottom panels*) expression in MCF-7 (*left panels*) and T47D (*right panels*) cells stably down-regulating FOXA1. The relative mRNA levels were calculated by normalization to the *RPS14* and *RPLP0* genes. B, Ectopic FOXA1 over-expression in MDA-MB-231 cells was unable to trigger E-cadherin expression even after *CDH1* promoter demethylation. Cells were treated daily with DNA demethylating agent 5-Azacytidine (AzaC) for a period of 3 days and *CDH1* mRNA levels were determined by quantitative real-time PCR analysis. Activation of *ESR1* expression was used as a control for AzaC treatment. The mRNA levels were normalized to the *RPS14* gene. The relative expression was calculated with respect to the corresponding untreated control. C, Removal HDAC constraint on chromatin could not make FOXA1 capable to induce E-cadherin expression in MDA-MB-231 cells. Cells were treated with HDAC inhibitor trichostatin A (TSA) for 3 days and *CDH1* mRNA levels were determined by quantitative real-time PCR analysis. E-cadherin expression in MCF-7 cells was used as a positive control. The mRNA levels were normalized to the *RPS14* gene. The relative expression was calculated with respect to the corresponding untreated control. D, Quantitative real-time PCR analyses of some well-known *CDH1* transcriptional repressors expression in MDA-MB-231 cells over-expressing FOXA1. The mRNAs levels were normalized to the *RPS14* and *RPLP0* genes. The relative expression of each gene was calculated with respect to empty vector control (MDA-ev cells, dashed line). In all cases, data represent the average ± SD of three independent experiments. *, $p<0.05$.

7.3.3 FOXA1 regulates the sensitivity of breast cancer cells to doxorubicin and paclitaxel

As FOXA1 has a definitive role in the endocrine therapy resistance in ER-positive breast cancer (Fu *et al.*, 2016), I aimed to determine how an experimental alteration of FOXA1 expression affects sensitivity of breast cancer cells to commonly used chemotherapeutics, such as doxorubicin and paclitaxel. Interestingly, FOXA1 down-regulation in both luminal MCF-7 and T47D breast cancer cells led to increase in sensitivity to doxorubicin and paclitaxel, as estimated by both short-term SRB staining and long-term clonogenic assays (**Figure 7.5 A-D and 7.6**). LD_{50} calculations from drug sensitivity curves indicated that MCF-7 cells down-regulating FOXA1 showed an increase in doxorubicin sensitivity between 6.3 and 7-fold, and paclitaxel sensitivity between 1.7 and 1.9-fold (**Table 7.1**). Similarly, T47D cells down-regulating FOXA1 exhibited an increase in sensitivity to doxorubicin by 2.0- to 2.8-fold and to paclitaxel by 1.8- to 3.2-fold (**Table 7.1**). Long-term clonogenic assays using a range of concentration of doxorubicin and paclitaxel revealed a significant decrease in drug resistant clones after FOXA1 knock-down in both MCF-7 and T47D cells, compared to their corresponding empty vector control (**Figure 7.6**). In fact, no surviving clones were observed with MCF-7 cells down-regulating FOXA1 beyond the concentration of 6.7 nM for doxorubicin and of 1 nM for paclitaxel, whereas there were still traces of drug resistant clones at 16.7 nM of doxorubicin and 2 nM of paclitaxel with control MCF-7 cells (pGIPZ) (**Figure 7.6 A and B**). Similarly, T47D cells down-regulating FOXA1 showed a significant decrease in the number of doxorubicin resistant clones at each drug concentration used (0.8-5.0 nM), compared to control T47D cells (pGIPZ) (**Figure 7.6 C**). Additionally, only a few drug-resistant clones up to 1 nM of paclitaxel were found in T47D cells down-regulating FOXA1, whereas control T47D cells showed a significant number of surviving clones even at the paclitaxel concentration raised to 3 nM (**Figure 7.6 D**).

As hormone signalling is essential for survival and proliferation of luminal breast cancer cells (Hilton, Clarke & Graham, 2018) and there has been a report demonstrating transient silencing of *FOXA1* leads to reduction in ERα expression in both luminal MCF-7 and T47D cells (Bernardo *et al.*, 2010), I aimed to identify whether a decrease or complete abolition of clones in stably FOXA1 down-regulated MCF-7 and T47D cells during the long-term experiment is due to deprivation of hormone receptors (ERα and PR) expression. Interestingly, RT-QPCR analysis indicated that stable FOXA1 knock-down in both MCF-7 and T47D cells did not cause reduction of *ESR1* and *PGR* expression (**Figure 7.7 A**),

suggesting that cells have compensated the effect of ERα down-regulation as observed after transient FOXA1 silencing (Bernardo *et al.*, 2010). Indeed, both *ESR1* and *PGR* mRNAs levels were found to be slightly elevated in MCF-7 and T47D cells down-regulating FOXA1, compared to corresponding control cells.

Conversely, drug sensitivity curves indicated ectopic over-expression of FOXA1 rendered the basal-like MDA-MB-231 cells resistant to both doxorubicin and paclitaxel (**Figure 7.5 E and F**). LD_{50} calculation indicated that MDA-MB-231 cells up-regulating FOXA1 showed an increase in doxorubicin resistance by 1.8-fold and paclitaxel resistance by 2.1-fold (**Table 7.1**), suggesting that an elevated FOXA1 expression leads to a MDR phenotype (Robey *et al.*, 2018).

As increased drug efflux due to elevated ABCB1 (P-glycoprotein) expression is one of main mechanisms through which cancer cells acquire resistance to mechanistically and structurally diverse chemotherapeutics (Robey *et al.*, 2018), I attempted to measure the expression of *ABCB1* in MDA-MB-231 cells over-expressing FOXA1 by RT-QPCR, but the cells showed either null or an extremely low *ABCB1* expression below the detection levels (Kumar *et al.*, 2021a). Equally, the luminal MCF-7 and T47D breast cancer cells do not express ABCB1 (Raguz *et al.*, 2004). Interrogation of another two genes expression involved in chemotherapy resistance, *ABCG2*, encoding an ABC transporter called breast cancer resistance protein (BCRP), and anti-apoptotic *BCL2*, indicated their up-regulation by 1.3- to 1.4-fold in MDA-MB-231 cells over-expressing FOXA1 (**Figure 7.7 B**), although it is unlikely that these modest up-regulation will be totally responsible for doxorubicin and paclitaxel resistance observed after FOXA1 over-expression (Yagüe *et al.*, 2003; Randle *et al.*, 2007).

Thus, FOXA1 is involved in the regulation of multidrug resistance in breast cancer cells.

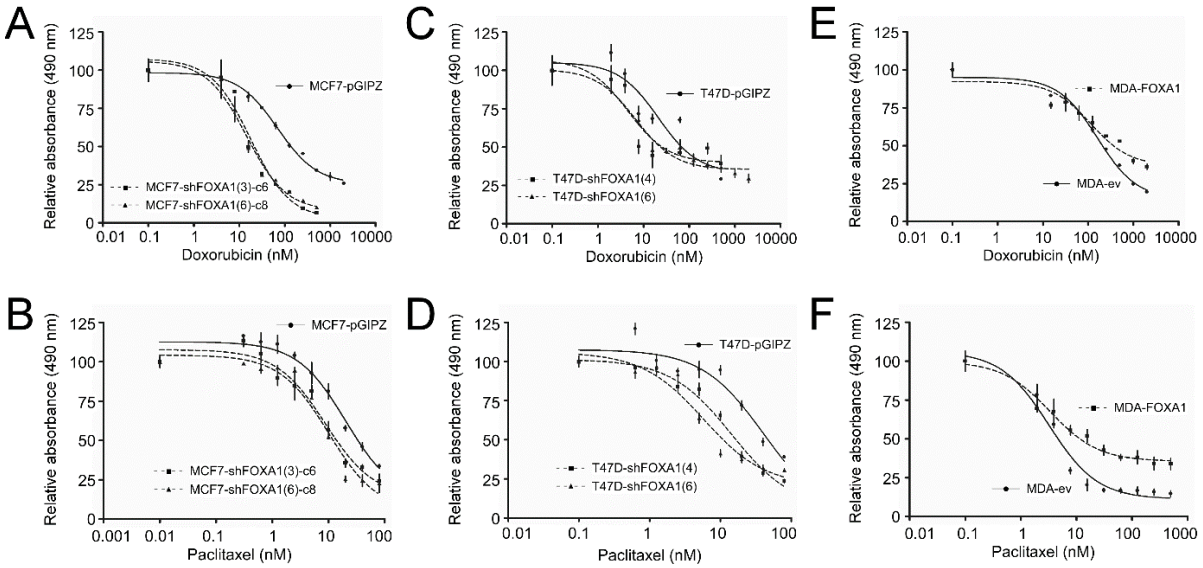


Figure 7.5: Experimental modulation of FOXA1 expression in breast cancer cells alters doxorubicin and paclitaxel sensitivity. Drug sensitivity curves, determined by sulphorhodamine B assays, for doxorubicin (*top panels*) and paclitaxel (*bottom panels*) in FOXA1 down-regulating MCF-7 (A, B) and T47D (C, D) cells, and MDA-MB-231 cells over-expressing FOXA1 (E, F). Cells were treated with a range of concentration of doxorubicin and paclitaxel for a length of time corresponding to their two population doubling times. The optical density (OD) was measured at 490 nm after solubilization of protein bound SRB stain. The relative absorbance was calculated by normalization to the untreated control x100. Data points represent the average ± SD from six replicates. The best-fit curves are obtained with GraphPad Prism software. Curves from three independent experiments were used to calculate the LD_{50} values (**Table 7.1**).

Table 7.1: Sensitivity of FOXA1-modulated breast cancer cells to doxorubicin and paclitaxel

Cell	FOXA1 modulation	LD_{50}[a] (nM)		Resistance ratio[b]	
		Doxorubicin	Paclitaxel	Doxorubicin	Paclitaxel
MDA-ev		199.8	5.5		
MDA-FOXA1	Up-regulation	364.8	11.7	1.8	2.1
MCF7-pGIPZ		128.0	28.6		
MCF7-shFOXA1(3)-c6	Down-regulation	20.2	15.2	-6.3	-1.9
MCF7-shFOXA1(6)-c8	Down-regulation	18.3	16.5	-7.0	-1.7
T47D-pGIPZ		53.0	32.6		
T47D-shFOXA1(4)	Down-regulation	26.5	18.1	-2.0	-1.8
T47D-shFOXA1(6)	Down-regulation	19.0	10.0	-2.8	-3.2

[a]All LD_{50} values from FOXA1-modulated cells were significant ($p<0.05$) when compared to their corresponding control cells

[b]Positive values indicate resistance; negative values indicate sensitivity

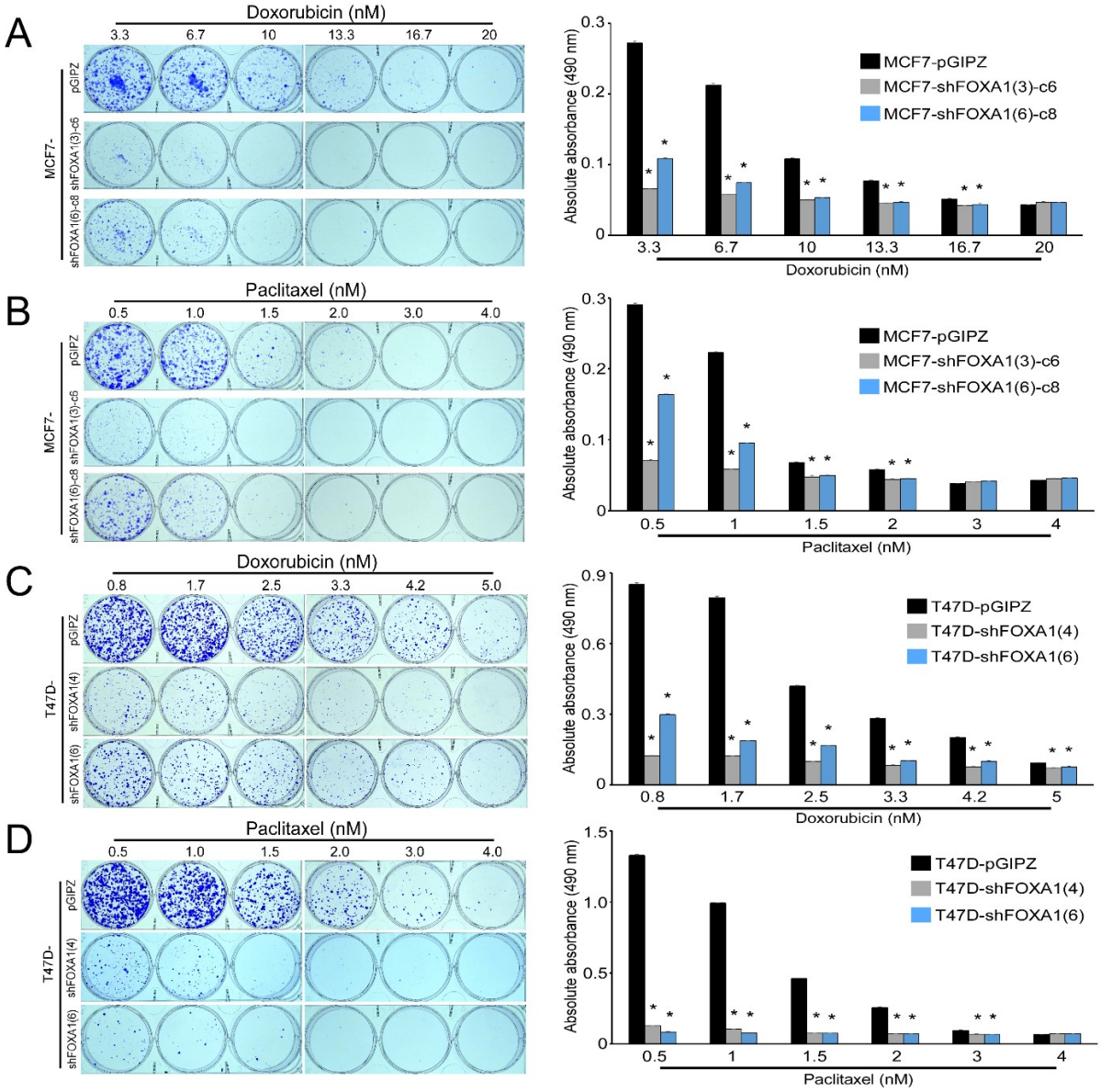


Figure 7.6: FOXA1 knock-down in breast cancer cells decreases long-term resistance to doxorubicin and paclitaxel. Clonogenic assay was employed to determine long-term resistance to doxorubicin and paclitaxel in FOXA1 down-regulating MCF-7 (A, B) and T47D (C, D) cells. Cells were seeded in 6-well plates (5 x 10^3 cells / well), treated with an initial 3-day pulse of doxorubicin, and paclitaxel, and resistant clones were allowed to grow for 14 days before crystal violet staining. The optical density (OD) of solubilized crystal violet stain was measured at 490 nm. Pictorial data show a representative picture of at least three independent experiments. Numerical data represent average ± SD of three independent experiments. *, $p<0.05$.

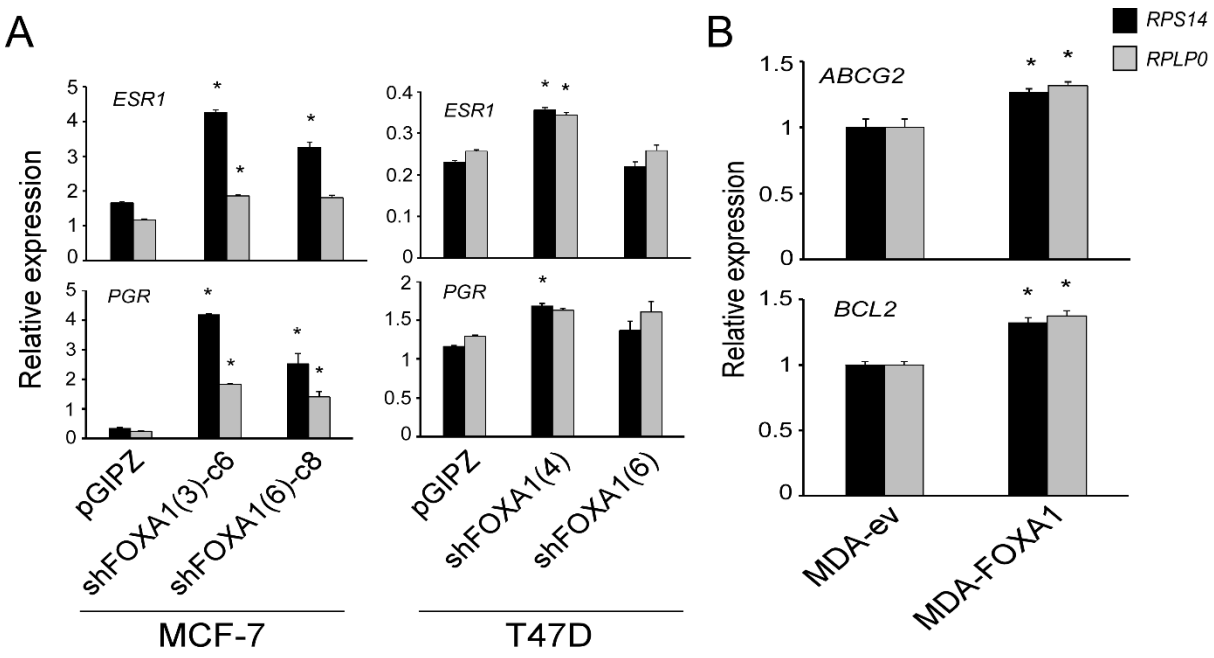


Figure 7.7: Analysis of hormone receptors and key drug resistance markers expression upon FOXA1 modulation. A, FOXA1 down-regulation did not cause a decrease in *ESR1* and *PGR* expression. Quantitative real-time PCR analyses of *ESR1* (*upper panels*) and *PGR* (*lower panels*) expression in luminal MCF-7 (*left panels*) and T47D (*right panels*) cells each stably down-regulating FOXA1 or carrying empty vector control. The relative mRNA levels were calculated by normalization to the *RPS14* and *RPLP0* genes. B, FOXA1 over-expression led to up-regulation of an ABC transporter, *ABCG2*, and anti-apoptotic marker, *BCL2*. Quantitative real-time PCR analyses of *ABCG2* and *BCL2* expression in MDA-MB-231 cells stably over-expressing FOXA1. The mRNAs levels were normalized to the *RPS14* and *RPLP0* genes. The relative expression of each gene was calculated with respect to empty vector control (MDA-ev cells). In all cases, data represent the average ± SD of three independent experiments. *, $p<0.05$.

7.3.4 FOXA1 regulates anchorage independence in breast cancer cells

Drug resistance is often associated with acquisition of stem cell-like phenotypes, such as anchorage-independent growth capacity (Wang *et al.*, 2010; Asaduzzaman *et al.*, 2017). This also enables the cancer cells to survive in the circulation, thereby playing an important role in the metastatic colonization (Mani *et al.*, 2008). Thus, the cellular phenotypes acquired during chemotherapy resistance promote disease metastasis, creating a double burden. As I have demonstrated that FOXA1 is involved in the regulation of chemotherapy resistance in breast cancer cells, next I aimed to assess whether the experimental modulation of its expression would affect the anchorage-independent growth capacity. Growth in soft agar indicated that both MCF-7 and T47D cells each down-regulating FOXA1 showed a decrease in cloning efficiency up to approximately 4-fold, compared to their corresponding control cells (**Figure 7.8 A and B**). Similarly, formation of mammospheres in liquid culture, another *in vitro* assay to assess anchorage independence, revealed that FOXA1 down-regulation in both luminal MCF-7 and T47D breast cancer cells led to a significant reduction in sphere forming efficiency (**Figure 7.8 C and D**). Thus, down-regulation of FOXA1 in breast cancer cells decreased anchorage independence. Conversely, FOXA1 over-expression in basal-like MDA-MB-231 cells promoted the anchorage independent growth capacity, with approximately 2-fold increase in mammosphere forming efficiency in liquid culture, compared to empty vector control (**Figure 7.8 E**). MDA-MB-231 cells did not form robust clones in the soft agar assay, a phenomenon also observed with another basal-like HS578T breast cancer cells (**Chapter 4**). In line with this phenotypic alteration of increased anchorage independence with FOXA1 over-expression, RT-QPCR data also indicated an up-regulation of stem cell marker *NANOG* in MDA-MB-231 cells over-expressing FOXA1 (**Figure 7.8 F**).

Overall, these data indicate FOXA1 regulates anchorage independence in breast cancer cells and hence attributing that FOXA1's involvement in the regulation of MDR in breast cancer might be through modulating stemness.

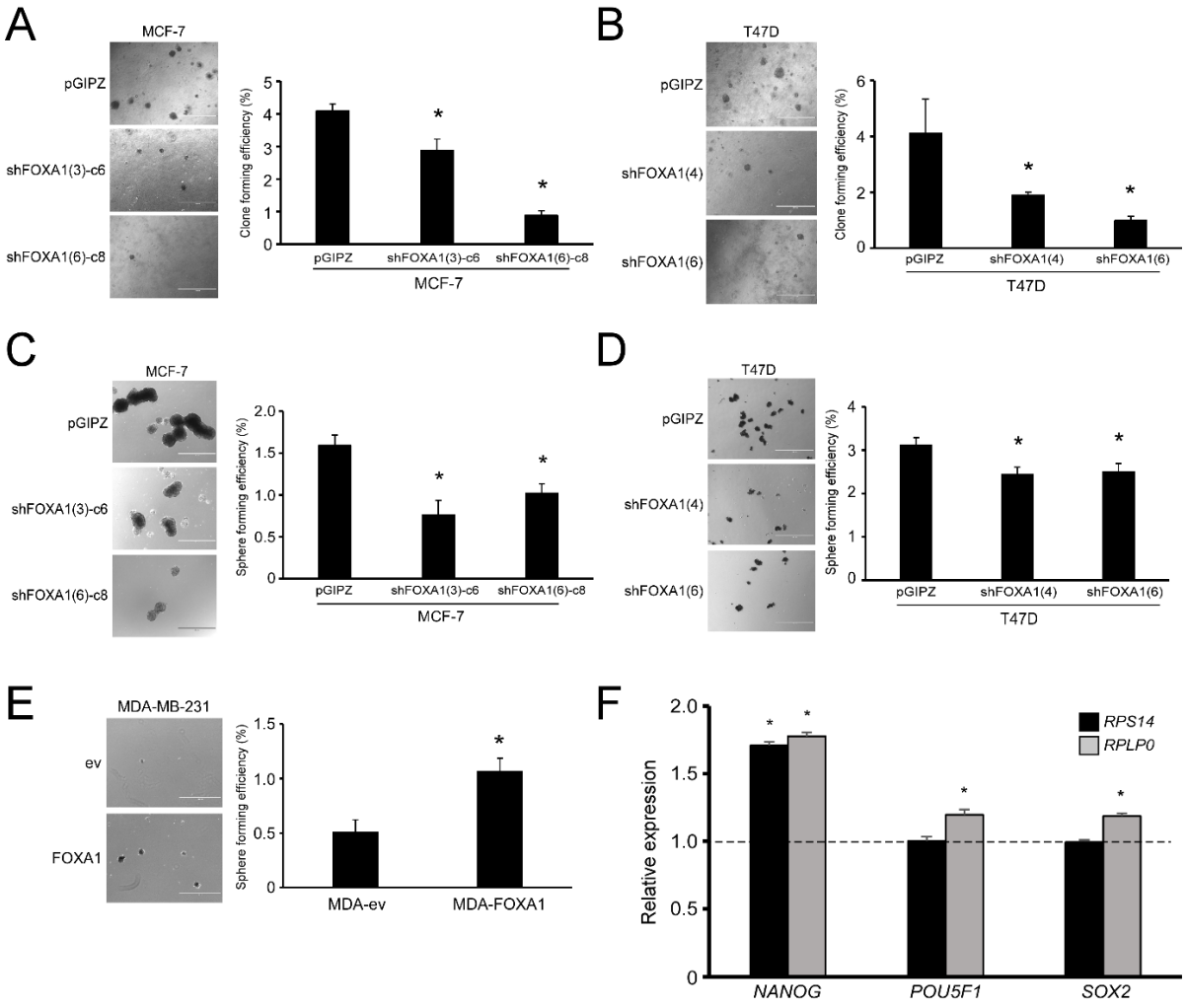


Figure 7.8: Experimental modulation of FOXA1 expression alters anchorage independence in breast cancer cells. Anchorage independent growth assays included growth in soft agar (A, B) and mammosphere formation in liquid culture (C-E) and were used for *in vitro* assessment of CSC phenotype in MCF-7 (A, C) and T47D (B, D) cells each down-regulating FOXA1, and MDA-MB-231 cells over-expressing FOXA1 (E). A-B, Soft agar colony formation assay: Cells (2 x 10^4 / well) were seeded in 6-well plates with medium containing soft agar and the formation of colonies was determined after 4 weeks of culture. C-E, Mammosphere formation assay: Cells (4 x 10^3 / well) were seeded in 6-well low-attachment plates with appropriate culture medium and the spheres were counted after two weeks of culture. In all cases, clones or spheres larger than 100 µm in diameter were counted. Clone or sphere forming efficiency was calculated relative to the total number of plated cells x100. Pictorial data are representatives of at least three independent experiments. Numerical data represent the average ± SD of three independent experiments. Bar represents 1000 µm. F, Quantitative real-time PCR analyses of some well-known CSC marker genes expression in MDA-MB-231 cells over-expressing FOXA1. The mRNAs levels were normalized to the *RPS14* and *RPLP0* genes. The relative expression of each gene was calculated with respect to empty vector control (MDA-ev cells, dashed line). Data represent the average ± SD of three independent experiments. *, $p<0.05$.

7.4 Discussion

During disease progression, cancer cells acquire some new phenotypes, such as drug resistance and stemness, which help their survival and proliferation (Hanahan & Weinberg, 2011). Here, I demonstrate, using breast cancer cellular models, that FOXA1 as a key mediator of MDR and anchorage independence. Although FOXA1's involvement in chemotherapy response has not been studied before, several reports indicate that FOXA1 contributes to the endocrine resistance in ER-positive breast cancer (Hurtado *et al.*, 2011; Ross-Innes *et al.*, 2012; Fu *et al.*, 2016). FOXA1, together with GRHL2, promotes the expression and activity of ligand-receptor complex LYPD3/ARG2, which contributes to the development of resistance to endocrine therapy (Cocce *et al.*, 2019). Additionally, FOXA1 reprograms ER binding in therapy resistant ER-positive disease and its expression is correlated with distant metastasis (Ross-Innes *et al.*, 2012).

While the FOXA1 function in traditional chemotherapy resistance has not been investigated in breast cancer, it appears to promote cell cycle progression by up-regulating cyclin B1 expression in chondrosarcoma, a highly chemo- and radiation-refractory malignant bone tumor (Lin *et al.*, 2018). Here, the data presented indicate that FOXA1 determines the resistance of breast cancer cells to doxorubicin and paclitaxel. MDR poses a significant treatment challenge in clinical settings, as the tumor cells acquire resistance simultaneously to structurally and mechanistically diverse drugs (Robey *et al.*, 2018). In metastatic breast cancer patients treated with first-line anthracycline- and taxanes-based chemotherapy, the response rates are found to be between 30 to 70% and most patients initially responding to the treatment tend to show disease progression within as short as six months, reflecting a non-durable pattern of chemotherapy response (Rivera & Gomez, 2010). An earlier study identified transcriptomic changes in both luminal MCF-7 and T47D cells upon transient silencing of FOXA1 (Bernardo *et al.*, 2013). However, this study neither did address cells response to drug nor its gene signatures included any of the traditional markers related to MDR, such as membrane bound efflux pumps or apoptotic proteins (Gottesman, 2002). Moreover, a cellular model with stably altered expression of a particular gene or multiple genes, like the ones generated in this study, gives a more reliable reflection of associated phenotypes than these obtained after transient alteration, thus highlighting further need for transcriptomic analysis with these cell models. Elucidating the mechanisms behind MDR can help identify targets for development of new drug candidates as well as develop novel treatment strategies aiming to improve clinical outcomes. Despite many years of research

pharmacological targeting of ABC transporters for modulating MDR could not bring a new treatment weapon into clinical practice. Thus, targeting regulators of MDR might represent an alternative avenue for the development of new cancer treatment. Although the molecules down-stream FOXA1 regulating MDR were not identified, the data represented here clearly supports a role for FOXA1 in the regulation of genes dictating breast cancer cellular response to doxorubicin and paclitaxel.

Using 3D cultures as an *in vitro* surrogate for tumor formation, I found that FOXA1 promotes anchorage independence, a key phenotype of cancer stem or tumor initiating cells (Weiswald, Bellet & Dangles-Marie, 2015). Ectopic over-expression of FOXA1 in MDA-MB-231 cells increased the tumor initiating cell population, as evident by the increased mammosphere forming efficiency in liquid culture. In contrast, FOXA1 down-regulation in both MCF-7 and T47D cells led to opposite effect, with reduction in the mammosphere formation capacity and growth in soft agar. In addition to the role in acquisition of drug resistance, cancer stem cells also contribute to the development of metastases (Luo, Brooks & Wicha, 2015). Thus, FOXA1 may play a vital role in disease progression by regulating genes involved in tumor formation and chemotherapy resistance.

FOXA1, as of EP300 and RUNX1, functions as an up-regulating transcription factor for *CDH1*, a gene encoding E-cadherin (Liu *et al.*, 2005). As loss of E-cadherin contributes to metastasis (Onder *et al.*, 2008), and EP300 down-regulation in MCF-7 cells leads to a decrease in E-cadherin expression (Asaduzzaman *et al.*, 2017), I initially postulated that experimental down-regulation FOXA1 expression would cause a reduction in E-cadherin levels. However, no alteration in E-cadherin expression was observed in both MCF-7 and T47D cells upon FOXA1 knock-down. Importantly, these cells showed an up-regulation of other positive regulators of E-cadherin, *EP300* and *RUNX1*, suggesting that any effect on E-cadherin expression incurred due to FOXA1 down-regulation might be compensated by up-regulating other two transcriptional activators of *CDH1*. As this is not evident with EP300 knock-down (Asaduzzaman *et al.*, 2017), a certain hierarchy in the transcriptional regulation *CDH1* expression must exist. Similarly, FOXA1 over-expression in MDA-MB-231 cells did not cause E-cadherin expression even after removal of HDAC constraint on chromatin and demethylation of *CDH1* promoter, suggesting that FOXA1 alone is unable to trigger E-cadherin expression.

The involvement of FOXA1 in promoting chemotherapeutic resistance and anchorage independence supports its role in orchestrating programs responsible for making breast cancer cells more aggressive. As MDR is a prime cause of cancer associated death in most patients (Robey *et al.*, 2018), the future identification of MDR effectors down-stream from FOXA1 may unveil new targeted therapeutic modalities to reduce breast cancer mortality.

Chapter 8: Discussion and future directions

In breast cancer, therapy failure owing to emergence of drug resistance always poses a significant challenge to the clinicians, as this contributes to disease relapse and morbidity. Despite the advent of many new targeted therapies, drug resistance still remains an unresolved clinical problem (Lage, 2008). Thus, there is a constant thrust unveiling the molecular mechanisms behind the chemotherapy resistance to identify the new targets for drug development. The present study aimed to identify the potential regulators of chemotherapy resistance in breast cancer, with a particular focus on metaplastic breast cancer, a treatment recalcitrant breast cancer subtype (Al Sayed *et al.*, 2006; Weigelt *et al.*, 2014; Al-Hilli *et al.*, 2019). Here, I report molecular and phenotypic characteristics of a novel MBC derived cell line, which shows resemblance to MBC subclass 1 (Lien *et al.*, 2007). Multidrug resistant cells generated from this metaplastic breast cancer derived cell line showed an up-regulation of the transcription factor FOXC1. Experimental silencing of FOXC1 in these cells reversed the MDR phenotype, highlighting a new pathway mediated by the upregulation of FOXC1 in breast cancer multidrug resistance. Further analysis revealed that FOXC1's involvement in MDR was not exclusive to MBC derived cells, rather it also contributed to the acquisition of MDR in basal-like breast cancer cells. Importantly, genome-wide expression analysis indicated that MDR phenotype in metaplastic breast cancer derived cells was accompanied by up-regulation of *TGFB2*, encoding an isoform of cytokine TGF-β. Inhibition of this pathway by treatment with galunisertib, an inhibitor of type I TGF-β receptor (Akhurst & Hata, 2012; Herbertz *et al.*, 2015), led to reversal of MDR phenotype, together with down-regulation of FOXC1, suggesting that FOXC1 functions down-stream TGF-β signalling cascade regulating MDR in metaplastic breast cancer derived cells. As miRs offer another layer of control in gene expression, I also studied miR expression profiling of MBC derived MDR cellular models. Interestingly, miR-495-3p, which targets both *TGFB2* and *FOXC1* (Xu *et al.*, 2016; Welten *et al.*, 2017; Elian, Yan & Walter, 2018), was significantly down-regulated in metaplastic breast cancer derived MDR cells. Experimental up-regulation of this miR with miR-495 mimic reversed the MDR phenotype in these drug-resistant cells, together with down-regulation of both *TGFB2* and *FOXC1*. In contrast, inhibition of miR-495-3p resulted in acquisition of MDR phenotype in drug sensitive parental cells, with up-regulation of both *TGFB2* and *FOXC1*. This highlights a novel miR-495-3p regulatory pathway controlling MDR in metaplastic breast cancer derived cells via FOXC1 and the TGF-β pathway (**Figure 8.1 A**).

Additionally, FOXA1, another member of FOX transcription factor family, contributes to the MDR in breast cancer cells. Experimental down-regulation of FOXA1 in luminal breast cancer cells led to increase in doxorubicin and paclitaxel sensitivity, whereas its over-expression in basal-like breast cancer cells caused an increase in resistance to both drugs (**Figure 8.1 B**).

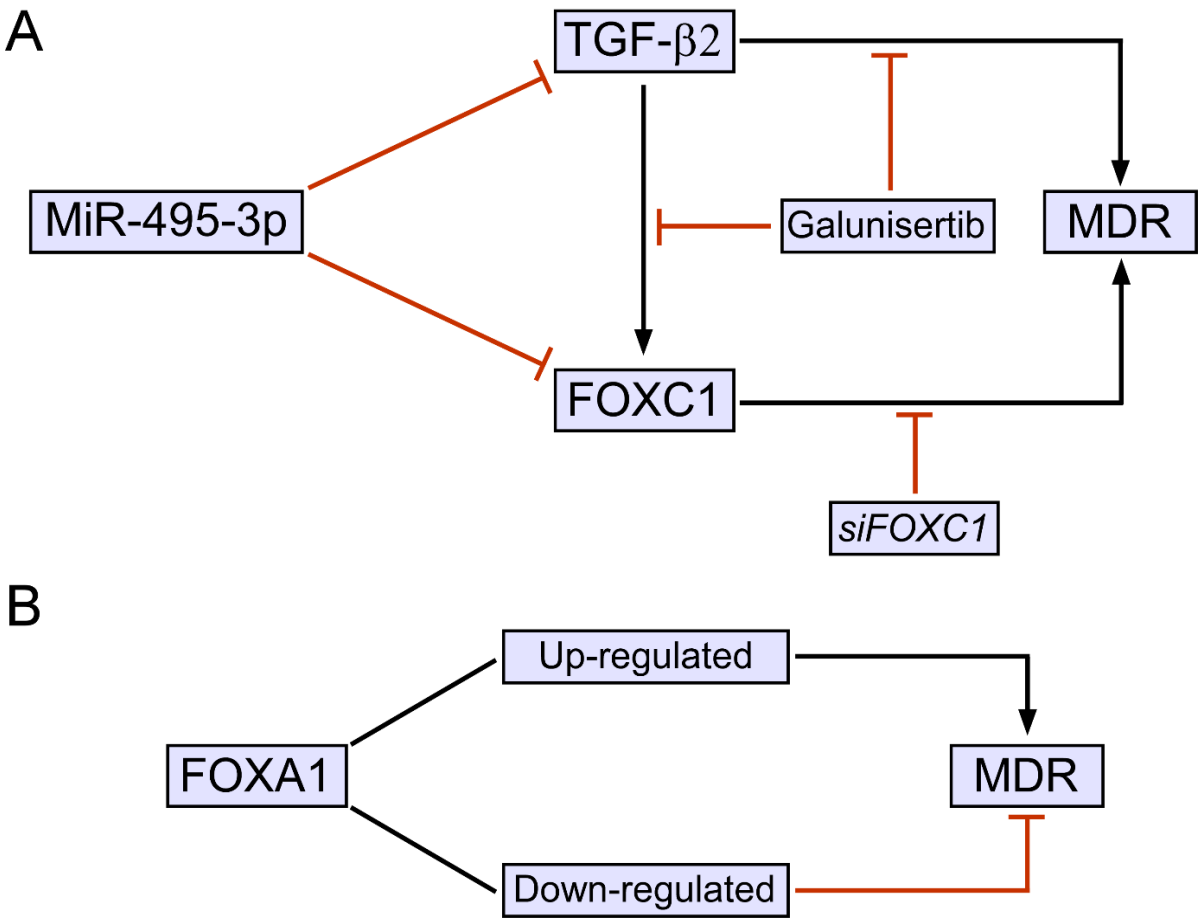


Figure 8.1: Regulators of multidrug resistance in breast cancer cells. A, Interplay between FOXC1, TGF-β and miR-495-3p regulating MDR in metaplastic breast cancer derived cells. B, FOXA1 regulates chemoresistance in breast cancer cells. Black arrows represent activation; red lines represent inhibition or repression of gene expression.

Currently, the standard care for MBC with systemic therapies is the same that used for other TNBCs. However, this brings less favorable clinical outcomes in MBC patents, compared to conventional TNBC (Jung *et al.*, 2010; Chen *et al.*, 2011). Thus, treating MBCs as conventional TNBCs is not a judicious approach for their clinical management. This requires treatment modalities specifically targeted against MBC. Several studies indicate multiple molecular alterations in MBC, such as overexpression of EGFR and PD-L1, and frequent mutations in *PIK3CA* and *TP53* genes, among others (Reddy *et al.*, 2020). Thus, developing new therapeutics targeting these molecular alterations could offer new hope in the treatment of this notorious category of breast cancer. Supporting this notion, a study indicated that an MBC patient harbouring a *PIK3CA* mutation showed an improved clinical benefit to a combination systemic chemotherapy of paclitaxel and buparlisib, a pan-class I PI3K inhibitor (Yang, Chen & Lu, 2019). Similarly, another study showed that nivolumab, an anti-PD-1 drug, given in combination with ipilimumab, an anti-CTLA4 monoclonal antibody, is clinically effective in advanced MBC, with three patients shows durable response in a small cohort of 17 patients (Adams *et al.*, 2020).

However, an alternative, possibly the best, strategy in developing new therapeutics against this notorious cancer subtype would be targeting the molecules that drive chemoresistance, thereby improving or retaining the sensitivity of the tumours to conventional chemotherapeutics. The data presented here indicates that higher expression of transcription factor FOXC1 contributes to the acquired multidrug resistance in metaplastic breast cancer derived cells. Silencing FOXC1 expression significantly increases the sensitivity of the cells to the conventional chemotherapeutics, doxorubicin and paclitaxel, thus offering a promising target for new therapeutics development. Moreover, IHC staining of breast cancer tissue specimen for FOXC1 could be used as a pathological test in clinics to assess the possible chemotherapeutic efficacy. Therapeutic modalities aiming to inhibit either transcriptional activity or expression of FOXC1 would provide improved clinical outcome not only for patients with metaplastic breast carcinoma, but also with other basal-like breast cancer subtype, which express comparatively higher levels of FOXC1 (Han *et al.*, 2017). Designing small molecule inhibitors of FOXC1 could be an attractive avenue for new drug development, as this approach has already been proven to be promising for inhibition of FOXM1, another FOX transcription factor (Adami & Ye, 2007). A study shows that thiazole antibiotics, Siomycin A and thiostrepton, inhibit FOXM1 transcriptional activity, leading to induction of apoptosis in cancer cells (Bhat, Halasi & Gartel, 2009). Interestingly, FOXC1

stability is greatly increased when phosphorylated at Ser-272 by EGF-activated ERK1/2-MAPK signalling pathway. Pharmacological inhibition of this pathway reduces the steady state levels FOXC1 protein (Berry, Mirzayans & Walter, 2006). This provides another option to test whether a combination of MEK inhibitor and conventional chemotherapeutics could benefit by increasing the sensitivity to chemotherapy. Another study reported that EGF-induced activation of EGFR leads to up-regulation of FOXC1 in BLBC cells via both Ras/ERK and PI3K/AKT signalling pathways (Jin *et al.*, 2014). Thus, inhibition of PI3K/AKT pathways by small molecule inhibitor, such as buparlisib, could be explored future, with an aim to increase chemotherapeutic efficacy upon FOXC1 down-regulation.

Equally, transcriptional silencing FOXC1 through siRNA-loaded nanoparticle drug delivery system could be another potential future drug development strategy. Although there are currently no Food and Drug Administration (FDA) approved siRNA-based therapeutics for cancer treatment, several siRNA-nanoparticles targeting different hallmarks of breast cancer are in process of development (Ngamcherdtrakul & Yantasee, 2019). For instance, nanoparticle carrying siRNA targeting P-glycoprotein (ABCB1) and doxorubicin significantly increases the intracellular concentration of doxorubicin when delivered to a MDR ectopic breast tumour (Meng *et al.*, 2013). Similarly, co-delivery of siRNA targeting ABCC1 and doxorubicin significantly improves doxorubicin efficacy (Deng *et al.*, 2013).

Although the data presented in this thesis explicitly describe MDR regulation by FOXC1 in breast cancer cells, we currently do not know the FOXC1 down-stream effectors involved in such regulation. Several studies indicate that FOXC1 regulates the BLBC cellular phenotypes via activating multiple signalling pathways, such as NF-κB and Notch (Han *et al.*, 2017; Elian, Yan & Walter, 2018). Thus, future identification of down-stream effectors of FOXC1 responsible for MDR in breast cancer cells is of utmost importance, as this could introduce more druggable targets. Consequently, transcriptome-wide and RNA-seq analyses using breast cancer cellular models with experimentally modulated FOXC1 expression is warranted in the future to identify altered gene expression profiles upon FOXC1 modulation. In addition, ChIP-seq analysis could help to identify the down-stream targets of FOXC1. Collectively, these data will help establish mechanisms visualising how FOXC1 regulates MDR in breast cancer cells.

Data presented here indicate that TGF-β2 contributes to MDR in metaplastic breast cancer derived cells either directly or via regulating FOXC1 expression. Thus, this offers a

promising target for the development of new therapeutics for this breast cancer subtype and such approaches to inhibit TGF-β pathway might include either targeted TGF-β2 suppression or the inhibition of TGF-β receptor (Neuzillet *et al.*, 2015). Several TGF-β2 inhibitors already in the development for many different carcinomas could be repurposed to assess their potential in reversing the MDR in metaplastic breast carcinoma. For example, trabedersen, an antisense oligodeoxynucleotide targeting TGF-β2, at 10 μM dose showed superior safety and efficacy compared to standard chemotherapy (temozolomide or procarbazine/lomustine/ vincristine) for patients with high-grade glioma (Bogdahn *et al.*, 2011). Similarly, a recently developed antisense oligonucleotide targeting TGF-β2, ISTH0047, caused significant prolongation in the survival of glioma-bearing mice (Papachristodoulou *et al.*, 2019) and prevented lung metastasis in a human breast cancer orthotopic mouse model (Huber-Ruano *et al.*, 2017). Fresolimumab, a TGF-β-neutralizing monoclonal antibody, exhibited acceptable safety and anti-tumour activity for patients mostly with advanced melanoma (Morris *et al.*, 2014).

Inhibition of TGF-β receptors with small molecule inhibitors might be another avenue for developing new therapeutics for tackling chemotherapy resistance in MBC. The present study demonstrated the potential of galunisertib, a small molecule inhibitor of type I TGF-β receptor (TβR-I) already in clinical trials for several different cancers, including pancreatic cancer, glioblastoma, and hepatocellular carcinoma (Akhurst & Hata, 2012; Herbertz *et al.*, 2015), in reversing the resistance to doxorubicin or paclitaxel in metaplastic breast cancer derived cellular models. This warrants further corroboration from *in vivo* studies demonstrating safety and efficacy of combination therapy of galunisertib and conventional chemotherapeutics (such as doxorubicin or paclitaxel) in sustaining drug sensitivity, thereby achieving improved clinical outcome. Similarly, vactosertib, another molecule belonging to the class of TGF-β type I receptor kinase (TβR-I) inhibitor currently in a phase I clinical trial for multiple myeloma (NCT03143985) (Kim *et al.*, 2018), could be explored future for repurpose in reversing the chemotherapy resistance in MBC.

Interestingly, the present study demonstrates that the TGF-β-FOXC1 axis regulates MDR in metaplastic breast cancer derived cells. TGF-β signalling functions through diverse down-stream molecules and co-operates with other signalling pathways, including Notch, WNT/β-catenin, NF-κB and RTK, to promote EMT (Heldin, Landström & Moustakas, 2009; Wang & Zhou, 2011). Thus, future identification of more down-stream effectors of TGF-β

contributing MDR in metaplastic breast cancer might add further targets for new drug development.

Finally, moving to the upper layer of hierarchy controlling both MDR regulators TGF-β2 and FOXC1, miR expression profiling identified miR-495-3p, which was significantly down-regulated in metaplastic breast cancer derived MDR cells. Data presented here indicates that this miR negatively regulates the MDR in metaplastic breast cancer derived cells via FOXC1 and the TGF-β pathway. Thus, miR-495-3p-mediated regulation of *TGFB2* and FOXC1 could be used in synergy with chemotherapeutics, such as doxorubicin and paclitaxel, to achieve enhanced and durable cytotoxic effects, thereby improved clinical outcomes in patients with MBC. Therapeutic modalities incorporating nanoparticles loaded with miR-495-3p only or in combination with a cytotoxic drug (such as, doxorubicin or paclitaxel) could offer promising treatment options against this aggressive breast cancer subtype. Several studies reported that miRs in combination with chemotherapeutics significantly enhanced the therapeutic efficacy of the cytotoxic drugs (Lee *et al.*, 2019). For instance, co-delivery of miR-34a, which targets anti-apoptotic marker BCL-2, and doxorubicin shows significantly augmented anti-tumour activity of the chemotherapeutic in human TNBC-bearing mouse model (Deng *et al.*, 2014). Similarly, combination therapy of miR-7 and paclitaxel exhibits enhanced chemotherapeutic efficacy of paclitaxel in ovarian cancer both *in vitro* and *in vivo*. As paclitaxel-induced activation of EGFR/ERK pathway is the major cause of acquired resistance to the drug, concurrent delivery of miR-7, which supresses EGFR/ERK pathway, aids in sensitizing the cells to paclitaxel, thereby help achieving sustained and improved therapeutic response (Cui *et al.*, 2018).

Furthermore, the present study also indicates FOXA1 contributes to the acquisition of MDR in breast cancer cells. FOXA1's involvement in poor disease prognosis has also been described in previous reports. For instance, a recent study investigating FOXA1 expression in 113 invasive breast cancer clinical samples indicates that FOXA1 expression is higher in tumour tissues and is positively associated tumour size and lymph node metastasis, among others. Importantly, patients with high FOXA1 expression tend to show worse overall and relapse-free survivals (Zhang *et al.*, 2020c). Similarly, another study analysing 333 non-metastatic TNBC clinical samples shows that patients with androgen receptor (AR)+/FOXA1+ are associated with significantly lower overall and recurrence-free survivals (Guiu *et al.*, 2018). Thus, accumulated evidence from present study and previous reports

indicates that FOXA1 could be a potential therapeutic target for development of new targeted treatment modalities for patients with breast cancer.

As the data presented clearly indicates FOXA1's role in chemotherapy resistance in breast cancer cells, future identification of up-restream regulators and down-stream effectors of FOXA1 involved in chemoresistance is crucial for identification more targets for drug development aiming to combat therapy resistance problem in breast cancer. Recently, using prostate cancer cellular model a study shows that methylation of FOXA1 by enhancer of zeste homolog 2 (EZH2) increases the protein stability. Inhibition of EZH2 by its inhibitor (tazemetostat, EPZ-6438) attenuates the FOXA1-driven prostate cancer growth (Park *et al.*, 2021). It remains to be studied whether inhibition of EZH2 in breast cancer cells reverses FOXA1-mediated chemotherapy resistance. Importantly, transcriptome-wide expression and ChIP-seq analyses in FOXA1 expression modulated breast cancer cellular model are warranted to identify FOXA1-regulated genes responsible for multidrug resistance.

Overall, the present study reveals some novel regulators of multidrug resistance in breast cancer cells. This information will be crucial for the development of targeted therapies to reduce the breast cancer mortality, as well as offers promising avenue for future research.

Chapter 9: References

Abdin, S.M., Tolba, M.F., Zaher, D.M. & Omar, H.A. (2021) Nuclear factor-κB signaling inhibitors revert multidrug-resistance in breast cancer cells. *Chemico-Biological Interactions*. 340 (March), 109450. Available from: doi:10.1016/j.cbi.2021.109450.

Abe, O., Abe, R., Enomoto, K., Kikuchi, K., et al. (2005) Effects of radiotherapy and of differences in the extent of surgery for early breast cancer on local recurrence and 15-year survival: An overview of the randomised trials. *The Lancet*. 366 (9503), 2087–2106. Available from: doi:10.1016/S0140-6736(05)67887-7.

Abouharb, S. & Moulder, S. (2015) Metaplastic Breast Cancer: Clinical Overview and Molecular Aberrations for Potential Targeted Therapy. *Current Oncology Reports*. 17 (3), 10. Available from: doi:10.1007/s11912-014-0431-z.

Adami, G.R. & Ye, H. (2007) Future roles for FoxM1 inhibitors in cancer treatments. *Future Oncology*. 3 (1), 1–3. Available from: doi:10.2217/14796694.3.1.1.

Adams, C., Cazzanelli, G., Rasul, S., Hitchinson, B., et al. (2015) Apoptosis inhibitor TRIAP1 is a novel effector of drug resistance. *Oncology Reports*. 34 (1), 415–422. Available from: doi:10.3892/or.2015.3988.

Adams, S., Othus, M., Patel, S.P., Chae, Y.K., et al. (2020) Dual anti-CTLA-4 and anti-PD-1 blockade in metaplastic carcinoma of the breast: Dart (SWOG S1609, Cohort 36). *Journal of Clinical Oncology*. 38 (15_suppl), 1073–1073. Available from: doi:10.1200/jco.2020.38.15_suppl.1073.

Akada, M., Crnogorac-Jurcevic, T., Lattimore, S., Mahon, P., et al. (2005) Intrinsic chemoresistance to gemcitabine is associated with decreased expression of BNIP3 in pancreatic cancer. *Clinical Cancer Research*. 11 (8), 3094–3101. Available from: doi:10.1158/1078-0432.CCR-04-1785.

Akhurst, R.J. & Hata, A. (2012) Targeting the TGFβ signalling pathway in disease. *Nature reviews. Drug discovery*. 11 (10), 790–811. Available from: doi:10.1038/nrd3810.

Al-Hilli, Z., Choong, G., Keeney, M.G., Visscher, D.W., et al. (2019) Metaplastic breast cancer has a poor response to neoadjuvant systemic therapy. *Breast Cancer Research and Treatment*. 176 (3), 709–716. Available from: doi:10.1007/s10549-019-05264-2.

Alamgeer, M., Ganju, V., Kumar, B., Fox, J., et al. (2014) Changes in aldehyde dehydrogenase-1 expression during neoadjuvant chemotherapy predict outcome in locally advanced breast cancer. *Breast Cancer Research*. 16 (2), R44. Available from: doi:10.1186/bcr3648.

Al Sayed, A.D., El Weshi, A.N., Tulbah, A.M., Rahal, M.M., et al. (2006) Metaplastic carcinoma of the breast Clinical presentation, treatment results and prognostic factors. *Acta Oncologica*. 45 (2), 188–195. Available from: doi:10.1080/02841860500513235.

American Cancer Society (2017) *About Breast Cancer*. Breast Cancer Facts and Figures. Available from: https://www.cancer.org/content/dam/CRC/PDF/Public/8577.00.pdf [Accessed: 13 January 2021].

American Cancer Society (2019a) *Breast Cancer: Treating Breast Cancer*. American Cancer Society. Available from: https://www.cancer.org/cancer/breast-cancer/treatment.html [Accessed: 13 January 2021].

American Cancer Society (2019b) *Non-cancerous Breast Conditions*. American Cancer Society. Available from: https://www.cancer.org/content/dam/CRC/PDF/Public/5034.00.pdf [Accessed: 13 January 2021].

Anandappa, G., Lampis, A., Cunningham, D., Khan, K.H., et al. (2019) MiR-31-3p expression and benefit from anti-EGFR inhibitors in metastatic colorectal cancer patients enrolled in the prospective phase II PROSPECT-C trial. *Clinical Cancer Research*. 25 (13), 3830–3838. Available from: doi:10.1158/1078-0432.CCR-18-3769.

Arlt, A., Gehrz, A., Müerköster, S., Vorndamm, J., et al. (2003) Role of NF-κB and Akt/PI3K in the resistance of pancreatic carcinoma cell lines against gemcitabine-induced cell death. *Oncogene*. 22 (21), 3243–3251. Available from: doi:10.1038/sj.onc.1206390.

Arner, E.N., Du, W. & Brekken, R.A. (2019) Behind the Wheel of Epithelial Plasticity in KRAS-Driven Cancers. *Frontiers in Oncology*. 9 (October). Available from: doi:10.3389/fonc.2019.01049.

Arumugam, T., Ramachandran, V., Fournier, K.F., Wang, H., et al. (2009) Epithelial to Mesenchymal Transition Contributes to Drug Resistance in Pancreatic Cancer. *Cancer Research*. 69 (14), 5820–5828. Available from: doi:10.1158/0008-5472.CAN-08-2819.

Asaduzzaman, M., Constantinou, S., Min, H., Gallon, J., et al. (2017) Tumour suppressor

EP300, a modulator of paclitaxel resistance and stemness, is downregulated in metaplastic breast cancer. *Breast Cancer Research and Treatment*. 163 (3), 461–474. Available from: doi:10.1007/s10549-017-4202-z.

Augello, M.A., Hickey, T.E. & Knudsen, K.E. (2011) FOXA1: Master of steroid receptor function in cancer. *EMBO Journal*. 30 (19), 3885–3894. Available from: doi:10.1038/emboj.2011.340.

Autier, P., Boniol, M., La Vecchia, C., LaVecchia, C., et al. (2010) Disparities in breast cancer mortality trends between 30 European countries: retrospective trend analysis of WHO mortality database. *BMJ (Clinical research ed.)*. 341 (aug11 1), c3620. Available from: doi:10.1136/bmj.c3620.

Avgeris, M., Papachristopoulou, G., Polychronis, A. & Scorilas, A. (2011) Down-regulation of kallikrein-related peptidase 5 (KLK5) expression in breast cancer patients: A biomarker for the differential diagnosis of breast lesions. *Clinical Proteomics*. 8 (1), 5. Available from: doi:10.1186/1559-0275-8-5.

Badve, S., Turbin, D., Thorat, M.A., Morimiya, A., et al. (2007) FOXA1 Expression in Breast Cancer—Correlation with Luminal Subtype A and Survival. *Clinical Cancer Research*. 13 (15), 4415–4421. Available from: doi:10.1158/1078-0432.CCR-07-0122.

Baguley, B.C. (2010) Multiple Drug Resistance Mechanisms in Cancer. *Molecular Biotechnology*. 46 (3), 308–316. Available from: doi:10.1007/s12033-010-9321-2.

Bai, W.-D., Ye, X.-M., Zhang, M.-Y., Zhu, H.-Y., et al. (2014) MiR-200c suppresses TGF-β signaling and counteracts trastuzumab resistance and metastasis by targeting ZNF217 and ZEB1 in breast cancer. *International Journal of Cancer*. 135 (6), 1356–1368. Available from: doi:10.1002/ijc.28782.

Balic, M., Lin, H., Young, L., Hawes, D., et al. (2006) Most Early Disseminated Cancer Cells Detected in Bone Marrow of Breast Cancer Patients Have a Putative Breast Cancer Stem Cell Phenotype. *Clinical Cancer Research*. 12 (19), 5615–5621. Available from: doi:10.1158/1078-0432.CCR-06-0169.

Bandyopadhyay, A., Wang, L., Agyin, J., Tang, Y., et al. (2010) Doxorubicin in Combination with a Small TGFβ Inhibitor: A Potential Novel Therapy for Metastatic Breast Cancer in Mouse Models Kurt Anderson (ed.). *PLoS ONE*. 5 (4), e10365. Available from:

doi:10.1371/journal.pone.0010365.

Beatty, J.D., Atwood, M., Tickman, R. & Reiner, M. (2006) Metaplastic breast cancer: clinical significance. *American Journal of Surgery*. 191 (5), 657–664. Available from: doi:10.1016/j.amjsurg.2006.01.038.

Bentires-Alj, M., Barbu, V., Fillet, M., Chariot, A., et al. (2003) NF-κB transcription factor induces drug resistance through MDR1 expression in cancer cells. *Oncogene*. 22 (1), 90–97. Available from: doi:10.1038/sj.onc.1206056.

Bergamaschi, A., Kim, Y.H., Wang, P., Sørlie, T., et al. (2006) Distinct patterns of DNA copy number alteration are associated with different clinicopathological features and gene-expression subtypes of breast cancer. *Genes, Chromosomes and Cancer*. 45 (11), 1033–1040. Available from: doi:10.1002/gcc.20366.

Bernardo, G.M., Bebek, G., Ginther, C.L., Sizemore, S.T., et al. (2013) FOXA1 represses the molecular phenotype of basal breast cancer cells. *Oncogene*. 32 (5), 554–563. Available from: doi:10.1038/onc.2012.62.

Bernardo, G.M., Lozada, K.L., Miedler, J.D., Harburg, G., et al. (2010) FOXA1 is an essential determinant of ERα expression and mammary ductal morphogenesis. *Development*. 137 (12), 2045–2054. Available from: doi:10.1242/dev.043299.

Bernaudo, S., Salem, M., Qi, X., Zhou, W., et al. (2016) Cyclin G2 inhibits epithelial-to-mesenchymal transition by disrupting Wnt/β-catenin signaling. *Oncogene*. 35 (36), 4816–4827. Available from: doi:10.1038/onc.2016.15.

Berry, F.B., Mirzayans, F. & Walter, M.A. (2006) Regulation of FOXC1 Stability and Transcriptional Activity by an Epidermal Growth Factor-activated Mitogen-activated Protein Kinase Signaling Cascade. *Journal of Biological Chemistry*. 281 (15), 10098–10104. Available from: doi:10.1074/jbc.M513629200.

Berry, F.B., Saleem, R.A. & Walter, M.A. (2002) FOXC1 Transcriptional Regulation Is Mediated by N- and C-terminal Activation Domains and Contains a Phosphorylated Transcriptional Inhibitory Domain. *Journal of Biological Chemistry*. 277 (12), 10292–10297. Available from: doi:10.1074/jbc.M110266200.

Berx, G., Becker, K.F., Höfler, H. & Van Roy, F. (1998) Mutations of the human E-cadherin (CDH1) gene. *Human Mutation*. 12 (4), 226–237. Available from:

doi:10.1002/(SICI)1098-1004(1998)12:4<226::AID-HUMU2>3.0.CO;2-D.

Bhat, U.G., Halasi, M. & Gartel, A.L. (2009) Thiazole Antibiotics Target FoxM1 and Induce Apoptosis in Human Cancer Cells Mikhail V. Blagosklonny (ed.). *PLoS ONE*. 4 (5), e5592. Available from: doi:10.1371/journal.pone.0005592.

Bhateja, P., Cherian, M., Majumder, S. & Ramaswamy, B. (2019) The Hedgehog Signaling Pathway: A Viable Target in Breast Cancer? *Cancers*. 11 (8), 1126. Available from: doi:10.3390/cancers11081126.

Bhola, N.E., Balko, J.M., Dugger, T.C., Kuba, M.G., et al. (2013) TGF-β inhibition enhances chemotherapy action against triple-negative breast cancer. *Journal of Clinical Investigation*. 123 (3), 1348–1358. Available from: doi:10.1172/JCI65416.

Bian, T., Lin, Q., Wu, Z., Cui, C., et al. (2016) Metaplastic carcinoma of the breast: Imaging and pathological features. *Oncology Letters*. 12 (5), 3975–3980. Available from: doi:10.3892/ol.2016.5177.

Bierie, B. & Moses, H.L. (2006) Tumour microenvironment - TGFB: The molecular Jekyll and Hyde of cancer. *Nature Reviews Cancer*. 6 (7), 506–520. Available from: doi:10.1038/nrc1926.

Bogdahn, U., Hau, P., Stockhammer, G., Venkataramana, N.K., et al. (2011) Targeted therapy for high-grade glioma with the TGF- 2 inhibitor trabedersen: results of a randomized and controlled phase IIb study. *Neuro-Oncology*. 13 (1), 132–142. Available from: doi:10.1093/neuonc/noq142.

Bonci, D., Coppola, V., Musumeci, M., Addario, A., et al. (2008) The miR-15a-miR-16-1 cluster controls prostate cancer by targeting multiple oncogenic activities. *Nature Medicine*. 14 (11), 1271–1277. Available from: doi:10.1038/nm.1880.

Bonnet, D. & Dick, J.E. (1997) Human Acute Myeloid Leukaemia is organised as a heirarchy that originates from a primitive haematopoetic cell. *Nature Medicine*. 3 (7), 730–737. Available from: http://www.nature.com/naturemedicine.

Borgna, S., Armellin, M., Di Gennaro, A., Maestro, R., et al. (2012) Mesenchymal traits are selected along with stem features in breast cancer cells grown as mammospheres. *Cell Cycle*. 11 (22), 4242–4251. Available from: doi:10.4161/cc.22543.

Borowicz, S., Van Scoyk, M., Avasarala, S., Karuppusamy Rathinam, M.K., et al. (2014) The

soft agar colony formation assay. *Journal of Visualized Experiments*. (92), e51998. Available from: doi:10.3791/51998.

Borst, P. & Oude Elferink, R. (2002) Mammalian ABC transporters in health and disease. *Annual Review of Biochemistry*. 71, 537–592. Available from: doi:10.1146/annurev.biochem.71.102301.093055.

Brabletz, T., Jung, A., Spaderna, S., Hlubek, F., et al. (2005) Migrating cancer stem cells — an integrated concept of malignant tumour progression. *Nature Reviews Cancer*. 5 (9), 744–749. Available from: doi:10.1038/nrc1694.

Bradbury, P.A. & Middleton, M.R. (2004) DNA repair pathways in drug resistance in melanoma. *Anti-Cancer Drugs*. 15 (5), 421–426. Available from: doi:10.1097/01.cad.0000127665.74096.93.

Bray, F., Ferlay, J., Soerjomataram, I., Siegel, R.L., et al. (2018) Global cancer statistics 2018: GLOBOCAN estimates of incidence and mortality worldwide for 36 cancers in 185 countries. *CA: A Cancer Journal for Clinicians*. 68 (6), 394–424. Available from: doi:10.3322/caac.21492.

Brenner, R.J., Turner, R.R., Schiller, V., Arndt, R.D., et al. (1998) Metaplastic carcinoma of the breast: Report of three cases. *Cancer*. 82 (6), 1082–1087. Available from: doi:10.1002/(SICI)1097-0142(19980315)82:6<1082::AID-CNCR11>3.0.CO;2-2.

Brodie, A. & Sabnis, G. (2011) Adaptive changes result in activation of alternate signaling pathways and acquisition of resistance to aromatase inhibitors. *Clinical Cancer Research*. 17 (13), 4208–4213. Available from: doi:10.1158/1078-0432.CCR-10-2920.

Brown, J.M. & Attardi, L.D. (2005) The role of apoptosis in cancer development and treatment response. *Nature Reviews Cancer*. 5 (March), 231–237. Available from: doi:10.1038/nrc1560.

Bryan, E.J., Jokubaitis, V.J., Chamberlain, N.L., Baxter, S.W., et al. (2002) Mutation analysis of EP300 in colon, breast and ovarian carcinomas. *International Journal of Cancer*. 102 (2), 137–141. Available from: doi:10.1002/ijc.10682.

Byers, L.A., Diao, L., Wang, J., Saintigny, P., et al. (2013) An Epithelial–Mesenchymal Transition Gene Signature Predicts Resistance to EGFR and PI3K Inhibitors and Identifies Axl as a Therapeutic Target for Overcoming EGFR Inhibitor Resistance.

Clinical Cancer Research. 19 (1), 279–290. Available from: doi:10.1158/1078-0432.CCR-12-1558.

Calin, G.A., Dumitru, C.D., Shimizu, M., Bichi, R., et al. (2002) Frequent deletions and down-regulation of micro-RNA genes miR15 and miR16 at 13q14 in chronic lymphocytic leukemia. *Proceedings of the National Academy of Sciences of the United States of America*. 99 (24), 15524–15529. Available from: doi:10.1073/pnas.242606799.

Calin, G.A., Sevignani, C., Dumitru, C.D., Hyslop, T., et al. (2004) Human microRNA genes are frequently located at fragile sites and genomic regions involved in cancers. *Proceedings of the National Academy of Sciences of the United States of America*. 101 (9), 2999–3004. Available from: doi:10.1073/pnas.0307323101.

Cameron, M.D., Schmidt, E.E., Kerkvliet, N., Nadkarni, K. V., et al. (2000) Temporal progression of metastasis in lung: Cell survival, dormancy, and location dependence of metastatic inefficiency. *Cancer Research*. 60 (9), 2541–2546. Available from: http://www.ncbi.nlm.nih.gov/pubmed/10811137.

Cao, S., Wang, Z., Gao, X., He, W., et al. (2018) FOXC1 induces cancer stem cell-like properties through upregulation of beta-catenin in NSCLC. *Journal of Experimental & Clinical Cancer Research*. 37 (1), 220. Available from: doi:10.1186/s13046-018-0894-0.

Cao, X., Wang, C., Liu, J. & Zhao, B. (2020) Regulation and functions of the Hippo pathway in stemness and differentiation. *Acta Biochimica et Biophysica Sinica*. 52 (7), 736–748. Available from: doi:10.1093/abbs/gmaa048.

Cardoso, F., Bedard, P.L., Winer, E.P., Pagani, O., et al. (2009) International guidelines for management of metastatic breast cancer: Combination vs sequential single-agent chemotherapy. *Journal of the National Cancer Institute*. 101 (17), 1174–1181. Available from: doi:10.1093/jnci/djp235.

Carroll, J.S. & Brown, M. (2006) Estrogen receptor target gene: An evolving concept. *Molecular Endocrinology*. 20 (8), 1707–1714. Available from: doi:10.1210/me.2005-0334.

Carroll, J.S., Liu, X.S., Brodsky, A.S., Li, W., et al. (2005) Chromosome-Wide Mapping of Estrogen Receptor Binding Reveals Long-Range Regulation Requiring the Forkhead

Protein FoxA1. *Cell*. 122 (1), 33–43. Available from: doi:10.1016/j.cell.2005.05.008.

Carter, C.L., Allen, C. & Henson, D.E. (1989) Relation of tumor size, lymph node status, and survival in 24,740 breast cancer cases. *Cancer*. 63 (1), 181–187. Available from: doi:10.1002/1097-0142(19890101)63:1<181::AID-CNCR2820630129>3.0.CO;2-H.

Carvalho, B.S. & Irizarry, R.A. (2010) A framework for oligonucleotide microarray preprocessing. *Bioinformatics*. 26 (19), 2363–2367. Available from: doi:10.1093/bioinformatics/btq431.

Castilla, M.Á., Díaz-Martín, J., Sarrió, D., Romero-Pérez, L., et al. (2012) MicroRNA-200 Family Modulation in Distinct Breast Cancer Phenotypes Elad Katz (ed.). *PLoS ONE*. 7 (10), e47709. Available from: doi:10.1371/journal.pone.0047709.

Celis, J.E., Kruhøffer, M., Gromova, I., Frederiksen, C., et al. (2000) Gene expression profiling: monitoring transcription and translation products using DNA microarrays and proteomics. *FEBS Letters*. 480 (1), 2–16. Available from: doi:10.1016/S0014-5793(00)01771-3.

Chambers, A.F., Groom, A.C. & MacDonald, I.C. (2002) Dissemination and growth of cancer cells in metastatic sites. *Nature Reviews Cancer*. 2 (8), 563–572. Available from: doi:10.1038/nrc865.

Charafe-Jauffret, E., Ginestier, C., Monville, F., Finetti, P., et al. (2006) Gene expression profiling of breast cell lines identifies potential new basal markers. *Oncogene*. 25 (15), 2273–2284. Available from: doi:10.1038/sj.onc.1209254.

Chen, G.Q., Zhao, Z.W., Zhou, H.Y., Liu, Y.J., et al. (2010) Systematic analysis of microRNA involved in resistance of the MCF-7 human breast cancer cell to doxorubicin. *Medical Oncology*. 27 (2), 406–415. Available from: doi:10.1007/s12032-009-9225-9.

Chen, H., Xu, L., Shan, Z. li, Chen, S., et al. (2020) GPX8 is transcriptionally regulated by FOXC1 and promotes the growth of gastric cancer cells through activating the Wnt signaling pathway. *Cancer Cell International*. 20 (1), 596. Available from: doi:10.1186/s12935-020-01692-z.

Chen, I.C., Lin, C.H., Huang, C.S., Lien, H.C., et al. (2011) Lack of efficacy to systemic chemotherapy for treatment of metaplastic carcinoma of the breast in the modern era.

Breast Cancer Research and Treatment. 130 (1), 345–351. Available from: doi:10.1007/s10549-011-1686-9.

Chen, J., Tian, W., He, H., Chen, F., et al. (2018a) Downregulation of miR-200c-3p contributes to the resistance of breast cancer cells to paclitaxel by targeting SOX2. *Oncology Reports*. 40 (6), 3821–3829. Available from: doi:10.3892/or.2018.6735.

Chen, S., Jiao, S., Jia, Y. & Li, Y. (2016) Effects of targeted silencing of FOXC1 gene on proliferation and in vitro migration of human non-small-cell lung carcinoma cells. *American Journal of Translational Research*. 8 (8), 3309–3318.

Chen, S., Wu, J., Jiao, K., Wu, Q., et al. (2018b) MicroRNA-495-3p inhibits multidrug resistance by modulating autophagy through GRP78/mTOR axis in gastric cancer. *Cell Death and Disease*. 9 (11), 1070. Available from: doi:10.1038/s41419-018-0950-x.

Chen, Y., Bieber, M.M. & Teng, N.N.H. (2014) Hedgehog signaling regulates drug sensitivity by targeting ABC transporters ABCB1 and ABCG2 in epithelial ovarian cancer. *Molecular Carcinogenesis*. 53 (8), 625–634. Available from: doi:10.1002/mc.22015.

Chen, Y., Sun, Y., Chen, L., Xu, X., et al. (2013) MiRNA-200c increases the sensitivity of breast cancer cells to doxorubicin through the suppression of E-cadherin-mediated PTEN/Akt signaling. *Molecular Medicine Reports*. 7 (5), 1579–1584. Available from: doi:10.3892/mmr.2013.1403.

Cheng, G.Z., Chan, J., Wang, Q., Zhang, W., et al. (2007) Twist Transcriptionally Up-regulates AKT2 in Breast Cancer Cells Leading to Increased Migration, Invasion, and Resistance to Paclitaxel. *Cancer Research*. 67 (5), 1979–1987. Available from: doi:10.1158/0008-5472.CAN-06-1479.

Chin, K., DeVries, S., Fridlyand, J., Spellman, P.T., et al. (2006) Genomic and transcriptional aberrations linked to breast cancer pathophysiologies. *Cancer Cell*. 10 (6), 529–541. Available from: doi:10.1016/j.ccr.2006.10.009.

Cirillo, L.A. & Zaret, K.S. (2007) Specific Interactions of the Wing Domains of FOXA1 Transcription Factor with DNA. *Journal of Molecular Biology*. 366 (3), 720–724. Available from: doi:10.1016/j.jmb.2006.11.087.

Clark, K.L., Halay, E.D., Lai, E. & Burley, S.K. (1993) Co-crystal structure of the HNF-

3/fork head DNA-recognition motif resembles histone H5. *Nature*. 364 (6436), 412–420. Available from: doi:10.1038/364412a0.

Cocce, K.J., Jasper, J.S., Desautels, T.K., Everett, L., et al. (2019) The Lineage Determining Factor GRHL2 Collaborates with FOXA1 to Establish a Targetable Pathway in Endocrine Therapy-Resistant Breast Cancer. *Cell Reports*. 29 (4), 889–903.e10. Available from: doi:10.1016/j.celrep.2019.09.032.

Craene, B. De & Berx, G. (2013) Regulatory networks defining EMT during cancer initiation and progression. *Nature Reviews Cancer*. 13 (2), 97–110. Available from: doi:10.1038/nrc3447.

Creighton, C.J., Chang, J.C. & Rosen, J.M. (2010) Epithelial-mesenchymal transition (EMT) in tumor-initiating cells and its clinical implications in breast cancer. *Journal of Mammary Gland Biology and Neoplasia*. 15 (2), 253–260. Available from: doi:10.1007/s10911-010-9173-1.

Cristea, S. & Polyak, K. (2018) Dissecting the mammary gland one cell at a time. *Nature Communications*. 9 (1), 2473. Available from: doi:10.1038/s41467-018-04905-2.

Cui, X., Sun, Y., Shen, M., Song, K., et al. (2018) Enhanced Chemotherapeutic Efficacy of Paclitaxel Nanoparticles Co-delivered with MicroRNA-7 by Inhibiting Paclitaxel-Induced EGFR/ERK pathway Activation for Ovarian Cancer Therapy. *ACS Applied Materials & Interfaces*. 10 (9), 7821–7831. Available from: doi:10.1021/acsami.7b19183.

D'Andrea, F.P., Safwat, A., Kassem, M., Gautier, L., et al. (2011) Cancer stem cell overexpression of nicotinamide N-methyltransferase enhances cellular radiation resistance. *Radiotherapy and Oncology*. 99 (3), 373–378. Available from: doi:10.1016/j.radonc.2011.05.086.

Dai, D. nian, Li, Y., Chen, B., Du, Y., et al. (2017) Elevated expression of CST1 promotes breast cancer progression and predicts a poor prognosis. *Journal of Molecular Medicine*. 95 (8), 873–886. Available from: doi:10.1007/s00109-017-1537-1.

Dai, H., Xu, L.Y., Qian, Q., Zhu, Q.W., et al. (2019) MicroRNA-222 promotes drug resistance to doxorubicin in breast cancer via regulation of miR-222/bim pathway. *Bioscience Reports*. 39 (7), 1–9. Available from: doi:10.1042/BSR20190650.

Dalal, B.I., Keown, P.A. & Greenberg, A.H. (1993) Immunocytochemical localization of secreted transforming growth factor- β1 to the advancing edges of primary tumors and to lymph node metastases of human mammary carcinoma. *American Journal of Pathology*. 143 (2), 381–389. Available from: http://www.ncbi.nlm.nih.gov/pubmed/8393616.

Dallas, N.A., Xia, L., Fan, F., Gray, M.J., et al. (2009) Chemoresistant Colorectal Cancer Cells, the Cancer Stem Cell Phenotype and Increased Sensitivity to Insulin-like Growth Factor Receptor-1 Inhibition. *Cancer Research*. 69 (5), 1951–1957. Available from: doi:10.1158/0008-5472.CAN-08-2023.

Das, S., Mukherjee, P., Chatterjee, R., Jamal, Z., et al. (2019) Enhancing Chemosensitivity of Breast Cancer Stem Cells by Downregulating SOX2 and ABCG2 Using Wedelolactone-encapsulated Nanoparticles. *Molecular Cancer Therapeutics*. 18 (3), 680–692. Available from: doi:10.1158/1535-7163.MCT-18-0409.

Dave, B., Mittal, V., Tan, N.M. & Chang, J.C. (2012) Epithelial-mesenchymal transition, cancer stem cells and treatment resistance. *Breast Cancer Research*. 14 (1), 202. Available from: doi:10.1186/bcr2938.

Davis, R.E., Brown, K.D., Siebenlist, U. & Staudt, L.M. (2001) Constitutive Nuclear Factor κB Activity Is Required for Survival of Activated B Cell–like Diffuse Large B Cell Lymphoma Cells. *Journal of Experimental Medicine*. 194 (12), 1861–1874. Available from: doi:10.1084/jem.194.12.1861.

Dean, M., Fojo, T. & Bates, S. (2005) Tumour stem cells and drug resistance. *Nature Reviews Cancer*. 5 (4), 275–284. Available from: doi:10.1038/nrc1590.

Dejeux, E., Rønneberg, J.A., Solvang, H., Bukholm, I., et al. (2010) DNA methylation profiling in doxorubicin treated primary locally advanced breast tumours identifies novel genes associated with survival and treatment response. *Molecular Cancer*. 9 (1), 68. Available from: doi:10.1186/1476-4598-9-68.

Della Corte, C.M., Bellevicine, C., Vicidomini, G., Vitagliano, D., et al. (2015) SMO Gene Amplification and Activation of the Hedgehog Pathway as Novel Mechanisms of Resistance to Anti-Epidermal Growth Factor Receptor Drugs in Human Lung Cancer. *Clinical Cancer Research*. 21 (20), 4686–4697. Available from: doi:10.1158/1078-0432.CCR-14-3319.

Delou, J.M.A., Souza, A.S.O., Souza, L.C.M. & Borges, H.L. (2019) Highlights in Resistance Mechanism Pathways for Combination Therapy. *Cells*. 8 (9), 1013. Available from: doi:10.3390/cells8091013.

Deng, J.J., Zhang, W., Xu, X.M., Zhang, F., et al. (2016) Twist mediates an aggressive phenotype in human colorectal cancer cells. *International Journal of Oncology*. 48 (3), 1117–1124. Available from: doi:10.3892/ijo.2016.3342.

Deng, X., Cao, M., Zhang, J., Hu, K., et al. (2014) Hyaluronic acid-chitosan nanoparticles for co-delivery of MiR-34a and doxorubicin in therapy against triple negative breast cancer. *Biomaterials*. 35 (14), 4333–4344. Available from: doi:10.1016/j.biomaterials.2014.02.006.

Deng, Z.J., Morton, S.W., Ben-Akiva, E., Dreaden, E.C., et al. (2013) Layer-by-Layer Nanoparticles for Systemic Codelivery of an Anticancer Drug and siRNA for Potential Triple-Negative Breast Cancer Treatment. *ACS Nano*. 7 (11), 9571–9584. Available from: doi:10.1021/nn4047925.

DeSantis, C.E., Ma, J., Gaudet, M.M., Newman, L.A., et al. (2019) Breast cancer statistics, 2019. *CA: A Cancer Journal for Clinicians*. 69 (6), 438–451. Available from: doi:10.3322/caac.21583.

Dietel, M., Lage, H., Arps, H. & Niendorf, A. (1990) Membrane Vesicle Formation Due to Acquired Mitoxantrone Resistance in Human Gastric Carcinoma Cell Line EPG85–257. *Cancer Research*. 50 (18), 6100–6106. Available from: http://www.ncbi.nlm.nih.gov/pubmed/1975514.

Dirks, W.G., MacLeod, R.A.F., Nakamura, Y., Kohara, A., et al. (2010) Cell line cross-contamination initiative: An interactive reference database of STR profiles covering common cancer cell lines. *International Journal of Cancer*. 126 (1), 303–304. Available from: doi:10.1002/ijc.24999.

Djomehri, S.I., Gonzalez, M.E., da Veiga Leprevost, F., Tekula, S.R., et al. (2020) Quantitative proteomic landscape of metaplastic breast carcinoma pathological subtypes and their relationship to triple-negative tumors. *Nature Communications*. 11 (1), 1–15. Available from: doi:10.1038/s41467-020-15283-z.

Domingo-Domenech, J., Vidal, S.J., Rodriguez-Bravo, V., Castillo-Martin, M., et al. (2012)

Suppression of Acquired Docetaxel Resistance in Prostate Cancer through Depletion of Notch- and Hedgehog-Dependent Tumor-Initiating Cells. *Cancer Cell*. 22 (3), 373–388. Available from: doi:10.1016/j.ccr.2012.07.016.

Dong, B., Li, S., Zhu, S., Yi, M., et al. (2021) MiRNA-mediated EMT and CSCs in cancer chemoresistance. *Experimental Hematology & Oncology*. 10 (1), 12. Available from: doi:10.1186/s40164-021-00206-5.

Du, B. & Shim, J. (2016) Targeting Epithelial–Mesenchymal Transition (EMT) to Overcome Drug Resistance in Cancer. *Molecules*. 21 (7), 965. Available from: doi:10.3390/molecules21070965.

Duhachek-Muggy, S., Qi, Y., Wise, R., Alyahya, L., et al. (2017) Metalloprotease-disintegrin ADAM12 actively promotes the stem cell-like phenotype in claudin-low breast cancer. *Molecular Cancer*. 16 (1), 32. Available from: doi:10.1186/s12943-017-0599-6.

EBCTCG (2005) Effects of chemotherapy and hormonal therapy for early breast cancer on recurrence and 15-year survival: an overview of the randomised trials. *Lancet*. 365 (9472), 1687–1717. Available from: doi:10.1016/S0140-6736(05)66544-0.

Eeckhoute, J., Carroll, J.S., Geistlinger, T.R., Torres-Arzayus, M.I., et al. (2006) A cell-type-specific transcriptional network required for estrogen regulation of cyclin D1 and cell cycle progression in breast cancer. *Genes and Development*. 20 (18), 2513–2526. Available from: doi:10.1101/gad.1446006.

Elian, F.A., Yan, E. & Walter, M.A. (2018) FOXC1, the new player in the cancer sandbox. *Oncotarget*. 9 (8), 8165–8178. Available from: doi:10.18632/oncotarget.22742.

El Zein, D., Hughes, M., Kumar, S., Peng, X., et al. (2017) Metaplastic Carcinoma of the Breast Is More Aggressive Than Triple-negative Breast Cancer: A Study From a Single Institution and Review of Literature. *Clinical Breast Cancer*. 17 (5), 382–391. Available from: doi:10.1016/j.clbc.2017.04.009.

Esteller, M. (2007) Epigenetic gene silencing in cancer: The DNA hypermethylome. *Human Molecular Genetics*. 16 (R1), R50–R59. Available from: doi:10.1093/hmg/ddm018.

Eun, J.W., Kim, H.S., Shen, Q., Yang, H.D., et al. (2018) MicroRNA-495-3p functions as a tumor suppressor by regulating multiple epigenetic modifiers in gastric carcinogenesis. *The Journal of Pathology*. 244 (1), 107–119. Available from: doi:10.1002/path.4994.

Falkenberg, N., Anastasov, N., Rappl, K., Braselmann, H., et al. (2013) MiR-221/-222 differentiate prognostic groups in advanced breast cancers and influence cell invasion. *British Journal of Cancer*. 109 (10), 2714–2723. Available from: doi:10.1038/bjc.2013.625.

Fan, H., Wang, W., Yan, J., Xiao, L., et al. (2018) Prognostic significance of CXCR7 in cancer patients: A meta-analysis. *Cancer Cell International*. 18 (1), 1–16. Available from: doi:10.1186/s12935-018-0702-0.

Fan, W., Chang, J. & Fu, P. (2015) Endocrine therapy resistance in breast cancer: Current status, possible mechanisms and overcoming strategies. *Future Medicinal Chemistry*. 7 (12), 1511–1519. Available from: doi:10.4155/fmc.15.93.

Ferguson, A.T., Vertino, P.M., Spitzner, J.R., Baylin, S.B., et al. (1997) Role of estrogen receptor gene demethylation and DNA methyltransferase- DNA adduct formation in 5-aza-2'-deoxycytidine-induced cytotoxicity in human breast cancer cells. *Journal of Biological Chemistry*. 272 (51), 32260–32266. Available from: doi:10.1074/jbc.272.51.32260.

Ferreira, C.G., Tolis, C. & Giaccone, G. (1999) p53 and chemosensitivity. *Annals of Oncology*. 10 (9), 1011–1022. Available from: doi:10.1023/A:1008361818480.

Fidler, I.J. (2002) The organ microenvironment and cancer metastasis. *Differentiation*. 70 (9–10), 498–505. Available from: doi:10.1046/j.1432-0436.2002.700904.x.

Fidler, I.J. (2003) The pathogenesis of cancer metastasis: the 'seed and soil' hypothesis revisited. *Nature Reviews Cancer*. 3 (6), 453–458. Available from: doi:10.1038/nrc1098.

Fischer, A.N.M., Fuchs, E., Mikula, M., Huber, H., et al. (2007) PDGF essentially links TGF-β signaling to nuclear β-catenin accumulation in hepatocellular carcinoma progression. *Oncogene*. 26 (23), 3395–3405. Available from: doi:10.1038/sj.onc.1210121.

Fu, X., Creighton, C.J., Biswal, N.C., Kumar, V., et al. (2014) Overcoming endocrine resistance due to reduced PTEN levels in estrogen receptor-positive breast cancer by co-targeting mammalian target of rapamycin, protein kinase B, or mitogen-activated protein kinase kinase. *Breast Cancer Research*. 16 (5), 430. Available from: doi:10.1186/s13058-014-0430-x.

Fu, X., Jeselsohn, R., Pereira, R., Hollingsworth, E.F., et al. (2016) FOXA1 overexpression

mediates endocrine resistance by altering the ER transcriptome and IL-8 expression in ER-positive breast cancer. *Proceedings of the National Academy of Sciences*. 113 (43), E6600–E6609. Available from: doi:10.1073/pnas.1612835113.

Fujita, Y., Kojima, K., Hamada, N., Ohhashi, R., et al. (2008) Effects of miR-34a on cell growth and chemoresistance in prostate cancer PC3 cells. *Biochemical and Biophysical Research Communications*. 377 (1), 114–119. Available from: doi:10.1016/j.bbrc.2008.09.086.

Gan, Y., Wientjes, M.G. & Au, J.L.S. (2006) Expression of basic fibroblast growth factor correlates with resistance to paclitaxel in human patient tumors. *Pharmaceutical Research*. 23 (6), 1324–1331. Available from: doi:10.1007/s11095-006-0136-6.

Gao, Y.T., Chen, X.B. & Liu, H.L. (2016) Up-regulation of miR-370-3p restores glioblastoma multiforme sensitivity to temozolomide by influencing MGMT expression. *Scientific Reports*. 6 (1), 32972. Available from: doi:10.1038/srep32972.

García-Aranda, M., Pérez-Ruiz, E. & Redondo, M. (2018) Bcl-2 inhibition to overcome resistance to chemo-and immunotherapy. *International Journal of Molecular Sciences*. 19 (12), 3950. Available from: doi:10.3390/ijms19123950.

Gayther, S.A., Batley, S.J., Linger, L., Bannister, A., et al. (2000) Mutations truncating the EP300 acetylase in human cancers. *Nature Genetics*. 24 (3), 300–303. Available from: doi:10.1038/73536.

Geiger, T.R. & Peeper, D.S. (2009) Metastasis mechanisms. *Biochimica et Biophysica Acta - Reviews on Cancer*. 1796 (2), 293–308. Available from: doi:10.1016/j.bbcan.2009.07.006.

Gerhardt, J., Montani, M., Wild, P., Beer, M., et al. (2012) FOXA1 promotes tumor progression in prostate cancer and represents a novel hallmark of castration-resistant prostate cancer. *American Journal of Pathology*. 180 (2), 848–861. Available from: doi:10.1016/j.ajpath.2011.10.021.

Gerson, S.L. (2004) MGMT: Its role in cancer aetiology and cancer therapeutics. *Nature Reviews Cancer*. 4 (4), 296–307. Available from: doi:10.1038/nrc1319.

Gibbs, G.M., Roelants, K. & O'Bryan, M.K. (2008) The CAP superfamily: Cysteine-rich secretory proteins, antigen 5, and pathogenesis-related 1 proteins - Roles in

reproduction, cancer, and immune defense. *Endocrine Reviews*. 29 (7), 865–897. Available from: doi:10.1210/er.2008-0032.

Giordano, S.H. (2003) Update on Locally Advanced Breast Cancer. *The Oncologist*. 8 (6), 521–530. Available from: doi:10.1634/theoncologist.8-6-521.

Gjerstorff, M.F. & Ditzel, H.J. (2008) An overview of the GAGE cancer/testis antigen family with the inclusion of newly identified members. *Tissue Antigens*. 71 (3), 187–192. Available from: doi:10.1111/j.1399-0039.2007.00997.x.

Goldhirsch, A., Wood, W.C., Gelber, R.D., Coates, A.S., et al. (2007) Progress and promise: Highlights of the international expert consensus on the primary therapy of early breast cancer 2007. *Annals of Oncology*. 18 (7), 1133–1144. Available from: doi:10.1093/annonc/mdm271.

Gomm, J.J., Coope, R.C., Browne, P.J. & Coombes, R.C. (1997) Separated human breast epithelial and myoepithelial cells have different growth factor requirements in vitro but can reconstitute normal breast lobuloalveolar structure. *Journal of Cellular Physiology*. 171 (1), 11–19. Available from: doi:10.1002/(SICI)1097-4652(199704)171:1<11::AID-JCP2>3.0.CO;2-K.

González-Martínez, S., Pérez-Mies, B., Carretero-Barrio, I., Palacios-Berraquero, M.L., et al. (2020) Molecular features of metaplastic breast carcinoma: An infrequent subtype of triple negative breast carcinoma. *Cancers*. 12 (7), 1–13. Available from: doi:10.3390/cancers12071832.

Goodman, R.H. & Smolik, S. (2000) CBP/p300 in cell growth, transformation, and development. *Genes and Development*. 14 (13), 1553–1577. Available from: doi:10.1101/gad.14.13.1553.

Gottesman, M.M. (2002) Mechanisms of Cancer Drug Resistance. *Annual Review of Medicine*. 53 (1), 615–627. Available from: doi:10.1146/annurev.med.53.082901.103929.

Gottesman, M.M. & Pastan, I. (1993) Biochemistry of Multidrug Resistance Mediated by the Multidrug Transporter. *Annual Review of Biochemistry*. 62 (1), 385–427. Available from: doi:10.1146/annurev.bi.62.070193.002125.

Gotzmann, J., Mikula, M., Eger, A., Schulte-Hermann, R., et al. (2004) Molecular aspects of

epithelial cell plasticity: implications for local tumor invasion and metastasis. *Mutation Research/Reviews in Mutation Research*. 566 (1), 9–20. Available from: doi:10.1016/S1383-5742(03)00033-4.

Gregory, P.A., Bert, A.G., Paterson, E.L., Barry, S.C., et al. (2008) The miR-200 family and miR-205 regulate epithelial to mesenchymal transition by targeting ZEB1 and SIP1. *Nature Cell Biology*. 10 (5), 593–601. Available from: doi:10.1038/ncb1722.

Guiu, S., Mollevi, C., Charon-Barra, C., Boissière, F., et al. (2018) Prognostic value of androgen receptor and FOXA1 co-expression in non-metastatic triple negative breast cancer and correlation with other biomarkers. *British Journal of Cancer*. 119 (1), 76–79. Available from: doi:10.1038/s41416-018-0142-6.

Guo, L., Liu, Y., Bai, Y., Sun, Y., et al. (2010) Gene expression profiling of drug-resistant small cell lung cancer cells by combining microRNA and cDNA expression analysis. *European Journal of Cancer*. 46 (9), 1692–1702. Available from: doi:10.1016/j.ejca.2010.02.043.

Guo, W., Keckesova, Z., Donaher, J.L., Shibue, T., et al. (2012) Slug and Sox9 Cooperatively Determine the Mammary Stem Cell State. *Cell*. 148 (5), 1015–1028. Available from: doi:10.1016/j.cell.2012.02.008.

Gupta, G.P. & Massagué, J. (2006) Cancer Metastasis: Building a Framework. *Cell*. 127 (4), 679–695. Available from: doi:10.1016/j.cell.2006.11.001.

Hackett, A.J., Smith, H.S., Springer, E.L., Owens, R.B., et al. (1977) Two syngeneic cell lines from human breast tissue: The aneuploid mammary epithelial (Hs578T) and the diploid myoepithelial (Hs578Bst) cell lines. *Journal of the National Cancer Institute*. 58 (6), 1795–1806. Available from: doi:10.1093/jnci/58.6.1795.

Hall, M.D., Handley, M.D. & Gottesman, M.M. (2009) Is resistance useless? Multidrug resistance and collateral sensitivity. *Trends in Pharmacological Sciences*. 30 (10), 546–556. Available from: doi:10.1016/j.tips.2009.07.003.

Han, B., Bhowmick, N., Qu, Y., Chung, S., et al. (2017) FOXC1: An emerging marker and therapeutic target for cancer. *Oncogene*. 36 (28), 3957–3963. Available from: doi:10.1038/onc.2017.48.

Han, B., Qu, Y., Jin, Y., Yu, Y., et al. (2015) FOXC1 Activates Smoothened-Independent

Hedgehog Signaling in Basal-like Breast Cancer. *Cell Reports*. 13 (5), 1046–1058. Available from: doi:10.1016/j.celrep.2015.09.063.

Han, M., Hu, J., Lu, P., Cao, H., et al. (2020) Exosome-transmitted miR-567 reverses trastuzumab resistance by inhibiting ATG5 in breast cancer. *Cell Death and Disease*. 11 (1), 43. Available from: doi:10.1038/s41419-020-2250-5.

Hanahan, D. & Weinberg, R.A. (2011) Hallmarks of cancer: The next generation. *Cell*. 144 (5), 646–674. Available from: doi:10.1016/j.cell.2011.02.013.

Hannenhalli, S. & Kaestner, K.H. (2009) The evolution of Fox genes and their role in development and disease. *Nature Reviews Genetics*. 10 (4), 233–240. Available from: doi:10.1038/nrg2523.

Harbeck, N., Penault-Llorca, F., Cortes, J., Gnant, M., et al. (2019) Breast cancer. *Nature Reviews Disease Primers*. 5 (1), 66. Available from: doi:10.1038/s41572-019-0111-2.

Hata, T., Mokutani, Y., Takahashi, H., Inoue, A., et al. (2017) Identification of microRNA-487b as a negative regulator of liver metastasis by regulation of KRAS in colorectal cancer. *International Journal of Oncology*. 50 (2), 487–496. Available from: doi:10.3892/ijo.2016.3813.

Hayes, M.J., Thomas, D., Emmons, A., Giordano, T.J., et al. (2008) Genetic changes of Wnt pathway genes are common events in metaplastic carcinomas of the breast. *Clinical Cancer Research*. 14 (13), 4038–4044. Available from: doi:10.1158/1078-0432.CCR-07-4379.

He, L., Thomson, J.M., Hemann, M.T., Hernando-Monge, E., et al. (2005) A microRNA polycistron as a potential human oncogene. *Nature*. 435 (7043), 828–833. Available from: doi:10.1038/nature03552.

He, X., Ji, J., Dong, R., Liu, H., et al. (2019) Prognosis in different subtypes of metaplastic breast cancer: a population-based analysis. *Breast Cancer Research and Treatment*. 173 (2), 329–341. Available from: doi:10.1007/s10549-018-5005-6.

Heidel, F.H., Bullinger, L., Feng, Z., Wang, Z., et al. (2012) Genetic and Pharmacologic Inhibition of β-Catenin Targets Imatinib-Resistant Leukemia Stem Cells in CML. *Cell Stem Cell*. 10 (4), 412–424. Available from: doi:10.1016/j.stem.2012.02.017.

Heldin, C.-H., Landström, M. & Moustakas, A. (2009) Mechanism of TGF-β signaling to

growth arrest, apoptosis, and epithelial–mesenchymal transition. *Current Opinion in Cell Biology*. 21 (2), 166–176. Available from: doi:10.1016/j.ceb.2009.01.021.

Hemmati, H.D., Nakano, I., Lazareff, J.A., Masterman-Smith, M., et al. (2003) Cancerous stem cells can arise from pediatric brain tumors. *Proceedings of the National Academy of Sciences of the United States of America*. 100 (25), 15178–15183. Available from: doi:10.1073/pnas.2036535100.

Hennessy, B.T., Giordano, S., Broglio, K., Duan, Z., et al. (2006) Biphasic metaplastic sarcomatoid carcinoma of the breast. *Annals of Oncology*. 17 (4), 605–613. Available from: doi:10.1093/annonc/mdl006.

Hennessy, B.T., Gonzalez-Angulo, A.M., Stemke-Hale, K., Gilcrease, M.Z., et al. (2009) Characterization of a naturally occurring breast cancer subset enriched in epithelial-to-mesenchymal transition and stem cell characteristics. *Cancer Research*. 69 (10), 4116–4124. Available from: doi:10.1158/0008-5472.CAN-08-3441.

Herbertz, S., Sawyer, J.S., Stauber, A.J., Gueorguieva, I., et al. (2015) Clinical development of galunisertib (Ly2157299 monohydrate), a small molecule inhibitor of transforming growth factor-beta signaling pathway. *Drug Design, Development and Therapy*. 9, 4479–4499. Available from: doi:10.2147/DDDT.S86621.

Hermann, P.C., Huber, S.L., Herrler, T., Aicher, A., et al. (2007) Distinct Populations of Cancer Stem Cells Determine Tumor Growth and Metastatic Activity in Human Pancreatic Cancer. *Cell Stem Cell*. 1 (3), 313–323. Available from: doi:10.1016/j.stem.2007.06.002.

Hilton, H.N., Clarke, C.L. & Graham, J.D. (2018) Estrogen and progesterone signalling in the normal breast and its implications for cancer development. *Molecular and Cellular Endocrinology*. 466, 2–14. Available from: doi:10.1016/j.mce.2017.08.011.

Hirohashi, S. (1998) Inactivation of the E-Cadherin-Mediated Cell Adhesion System in Human Cancers. *The American Journal of Pathology*. 153 (2), 333–339. Available from: doi:10.1016/S0002-9440(10)65575-7.

Hirschmann-Jax, C., Foster, A.E., Wulf, G.G., Nuchtern, J.G., et al. (2004) A distinct ‘side population’ of cells with high drug efflux capacity in human tumor cells. *Proceedings of the National Academy of Sciences of the United States of America*. 101 (39), 14228–

14233. Available from: doi:10.1073/pnas.0400067101.

Hollestelle, A., Peeters, J.K., Smid, M., Timmermans, M., et al. (2013) Loss of E-cadherin is not a necessity for epithelial to mesenchymal transition in human breast cancer. *Breast Cancer Research and Treatment*. 138 (1), 47–57. Available from: doi:10.1007/s10549-013-2415-3.

Holliday, D.L., Brouilette, K.T., Markert, A., Gordon, L.A., et al. (2009) Novel multicellular organotypic models of normal and malignant breast: Tools for dissecting the role of the microenvironment in breast cancer progression. *Breast Cancer Research*. 11 (1), R3. Available from: doi:10.1186/bcr2218.

Holliday, D.L. & Speirs, V. (2011) Choosing the right cell line for breast cancer research. *Breast Cancer Research*. 13 (4), 215. Available from: doi:10.1186/bcr2889.

Hollier, B.G., Tinnirello, A.A., Werden, S.J., Evans, K.W., et al. (2013) FOXC2 Expression Links Epithelial–Mesenchymal Transition and Stem Cell Properties in Breast Cancer. *Cancer Research*. 73 (6), 1981–1992. Available from: doi:10.1158/0008-5472.CAN-12-2962.

Holohan, C., Van Schaeybroeck, S., Longley, D.B. & Johnston, P.G. (2013) Cancer drug resistance: An evolving paradigm. *Nature Reviews Cancer*. 13 (10), 714–726. Available from: doi:10.1038/nrc3599.

Hopkins, A., Coatham, M.L. & Berry, F.B. (2017) FOXC1 Regulates FGFR1 Isoform Switching to Promote Invasion Following TGFβ-Induced EMT. *Molecular Cancer Research*. 15 (10), 1341–1353. Available from: doi:10.1158/1541-7786.MCR-17-0185.

Hortobagyi, G.N. (1994) Multidisciplinary management of advanced primary and metastatic breast cancer. *Cancer*. 74 (1 S), 416–423. Available from: doi:10.1002/cncr.2820741329.

Hsu, H.-H., Kuo, W.-W., Shih, H.-N., Cheng, S.-F., et al. (2019) FOXC1 Regulation of miR-31-5p Confers Oxaliplatin Resistance by Targeting LATS2 in Colorectal Cancer. *Cancers*. 11 (10), 1576. Available from: doi:10.3390/cancers11101576.

Hu, Q., Chen, W.X., Zhong, S.L., Zhang, J.Y., et al. (2014a) MicroRNA-452 contributes to the docetaxel resistance of breast cancer cells. *Tumor Biology*. 35 (7), 6327–6334. Available from: doi:10.1007/s13277-014-1834-z.

Hu, Q., Tong, S., Zhao, X., Ding, W., et al. (2015) Periostin Mediates TGF-β-Induced Epithelial Mesenchymal Transition in Prostate Cancer Cells. *Cellular Physiology and Biochemistry*. 36 (2), 799–809. Available from: doi:10.1159/000430139.

Hu, W.Z., Tan, C.L., He, Y.J., Zhang, G.Q., et al. (2018) Functional miRNAs in breast cancer drug resistance. *OncoTargets and Therapy*. 11, 1529–1541. Available from: doi:10.2147/OTT.S152462.

Hu, Y., Li, K., Asaduzzaman, M., Cuella, R., et al. (2016a) MIR-106b~25 cluster regulates multidrug resistance in an ABC transporter-independent manner via downregulation of EP300. *Oncology Reports*. 35 (2), 1170–1178. Available from: doi:10.3892/or.2015.4412.

Hu, Y., Li, S., Yang, M., Yan, C., et al. (2014b) Sorcin silencing inhibits epithelial-to-mesenchymal transition and suppresses breast cancer metastasis in vivo. *Breast Cancer Research and Treatment*. 143 (2), 287–299. Available from: doi:10.1007/s10549-013-2809-2.

Hu, Y., Qiu, Y., Yagüe, E., Ji, W., et al. (2016b) MiRNA-205 targets VEGFA and FGF2 and regulates resistance to chemotherapeutics in breast cancer. *Cell Death and Disease*. 7 (6), e2291. Available from: doi:10.1038/cddis.2016.194.

Hu, Y., Xu, K. & Yagüe, E. (2015) miR-218 targets survivin and regulates resistance to chemotherapeutics in breast cancer. *Breast Cancer Research and Treatment*. 151 (2), 269–280. Available from: doi:10.1007/s10549-015-3372-9.

Huang, J., Li, H. & Ren, G. (2015) Epithelial-mesenchymal transition and drug resistance in breast cancer (Review). *International Journal of Oncology*. 47 (3), 840–848. Available from: doi:10.3892/ijo.2015.3084.

Huang, K., Sun, Z., Ding, B., Jiang, X., et al. (2019) Suppressing hedgehog signaling reverses drug resistance of refractory acute myeloid leukemia. *OncoTargets and Therapy*. 12, 7477–7488. Available from: doi:10.2147/OTT.S216628.

Huang, L., Huang, Z., Fan, Y., He, L., et al. (2017) FOXC1 promotes proliferation and epithelial-mesenchymal transition in cervical carcinoma through the PI3K-Akt signal pathway. *American Journal of Translational Research*. 9 (3), 1297–1306.

Huang, W., Chen, Z., Zhang, L., Tian, D., et al. (2015) Interleukin-8 Induces Expression of

FOXC1 to Promote Transactivation of CXCR1 and CCL2 in Hepatocellular Carcinoma Cell Lines and Formation of Metastases in Mice. *Gastroenterology*. 149 (4), 1053–1067.e14. Available from: doi:10.1053/j.gastro.2015.05.058.

Huber-Ruano, I., Raventós, C., Cuartas, I., Sánchez-Jaro, C., et al. (2017) An antisense oligonucleotide targeting TGF-β2 inhibits lung metastasis and induces CD86 expression in tumor-associated macrophages. *Annals of Oncology*. 28 (9), 2278–2285. Available from: doi:10.1093/annonc/mdx314.

Huber, M.A., Kraut, N. & Beug, H. (2005) Molecular requirements for epithelial–mesenchymal transition during tumor progression. *Current Opinion in Cell Biology*. 17 (5), 548–558. Available from: doi:10.1016/j.ceb.2005.08.001.

Hurtado, A., Holmes, K.A., Ross-Innes, C.S., Schmidt, D., et al. (2011) FOXA1 is a key determinant of estrogen receptor function and endocrine response. *Nature Genetics*. 43 (1), 27–33. Available from: doi:10.1038/ng.730.

Hyter, S., Hirst, J., Pathak, H., Pessetto, Z.Y., et al. (2018) Developing a genetic signature to predict drug response in ovarian cancer. *Oncotarget*. 9 (19), 14828–14848. Available from: doi:10.18632/oncotarget.23663.

Jacobsen, F., Kraft, J., Schroeder, C., Hube-Magg, C., et al. (2017) Up-regulation of Biglycan is Associated with Poor Prognosis and PTEN Deletion in Patients with Prostate Cancer. *Neoplasia (United States)*. 19 (9), 707–715. Available from: doi:10.1016/j.neo.2017.06.003.

Jain, R.K., Mehta, R.J., Nakshatri, H., Idrees, M.T., et al. (2011) High-level expression of forkhead-box protein A1 in metastatic prostate cancer. *Histopathology*. 58 (5), 766–772. Available from: doi:10.1111/j.1365-2559.2011.03796.x.

JAMA (1991) Treatment of Early-Stage Breast Cancer. *JAMA: The Journal of the American Medical Association*. 265 (3), 391–395. Available from: doi:10.1001/jama.1991.03460030097037.

Jang, J.S., Jeon, H.S., Sun, Z., Aubry, M.C., et al. (2012) Increased miR-708 expression in NSCLC and its association with poor survival in lung adenocarcinoma from never smokers. *Clinical Cancer Research*. 18 (13), 3658–3667. Available from: doi:10.1158/1078-0432.CCR-11-2857.

Januchowski, R., Zawierucha, P., Ruciński, M., Nowicki, M., et al. (2014) Extracellular matrix proteins expression profiling in chemoresistant variants of the A2780 ovarian cancer cell line. *BioMed Research International*. 2014 (4), 1–9. Available from: doi:10.1155/2014/365867.

Jemal, A., Bray, F., Center, M.M., Ferlay, J., et al. (2011) Global cancer statistics. *CA: A Cancer Journal for Clinicians*. 61 (2), 69–90. Available from: doi:10.3322/caac.20107.

Jensen, T.W., Ray, T., Wang, J., Li, X., et al. (2015) Diagnosis of Basal-Like Breast Cancer Using a FOXC1-Based Assay. *JNCI: Journal of the National Cancer Institute*. 107 (8), 1–9. Available from: doi:10.1093/jnci/djv148.

Ji, J., Yamashita, T., Budhu, A., Forgues, M., et al. (2009a) Identification of MicroRNA-181 by genome-wide screening as a critical player in EpCAM - Positive hepatic cancer stem cells. *Hepatology*. 50 (2), 472–480. Available from: doi:10.1002/hep.22989.

Ji, Q., Hao, X., Zhang, M., Tang, W., et al. (2009b) MicroRNA miR-34 inhibits human pancreatic cancer tumor-initiating cells Eric J. Bernhard (ed.). *PLoS ONE*. 4 (8), e6816. Available from: doi:10.1371/journal.pone.0006816.

Jiang, L., He, D., Yang, D., Chen, Z., et al. (2014) MiR-489 regulates chemoresistance in breast cancer via epithelial mesenchymal transition pathway. *FEBS Letters*. 588 (11), 2009–2015. Available from: doi:10.1016/j.febslet.2014.04.024.

Jiao, X., Zhao, L., Ma, M., Bai, X., et al. (2013) MiR-181a enhances drug sensitivity in mitoxantone-resistant breast cancer cells by targeting breast cancer resistance protein (BCRP/ABCG2). *Breast Cancer Research and Treatment*. 139 (3), 717–730. Available from: doi:10.1007/s10549-013-2607-x.

Jin, H.-J., Zhao, J.C., Ogden, I., Bergan, R.C., et al. (2013) Androgen Receptor-Independent Function of FoxA1 in Prostate Cancer Metastasis. *Cancer Research*. 73 (12), 3725–3736. Available from: doi:10.1158/0008-5472.CAN-12-3468.

Jin, Y., Han, B., Chen, J., Wiedemeyer, R., et al. (2014) FOXC1 is a Critical Mediator of EGFR Function in Human Basal-like Breast Cancer. *Annals of Surgical Oncology*. 21 (4), 758–766. Available from: doi:10.1245/s10434-014-3980-3.

Johnstone, R.W., Ruefli, A.A. & Lowe, S.W. (2002) Apoptosis: A link between cancer genetics and chemotherapy. *Cell*. 108 (2), 153–164. Available from: doi:10.1016/S0092-

8674(02)00625-6.

Joneja, U., Vranic, S., Swensen, J., Feldman, R., et al. (2017) Comprehensive profiling of metaplastic breast carcinomas reveals frequent overexpression of programmed death-ligand 1. *Journal of Clinical Pathology*. 70 (3), 255–259. Available from: doi:10.1136/jclinpath-2016-203874.

Jones, P.A. & Baylin, S.B. (2007) The Epigenomics of Cancer. *Cell*. 128 (4), 683–692. Available from: doi:10.1016/j.cell.2007.01.029.

Ju, J., Zhu, A.-J. & Yuan, P. (2018) Progress in targeted therapy for breast cancer. *Chronic Diseases and Translational Medicine*. 4 (3), 164–175. Available from: doi:10.1016/j.cdtm.2018.04.002.

Jung, S.Y., Kim, H.Y., Nam, B.H., Min, S.Y., et al. (2010) Worse prognosis of metaplastic breast cancer patients than other patients with triple-negative breast cancer. *Breast Cancer Research and Treatment*. 120 (3), 627–637. Available from: doi:10.1007/s10549-010-0780-8.

Kajita, M., McClinic, K.N. & Wade, P.A. (2004) Aberrant Expression of the Transcription Factors Snail and Slug Alters the Response to Genotoxic Stress. *Molecular and Cellular Biology*. 24 (17), 7559–7566. Available from: doi:10.1128/MCB.24.17.7559-7566.2004.

Kalluri, R. & Neilson, E.G. (2003) Epithelial-mesenchymal transition and its implications for fibrosis. *Journal of Clinical Investigation*. 112 (12), 1776–1784. Available from: doi:10.1172/JCI200320530.

Kalluri, R. & Weinberg, R.A. (2009) The basics of epithelial-mesenchymal transition. *Journal of Clinical Investigation*. 119 (6), 1420–1428. Available from: doi:10.1172/JCI39104.

Kang, M.H., Singaraja, R. & Hayden, M.R. (2010) Adenosine-triphosphate-binding cassette transporter-1 trafficking and function. *Trends in Cardiovascular Medicine*. 20 (2), 41–49. Available from: doi:10.1016/j.tcm.2010.03.006.

Kao, J., Salari, K., Bocanegra, M., Choi, Y.-L., et al. (2009) Molecular Profiling of Breast Cancer Cell Lines Defines Relevant Tumor Models and Provides a Resource for Cancer Gene Discovery Mikhail V. Blagosklonny (ed.). *PLoS ONE*. 4 (7), e6146. Available from: doi:10.1371/journal.pone.0006146.

Khan, S., Brougham, C.L., Ryan, J., Sahrudin, A., et al. (2013) miR-379 Regulates Cyclin B1 Expression and Is Decreased in Breast Cancer Anna Alisi (ed.). *PLoS ONE*. 8 (7), e68753. Available from: doi:10.1371/journal.pone.0068753.

Kim, B.-G., Choi, S.H., Luo, G., Sergeeva, O., et al. (2018) Vactosertib, a TGF-ß Receptor I Kinase/ALK5 Inhibitor, Diminishes Tumor Progression and Bone Disease in a Mouse Model of Multiple Myeloma and Overcomes Resistance to Proteasome Inhibitors. *Blood*. 132 (Supplement 1), 1918–1918. Available from: doi:10.1182/blood-2018-99-117852.

Kitamura, T., Qian, B.Z., Soong, D., Cassetta, L., et al. (2015) CCL2-induced chemokine cascade promotes breast cancer metastasis by enhancing retention of metastasis-associated macrophages. *Journal of Experimental Medicine*. 212 (7), 1043–1059. Available from: doi:10.1084/jem.20141836.

Klarmann, G.J., Decker, A. & Farrar, W.L. (2008) Epigenetic gene silencing in the Wnt pathway in breast cancer. *Epigenetics*. 3 (2), 59–63. Available from: doi:10.4161/epi.3.2.5899.

Koinuma, K., Yamashita, Y., Liu, W., Hatanaka, H., et al. (2006) Epigenetic silencing of AXIN2 in colorectal carcinoma with microsatellite instability. *Oncogene*. 25 (1), 139–146. Available from: doi:10.1038/sj.onc.1209009.

Kong, Q., Han, J., Deng, H., Wu, F., et al. (2018) miR-431-5p alters the epithelial-to-mesenchymal transition markers by targeting UROC28 in hepatoma cells. *OncoTargets and Therapy*. 11, 6489–6503. Available from: doi:10.2147/OTT.S173840.

Kotiyal, S. & Bhattacharya, S. (2014) Breast cancer stem cells, EMT and therapeutic targets. *Biochemical and Biophysical Research Communications*. 453 (1), 112–116. Available from: doi:10.1016/j.bbrc.2014.09.069.

Koury, J., Zhong, L. & Hao, J. (2017) Targeting Signaling Pathways in Cancer Stem Cells for Cancer Treatment. *Stem Cells International*. 2017, 1–10. Available from: doi:10.1155/2017/2925869.

Krubasik, D., Iyer, N.G., English, W.R., Ahmed, A.A., et al. (2006) Absence of p300 induces cellular phenotypic changes characteristic of epithelial to mesenchyme transition. *British Journal of Cancer*. 94 (9), 1326–1332. Available from: doi:10.1038/sj.bjc.6603101.

Kumar, S., Kishimoto, H., Chua, H.L., Badve, S., et al. (2003) Interleukin-1α Promotes Tumor Growth and Cachexia in MCF-7 Xenograft Model of Breast Cancer. *American Journal of Pathology*. 163 (6), 2531–2541. Available from: doi:10.1016/S0002-9440(10)63608-5.

Kumar, U., Ardasheva, A., Mahmud, Z., Coombes, R.C., et al. (2021a) FOXA1 is a determinant of drug resistance in breast cancer cells. *Breast Cancer Research and Treatment*. 186 (2), 317–326. Available from: doi:10.1007/s10549-020-06068-5.

Kumar, V., Vashishta, M., Kong, L., Wu, X., et al. (2021b) The Role of Notch, Hedgehog, and Wnt Signaling Pathways in the Resistance of Tumors to Anticancer Therapies. *Frontiers in Cell and Developmental Biology*. 9 (April), 1–24. Available from: doi:10.3389/fcell.2021.650772.

Kume, T., Deng, K. & Hogan, B.L. (2000) Murine forkhead/winged helix genes Foxc1 (Mf1) and Foxc2 (Mfh1) are required for the early organogenesis of the kidney and urinary tract. *Development*. 127 (7), 1387–1395. Available from: doi:10.1242/dev.127.7.1387.

Kume, T., Deng, K.Y., Winfrey, V., Gould, D.B., et al. (1998) The forkhead/winged helix gene Mf1 is disrupted in the pleiotropic mouse mutation congenital hydrocephalus. *Cell*. 93 (6), 985–996. Available from: doi:10.1016/S0092-8674(00)81204-0.

Kutanzi, K.R., Yurchenko, O. V., Beland, F.A., Checkhun, V.F., et al. (2011) MicroRNA-mediated drug resistance in breast cancer. *Clinical Epigenetics*. 2 (2), 171–185. Available from: doi:10.1007/s13148-011-0040-8.

Laganière, J., Deblois, G. & Giguère, V. (2005) Functional genomics identifies a mechanism for estrogen activation of the retinoic acid receptor 1 gene in breast cancer cells. *Molecular Endocrinology*. 19 (6), 1584–1592. Available from: doi:10.1210/me.2005-0040.

Lage, H. (2008) An overview of cancer multidrug resistance: a still unsolved problem. *Cellular and Molecular Life Sciences*. 65 (20), 3145–3167. Available from: doi:10.1007/s00018-008-8111-5.

Lage, H. & Dietel, M. (2000) Effect of the breast-cancer resistance protein on atypical multidrug resistance. *Lancet Oncology*. 1 (3), 169–175. Available from: doi:10.1016/S1470-2045(00)00032-2.

Lage, H. & Dietel, M. (1999) Involvement of the DNA mismatch repair system in antineoplastic drug resistance. *Journal of Cancer Research and Clinical Oncology*. 125 (3–4), 156–165. Available from: doi:10.1007/s004320050258.

Lam, E.W.F., Brosens, J.J., Gomes, A.R. & Koo, C.Y. (2013) Forkhead box proteins: Tuning forks for transcriptional harmony. *Nature Reviews Cancer*. 13 (7), 482–495. Available from: doi:10.1038/nrc3539.

Lamouille, S., Xu, J. & Derynck, R. (2014) Molecular mechanisms of epithelial-mesenchymal transition. *Nature Reviews Molecular Cell Biology*. 15 (3), 178–196. Available from: doi:10.1038/nrm3758.

Lang, J.-Y., Hsu, J.L., Meric-Bernstam, F., Chang, C.-J., et al. (2011) BikDD Eliminates Breast Cancer Initiating Cells and Synergizes with Lapatinib for Breast Cancer Treatment. *Cancer Cell*. 20 (3), 341–356. Available from: doi:10.1016/j.ccr.2011.07.017.

Langlands, F., Cornford, E., Rakha, E., Dall, B., et al. (2016) Imaging overview of metaplastic carcinomas of the breast: A large study of 71 cases. *British Journal of Radiology*. 89 (1064), 20140644. Available from: doi:10.1259/bjr.20140644.

Lee, S.W.L., Paoletti, C., Campisi, M., Osaki, T., et al. (2019) MicroRNA delivery through nanoparticles. *Journal of Controlled Release*. 313 (October), 80–95. Available from: doi:10.1016/j.jconrel.2019.10.007.

Lee, Y.-M., Oh, M.H., Go, J.-H., Han, K., et al. (2020) Molecular subtypes of triple-negative breast cancer: understanding of subtype categories and clinical implication. *Genes & Genomics*. 42 (12), 1381–1387. Available from: doi:10.1007/s13258-020-01014-7.

Lehmann, O.J., Sowden, J.C., Carlsson, P., Jordan, T., et al. (2003) Fox's in development and disease. *Trends in Genetics*. 19 (6), 339–344. Available from: doi:10.1016/S0168-9525(03)00111-2.

Lei, J., Fan, L., Wei, G., Chen, X., et al. (2015) Gli-1 is crucial for hypoxia-induced epithelial-mesenchymal transition and invasion of breast cancer. *Tumor Biology*. 36 (4), 3119–3126. Available from: doi:10.1007/s13277-014-2948-z.

Leibl, S., Gogg-Kammerer, M., Sommersacher, A., Denk, H., et al. (2005) Metaplastic breast carcinomas: Are they of myoepithelial differentiation? Immunohistochemical profile of

the sarcomatoid subtype using novel myoepithelial markers. *American Journal of Surgical Pathology*. 29 (3), 347–353. Available from: doi:10.1097/01.pas.0000152133.60278.d2.

Leivonen, S.K., Icay, K., Jäntti, K., Siren, I., et al. (2017) MicroRNAs regulate key cell survival pathways and mediate chemosensitivity during progression of diffuse large B-cell lymphoma. *Blood Cancer Journal*. 7 (12), 654. Available from: doi:10.1038/s41408-017-0033-8.

Leo, F., Bartels, S., Mägel, L., Framke, T., et al. (2016) Prognostic factors in the myoepithelial-like spindle cell type of metaplastic breast cancer. *Virchows Archiv*. 469 (2), 191–201. Available from: doi:10.1007/s00428-016-1950-9.

Leong, K.G., Niessen, K., Kulic, I., Raouf, A., et al. (2007) Jagged1-mediated Notch activation induces epithelial-to-mesenchymal transition through Slug-induced repression of E-cadherin. *The Journal of Experimental Medicine*. 204 (12), 2935–2948. Available from: doi:10.1084/jem.20071082.

Li, J., Liu, H., Yu, J. & Yu, H. (2015) Chemoresistance to doxorubicin induces epithelial-mesenchymal transition via upregulation of transforming growth factor β signaling in HCT116 colon cancer cells. *Molecular Medicine Reports*. 12 (1), 192–198. Available from: doi:10.3892/mmr.2015.3356.

Li, J., Yang, X., Guan, H., Mizokami, A., et al. (2016a) Exosome-derived microRNAs contribute to prostate cancer chemoresistance. *International Journal of Oncology*. 49 (2), 838–846. Available from: doi:10.3892/ijo.2016.3560.

Li, J., Zhao, X., Wang, D., He, W., et al. (2016b) Up-regulated expression of phospholipase C, β1 is associated with tumor cell proliferation and poor prognosis in hepatocellular carcinoma. *OncoTargets and Therapy*. 9, 1697–1706. Available from: doi:10.2147/OTT.S97189.

Li, M., Gao, M., Xie, X., Zhang, Y., et al. (2019a) MicroRNA-200c reverses drug resistance of human gastric cancer cells by targeting regulation of the NER-ERCC3/4 pathway. *Oncology Letters*. 18 (1), 145–152. Available from: doi:10.3892/ol.2019.10304.

Li, Q., Wei, P., Wu, J., Zhang, M., et al. (2019b) The FOXC1/FBP1 signaling axis promotes colorectal cancer proliferation by enhancing the Warburg effect. *Oncogene*. 38 (4), 483–

496. Available from: doi:10.1038/s41388-018-0469-8.

Li, R., Chung, A.C.K., Dong, Y., Yang, W., et al. (2013) The microRNA miR-433 promotes renal fibrosis by amplifying the TGF-β/Smad3-Azin1 pathway. *Kidney International*. 84 (6), 1129–1144. Available from: doi:10.1038/ki.2013.272.

Li, S., Fong, K., Gritsina, G., Zhang, A., et al. (2019c) Activation of MAPK Signaling by CXCR7 Leads to Enzalutamide Resistance in Prostate Cancer. *Cancer Research*. 79 (10), 2580–2592. Available from: doi:10.1158/0008-5472.CAN-18-2812.

Li, X., Lewis, M.T., Huang, J., Gutierrez, C., et al. (2008) Intrinsic resistance of tumorigenic breast cancer cells to chemotherapy. *Journal of the National Cancer Institute*. 100 (9), 672–679. Available from: doi:10.1093/jnci/djn123.

Li, Y., Vandenboom, T.G., Kong, D., Wang, Z., et al. (2009) Up-regulation of miR-200 and let-7 by natural agents leads to the reversal of epithelial-to-mesenchymal transition in gemcitabine-resistant pancreatic cancer cells. *Cancer Research*. 69 (16), 6704–6712. Available from: doi:10.1158/0008-5472.CAN-09-1298.

Liang, C.-C., Park, A.Y. & Guan, J.-L. (2007) In vitro scratch assay: a convenient and inexpensive method for analysis of cell migration in vitro. *Nature Protocols*. 2 (2), 329–333. Available from: doi:10.1038/nprot.2007.30.

Liang, Z., Wu, H., Xia, J., Li, Y., et al. (2010) Involvement of miR-326 in chemotherapy resistance of breast cancer through modulating expression of multidrug resistance-associated protein 1. *Biochemical Pharmacology*. 79 (6), 817–824. Available from: doi:10.1016/j.bcp.2009.10.017.

Liberzon, A., Birger, C., Thorvaldsdóttir, H., Ghandi, M., et al. (2015) The Molecular Signatures Database Hallmark Gene Set Collection. *Cell Systems*. 1 (6), 417–425. Available from: doi:10.1016/j.cels.2015.12.004.

Lien, H.C., Hsiao, Y.H., Lin, Y.S., Yao, Y.T., et al. (2007) Molecular signatures of metaplastic carcinoma of the breast by large-scale transcriptional profiling: Identification of genes potentially related to epithelial-mesenchymal transition. *Oncogene*. 26 (57), 7859–7871. Available from: doi:10.1038/sj.onc.1210593.

Lin, L., Miller, C.T., Contreras, J.I., Prescott, M.S., et al. (2002) The hepatocyte nuclear factor 3 α gene, HNF3α (FOXA1), on chromosome band 14q13 is amplified and

overexpressed in esophageal and lung adenocarcinomas. *Cancer Research*. 62 (18), 5273–5279. Available from: http://www.ncbi.nlm.nih.gov/pubmed/12234996.

Lin, X.-J., He, C.-L., Sun, T., Duan, X.-J., et al. (2017) hsa-miR-485-5p reverses epithelial to mesenchymal transition and promotes cisplatin-induced cell death by targeting PAK1 in oral tongue squamous cell carcinoma. *International Journal of Molecular Medicine*. 40 (1), 83–89. Available from: doi:10.3892/ijmm.2017.2992.

Lin, Z.-S., Chung, C.-C., Liu, Y.-C., Chen, T.-M., et al. (2018) FOXA1 transcriptionally up-regulates cyclin B1 expression to enhance chondrosarcoma progression. *American journal of cancer research*. 8 (10), 1989–2004. Available from: http://www.ncbi.nlm.nih.gov/pubmed/30416851.

Litière, S., Werutsky, G., Fentiman, I.S., Rutgers, E., et al. (2012) Breast conserving therapy versus mastectomy for stage I-II breast cancer: 20 year follow-up of the EORTC 10801 phase 3 randomised trial. *The Lancet Oncology*. 13 (4), 412–419. Available from: doi:10.1016/S1470-2045(12)70042-6.

Liu, B., Xu, T., Xu, X., Cui, Y., et al. (2018a) Biglycan promotes the chemotherapy resistance of colon cancer by activating NF-κB signal transduction. *Molecular and Cellular Biochemistry*. 449 (1–2), 285–294. Available from: doi:10.1007/s11010-018-3365-1.

Liu, D., Wu, J., Lin, C., Andriani, L., et al. (2020) Breast Subtypes and Prognosis of Breast Cancer Patients With Initial Bone Metastasis: A Population-Based Study. *Frontiers in Oncology*. 10 (December), 1–12. Available from: doi:10.3389/fonc.2020.580112.

Liu, H., Patel, M.R., Prescher, J.A., Patsialou, A., et al. (2010) Cancer stem cells from human breast tumors are involved in spontaneous metastases in orthotopic mouse models. *Proceedings of the National Academy of Sciences of the United States of America*. 107 (42), 18115–18120. Available from: doi:10.1073/pnas.1006732107.

Liu, J., Wang, L., Su, Z., Wu, W., et al. (2014) A reciprocal antagonism between miR-376c and TGF-β signaling regulates neural differentiation of human pluripotent stem cells. *The FASEB Journal*. 28 (11), 4642–4656. Available from: doi:10.1096/fj.13-249342.

Liu, Q., Zhang, H., Jiang, X., Qian, C., et al. (2017) Factors involved in cancer metastasis: A better understanding to 'seed and soil' hypothesis. *Molecular Cancer*. 16 (1), 176.

Available from: doi:10.1186/s12943-017-0742-4.

Liu, R., Wang, X., Chen, G.Y., Dalerba, P., et al. (2007) The Prognostic Role of a Gene Signature from Tumorigenic Breast-Cancer Cells. *New England Journal of Medicine*. 356 (3), 217–226. Available from: doi:10.1056/nejmoa063994.

Liu, S., Lee, J.S., Jie, C., Park, M.H., et al. (2018b) HER2 overexpression triggers an IL1a proinflammatory circuit to drive tumorigenesis and promote chemotherapy resistance. *Cancer Research*. 78 (8), 2040–2051. Available from: doi:10.1158/0008-5472.CAN-17-2761.

Liu, Y.-N., Lee, W.-W., Wang, C.-Y., Chao, T.-H., et al. (2005) Regulatory mechanisms controlling human E-cadherin gene expression. *Oncogene*. 24 (56), 8277–8290. Available from: doi:10.1038/sj.onc.1208991.

Liu, Z., Liu, H., Desai, S., Schmitt, D.C., et al. (2013) MiR-125b functions as a key mediator for snail-induced stem cell propagation and chemoresistance. *Journal of Biological Chemistry*. 288 (6), 4334–4345. Available from: doi:10.1074/jbc.M112.419168.

Lombardo, Y., Filipovic, A., Molyneux, G., Periyasamy, M., et al. (2012) Nicastrin regulates breast cancer stem cell properties and tumor growth in vitro and in vivo. *Proceedings of the National Academy of Sciences*. 109 (41), 16558–16563. Available from: doi:10.1073/pnas.1206268109.

Lou, C., Xiao, M., Cheng, S., Lu, X., et al. (2016) MiR-485-3p and mir-485-5p suppress breast cancer cell metastasis by inhibiting PGC-1α expression. *Cell Death and Disease*. 7 (3), e2159. Available from: doi:10.1038/cddis.2016.27.

Lou, H. & Dean, M. (2007) Targeted therapy for cancer stem cells: The patched pathway and ABC transporters. *Oncogene*. 26 (9), 1357–1360. Available from: doi:10.1038/sj.onc.1210200.

Lu, X., Wang, Z., Huang, H. & Wang, H. (2020) Hedgehog signaling promotes multidrug resistance by regulation of ABC transporters in oral squamous cell carcinoma. *Journal of Oral Pathology & Medicine*. 49 (9), 897–906. Available from: doi:10.1111/jop.13050.

Luo, M., Brooks, M. & Wicha, M. (2015) Epithelial-Mesenchymal Plasticity of Breast Cancer Stem Cells: Implications for Metastasis and Therapeutic Resistance. *Current*

Pharmaceutical Design. 21 (10), 1301–1310. Available from: doi:10.2174/138161282166614121112060 4.

Luo, M., Clouthier, S.G., Deol, Y., Liu, S., et al. (2015) Breast Cancer Stem Cells: Current Advances and Clinical Implications. In: *Methods in Molecular Biology*. pp. 1–49. Available from: doi:10.1007/978-1-4939-2519-3_1.

Lupien, M. & Brown, M. (2009) Cistromics of hormone-dependent cancer. *Endocrine-Related Cancer*. 16 (2), 381–389. Available from: doi:10.1677/ERC-09-0038.

Ma, L., Young, J., Prabhala, H., Pan, E., et al. (2010) miR-9, a MYC/MYCN-activated microRNA, regulates E-cadherin and cancer metastasis. *Nature Cell Biology*. 12 (3), 247–256. Available from: doi:10.1038/ncb2024.

Ma, M.T., He, M., Wang, Y., Jiao, X.Y., et al. (2013) MiR-487a resensitizes mitoxantrone (MX)-resistant breast cancer cells (MCF-7/MX) to MX by targeting breast cancer resistance protein (BCRP/ABCG2). *Cancer Letters*. 339 (1), 107–115. Available from: doi:10.1016/j.canlet.2013.07.016.

Ma, Y., Duan, J. & Hao, X. (2020) Down-regulated HDAC3 elevates microRNA-495-3p to restrain epithelial-mesenchymal transition and oncogenicity of melanoma cells via reducing TRAF5. *Journal of Cellular and Molecular Medicine*. 24 (22), 12933–12944. Available from: doi:10.1111/jcmm.15885.

Mahmud, Z., Asaduzzaman, M., Kumar, U., Masrour, N., et al. (2019) Oncogenic EP300 can be targeted with inhibitors of aldo-keto reductases. *Biochemical Pharmacology*. 163 (May), 391–403. Available from: doi:10.1016/j.bcp.2019.03.009.

Majem, B., Parrilla, A., Jiménez, C., Suárez-Cabrera, L., et al. (2019) MicroRNA-654-5p suppresses ovarian cancer development impacting on MYC, WNT and AKT pathways. *Oncogene*. 38 (32), 6035–6050. Available from: doi:10.1038/s41388-019-0860-0.

Malanchi, I., Santamaria-Martínez, A., Susanto, E., Peng, H., et al. (2012) Interactions between cancer stem cells and their niche govern metastatic colonization. *Nature*. 481 (7379), 85–89. Available from: doi:10.1038/nature10694.

Manavalan, T.T., Teng, Y., Litchfield, L.M., Muluhngwi, P., et al. (2013) Reduced Expression of miR-200 Family Members Contributes to Antiestrogen Resistance in LY2 Human Breast Cancer Cells Aamir Ahmad (ed.). *PLoS ONE*. 8 (4), e62334. Available

from: doi:10.1371/journal.pone.0062334.

Mani, S.A., Guo, W., Liao, M.-J., Eaton, E.N., et al. (2008) The Epithelial-Mesenchymal Transition Generates Cells with Properties of Stem Cells. *Cell*. 133 (4), 704–715. Available from: doi:10.1016/j.cell.2008.03.027.

Maretzky, T., Reiss, K., Ludwig, A., Buchholz, J., et al. (2005) ADAM10 mediates E-cadherin shedding and regulates epithelial cell-cell adhesion, migration, and β-catenin translocation. *Proceedings of the National Academy of Sciences of the United States of America*. 102 (26), 9182–9187. Available from: doi:10.1073/pnas.0500918102.

Mashima, T. & Tsuruo, T. (2005) Defects of the apoptotic pathway as therapeutic target against cancer. *Drug Resistance Updates*. 8 (6), 339–343. Available from: doi:10.1016/j.drup.2005.11.001.

Massagué, J. (2008) TGFβ in Cancer. *Cell*. 134 (2), 215–230. Available from: doi:10.1016/j.cell.2008.07.001.

Massarweh, S., Osborne, C.K., Creighton, C.J., Qin, L., et al. (2008) Tamoxifen resistance in breast tumors is driven by growth factor receptor signaling with repression of classic estrogen receptor genomic function. *Cancer Research*. 68 (3), 826–833. Available from: doi:10.1158/0008-5472.CAN-07-2707.

Masters, J.R., Thomson, J.A., Daly-Burns, B., Reid, Y.A., et al. (2001) Short tandem repeat profiling provides an international reference standard for human cell lines. *Proceedings of the National Academy of Sciences*. 98 (14), 8012–8017. Available from: doi:10.1073/pnas.121616198.

Maughan, K.L., Lutterbie, M.A. & Ham, P.S. (2010) Treatment of breast cancer. *American Family Physician*. 81 (11), 1339–1346. Available from: doi:10.1056/nejm199810013391407.

McCart Reed, A.E., Kalaw, E., Nones, K., Bettington, M., et al. (2019) Phenotypic and molecular dissection of metaplastic breast cancer and the prognostic implications. *The Journal of Pathology*. 247 (2), 214–227. Available from: doi:10.1002/path.5184.

McMullen, E.R., Zoumberos, N.A. & Kleer, C.G. (2019) Metaplastic breast carcinoma update on histopathology and molecular alterations. *Archives of Pathology and Laboratory Medicine*. 143 (12), 1492–1496. Available from: doi:10.5858/arpa.2019-

0396-RA.

McQuerry, J.A., Jenkins, D.F., Yost, S.E., Zhang, Y., et al. (2019) Pathway activity profiling of growth factor receptor network and stemness pathways differentiates metaplastic breast cancer histological subtypes. *BMC Cancer*. 19 (1), 881. Available from: doi:10.1186/s12885-019-6052-z.

Mears, A.J., Jordan, T., Mirzayans, F., Dubois, S., et al. (1998) Mutations of the forkhead/winged-helix gene, FKHL7, in patients with Axenfeld-Rieger anomaly. *American Journal of Human Genetics*. 63 (5), 1316–1328. Available from: doi:10.1086/302109.

Meng, F., Henson, R., Lang, M., Wehbe, H., et al. (2006) Involvement of Human Micro-RNA in Growth and Response to Chemotherapy in Human Cholangiocarcinoma Cell Lines. *Gastroenterology*. 130 (7), 2113–2129. Available from: doi:10.1053/j.gastro.2006.02.057.

Meng, H., Mai, W.X., Zhang, H., Xue, M., et al. (2013) Codelivery of an Optimal Drug/siRNA Combination Using Mesoporous Silica Nanoparticles To Overcome Drug Resistance in Breast Cancer in Vitro and in Vivo. *ACS Nano*. 7 (2), 994–1005. Available from: doi:10.1021/nn3044066.

Meng, Z., Fu, X., Chen, X., Zeng, S., et al. (2010) miR-194 is a marker of hepatic epithelial cells and suppresses metastasis of liver cancer cells in mice. *Hepatology*. 52 (6), 2148–2157. Available from: doi:10.1002/hep.23915.

Merchant, A.A. & Matsui, W. (2010) Targeting Hedgehog — a Cancer Stem Cell Pathway. *Clinical Cancer Research*. 16 (12), 3130–3140. Available from: doi:10.1158/1078-0432.CCR-09-2846.

Miettinen, P.J., Ebner, R., Lopez, A.R. & Derynck, R. (1994) TGF-beta induced transdifferentiation of mammary epithelial cells to mesenchymal cells: involvement of type I receptors. *The Journal of cell biology*. 127 (6 Pt 2), 2021–2036. Available from: doi:10.1083/jcb.127.6.2021.

Miller, T.E., Ghoshal, K., Ramaswamy, B., Roy, S., et al. (2008) MicroRNA-221/222 confers tamoxifen resistance in breast cancer by targeting p27Kip1. *Journal of Biological Chemistry*. 283 (44), 29897–29903. Available from: doi:10.1074/jbc.M804612200.

Mills, M.N., Yang, G.Q., Oliver, D.E., Liveringhouse, C.L., et al. (2018) Histologic heterogeneity of triple negative breast cancer: A National Cancer Centre Database analysis. *European Journal of Cancer*. 98, 48–58. Available from: doi:10.1016/j.ejca.2018.04.011.

Min, C., Eddy, S.F., Sherr, D.H. & Sonenshein, G.E. (2008) NF-κB and epithelial to mesenchymal transition of cancer. *Journal of Cellular Biochemistry*. 104 (3), 733–744. Available from: doi:10.1002/jcb.21695.

Morel, A.-P., Lièvre, M., Thomas, C., Hinkal, G., et al. (2008) Generation of Breast Cancer Stem Cells through Epithelial-Mesenchymal Transition Juha Klefstrom (ed.). *PLoS ONE*. 3 (8), e2888. Available from: doi:10.1371/journal.pone.0002888.

Morita, T., Mayanagi, T. & Sobue, K. (2007) Dual roles of myocardin-related transcription factors in epithelial-mesenchymal transition via slug induction and actin remodeling. *Journal of Cell Biology*. 179 (5), 1027–1042. Available from: doi:10.1083/jcb.200708174.

Morris, J.C., Tan, A.R., Olencki, T.E., Shapiro, G.I., et al. (2014) Phase I Study of GC1008 (Fresolimumab): A Human Anti-Transforming Growth Factor-Beta (TGFβ) Monoclonal Antibody in Patients with Advanced Malignant Melanoma or Renal Cell Carcinoma Jose Luis Perez-Gracia (ed.). *PLoS ONE*. 9 (3), e90353. Available from: doi:10.1371/journal.pone.0090353.

Mutlu, M., Raza, U., Saatci, Ö., Eyüpoğlu, E., et al. (2016) miR-200c: a versatile watchdog in cancer progression, EMT, and drug resistance. *Journal of Molecular Medicine*. 94 (6), 629–644. Available from: doi:10.1007/s00109-016-1420-5.

Myatt, S.S. & Lam, E.W.F. (2007) The emerging roles of forkhead box (Fox) proteins in cancer. *Nature Reviews Cancer*. 7 (11), 847–859. Available from: doi:10.1038/nrc2223.

Nagao, K., Tomioka, M. & Ueda, K. (2011) Function and regulation of ABCA1 - membrane meso-domain organization and reorganization. *FEBS Journal*. 278 (18), 3190–3203. Available from: doi:10.1111/j.1742-4658.2011.08170.x.

Nakshatri, H. & Badve, S. (2009) FOXA1 in breast cancer. *Expert Reviews in Molecular Medicine*. 11 (March 2009), e8. Available from: doi:10.1017/S1462399409001008.

Natoni, A., Macauley, M.S. & O'Dwyer, M.E. (2016) Targeting selectins and their ligands in

cancer. *Frontiers in Oncology*. 6 (APR), 1–12. Available from: doi:10.3389/fonc.2016.00093.

Natsagdorj, A., Izumi, K., Hiratsuka, K., Machioka, K., et al. (2019) CCL2 induces resistance to the antiproliferative effect of cabazitaxel in prostate cancer cells. *Cancer Science*. 110 (1), 279–288. Available from: doi:10.1111/cas.13876.

Nedeljković, M. & Damjanović, A. (2019) Mechanisms of Chemotherapy Resistance in Triple-Negative Breast Cancer—How We Can Rise to the Challenge. *Cells*. 8 (9), 957. Available from: doi:10.3390/cells8090957.

Nelson, R.A., Guye, M.L., Luu, T. & Lai, L.L. (2015) Survival Outcomes of Metaplastic Breast Cancer Patients: Results from a US Population-based Analysis. *Annals of Surgical Oncology*. 22 (1), 24–31. Available from: doi:10.1245/s10434-014-3890-4.

Neuzillet, C., Tijeras-Raballand, A., Cohen, R., Cros, J., et al. (2015) Targeting the TGFβ pathway for cancer therapy. *Pharmacology & Therapeutics*. 147, 22–31. Available from: doi:10.1016/j.pharmthera.2014.11.001.

Neve, R.M., Chin, K., Fridlyand, J., Yeh, J., et al. (2006) A collection of breast cancer cell lines for the study of functionally distinct cancer subtypes. *Cancer Cell*. 10 (6), 515–527. Available from: doi:10.1016/j.ccr.2006.10.008.

Neves, M., Fumagalli, A., van den Bor, J., Marin, P., et al. (2019) The role of ACKR3 in breast, lung, and brain cancer. *Molecular Pharmacology*. 96 (6), 819–825. Available from: doi:10.1124/mol.118.115279.

Ngamcherdtrakul, W. & Yantasee, W. (2019) siRNA therapeutics for breast cancer: recent efforts in targeting metastasis, drug resistance, and immune evasion. *Translational Research*. 214, 105–120. Available from: doi:10.1016/j.trsl.2019.08.005.

Nielsen, T.O., Hsu, F.D., Jensen, K., Cheang, M., et al. (2004) Immunohistochemical and Clinical Characterization of the Basal-Like Subtype of Invasive Breast Carcinoma. *Clinical Cancer Research*. 10 (16), 5367–5374. Available from: doi:10.1158/1078-0432.CCR-04-0220.

Nieto, M.A. (2013) Epithelial plasticity: A common theme in embryonic and cancer cells. *Science*. 342 (6159), 1234850. Available from: doi:10.1126/science.1234850.

Nishijima, N., Seike, M., Soeno, C., Chiba, M., et al. (2016) miR-200/ZEB axis regulates

sensitivity to nintedanib in non-small cell lung cancer cells. *International Journal of Oncology*. 48 (3), 937–944. Available from: doi:10.3892/ijo.2016.3331.

Nishimura, D.Y., Swiderski, R.E., Alward, W.L.M., Searby, C.C., et al. (1998) The forkhead transcription factor gene FKHL7 is responsible for glaucoma phenotypes which map to 6p25. *Nature Genetics*. 19 (2), 140–147. Available from: doi:10.1038/493.

Nucera, C., Eeckhoute, J., Finn, S., Carroll, J.S., et al. (2009) FOXA1 is a potential oncogene in anaplastic thyroid carcinoma. *Clinical Cancer Research*. 15 (11), 3680–3689. Available from: doi:10.1158/1078-0432.CCR-08-3155.

Nurmik, M., Ullmann, P., Rodriguez, F., Haan, S., et al. (2020) In search of definitions: Cancer-associated fibroblasts and their markers. *International Journal of Cancer*. 146 (4), 895–905. Available from: doi:10.1002/ijc.32193.

O'Brien, C.A., Pollett, A., Gallinger, S. & Dick, J.E. (2007) A human colon cancer cell capable of initiating tumour growth in immunodeficient mice. *Nature*. 445 (7123), 106–110. Available from: doi:10.1038/nature05372.

Oba, T., Izumi, H. & Ito, K.I. (2016) ABCB1 and ABCC11 confer resistance to eribulin in breast cancer cell lines. *Oncotarget*. 7 (43), 70011–70027. Available from: doi:10.18632/oncotarget.11727.

Ogryzko, V. V., Schiltz, R.L., Russanova, V., Howard, B.H., et al. (1996) The transcriptional coactivators p300 and CBP are histone acetyltransferases. *Cell*. 87 (5), 953–959. Available from: doi:10.1016/S0092-8674(00)82001-2.

Ohka, F., Natsume, A., Motomura, K., Kishida, Y., et al. (2011) The global DNA methylation surrogate LINE-1 methylation is correlated with MGMT promoter methylation and is a better prognostic factor for glioma Maciej S. Lesniak (ed.). *PLoS ONE*. 6 (8), e23332. Available from: doi:10.1371/journal.pone.0023332.

Ohm, J.E., McGarvey, K.M., Yu, X., Cheng, L., et al. (2007) A stem cell-like chromatin pattern may predispose tumor suppressor genes to DNA hypermethylation and heritable silencing. *Nature Genetics*. 39 (2), 237–242. Available from: doi:10.1038/ng1972.

Okada, H. & Mak, T.W. (2004) Pathways of apoptotic and non-apoptotic death in tumour cells. *Nature Reviews Cancer*. 4 (8), 592–603. Available from: doi:10.1038/nrc1412.

Onder, T.T., Gupta, P.B., Mani, S.A., Yang, J., et al. (2008) Loss of E-Cadherin Promotes

Metastasis via Multiple Downstream Transcriptional Pathways. *Cancer Research*. 68 (10), 3645–3654. Available from: doi:10.1158/0008-5472.CAN-07-2938.

Ong, C.T., Campbell, B.M., Thomas, S.M., Greenup, R.A., et al. (2018) Metaplastic Breast Cancer Treatment and Outcomes in 2500 Patients: A Retrospective Analysis of a National Oncology Database. *Annals of Surgical Oncology*. 25 (8), 2249–2260. Available from: doi:10.1245/s10434-018-6533-3.

Orlowski, R.Z. & Baldwin, A.S. (2002) NF-κB as a therapeutic target in cancer. *Trends in Molecular Medicine*. 8 (8), 385–389. Available from: doi:10.1016/S1471-4914(02)02375-4.

Orosco, A., Fromigué, O., Bazille, C., Entz-Werle, N., et al. (2007) Syndecan-2 affects the basal and chemotherapy-induced apoptosis in osteosarcoma. *Cancer Research*. 67 (8), 3708–3715. Available from: doi:10.1158/0008-5472.CAN-06-4164.

Ouyang, M., Li, Y., Ye, S., Ma, J., et al. (2014) MicroRNA profiling implies new markers of chemoresistance of triple-negative breast cancer Pranela Rameshwar (ed.). *PLoS ONE*. 9 (5), e96228. Available from: doi:10.1371/journal.pone.0096228.

Ozdamar, B., Bose, R., Barrios-Rodiles, M., Wang, H.R., et al. (2005) Regulation of the polarity protein Par6 by TGFβ receptors controls epithelial cell plasticity. *Science*. 307 (5715), 1603–1609. Available from: doi:10.1126/science.1105718.

Padua, D., Zhang, X.H.F., Wang, Q., Nadal, C., et al. (2008) TGFβ Primes Breast Tumors for Lung Metastasis Seeding through Angiopoietin-like 4. *Cell*. 133 (1), 66–77. Available from: doi:10.1016/j.cell.2008.01.046.

Pampalakis, G., Obasuyi, O., Papadodima, O., Chatziioannou, A., et al. (2014) The KLK5 protease suppresses breast cancer by repressing the mevalonate pathway. *Oncotarget*. 5 (9), 2390–2403. Available from: doi:10.18632/oncotarget.1235.

Pan, X., Hong, X., Lai, J., Cheng, L., et al. (2020) Exosomal MicroRNA-221-3p Confers Adriamycin Resistance in Breast Cancer Cells by Targeting PIK3R1. *Frontiers in Oncology*. 10 (April), 1–14. Available from: doi:10.3389/fonc.2020.00441.

Pandya, K., Meeke, K., Clementz, A.G., Rogowski, A., et al. (2011) Targeting both Notch and ErbB-2 signalling pathways is required for prevention of ErbB-2-positive breast tumour recurrence. *British Journal of Cancer*. 105 (6), 796–806. Available from:

doi:10.1038/bjc.2011.321.

Papachristodoulou, A., Silginer, M., Weller, M., Schneider, H., et al. (2019) Therapeutic Targeting of TGFβ Ligands in Glioblastoma Using Novel Antisense Oligonucleotides Reduces the Growth of Experimental Gliomas. *Clinical Cancer Research*. 25 (23), 7189–7201. Available from: doi:10.1158/1078-0432.CCR-17-3024.

Park, H.S., Park, S., Kim, J.H., Lee, J.H., et al. (2010) Clinicopathologic features and outcomes of metaplastic breast Carcinoma: Comparison with invasive ductal carcinoma of the breast. *Yonsei Medical Journal*. 51 (6), 864–869. Available from: doi:10.3349/ymj.2010.51.6.864.

Park, S.H., Fong, K., Kim, J., Wang, F., et al. (2021) Posttranslational regulation of FOXA1 by Polycomb and BUB3/USP7 deubiquitin complex in prostate cancer. *Science Advances*. 7 (15), eabe2261. Available from: doi:10.1126/sciadv.abe2261.

Park, S.M., Gaur, A.B., Lengyel, E. & Peter, M.E. (2008) The miR-200 family determines the epithelial phenotype of cancer cells by targeting the E-cadherin repressors ZEB1 and ZEB2. *Genes and Development*. 22 (7), 894–907. Available from: doi:10.1101/gad.1640608.

Partridge, A.H., Burstein, H.J. & Winer, E.P. (2001) Side Effects of Chemotherapy and Combined Chemohormonal Therapy in Women With Early-Stage Breast Cancer. *JNCI Monographs*. 2001 (30), 135–142. Available from: doi:10.1093/oxfordjournals.jncimonographs.a003451.

Patani, N., Jiang, W.G. & Mokbel, K. (2011) Brain-derived neurotrophic factor expression predicts adverse pathological & clinical outcomes in human breast cancer. *Cancer Cell International*. 11 (1), 23. Available from: doi:10.1186/1475-2867-11-23.

Perou, C.M., Sørlie, T., Eisen, M.B., van de Rijn, M., et al. (2000) Molecular portraits of human breast tumours. *Nature*. 406 (6797), 747–752. Available from: doi:10.1038/35021093.

Pezzi, C.M., Patel-Parekh, L., Cole, K., Franko, J., et al. (2006) Characteristics and Treatment of Metaplastic Breast Cancer: Analysis of 892 Cases from the National Cancer Data Base. *Annals of Surgical Oncology*. 14 (1), 166–173. Available from: doi:10.1245/s10434-006-9124-7.

Phi, L.T.H., Sari, I.N., Yang, Y., Lee, S.-H., et al. (2018) Cancer Stem Cells (CSCs) in Drug Resistance and their Therapeutic Implications in Cancer Treatment. *Stem Cells International*. 2018, 1–16. Available from: doi:10.1155/2018/5416923.

Piscuoglio, S., Ng, C.K.Y., Geyer, F.C., Burke, K.A., et al. (2017) Genomic and transcriptomic heterogeneity in metaplastic carcinomas of the breast. *npj Breast Cancer*. 3 (1), 48. Available from: doi:10.1038/s41523-017-0048-0.

Pluchino, K.M., Hall, M.D., Goldsborough, A.S., Callaghan, R., et al. (2012) Collateral sensitivity as a strategy against cancer multidrug resistance. *Drug Resistance Updates*. 15 (1–2), 98–105. Available from: doi:10.1016/j.drup.2012.03.002.

Po, A., Citarella, A., Catanzaro, G., Besharat, Z.M., et al. (2020) Hedgehog-GLI signalling promotes chemoresistance through the regulation of ABC transporters in colorectal cancer cells. *Scientific Reports*. 10 (1), 1–14. Available from: doi:10.1038/s41598-020-70871-9.

Poste, G. & Fidler, I.J. (1980) The pathogenesis of cancer metastasis. *Nature*. 283 (5743), 139–146. Available from: doi:10.1038/283139a0.

Potenta, S., Zeisberg, E. & Kalluri, R. (2008) The role of endothelial-to-mesenchymal transition in cancer progression. *British Journal of Cancer*. 99 (9), 1375–1379. Available from: doi:10.1038/sj.bjc.6604662.

Powell, A.A., Talasaz, A.H., Zhang, H., Coram, M.A., et al. (2012) Single Cell Profiling of Circulating Tumor Cells: Transcriptional Heterogeneity and Diversity from Breast Cancer Cell Lines Wei-Chun Chin (ed.). *PLoS ONE*. 7 (5), e33788. Available from: doi:10.1371/journal.pone.0033788.

Pu, Y., Zhao, F., Li, Y., Cui, M., et al. (2017) The miR-34a-5p promotes the multi-chemoresistance of osteosarcoma via repression of the AGTR1 gene. *BMC Cancer*. 17 (1), 45. Available from: doi:10.1186/s12885-016-3002-x.

Raguz, S., Adams, C., Masrour, N., Rasul, S., et al. (2013) Loss of O6-methylguanine-DNA methyltransferase confers collateral sensitivity to carmustine in topoisomerase II-mediated doxorubicin resistant triple negative breast cancer cells. *Biochemical Pharmacology*. 85 (2), 186–196. Available from: doi:10.1016/j.bcp.2012.10.020.

Raguz, S., De Bella, M.T., Tripuraneni, G., Slade, M.J., et al. (2004) Activation of the MDR1

Upstream Promoter in Breast Carcinoma As A Surrogate for Metastatic Invasion. *Clinical Cancer Research*. 10 (8), 2776–2783. Available from: doi:10.1158/1078-0432.CCR-03-0517.

Rakha, E.A., Reis-Filho, J.S. & Ellis, I.O. (2008) Basal-like breast cancer: A critical review. *Journal of Clinical Oncology*. 26 (15), 2568–2581. Available from: doi:10.1200/JCO.2007.13.1748.

Rakha, E.A., Tan, P.H., Varga, Z., Tse, G.M., et al. (2015) Prognostic factors in metaplastic carcinoma of the breast: a multi-institutional study. *British Journal of Cancer*. 112 (2), 283–289. Available from: doi:10.1038/bjc.2014.592.

Ran, L., Hong, T., Xiao, X., Xie, L., et al. (2017) GABARAPL1 acts as a potential marker and promotes tumor proliferation and metastasis in triple negative breast cancer. *Oncotarget*. 8 (43), 74519–74526. Available from: doi:10.18632/oncotarget.20159.

Randle, R.A., Raguz, S., Higgins, C.F. & Yagüe, E. (2007) Role of the highly structured 5′-end region of MDR1 mRNA in P-glycoprotein expression. *Biochemical Journal*. 406 (3), 445–455. Available from: doi:10.1042/BJ20070235.

Ray, P.S., Bagaria, S.P., Wang, J., Shamonki, J.M., et al. (2011) Basal-like breast cancer defined by FOXC1 expression offers superior prognostic value: A retrospective immunohistochemical study. *Annals of Surgical Oncology*. 18 (13), 3839–3847. Available from: doi:10.1245/s10434-011-1657-8.

Ray, P.S., Wang, J., Qu, Y., Sim, M.S., et al. (2010) FOXC1 is a potential prognostic biomarker with functional significance in basal-like breast cancer. *Cancer Research*. 70 (10), 3870–3876. Available from: doi:10.1158/0008-5472.CAN-09-4120.

Rayson, D., Adjei, A.A., Suman, V.J., Wold, L.E., et al. (1999) Metaplastic breast cancer: Prognosis and response to systemic therapy. *Annals of Oncology*. 10 (4), 413–419. Available from: doi:10.1023/A:1008329910362.

Raz, S., Sheban, D., Gonen, N., Stark, M., et al. (2014) Severe hypoxia induces complete antifolate resistance in carcinoma cells due to cell cycle arrest. *Cell Death and Disease*. 5 (2), e1067–e1067. Available from: doi:10.1038/cddis.2014.39.

Reddy, T.P., Rosato, R.R., Li, X., Moulder, S., et al. (2020) A comprehensive overview of metaplastic breast cancer: clinical features and molecular aberrations. *Breast Cancer*

Research. 22 (1), 121. Available from: doi:10.1186/s13058-020-01353-z.

Reik, W. (2007) Stability and flexibility of epigenetic gene regulation in mammalian development. *Nature*. 447 (7143), 425–432. Available from: doi:10.1038/nature05918.

Reinbolt, R.E., Mangini, N., Hill, J.L., Levine, L.B., et al. (2015) Endocrine Therapy in Breast Cancer: The Neoadjuvant, Adjuvant, and Metastatic Approach. *Seminars in Oncology Nursing*. 31 (2), 146–155. Available from: doi:10.1016/j.soncn.2015.02.002.

Reinhart, B.J., Slack, F.J., Basson, M., Pasquinelll, A.E., et al. (2000) The 21-nucleotide let-7 RNA regulates developmental timing in Caenorhabditis elegans. *Nature*. 403 (6772), 901–906. Available from: doi:10.1038/35002607.

Reinhold, W.C., Reimers, M.A., Maunakea, A.K., Kim, S., et al. (2007) Detailed DNA methylation profiles of the E-cadherin promoter in the NCI-60 cancer cells. *Molecular Cancer Therapeutics*. 6 (2), 391–403. Available from: doi:10.1158/1535-7163.MCT-06-0609.

Ring, A. & Dowsett, M. (2004) Mechanisms of tamoxifen resistance. *Endocrine-Related Cancer*. 11 (4), 643–658. Available from: doi:10.1677/erc.1.00776.

Rivera, E. & Gomez, H. (2010) Chemotherapy resistance in metastatic breast cancer: the evolving role of ixabepilone. *Breast Cancer Research*. 12 (S2), S2. Available from: doi:10.1186/bcr2573.

Robbins, C.M., Tembe, W.A., Baker, A., Sinari, S., et al. (2011) Copy number and targeted mutational analysis reveals novel somatic events in metastatic prostate tumors. *Genome Research*. 21 (1), 47–55. Available from: doi:10.1101/gr.107961.110.

Robey, R.W., Pluchino, K.M., Hall, M.D., Fojo, A.T., et al. (2018) Revisiting the role of ABC transporters in multidrug-resistant cancer. *Nature Reviews Cancer*. 18 (7), 452–464. Available from: doi:10.1038/s41568-018-0005-8.

Robinson, J.L.L., Hickey, T.E., Warren, A.Y., Vowler, S.L., et al. (2014) Elevated levels of FOXA1 facilitate androgen receptor chromatin binding resulting in a CRPC-like phenotype. *Oncogene*. 33 (50), 5666–5674. Available from: doi:10.1038/onc.2013.508.

Robinson, J.L.L., MacArthur, S., Ross-Innes, C.S., Tilley, W.D., et al. (2011) Androgen receptor driven transcription in molecular apocrine breast cancer is mediated by FoxA1. *EMBO Journal*. 30 (15), 3019–3027. Available from: doi:10.1038/emboj.2011.216.

Ross-Innes, C.S., Stark, R., Teschendorff, A.E., Holmes, K.A., et al. (2012) Differential oestrogen receptor binding is associated with clinical outcome in breast cancer. *Nature*. 481 (7381), 389–393. Available from: doi:10.1038/nature10730.

Ross, J.S., Badve, S., Wang, K., Sheehan, C.E., et al. (2015) Genomic Profiling of Advanced-Stage, Metaplastic Breast Carcinoma by Next-Generation Sequencing Reveals Frequent, Targetable Genomic Abnormalities and Potential New Treatment Options. *Archives of Pathology & Laboratory Medicine*. 139 (5), 642–649. Available from: doi:10.5858/arpa.2014-0200-OA.

Ru, P., Steele, R., Newhall, P., Phillips, N.J., et al. (2012) miRNA-29b suppresses prostate cancer metastasis by regulating epithelial-mesenchymal transition signaling. *Molecular Cancer Therapeutics*. 11 (5), 1166–1173. Available from: doi:10.1158/1535-7163.MCT-12-0100.

Ruan, K., Fang, X. & Ouyang, G. (2009) MicroRNAs: Novel regulators in the hallmarks of human cancer. *Cancer Letters*. 285 (2), 116–126. Available from: doi:10.1016/j.canlet.2009.04.031.

Rui, W., Bing, F., Hai-Zhu, S., Wei, D., et al. (2010) Identification of microRNA profiles in docetaxel-resistant human non-small cell lung carcinoma cells (SPC-A1). *Journal of Cellular and Molecular Medicine*. 14 (1–2), 206–214. Available from: doi:10.1111/j.1582-4934.2009.00964.x.

Sarrió, D., Rodriguez-Pinilla, S.M., Hardisson, D., Cano, A., et al. (2008) Epithelial-Mesenchymal Transition in Breast Cancer Relates to the Basal-like Phenotype. *Cancer Research*. 68 (4), 989–997. Available from: doi:10.1158/0008-5472.CAN-07-2017.

Sausville, E.A. & Holbeck, S.L. (2004) Transcription profiling of gene expression in drug discovery and development: the NCI experience. *European Journal of Cancer*. 40 (17), 2544–2549. Available from: doi:10.1016/j.ejca.2004.08.006.

Schinkel, A.H. & Jonker, J.W. (2003) Mammalian drug efflux transporters of the ATP binding cassette (ABC) family: an overview. *Advanced Drug Delivery Reviews*. 55 (1), 3–29. Available from: doi:10.1016/S0169-409X(02)00169-2.

Schmidmaier, R., Mörsdorf, K., Baumann, P., Emmerich, B., et al. (2006) Evidence for cell adhesion-mediated drug resistance of multiple myeloma cells in vivo. *International*

Journal of Biological Markers. 21 (4), 218–222. Available from: doi:10.5301/JBM.2008.1098.

Schröder, C., Witzel, I., Müller, V., Krenkel, S., et al. (2011) Prognostic value of intercellular adhesion molecule (ICAM)-1 expression in breast cancer. *Journal of Cancer Research and Clinical Oncology*. 137 (8), 1193–1201. Available from: doi:10.1007/s00432-011-0984-2.

Schwartz, T.L., Mogal, H., Papageorgiou, C., Veerapong, J., et al. (2013) Metaplastic breast cancer: histologic characteristics, prognostic factors and systemic treatment strategies. *Experimental Hematology & Oncology*. 2 (1), 31. Available from: doi:10.1186/2162-3619-2-31.

Sekiya, T. & Zaret, K.S. (2007) Repression by Groucho/TLE/Grg Proteins: Genomic Site Recruitment Generates Compacted Chromatin In Vitro and Impairs Activator Binding In Vivo. *Molecular Cell*. 28 (2), 291–303. Available from: doi:10.1016/j.molcel.2007.10.002.

Sengelaub, C.A., Navrazhina, K., Ross, J.B., Halberg, N., et al. (2016) PTPRN 2 and PLC β1 promote metastatic breast cancer cell migration through PI (4,5)P 2 -dependent actin remodeling . *The EMBO Journal*. 35 (1), 62–76. Available from: doi:10.15252/embj.201591973.

Shang, A., Zhou, C., Bian, G., Chen, W., et al. (2019) miR-381-3p restrains cervical cancer progression by downregulating FGF7. *Journal of Cellular Biochemistry*. 120 (1), 778–789. Available from: doi:10.1002/jcb.27438.

Shen, H., Li, L., Yang, S., Wang, D., et al. (2016) MicroRNA-29a contributes to drug-resistance of breast cancer cells to adriamycin through PTEN/AKT/GSK3β signaling pathway. *Gene*. 593 (1), 84–90. Available from: doi:10.1016/j.gene.2016.08.016.

Shibue, T. & Weinberg, R.A. (2017) EMT, CSCs, and drug resistance: The mechanistic link and clinical implications. *Nature Reviews Clinical Oncology*. 14 (10), 611–629. Available from: doi:10.1038/nrclinonc.2017.44.

Shimono, Y., Zabala, M., Cho, R.W., Lobo, N., et al. (2009) Downregulation of miRNA-200c Links Breast Cancer Stem Cells with Normal Stem Cells. *Cell*. 138 (3), 592–603. Available from: doi:10.1016/j.cell.2009.07.011.

Shipitsin, M., Campbell, L.L., Argani, P., Weremowicz, S., et al. (2007) Molecular Definition of Breast Tumor Heterogeneity. *Cancer Cell*. 11 (3), 259–273. Available from: doi:10.1016/j.ccr.2007.01.013.

Shirakihara, T., Horiguchi, K., Miyazawa, K., Ehata, S., et al. (2011) TGF-β regulates isoform switching of FGF receptors and epithelial-mesenchymal transition. *The EMBO Journal*. 30 (4), 783–795. Available from: doi:10.1038/emboj.2010.351.

Shlush, L.I., Mitchell, A., Heisler, L., Abelson, S., et al. (2017) Tracing the origins of relapse in acute myeloid leukaemia to stem cells. *Nature*. 547 (7661), 104–108. Available from: doi:10.1038/nature22993.

Singh, A. & Settleman, J. (2010) EMT, cancer stem cells and drug resistance: An emerging axis of evil in the war on cancer. *Oncogene*. 29 (34), 4741–4751. Available from: doi:10.1038/onc.2010.215.

Singh, S.K., Hawkins, C., Clarke, I.D., Squire, J.A., et al. (2004) Identification of human brain tumour initiating cells. *Nature*. 432 (7015), 396–401. Available from: doi:10.1038/nature03128.

Sizemore, S.T. & Keri, R.A. (2012) The forkhead box transcription factor FOXC1 promotes breast cancer invasion by inducing matrix metalloprotease 7 (MMP7) expression. *Journal of Biological Chemistry*. 287 (29), 24631–24640. Available from: doi:10.1074/jbc.M112.375865.

Skvortsova, I., Debbage, P., Kumar, V. & Skvortsov, S. (2015) Radiation resistance: Cancer stem cells (CSCs) and their enigmatic pro-survival signaling. *Seminars in Cancer Biology*. 35, 39–44. Available from: doi:10.1016/j.semcancer.2015.09.009.

Smith, A.P., Verrecchia, A., Fagà, G., Doni, M., et al. (2009) A positive role for Myc in TGFβ-induced Snail transcription and epithelial-to-mesenchymal transition. *Oncogene*. 28 (3), 422–430. Available from: doi:10.1038/onc.2008.395.

Snoussi, K., Strosberg, A.D., Bouaouina, N., Ahmed, S. Ben, et al. (2005) Genetic variation in pro-inflammatory cytokines (interleukin-1β, interleukin-1α and interleukin-6) associated with the aggressive forms, survival, and relapse prediction of breast carcinoma. *European Cytokine Network*. 16 (4), 253–260.

Solin, L.J., Kurtz, J., Fourquet, A., Amalric, R., et al. (1996) Fifteen-year results of breast-

conserving surgery and definitive breast irradiation for the treatment of ductal carcinoma in situ of the breast. *Journal of Clinical Oncology*. 14 (3), 754–763. Available from: doi:10.1200/JCO.1996.14.3.754.

Solin, L.J., Recht, A., Fourquet, A., Kurtz, J., et al. (1991) Ten-year results of breast-conserving surgery and definitive irradiation for intraductal carcinoma (ductal carcinoma in situ) of the breast. *Cancer*. 68 (11), 2337–2344. Available from: doi:10.1002/1097-0142(19911201)68:11<2337::AID-CNCR2820681102>3.0.CO;2-R.

Song, B., Wang, Y., Xi, Y., Kudo, K., et al. (2009) Mechanism of chemoresistance mediated by miR-140 in human osteosarcoma and colon cancer cells. *Oncogene*. 28 (46), 4065–4074. Available from: doi:10.1038/onc.2009.274.

Song, G., He, L., Yang, X., Yang, Y., et al. (2020) Identification of aberrant gene expression during breast ductal carcinoma in situ progression to invasive ductal carcinoma. *Journal of International Medical Research*. 48 (1), 030006051881536. Available from: doi:10.1177/0300060518815364.

Song, Y., Liu, X., Zhang, G., Song, H., et al. (2013) Unique clinicopathological features of metaplastic breast carcinoma compared with invasive ductal carcinoma and poor prognostic indicators. *World Journal of Surgical Oncology*. 11 (1), 129. Available from: doi:10.1186/1477-7819-11-129.

Song, Y., Washington, M.K. & Crawford, H.C. (2010) Loss of FOXA1/2 is essential for the epithelial-to-mesenchymal transition in pancreatic cancer. *Cancer Research*. 70 (5), 2115–2125. Available from: doi:10.1158/0008-5472.CAN-09-2979.

Sopel, M. (2010) The myoepithelial cell: Its role in normal mammary glands and breast cancer. *Folia Morphologica*. 69 (1), 1–14. Available from: http://www.ncbi.nlm.nih.gov/pubmed/20235044.

Sørlie, T., Perou, C.M., Tibshirani, R., Aas, T., et al. (2001) Gene expression patterns of breast carcinomas distinguish tumor subclasses with clinical implications. *Proceedings of the National Academy of Sciences of the United States of America*. 98 (19), 10869–10874. Available from: doi:10.1073/pnas.191367098.

Steinbichler, T.B., Dudás, J., Skvortsov, S., Ganswindt, U., et al. (2018) Therapy resistance mediated by cancer stem cells. *Seminars in Cancer Biology*. 53 (July), 156–167.

Available from: doi:10.1016/j.semcancer.2018.11.006.

Sterzyńska, K., Klejewski, A., Wojtowicz, K., Świerczewska, M., et al. (2018) The role of matrix gla protein (MGP) expression in paclitaxel and topotecan resistant ovarian cancer cell lines. *International Journal of Molecular Sciences*. 19 (10), 2901. Available from: doi:10.3390/ijms19102901.

Stingl, J., Raouf, A., Emerman, J.T. & Eaves, C.J. (2005) Epithelial Progenitors in the Normal Human Mammary Gland. *Journal of Mammary Gland Biology and Neoplasia*. 10 (1), 49–59. Available from: doi:10.1007/s10911-005-2540-7.

Strahl, B.D. & Allis, C.D. (2000) The language of covalent histone modifications. *Nature*. 403 (6765), 41–45. Available from: doi:10.1038/47412.

Strathdee, G. (2002) Epigenetic versus genetic alterations in the inactivation of E-cadherin. *Seminars in Cancer Biology*. 12 (5), 373–379. Available from: doi:10.1016/S1044-579X(02)00057-3.

Subramani, R., Camacho, F.A., Levin, C.I., Flores, K., et al. (2018) FOXC1 plays a crucial role in the growth of pancreatic cancer. *Oncogenesis*. 7 (7), 52. Available from: doi:10.1038/s41389-018-0061-7.

Subramaniam, D.S. & Isaacs, C. (2005) Utilizing prognostic and predictive factors in breast cancer. *Current Treatment Options in Oncology*. 6 (2), 147–159. Available from: doi:10.1007/s11864-005-0022-1.

Surowiak, P., Materna, V., Kaplenko, I., Spaczynski, M., et al. (2006) ABCC2 (MRP2, cMOAT) Can Be Localized in the Nuclear Membrane of Ovarian Carcinomas and Correlates with Resistance to Cisplatin and Clinical Outcome. *Clinical Cancer Research*. 12 (23), 7149–7158. Available from: doi:10.1158/1078-0432.CCR-06-0564.

Szakács, G., Paterson, J.K., Ludwig, J.A., Booth-Genthe, C., et al. (2006) Targeting multidrug resistance in cancer. *Nature Reviews Drug Discovery*. 5 (3), 219–234. Available from: doi:10.1038/nrd1984.

Takala, S., Heikkilä, P., Nevanlinna, H., Blomqvist, C., et al. (2019) Metaplastic carcinoma of the breast: Prognosis and response to systemic treatment in metastatic disease. *The Breast Journal*. 25 (3), 418–424. Available from: doi:10.1111/tbj.13234.

Takebe, N., Miele, L., Harris, P.J., Jeong, W., et al. (2015) Targeting Notch, Hedgehog, and

Wnt pathways in cancer stem cells: clinical update. *Nature Reviews Clinical Oncology*. 12 (8), 445–464. Available from: doi:10.1038/nrclinonc.2015.61.

Tan, S., Shi, H., Ba, M., Lin, S., et al. (2016a) MiR-409-3p sensitizes colon cancer cells to oxaliplatin by inhibiting Beclin-1-mediated autophagy. *International Journal of Molecular Medicine*. 37 (4), 1030–1038. Available from: doi:10.3892/ijmm.2016.2492.

Tan, X., Fu, Y., Chen, L., Lee, W., et al. (2016b) miR-671-5p inhibits epithelial-to-mesenchymal transition by downregulating FOXM1 expression in breast cancer. *Oncotarget*. 7 (1), 293–307. Available from: doi:10.18632/oncotarget.6344.

Tang, Y., Wang, Y., Deosarkar, S., Soroush, F., et al. (2015) Fast, stable induction of P-glycoprotein-mediated drug resistance in BT-474 breast cancer cells by stable transfection of ABCB1 gene. *Anticancer Research*. 35 (5), 2531–2538.

Tang, Y., Wu, B., Huang, S., Peng, X., et al. (2019) Downregulation of miR-505-3p predicts poor bone metastasis-free survival in prostate cancer. *Oncology Reports*. 41 (1), 57–66. Available from: doi:10.3892/or.2018.6826.

Tangen, I.L., Krakstad, C., Halle, M.K., Werner, H.M.J., et al. (2014) Switch in FOXA1 Status Associates with Endometrial Cancer Progression Natasha Kyprianou (ed.). *PLoS ONE*. 9 (5), e98069. Available from: doi:10.1371/journal.pone.0098069.

Tao, L., Wu, Y.Q. & Zhang, S.P. (2019) MiR-21-5p enhances the progression and paclitaxel resistance in drug-resistant breast cancer cell lines by targeting PDCD4. *Neoplasma*. 66 (05), 746–755. Available from: doi:10.4149/neo_2018_181207N930.

Tapia, M.A., González-Navarrete, I., Dalmases, A., Bosch, M., et al. (2007) Inhibition of the canonical IKK/NFκB pathway sensitizes human cancer cells to doxorubicin. *Cell Cycle*. 6 (18), 2284–2292. Available from: doi:10.4161/cc.6.18.4721.

Taube, J.H., Herschkowitz, J.I., Komurov, K., Zhou, A.Y., et al. (2010) Core epithelial-to-mesenchymal transition interactome gene-expression signature is associated with claudin-low and metaplastic breast cancer subtypes. *Proceedings of the National Academy of Sciences*. 107 (35), 15449–15454. Available from: doi:10.1073/pnas.1004900107.

Thiery, J.P. (2003) Epithelial–mesenchymal transitions in development and pathologies. *Current Opinion in Cell Biology*. 15 (6), 740–746. Available from:

doi:10.1016/j.ceb.2003.10.006.

Thiery, J.P. (2002) Epithelial–mesenchymal transitions in tumour progression. *Nature Reviews Cancer*. 2 (6), 442–454. Available from: doi:10.1038/nrc822.

Thorat, M.A., Marchio, C., Morimiya, A., Savage, K., et al. (2008) Forkhead box A1 expression in breast cancer is associated with luminal subtype and good prognosis. *Journal of Clinical Pathology*. 61 (3), 327–332. Available from: doi:10.1136/jcp.2007.052431.

Thuault, S., Tan, E.J., Peinado, H., Cano, A., et al. (2008) HMGA2 and Smads co-regulate SNAIL1 expression during induction of epithelial-to-mesenchymal transition. *Journal of Biological Chemistry*. 283 (48), 33437–33446. Available from: doi:10.1074/jbc.M802016200.

Tie, Y., Chen, C., Yang, Y., Qian, Z., et al. (2018) Upregulation of let-7f-5p promotes chemotherapeutic resistance in colorectal cancer by directly repressing several pro-apoptotic proteins. *Oncology Letters*. 15 (6), 8695–8702. Available from: doi:10.3892/ol.2018.8410.

Tkocz, D., Crawford, N.T., Buckley, N.E., Berry, F.B., et al. (2012) BRCA1 and GATA3 corepress FOXC1 to inhibit the pathogenesis of basal-like breast cancers. *Oncogene*. 31 (32), 3667–3678. Available from: doi:10.1038/onc.2011.531.

Tordonato, C., Di Fiore, P.P. & Nicassio, F. (2015) The role of non-coding RNAs in the regulation of stem cells and progenitors in the normal mammary gland and in breast tumors. *Frontiers in Genetics*. 6 (FEB), 1–16. Available from: doi:10.3389/fgene.2015.00072.

Tray, N., Taff, J. & Adams, S. (2019) Therapeutic landscape of metaplastic breast cancer. *Cancer Treatment Reviews*. 79 (March), 101888. Available from: doi:10.1016/j.ctrv.2019.08.004.

Tulotta, C. & Ottewell, P. (2018) The role of IL-1B in breast cancer bone metastasis. *Endocrine-Related Cancer*. 25 (7), R421–R434. Available from: doi:10.1530/ERC-17-0309.

Tümer, Z. & Bach-Holm, D. (2009) Axenfeld-Rieger syndrome and spectrum of PITX2 and FOXC1 mutations. *European Journal of Human Genetics*. 17 (12), 1527–1539.

Available from: doi:10.1038/ejhg.2009.93.

Vandewalle, V., Essaghir, A., Bollaert, E., Lenglez, S., et al. (2021) miR-15a-5p and miR-21-5p contribute to chemoresistance in cytogenetically normal acute myeloid leukaemia by targeting PDCD4, ARL2 and BTG2. *Journal of Cellular and Molecular Medicine*. 25 (1), 575–585. Available from: doi:10.1111/jcmm.16110.

Van Gelder, R.N., von Zastrow, M.E., Yool, A., Dement, W.C., et al. (1990) Amplified RNA synthesized from limited quantities of heterogeneous cDNA. *Proceedings of the National Academy of Sciences*. 87 (5), 1663–1667. Available from: doi:10.1073/pnas.87.5.1663.

van Rhenen, A., Feller, N., Kelder, A., Westra, A.H., et al. (2005) High Stem Cell Frequency in Acute Myeloid Leukemia at Diagnosis Predicts High Minimal Residual Disease and Poor Survival. *Clinical Cancer Research*. 11 (18), 6520–6527. Available from: doi:10.1158/1078-0432.CCR-05-0468.

Vichai, V. & Kirtikara, K. (2006) Sulforhodamine B colorimetric assay for cytotoxicity screening. *Nature Protocols*. 1 (3), 1112–1116. Available from: doi:10.1038/nprot.2006.179.

Vincent, T., Neve, E.P.A., Johnson, J.R., Kukalev, A., et al. (2009) A SNAIL1-SMAD3/4 transcriptional repressor complex promotes TGF-β mediated epithelial-mesenchymal transition. *Nature Cell Biology*. 11 (8), 943–950. Available from: doi:10.1038/ncb1905.

Visvader, J.E. & Lindeman, G.J. (2008) Cancer stem cells in solid tumours: Accumulating evidence and unresolved questions. *Nature Reviews Cancer*. 8 (10), 755–768. Available from: doi:10.1038/nrc2499.

Vlachos, I.S., Zagganas, K., Paraskevopoulou, M.D., Georgakilas, G., et al. (2015) DIANA-miRPath v3.0: Deciphering microRNA function with experimental support. *Nucleic Acids Research*. 43 (W1), W460–W466. Available from: doi:10.1093/nar/gkv403.

Wang, B., Wang, H. & Yang, Z. (2012) MiR-122 Inhibits Cell Proliferation and Tumorigenesis of Breast Cancer by Targeting IGF1R Partha Mukhopadhyay (ed.). *PLoS ONE*. 7 (10), e47053. Available from: doi:10.1371/journal.pone.0047053.

Wang, D., Garcia-Bassets, I., Benner, C., Li, W., et al. (2011) Reprogramming transcription by distinct classes of enhancers functionally defined by eRNA. *Nature*. 474 (7351),

390–397. Available from: doi:10.1038/nature10006.

Wang, H., Deng, Z., Chen, X., Cai, J., et al. (2019) Downregulation of miR-222-3p Reverses Doxorubicin-Resistance in LoVo Cells Through Upregulating Forkhead Box Protein P2 (FOXP2) Protein. *Medical Science Monitor*. 25, 2169–2178. Available from: doi:10.12659/MSM.913325.

Wang, H., Tan, G., Dong, L., Cheng, L., et al. (2012a) Circulating mir-125b as a marker predicting chemoresistance in breast cancer William C. S. Cho (ed.). *PLoS ONE*. 7 (4), e34210. Available from: doi:10.1371/journal.pone.0034210.

Wang, J., Li, L., Liu, S., Zhao, Y., et al. (2016a) FOXC1 promotes melanoma by activating MST1R/PI3K/AKT pathway and is associated with poor prognosis in melanoma. *Oncotarget*. 7 (51), 84375–84387. Available from: doi:10.18632/oncotarget.11224.

Wang, J., Ray, P.S., Sim, M., Zhou, X.Z., et al. (2012b) FOXC1 regulates the functions of human basal-like breast cancer cells by activating NF-κB signaling. *Oncogene*. 31 (45), 4798–4802. Available from: doi:10.1038/onc.2011.635.

Wang, J., Seebacher, N., Shi, H., Kan, Q., et al. (2017a) Novel strategies to prevent the development of multidrug resistance (MDR) in cancer. *Oncotarget*. 8 (48), 84559–84571. Available from: doi:10.18632/oncotarget.19187.

Wang, J., Xu, Y., Li, L., Wang, L., et al. (2017b) FOXC1 is associated with estrogen receptor alpha and affects sensitivity of tamoxifen treatment in breast cancer. *Cancer Medicine*. 6 (1), 275–287. Available from: doi:10.1002/cam4.990.

Wang, K., Guan, C., Fang, C., Jin, X., et al. (2018a) Clinical significance and prognostic value of forkhead box A1 expression in human epithelial ovarian cancer. *Oncology Letters*. 15 (4), 4457–4462. Available from: doi:10.3892/ol.2018.7899.

Wang, L., Chai, L., Ji, Q., Cheng, R., et al. (2018b) Forkhead box protein C1 promotes cell proliferation and invasion in human cervical cancer. *Molecular Medicine Reports*. 17 (3), 4392–4398. Available from: doi:10.3892/mmr.2018.8423.

Wang, L., Gu, F., Liu, C.Y., Wang, R.J., et al. (2013) High level of FOXC1 expression is associated with poor prognosis in pancreatic ductal adenocarcinoma. *Tumor Biology*. 34 (2), 853–858. Available from: doi:10.1007/s13277-012-0617-7.

Wang, Q., Li, W., Zhang, Y., Yuan, X., et al. (2009) Androgen Receptor Regulates a Distinct

Transcription Program in Androgen-Independent Prostate Cancer. *Cell*. 138 (2), 245–256. Available from: doi:10.1016/j.cell.2009.04.056.

Wang, T., Zhan, Q., Peng, X., Qiu, Z., et al. (2018c) CCL2 influences the sensitivity of lung cancer A549 cells to docetaxel. *Oncology Letters*. 16 (1), 1267–1274. Available from: doi:10.3892/ol.2018.8769.

Wang, W., Dong, Y., Li, X., Pan, Y., et al. (2020) MicroRNA-431 serves as a tumor inhibitor in breast cancer through targeting FGF9. *Oncology Letters*. 19 (1), 1001–1007. Available from: doi:10.3892/ol.2019.11126.

Wang, W., Zhang, L., Wang, Y., Ding, Y., et al. (2017c) Involvement of miR-451 in resistance to paclitaxel by regulating YWHAZ in breast cancer. *Cell Death & Disease*. 8 (10), e3071. Available from: doi:10.1038/cddis.2017.460.

Wang, X., Lin, M., Zhao, J., Zhu, S., et al. (2018d) TSPAN7 promotes the migration and proliferation of lung cancer cells via epithelial-to-mesenchymal transition. *OncoTargets and Therapy*. 11, 8815–8822. Available from: doi:10.2147/OTT.S167902.

Wang, Y. & Li, H. (2018) Identification of proteins associated with paclitaxel resistance of epithelial ovarian cancer using iTRAQ-based proteomics. *Oncology Letters*. 15 (6), 9793–9801. Available from: doi:10.3892/ol.2018.8600.

Wang, Y., Zhao, L., Xiao, Q., Jiang, L., et al. (2016b) miR-302a/b/c/d cooperatively inhibit BCRP expression to increase drug sensitivity in breast cancer cells. *Gynecologic Oncology*. 141 (3), 592–601. Available from: doi:10.1016/j.ygyno.2015.11.034.

Wang, Y. & Zhou, B.P. (2011) Epithelial-mesenchymal transition in breast cancer progression and metastasis. *Chinese Journal of Cancer*. 30 (9), 603–611. Available from: doi:10.5732/cjc.011.10226.

Wang, Z., Huang, C., Zeng, J., Deng, Q., et al. (2012c) Effects of the proapoptotic regulator Bcl-2/adenovirus EIB 19-kDa-interacting protein 3 on the chemosensitivity of human colon cancer cell lines. *Oncology Letters*. 4 (6), 1195–1202. Available from: doi:10.3892/ol.2012.933.

Wang, Z., Li, Y., Ahmad, A., Azmi, A.S., et al. (2010) Targeting miRNAs involved in cancer stem cell and EMT regulation: An emerging concept in overcoming drug resistance. *Drug Resistance Updates*. 13 (4–5), 109–118. Available from:

doi:10.1016/j.drup.2010.07.001.

Ward, A., Balwierz, A., Zhang, J.D., Küblbeck, M., et al. (2013) Re-expression of microRNA-375 reverses both tamoxifen resistance and accompanying EMT-like properties in breast cancer. *Oncogene*. 32 (9), 1173–1182. Available from: doi:10.1038/onc.2012.128.

Wei, L.X., Zhou, R.S., Xu, H.F., Wang, J.Y., et al. (2013) High expression of FOXC1 is associated with poor clinical outcome in non-small cell lung cancer patients. *Tumor Biology*. 34 (2), 941–946. Available from: doi:10.1007/s13277-012-0629-3.

Wei, T., Zhu, W., Fang, S., Zeng, X., et al. (2017) miR-495 promotes the chemoresistance of SCLC through the epithelial-mesenchymal transition via Etk/BMX. *American Journal of Cancer Research*. 7 (3), 628–646. Available from: http://www.ncbi.nlm.nih.gov/pubmed/28401017.

Weigelt, B., Eberle, C., Cowell, C.F., Ng, C.K.Y., et al. (2014) Metaplastic breast carcinoma: More than a special type. *Nature Reviews Cancer*. 14 (3), 147–148. Available from: doi:10.1038/nrc3637.

Weigelt, B., Kreike, B. & Reis-Filho, J.S. (2009) Metaplastic breast carcinomas are basal-like breast cancers: A genomic profiling analysis. *Breast Cancer Research and Treatment*. 117 (2), 273–280. Available from: doi:10.1007/s10549-008-0197-9.

Weisbrod, A.B., Zhang, L., Jain, M., Barak, S., et al. (2013) Altered PTEN, ATRX, CHGA, CHGB, and TP53 Expression Are Associated with Aggressive VHL-Associated Pancreatic Neuroendocrine Tumors. *Hormones and Cancer*. 4 (3), 165–175. Available from: doi:10.1007/s12672-013-0134-1.

Weiswald, L.-B., Bellet, D. & Dangles-Marie, V. (2015) Spherical Cancer Models in Tumor Biology. *Neoplasia*. 17 (1), 1–15. Available from: doi:10.1016/j.neo.2014.12.004.

Wellington, C.L., Walker, E.K.Y., Suarez, A., Kwok, A., et al. (2002) ABCA1 mRNA and protein distribution patterns predict multiple different roles and levels of regulation. *Laboratory Investigation*. 82 (3), 273–283. Available from: doi:10.1038/labinvest.3780421.

Welten, S.M.J., de Jong, R.C.M., Wezel, A., de Vries, M.R., et al. (2017) Inhibition of 14q32 microRNA miR-495 reduces lesion formation, intimal hyperplasia and plasma

cholesterol levels in experimental restenosis. *Atherosclerosis*. 261, 26–36. Available from: doi:10.1016/j.atherosclerosis.2017.04.011.

WHO, I.A. for R. on C. (Iarc). (n.d.) *Global Cancer Observatory: Population Facts Sheet*. Available from: https://gco.iarc.fr/today/fact-sheets-populations [Accessed: 9 December 2020].

Wilm, B., James, R.G., Schultheiss, T.M. & Hogan, B.L.M. (2004) The forkhead genes, Foxc1 and Foxc2, regulate paraxial versus intermediate mesoderm cell fate. *Developmental Biology*. 271 (1), 176–189. Available from: doi:10.1016/j.ydbio.2004.03.034.

Wong, S.H.M., Fang, C.M., Chuah, L.H., Leong, C.O., et al. (2018) E-cadherin: Its dysregulation in carcinogenesis and clinical implications. *Critical Reviews in Oncology/Hematology*. 121 (April 2017), 11–22. Available from: doi:10.1016/j.critrevonc.2017.11.010.

Woodhouse, E.C., Chuaqui, R.F. & Liotta, L.A. (1997) General mechanisms of metastasis. *Cancer*. 80 (8 SUPPL.), 1529–1537. Available from: doi:10.1002/(sici)1097-0142(19971015)80:8+<1529::aid-cncr2>3.0.co;2-f.

World Health Organization (n.d.) *Cancer*. Available from: https://www.who.int/news-room/fact-sheets/detail/cancer [Accessed: 1 June 2021].

Wu, J., Niu, Q., Yuan, J., Xu, X., et al. (2019) Novel compound cedrelone inhibits hepatocellular carcinoma progression via PBLD and Ras/Rap1. *Experimental and Therapeutic Medicine*. 18 (6), 4209–4220. Available from: doi:10.3892/etm.2019.8080.

Wu, Y., Ginther, C., Kim, J., Mosher, N., et al. (2012) Expression of Wnt3 Activates Wnt/β-Catenin Pathway and Promotes EMT-like Phenotype in Trastuzumab-Resistant HER2-Overexpressing Breast Cancer Cells. *Molecular Cancer Research*. 10 (12), 1597–1606. Available from: doi:10.1158/1541-7786.MCR-12-0155-T.

Wu, Y. & Zhou, B.P. (2010) TNF-α/NF-κB/Snail pathway in cancer cell migration and invasion. *British Journal of Cancer*. 102 (4), 639–644. Available from: doi:10.1038/sj.bjc.6605530.

Xia, L., Huang, W., Tian, D., Zhu, H., et al. (2013) Overexpression of forkhead box C1 promotes tumor metastasis and indicates poor prognosis in hepatocellular carcinoma.

Hepatology. 57 (2), 610–624. Available from: doi:10.1002/hep.26029.

Xiao, M., Yang, Z., Tang, X., Mu, L., et al. (2017) Clinicopathological characteristics and prognosis of metaplastic carcinoma of the breast. *Oncology Letters*. 14 (2), 1971–1978. Available from: doi:10.3892/ol.2017.6399.

Xiao, T., Xu, Z., Zhang, H., Geng, J., et al. (2019) TP53I11 suppresses epithelial-mesenchymal transition and metastasis of breast cancer cells. *BMB reports*. 52 (6), 379–384. Available from: doi:10.5483/BMBRep.2019.52.6.173.

Xu, Y., Shao, Q., Yao, H., Jin, Y., et al. (2014) Overexpression of FOXC1 correlates with poor prognosis in gastric cancer patients. *Histopathology*. 64 (7), 963–970. Available from: doi:10.1111/his.12347.

Xu, Y.L., Yao, R., Li, J., Zhou, Y.D., et al. (2017) FOXC1 overexpression is a marker of poor response to anthracycline-based adjuvant chemotherapy in sporadic triple-negative breast cancer. *Cancer Chemotherapy and Pharmacology*. 79 (6), 1205–1213. Available from: doi:10.1007/s00280-017-3319-4.

Xu, Y.Y., Tian, J., Hao, Q. & Yin, L.R. (2016) MicroRNA-495 downregulates FOXC1 expression to suppress cell growth and migration in endometrial cancer. *Tumor Biology*. 37 (1), 239–251. Available from: doi:10.1007/s13277-015-3686-6.

Xu, Z.Y., Ding, S.M., Zhou, L., Xie, H.Y., et al. (2012) FOXC1 contributes to microvascular invasion in primary hepatocellular carcinoma via regulating epithelial-mesenchymal transition. *International Journal of Biological Sciences*. 8 (8), 1130–1141. Available from: doi:10.7150/ijbs.4769.

Xuan, Y. & Wang, Y.N. (2017) Hypoxia/IL-1α axis promotes gastric cancer progression and drug resistance. *Journal of Digestive Diseases*. 18 (9), 511–520. Available from: doi:10.1111/1751-2980.12496.

Yagüe, E., Arance, A., Kubitza, L., O'Hare, M., et al. (2007) Ability to acquire drug resistance arises early during the tumorigenesis process. *Cancer Research*. 67 (3), 1130–1137. Available from: doi:10.1158/0008-5472.CAN-06-2574.

Yagüe, E., Armesilla, A.L., Harrison, G., Elliott, J., et al. (2003) P-glycoprotein (MDR1) expression in leukemic cells is regulated at two distinct steps, mRNA stabilization and translational initiation. *Journal of Biological Chemistry*. 278 (12), 10344–10352.

Available from: doi:10.1074/jbc.M211093200.

Yam, C., Mani, S.A. & Moulder, S.L. (2017) Targeting the Molecular Subtypes of Triple Negative Breast Cancer: Understanding the Diversity to Progress the Field. *The Oncologist*. 22 (9), 1086–1093. Available from: doi:10.1634/theoncologist.2017-0095.

Yang, H., Kong, W., He, L., Zhao, J.J., et al. (2008) MicroRNA expression profiling in human ovarian cancer: miR-214 induces cell survival and cisplatin resistance by targeting PTEN. *Cancer Research*. 68 (2), 425–433. Available from: doi:10.1158/0008-5472.CAN-07-2488.

Yang, J. & Weinberg, R.A. (2008) Epithelial-Mesenchymal Transition: At the Crossroads of Development and Tumor Metastasis. *Developmental Cell*. 14 (6), 818–829. Available from: doi:10.1016/j.devcel.2008.05.009.

Yang, M.H., Chen, I.C. & Lu, Y.S. (2019) PI3K inhibitor provides durable response in metastatic metaplastic carcinoma of the breast: A hidden gem in the BELLE-4 study. *Journal of the Formosan Medical Association*. 118 (9), 1333–1338. Available from: doi:10.1016/j.jfma.2018.12.004.

Yang, Q., Wang, Y., Lu, X., Zhao, Z., et al. (2015) MiR-125b regulates epithelial-mesenchymal transition via targeting Sema4C in paclitaxel-resistant breast cancer cells. *Oncotarget*. 6 (5), 3268–3279. Available from: doi:10.18632/oncotarget.3065.

Yao, H., Xia, D., Li, Z., Ren, L., et al. (2019) MiR-382 functions as tumor suppressor and chemosensitizer in colorectal cancer. *Bioscience Reports*. 39 (8), 1–8. Available from: doi:10.1042/BSR20180441.

Yin, Y., Xie, C.-M., Li, H., Tan, M., et al. (2019) The FBXW2–MSX2–SOX2 axis regulates stem cell property and drug resistance of cancer cells. *Proceedings of the National Academy of Sciences*. 116 (41), 20528–20538. Available from: doi:10.1073/pnas.1905973116.

Yokoyama, S., Arakawa, R., Wu, C.A., Iwamoto, N., et al. (2012) Calpain-mediated ABCA1 degradation: Post-translational regulation of ABCA1 for HDL biogenesis. *Biochimica et Biophysica Acta - Molecular and Cell Biology of Lipids*. 1821 (3), 547–551. Available from: doi:10.1016/j.bbalip.2011.07.017.

Yook, J.I., Li, X.-Y., Ota, I., Hu, C., et al. (2006) A Wnt–Axin2–GSK3β cascade regulates

Snail1 activity in breast cancer cells. *Nature Cell Biology*. 8 (12), 1398–1406. Available from: doi:10.1038/ncb1508.

Yoshida, M., Hata, K., Takashima, R., Ono, K., et al. (2015) The transcription factor Foxc1 is necessary for Ihh-Gli2-regulated endochondral ossification. *Nature Communications*. 6 (1), 6653. Available from: doi:10.1038/ncomms7653.

Yoshimura, K., Takeuchi, K., Nagasaki, K., Ogishima, S., et al. (2009) Prognostic value of matrix Gla protein in breast cancer. *Molecular medicine reports*. 2 (4), 549–553. Available from: doi:10.3892/mmr_00000135.

Yoshioka, Y., Minoura, K., Takahashi, R. u., Takeshita, F., et al. (2011) An integrative genomic analysis revealed the relevance of microRNA and gene expression for drug-resistance in human breast cancer cells. *Molecular Cancer*. 10, 1–16. Available from: doi:10.1186/1476-4598-10-135.

Yu-Rice, Y., Jin, Y., Han, B., Qu, Y., et al. (2016) FOXC1 is involved in ERα silencing by counteracting GATA3 binding and is implicated in endocrine resistance. *Oncogene*. 35 (41), 5400–5411. Available from: doi:10.1038/onc.2016.78.

Yu, F., Deng, H., Yao, H., Liu, Q., et al. (2010) Mir-30 reduction maintains self-renewal and inhibits apoptosis in breast tumor-initiating cells. *Oncogene*. 29 (29), 4194–4204. Available from: doi:10.1038/onc.2010.167.

Yu, F., Jiao, Y., Zhu, Y., Wang, Y., et al. (2012) MicroRNA 34c gene down-regulation via DNA methylation promotes self-renewal and epithelial-mesenchymal transition in breast tumor-initiating cells. *Journal of Biological Chemistry*. 287 (1), 465–473. Available from: doi:10.1074/jbc.M111.280768.

Yu, J., Wang, S., Zhao, W., Duan, J., et al. (2018) Mechanistic Exploration of Cancer Stem Cell Marker Voltage-Dependent Calcium Channel α2δ1 Subunit-mediated Chemotherapy Resistance in Small-Cell Lung Cancer. *Clinical Cancer Research*. 24 (9), 2148–2158. Available from: doi:10.1158/1078-0432.CCR-17-1932.

Yu, L.H., Huang, Q.W. & Zhou, X.H. (2019) Identification of Cancer Hallmarks Based on the Gene Co-expression Networks of Seven Cancers. *Frontiers in Genetics*. 10 (FEB), 1–10. Available from: doi:10.3389/fgene.2019.00099.

Yu, M., Bardia, A., Wittner, B.S., Stott, S.L., et al. (2013) Circulating Breast Tumor Cells

Exhibit Dynamic Changes in Epithelial and Mesenchymal Composition. *Science*. 339 (6119), 580–584. Available from: doi:10.1126/science.1228522.

Zeisberg, E.M., Tarnavski, O., Zeisberg, M., Dorfman, A.L., et al. (2007) Endothelial-to-mesenchymal transition contributes to cardiac fibrosis. *Nature Medicine*. 13 (8), 952–961. Available from: doi:10.1038/nm1613.

Zhang, H., Hu, L., Cheng, M., Wang, Q., et al. (2020a) The Hedgehog signaling pathway promotes chemotherapy resistance via multidrug resistance protein 1 in ovarian cancer. *Oncology Reports*. 44 (6), 2610–2620. Available from: doi:10.3892/or.2020.7798.

Zhang, Y., Liao, Y., Chen, C., Sun, W., et al. (2020b) p38-regulated FOXC1 stability is required for colorectal cancer metastasis. *The Journal of Pathology*. 250 (2), 217–230. Available from: doi:10.1002/path.5362.

Zhang, Y., Ma, J., Shi, C., Han, W., et al. (2020c) Roles and correlation of FOXA1 and ZIC1 in breast cancer. *Current Problems in Cancer*. 44 (5), 100559. Available from: doi:10.1016/j.currproblcancer.2020.100559.

Zhang, Y., Toy, K.A. & Kleer, C.G. (2012) Metaplastic breast carcinomas are enriched in markers of tumor-initiating cells and epithelial to mesenchymal transition. *Modern Pathology*. 25 (2), 178–184. Available from: doi:10.1038/modpathol.2011.167.

Zhao, G., Zhang, L., Qian, D., Sun, Y., et al. (2019) MiR-495-3p inhibits the cell proliferation, invasion and migration of osteosarcoma by targeting C1q/TNF-related protein 3. *OncoTargets and Therapy*. 12, 6133–6143. Available from: doi:10.2147/OTT.S193937.

Zhao, L., Wang, Y., Jiang, L., He, M., et al. (2016) MIR-302a/b/c/d cooperatively sensitizes breast cancer cells to adriamycin via suppressing P-glycoprotein(P-gp) by targeting MAP/ERK kinase kinase 1 (MEKK1). *Journal of Experimental and Clinical Cancer Research*. 35 (1), 25. Available from: doi:10.1186/s13046-016-0300-8.

Zheng, Q., Banaszak, L., Fracci, S., Basali, D., et al. (2013) Leptin receptor maintains cancer stem-like properties in triple negative breast cancer cells. *Endocrine-Related Cancer*. 20 (6), 797–808. Available from: doi:10.1530/ERC-13-0329.

Zhou, J., Qie, S., Fang, H. & Xi, J. (2020) MiR-487a-3p suppresses the malignant development of pancreatic cancer by targeting SMAD7. *Experimental and Molecular*

Pathology. 116 (April), 104489. Available from: doi:10.1016/j.yexmp.2020.104489.

Zhou, M., Liu, Z., Zhao, Y., Ding, Y., et al. (2010) MicroRNA-125b confers the resistance of breast cancer cells to paclitaxel through suppression of pro-apoptotic Bcl-2 antagonist killer 1 (Bak1) expression. *Journal of Biological Chemistry*. 285 (28), 21496–21507. Available from: doi:10.1074/jbc.M109.083337.

Zhou, X., Li, D., Wang, X., Zhang, B., et al. (2015) Galectin-1 is overexpressed in CD133+ human lung adenocarcinoma cells and promotes their growth and invasiveness. *Oncotarget*. 6 (5), 3111–3122. Available from: doi:10.18632/oncotarget.3076.

Zhou, Y., Hu, Y., Yang, M., Jat, P., et al. (2014) The miR-106b~25 cluster promotes bypass of doxorubicin-induced senescence and increase in motility and invasion by targeting the E-cadherin transcriptional activator EP300. *Cell Death and Differentiation*. 21 (3), 462–474. Available from: doi:10.1038/cdd.2013.167.

Zhu, B., Chen, W., Fu, Y., Cui, X., et al. (2020) Microrna-27a-3p reverses adriamycin resistance by targeting btg2 and activating pi3k/akt pathway in breast cancer cells. *OncoTargets and Therapy*. 13, 6873–6884. Available from: doi:10.2147/OTT.S256153.

Zhu, H. (2016) Forkhead box transcription factors in embryonic heart development and congenital heart disease. *Life Sciences*. 144, 194–201. Available from: doi:10.1016/j.lfs.2015.12.001.

Zhu, X., Shen, H., Yin, X., Long, L., et al. (2016) MiR-186 regulation of Twist1 and ovarian cancer sensitivity to cisplatin. *Oncogene*. 35 (3), 323–332. Available from: doi:10.1038/onc.2015.84.

Zhu, Y.-H., Yang, F., Zhang, S.-S., Zeng, T.-T., et al. (2013) High expression of biglycan is associated with poor prognosis in patients with esophageal squamous cell carcinoma. *International journal of clinical and experimental pathology*. 6 (11), 2497–2505. Available from: doi:10.3233/CBM-160469.

Zimmermann, M., Arachchige-Don, A.P.S., Donaldson, M.S., Patriarchi, T., et al. (2016) Cyclin G2 promotes cell cycle arrest in breast cancer cells responding to fulvestrant and metformin and correlates with patient survival. *Cell Cycle*. 15 (23), 3278–3295. Available from: doi:10.1080/15384101.2016.1243189.

Chapter 10: Appendices

Appendix I

Oligonucleotides used in this study

Gene	Forward/Reverse	Sequence (5'-3')
ABCG2	Forward	TGGCTGTCATGGCTTCAGTA
	Reverse	GCCACGTGATTCTTCCACAA
ADAMTS5	Forward	TCTAAGCCCTGGTCCAAATG
	Reverse	CGTGGTAGGTCCAGCAAA
BCL2	Forward	GATTGTGGCCTTCTTTGAG
	Reverse	GTTCACAAAGGCATCC
CACNA2D1	Forward	TCCTGAGAAAATGACAGTG
	Reverse	TGTCAGTAGGAATATGGACTG
CDH1	Forward	GATTCTGCTGCTCTTGCT
	Reverse	GTCAAAGTCCTGGTCCTC
EDIL3	Forward	TCGAAGACATTGCACTTTGC
	Reverse	ACCCAGAGGCTCAGAACAAC
EP300	Forward	TATCTTCCATTGCCATCCTC
	Reverse	CCTTGTAGTCATGGACAATAC
ERBB2	Forward	CCAGCCTGAATATGTGAAC
	Reverse	CCCCAAAGGCAAAAACG
ESR1	Forward	GGAGTGTACACATTTCTGTC
	Reverse	CAAAGTGTCTGTGATCTTGTC
FOXA1	Forward	GTGGCTCCAGGATGTTAGGA
	Reverse	GCCTGAGTTCATGTTGCTGA
FOXC1	Forward	CCTGAACGGCATCTACCAGT
	Reverse	ACCTTGACGAAGCACTCGTT
IL6	Forward	TTCCTGCAGAAAAAGGCAAAG
	Reverse	AAGCTGCGCAGAATGAGAT
ITGB4	Forward	ATCTGGACAACCTCAAGAAG
	Reverse	GCCAAATCCAATAGTGTAGTC
KCNE4	Forward	ATTTTGCCTAGAGCTTTGTC
	Reverse	AAAAGAAGCTTGTAACCCAC
LEPR	Forward	ATTTTCAGAAGAGAACGGAC
	Reverse	TACTCTATAGACTGTTGGGAAG
MCAM	Forward	CAATTTAACCACCCTCACAC
	Reverse	ATAGAGGAAATAGAGGACAGC
NANOG	Forward	CTATCCATCCTTGCAAATGTC
	Reverse	GTTCTGGTCTTCTGTTTCTTG

Oligonucleotides used in this study (Contd.)

Gene	Forward/Reverse	Sequence (5'-3')
PDGFA	Forward	AAGCAAGTATTGTAGCACTC
	Reverse	GTGAGTCCGTTTTGTTTTTG
PDGFRA	Forward	TCTGCTGCCTGGACAATATAAA
	Reverse	GCATTGTCTGAGTCCACACG
PD-L1	Forward	ATGCCCCATACAACAAAATC
	Reverse	GACATGTCAGTTCATGTTCAG
PGR	Forward	ATTCACTTTTTCACCAGGTC
	Reverse	AACCTGGCAATGATTTAGAC
POU5F1	Forward	CAACCTGGAGAATTTGTTCC
	Reverse	CTCAAAATCCTCTCGTTGTG
ROR1	Forward	CAAAGATTCTTACCTGACCC
	Reverse	AGGAGCATCATTTTTGAACC
RPLP0	Forward	GCAGCATCTACAACCCTGAAG
	Reverse	CACTGGCAACATTGCGGAC
RPS14	Forward	TCACCGCCCTACACATCAAACT
	Reverse	CTGCGAGTGCTGTCAGAGG
SLC25A12	Forward	ATCTGTTTTATGTGCTCCAG
	Reverse	TTTTCAAATGTCACCTCTCC
SNAI1	Forward	AGGCCATGTCCGGACCCACA
	Reverse	GTGGAGCAGGGACATTCGGGA
SNAI2	Forward	CAGTGATTATTTCCCCGTATC
	Reverse	CCCCAAAGATGAGGAGTATC
SOX2	Forward	ATAATAACAATCATCGGCGG
	Reverse	AAAAAGAGAGAGGCAAACTG
SPARC	Forward	ACCCGCTTTTTCGAGACC
	Reverse	CAAGATCCTTGTCGATATCCTTC
STAG2	Forward	TGAGGTGTTCCAGAAGATGATAAA
	Reverse	AGAAGAAAAATGTGTTTCTGACTCC
TGFB2	Forward	TCTAGGGTGGAAATGGATAC
	Reverse	GTATTATATAAGCTCAGGACCC
THBS1	Forward	ATTTCACCGCCTACAGATGG
	Reverse	TCCCTTCATACATCACCACTCTAA
THBS2	Forward	GTGCAGGAGCGTCAGATGT
	Reverse	GGGTTGGATAAACAGCCATC
TIMP3	Forward	CAGTACATCCACACGGAAGC
	Reverse	CCATCATAGACGCGACCTG

Oligonucleotides used in this study (Contd.)

Gene	Forward/Reverse	Sequence (5'-3')
TWIST1	Forward	CTAGATGTCATTGTTTCCAGAG
	Reverse	CCCTGTTTCTTTGAATTTGG
VIM	Forward	AGTCCACTGAGTACCGGAGAC
	Reverse	CATTTCACGCATCTGGCGTTC
ZEB1	Forward	TTACACCTTTGCATACAGAACCC
	Reverse	TTTACGATTACACCCAGACTGC
ZEB2	Forward	ATTTCAGGGAGAATTGCTTG
	Reverse	TGTTCGTATTTATGTCGCAG

Appendix II

Primary antibodies used in this study

Antibody	Species	Dilution	Manufacturer/supplier and catalogue number
FOXC1	rabbit	1:1000	Abcam, UK (Cat. No: ab24067)
FOXA1	mouse	1:500	Santa Cruz Biotechnology, USA (Cat. No: sc-101058)
E-cadherin	rabbit	1:1000	Cell Signalling Technology, UK (Cat. No: 3195)
N-cadherin	rabbit	1:1000	Cell Signalling Technology, UK (Cat. No: 4061)
Vimentin	rabbit	1:1000	Cell Signalling Technology, UK (Cat. No: 5741)
Snail	rabbit	1:1000	Cell Signalling Technology, UK (Cat. No: 3879)
Slug	rabbit	1:1000	Cell Signalling Technology, UK (Cat. No: 9585)
Zeb1	rabbit	1:1000	Cell Signalling Technology, UK (Cat. No: 3396)
β-actin	mouse	1:10,000	Abcam, UK (Cat. No: ab6276)

Appendix III

Publications associated with this thesis findings

1. Oncogenic EP300 can be targeted with inhibitors of aldo-keto reductases

Authors: Zimam Mahmud, Muhammad Asaduzzaman, Uttom Kumar, Nahal Masrour, Roman Jugov, R. Charles Coombes, Sami Shousha, Yunhui Hu, Eric W.-F. Lam and Ernesto Yagüe

Journal: Biochemical Pharmacology (Year: 2019; Volume: 163; Issue: May; Page: 391-403)

DOI: 10.1016/j.bcp.2019.03.009

URL: https://doi.org/10.1016/j.bcp.2019.03.009

2. FOXA1 is a determinant of drug resistance in breast cancer cells

Authors: Uttom Kumar, Anastasia Ardasheva, Zimam Mahmud, R. Charles Coombes and Ernesto Yagüe

Journal: Breast Cancer Research and Treatment (Year: 2021; Volume:186; Issue: 2; Page: 317-326)

DOI: 10.1007/s10549-020-06068-5

URL: https://doi.org/10.1007/s10549-020-06068-5

3. MicroRNA-495/TGF-β/FOXC1 axis regulates multidrug resistance in metaplastic breast cancer cells

Authors: Uttom Kumar, Yunhui Hu, Nahal Masrour, Marcos Castellanos-Uribe, Alison Harrod, Sean T. May, Simak Ali, Valerie Speirs, R. Charles Coombes and Ernesto Yagüe

Journal: Biochemical Pharmacology (Year: 2021; Volume: 192)

DOI: 10.1016/j.bcp.2021.114692

URL: https://doi.org/10.1016/j.bcp.2021.114692